UNIVERSITÉ DE STRASBOURG

ÉCOLE DOCTORALE 182

UMR-7550

THÈSE présentée par :

Khyati MALHAN

soutenue le : **21 Septembre 2018**

pour obtenir le grade de : **Docteur de l'Université de Strasbourg**

Discipline/ Spécialité : Astrophysique

Stellar Streams as Probes of Dark Matter:

Search and Dynamical Analysis

THÈSE dirigée par :
M. IBATA Rodrigo A. (CNRS DR2, Université de Strasbourg)

RAPPORTEURS :
M. BELLAZZINI Michele (First Researcher, University of Bologna)
M. ERKAL Denis (Lecturer of Astrophysics, University of Surrey)

AUTRES MEMBRES DU JURY :
Mme. Di MATTEO P., (Astronome Adjointe, Observatoire de Paris)
M. FOUESNEAU Morgan, (Postdoctoral Fellow, MPIA, Heidelberg)
Mme. LANCON Ariane, (Professeur, Université de Strasbourg)

PhD Research Publications

Listed below are the scientific papers that the candidate contributed to various research projects during his doctoral studies (2015-2018). Some of the listed articles have resulted in peer-reviewed publications, while others have been submitted.

A SIGNIFICANT CONTRIBUTION

1 **Following Ariadne's thread through the Gaia's maze: A population of entangled stellar streams surrounding the inner Galaxy**, 2018
Ibata, Rodrigo A.; Malhan, Khyati & Martin, Nicolas F.
Ready for submission

2 **Constraining the Milky Way Halo Potential with the GD-1 stellar stream**, 2018
Malhan, Khyati & Ibata, Rodrigo A.
Submitted to the *Monthly Notices of Royal Astronomical Society* (ADS entry)

3 **Phlegethon, a nearby** 75°**-long retrograde stellar stream**, 2018
Ibata, Rodrigo A.; Malhan, Khyati; Martin, Nicolas F.; Starkenburg, Else
Accepted to the *Astrophysical Journal* (ADS entry)

4 **Ghostly Tributaries to the Milky Way: Charting the Halo's Stellar Streams with the Gaia DR2 catalogue**, 2018
Malhan, Khyati; Ibata, Rodrigo A.; Martin, Nicolas F.
Accepted to the *Monthly Notices of Royal Astronomical Society* (ADS entry)

5 `STREAMFINDER II`**: A possible fanning structure parallel to the GD-1 stream in Pan-STARRS1**, 2018
Malhan, Khyati; Ibata, Rodrigo A.; Goldman, Bertrand; Martin, Nicolas F.; Magnier, Eugene; Chambers, Kenneth
Published in *Monthly Notices of Royal Astronomical Society* (ADS entry)

6 `STREAMFINDER I` **: A new algorithm to detect Stellar Streams**, 2018
Malhan, Khyati & Ibata, Rodrigo A.
Published in *Monthly Notices of Royal Astronomical Society* ADS entry)

7 **Measuring Sun's Velocity with Stellar Streams**, 2017
Malhan, Khyati & Ibata, Rodrigo
Published in *Monthly Notices of the Royal Astronomical Society* (ADS entry)

B IN COLLABORATION

1 **Blue horizontal branch stars in the Canada-France Imaging Survey I. The stellar halo of the Milky Way traced to large radius**, 2018
Guillaume F. Thomas, Alan McConnachie, Rodrigo A. Ibata, Patrick Cote, Nicolas Martin, Else Starkenburg, Raymond Carlberg, Sebastien Fabbro, Benoit Famaey, Nicholas Fantin, Stephen Gwyn, Vincent Henault-Brunet, Khyati Malhan, Julio Navarro, Annie C. Robin, Douglas Scott
Submitted to *Monthly Notices of the Royal Astronomical Society*

2 **Chemical Mapping of the Milky Way with The Canada-France Imaging Survey: A Non-parametric Metallicity-Distance Decomposition of the Galaxy**, 2017
Ibata, Rodrigo A.; McConnachie, Alan; Cuillandre, Jean-Charles; Fantin, Nicholas; Haywood, Misha; Martin, Nicolas F.; Bergeron, Pierre; Beckmann, Volker; Bernard, Edouard; Bonifacio, Piercarlo; Caffau, Elisabetta; Carlberg, Raymond; Côté, Patrick; Cabanac, Rémi; Chapman, Scott; Duc, Pierre-Alain; Durret, Florence; Famaey, Benoît; Fabbro, Sébastien; Gwyn, Stephen; Hammer, Francois; Hill, Vanessa; Hudson, Michael J.; Lançon, Ariane; Lewis, Geraint; Malhan, Khyati; di Matteo, Paola; McCracken, Henry; Mei, Simona; Mellier, Yannick; Navarro, Julio; Pires, Sandrine; Pritchet, Chris; Reylé, Celine; Richer, Harvey; Robin, Annie C.; Sánchez Jannsen, Rubén; Sawicki, Marcin; Scott, Douglas; Scottez, Vivien; Spekkens, Kristine; Starkenburg, Else; Thomas, Guillaume; Venn, Kim
Published in Astrophysical Journal (ADS entry)

3 **The Canada-France Imaging Survey: First Results from the u-Band Component**, 2017
Ibata, Rodrigo A.; McConnachie, Alan; Cuillandre, Jean-Charles; Fantin, Nicholas; Haywood, Misha; Martin, Nicolas F.; Bergeron, Pierre; Beckmann, Volker; Bernard, Edouard; Bonifacio, Piercarlo; Caffau, Elisabetta; Carlberg, Raymond; Côté, Patrick; Cabanac, Rémi; Chapman, Scott; Duc, Pierre-Alain; Durret, Florence; Famaey, Benoît; Fabbro, Sébastien; Gwyn, Stephen; Hammer, Francois; Hill, Vanessa; Hudson, Michael J.; Lançon, Ariane; Lewis, Geraint; Malhan, Khyati; di Matteo, Paola; McCracken, Henry; Mei, Simona; Mellier, Yannick; Navarro, Julio; Pires, Sandrine; Pritchet, Chris; Reylé, Celine; Richer, Harvey; Robin, Annie C.; Sánchez Jannsen, Rubén; Sawicki, Marcin; Scott, Douglas; Scottez, Vivien; Spekkens, Kristine; Starkenburg, Else; Thomas, Guillaume; Venn, Kim
Published in Astrophysical Journal (ADS entry)

Acknowledgements

I am truly lucky to have come across many wonderful people in my life. From some I learnt Science, from some I learnt life and from some I learnt both. I believe that I am an accumulation of their good character, their positive thoughts and their skillful nature. Each and every one of them is a share holder in all of my successes. Here, I would like to acknowledge and dedicate this thesis work to all of them who have played influential roles in my life, have been extremely helpful and have left a lasting impression on me.

I sincerely thank my PhD supervisor, Dr. Rodrigo A. Ibata, for giving me this exceptional opportunity, and introducing me to the field of astrophysics through such an interesting project. When I started my doctoral studies, I had no formal training in astrophysics. But his patience and diligent nature allowed me to swiftly make progress and gain knowledge about this field. All of my hard work during these three years was only a reciprocation of his conscientious nature and our daily interactions, that also made these three years really constructive and memorable for me. I respect and thank him for his great companionship throughout my PhD journey.

It is a pleasure to thank Dr. Nicolas F. Martin for all of his refreshing on/off Science discussions, that were always both entertaining and informative. I can not thank him enough for all the invaluable favours and kind gestures that he extended towards me. It was a great experience working with him, and I hope I get similar opportunties in the future as well. I am also very pleased to have interacted with Dr. Bertrand Goldman, and would like to thank him for all the useful and friendly advices (and sometimes pastries and cakes) that I received from him. I also wish to acknowledge comradeship and innumerable generous favours that I received from Dr. Guillaume F. Thomas and (soon to be Dr.) Nicolas Longeard during my stay in France. I always cherished our discussions over “Pint of Science”.

Its really imbecile to thank your family members, but its the norm. Thank you dadima (grandma), papa, mummy, bua (aunt), chachu (uncle), Ginni (my sister) and jij (brother-in-law) for your selfless love and unconditional support. You guys are amazingly good at it, kindly continue doing that.

One should choose his friends wisely. I am not sure if I did, but then I know I could not have found better ones. Achinthya Bhat, Sushant Gupta, Tanya Gera and Yoihenba Kongbam are to blame for igniting the passion for physics in me during my academic days. It was our discussions, brainstormings and competition that kept me motivated to learn and explore more and taught me to strive everyday to become better.

Lastly, and most importantly, I would like to thank all my academic teachers for being sources of immense knowledge and inspiration. The list starts from my kindergarten days and goes uptil MSc. KG Prinicpal ma’am (I regret I dont remember her name because we used to call her *Principal ma’am*), Farouk ma’am, Anu Malik ma’am, Shikha Malhotra ma’am, Prof. K.C. Singh, Prof. Patrick Das Gupta, Prof. Sarkar, Prof Sanjay Jain - thank you for being my *gurus*.

Abstract (FR)

La formation et l'évolution des galaxies dans l'univers est un phénomène énigmatique qui demeure encore inexpliqué. Plusieurs modèles ont été proposés pour expliquer la formation de notre Galaxie, mais ils restent imparfaits. Par exemple, la fraction de la population constituant le halo stellaire de la Voie Lactée s'étant formée *ex-situ* , c.a.d., par l'accrétion d'autres galaxies et amas d'étoiles plus petits, est encore inconnue. Ceci vient principalement de notre méconnaissance de la distribution complète du halo stellaire dans l'espace des phases. De plus, nous manquons encore d'un modèle suffisamment raisonnable du potentiel gravitationnel de la Voie Lactée, qui joue un rôle majeur dans notre compréhension de la dynamique galactique. Ceci provient principalement de notre incapacité à contraindre efficacement la distribution de matière noire sous-jacente de la Voie Lactée.

Dans le même temps, et seulement depuis peu, les *Courants Stellaires* se sont révélés être d'importants outils d'archéologie galactique qui ont le potentiel de résoudre les problèmes mentionnés précédemment. Les courants stellaires sont des structures orbitales qui se sont formées par la destruction de galaxies naines et d'amas d'étoiles par effet de marée. Dans la mesure où ces objets tracent des orbites dans le potentiel sous-jacent de la galaxie (Dehnen et al 2004), leur dynamique a de nombreuses applications en archéologie galactique. Par exemple, ils sont des traceurs sensibles à l'histoire de formation de la galaxie ainsi qu'à son potentiel gravitationnel (Eyre & Binney 2009; Law & Majewski 2010). Modéliser leur dynamique permet de sonder la distrubtion de matière noire dans la Voie Lactée (Ibata et al. 2001; Koposov et al. 2010; Newberg et al 2010, Bovy et al. 2016). Le nombre de courants stellaires pourrait également placer une limite basse sur le nombre de phénomènes d'accrétion ayant eu lieu avec notre Galaxie, quantifiant ainsi quelle fraction du halo stellaire vient de fusions hierarchiques successives, et ils peuvent même sonder les sous-halos de matière noire de faible masse prédit par ΛCDM (Erkal et al. 2016a; Carlberg et al. 2012). Plus encore, connaitre les orbites d'une partie de ces streams permettrait de reconstruire la fonction de distribution d'accrétion de halos (et donc probablement du halo en lui-même). Toutes ces analyses concernent directement les problèmes fondamentaux de "Formation Galactique". Quelques courants stellaires connus ont, par le passé, été sujet à une modélisation de leur dynamique, mais la distribution de matière noire et le potentiel gravitationnel de la Voie Lactée restent encore peu contraints. Ce problème apparait car (1) le manque de vitesse tangentielle et de mesures de distance fiables entrainent des erreurs systématiques (Gibbons et al. 2014), et l'on finit par obtenir des solutions dégénérées concernant la distribution de matière noire, mais également parce que (2) le manque d'un échantillon plus large de courants stellaires, à des distances à notre galaxies diverses, mène à la détermination de modèles de potentiels n'étant pas suffisamment contraints. La détection d'un plus grand nombre de courants stellaires est donc essentielle pour obtenir de meilleurs modèles décrivant le potentiel gravitationnel du halo de matière noire de notre Galaxie, ainsi valides jusqu'à des distances plus

grandes, oú ce potentiel n'est globalement pas contraint par d'autres traceurs.

Ce manuscrit de thèse est dédié à la détection et à l'analyse de la dynamique des courants stellaires de la Voie Lactée. La première partie de ce manuscrit présente un nouvel algorithme de détection, appelé STREAMFINDER, et son application sur le catalogue ESA/Gaia DR2 (Gaia collaboration 2016, Gaia collaboration 2018), tandis que la suite montre le pouvoir que la modélisation des courants stellaires possède pour obtenir de bonnes contraintes sur le potentiel gravitationnel et les paramètres fondamentaux de notre galaxie. L'étude a mené à des résultats intéressants et, pour la première fois, a permis de produire des cartes structurelles et cinématiques des courants stellaires du halo de la Voie Lactée. Elle a également permis d'obtenir des contraintes strictes sur le halo de matière noire de la Voie Lactée, mais également un aperçu de l'exploitation de la géométrie des courants stellaires pour mesurer la vitesse galactique du Soleil.

En premier lieu, la thèse traite de l'algorithme STREAMFINDER (**Malhan & Ibata 2018**), un puissant et nouvel algorithme construit pour détecter des courants stellaires fins et dynamiquement froids dans la Voie Lactée en utilisant les données ESA/Gaia. L'algorithme est une "recette" de détection de courants stellaires qui s'appuie autant que possible sur nos connaissances à-priori de ces structures. Il peut gérer des données hétérogènes qui sont une combinaison de positions et de paramètres dynamiques, et sa particularité réside dans sa capacité à chercher des courants dans l'entièreté des données d'une façon automatique et sa capacité à détecter des courants stellaires se trouvant sur des orbites complexes. Le coeur de l'algorithme consiste à tirer des orbites théoriques tests en utilisant les paramètres actuels de l'espace des phases des étoiles observées, le tout dans un potentiel réaliste de la Voie Lactée, puis à faire des calculs multidimensionnels basés à la fois sur la population stellaire et la distribution, dans l'espace des phases, des étoiles afin de détecter des groupes d'étoiles qui correspondent à un courant. Des tests préliminaires ont été réalisés en utilisant des courants artificiels N-corps, superposés sur GUMS, un mock du catalogue Gaia (Robin et al. 2012) avec des paramètres dynamiques dégradés pour atteindre la qualité des données Gaia. Les résultats ont montré que cet algorithme pouvait, en principe, découvrir des courants trés faiblement lumineux ($\Sigma_G \sim 33\,\mathrm{mag\,arcsec^{-2}}$, nombre d'étoiles par courant ~ 15) à partir du catalogue ESA/Gaia prévu en fin de mission. La conception de l'algorithme, son modus operandi et les résultats obtenus basés sur ces tests sont décrits en détails.

Ensuite, l'application de STREAMFINDER sur la base de données de mouvement propres de Pan-STARRSS1 (Chambers et al 2016, Magnier et al 2016) est traitée. Cette analyse faite avant la sortie des données ESA/Gaia DR2 a été essentielle pour tester la faisabilité de l'algorithme une fois appliqué à un jeu de données réaliste. L'étude a été menée dans un but comparatif entre la technique de "Match Filter" et STREAMFINDER en les appliquant toutes les deux sur un même sous-échantillon, limité en magnitude, des données Pan-STARRSS1 pour tenter de trouver le courant GD-1 déja connu (Grillmair & Dianatos 2006). Elle s'est soldée par la non-détection du courant en utilisant la technique de "Match Filter", alors que STREAMFINDER, lui, a permis de détecter le courant en question (**Malhan et al 2018**). De plus, l'algorithme a également trouvé un autre courant stellaire connu, PS1-E, au voisinage de GD-1. Cette analyse a permis de justifier le travail sur l'algorithme et également mettre en avant sa supériorité sur d'autres techniques de détection de courants stellaires.

La thèse se poursuit en présentant les résultats obtenus en utilisant l'algorithme STREAMFINDER sur le catalogue trés attendu, et publié récemment, de ESA/Gaia DR2. Cette analyse a été menée à bien afin de créer une carte panoramique des halos stellaires de la Voie Lactée. Elle a constitué

un test de l'algorithme qui s'est concentrée sur la détection de courants dans le halo galactique à des distances au Soleil au-delà de 5 kpc, ainsi qu'à des latitudes galactiques $|b| > 30°$. Un riche résau de courants stellaires entremêlés dans le halo a été trouvé, avec une cohérence en terme de cinématique souvent frappante. En plus de la détection de courants déja connus, comme GD-1 (Grillmair & Dianatos 2006), Orphan (Grillmair 2006), Indus et Jhelum (Shipp et al 2018), 5 nouveaux courants ont été découverts, et nommés Gaia - 1,2,3,4 and 5. Cette analyse a, pour la première fois, produit des cartes structurelles et cinématiques du halo de la Voie Lactée (**Malhan, Ibata & Martin 2018**). La thèse détaille également ces découvertes.

Une partie de cette thèse a egalement été consacrée à la modélisation de la dynamique de ces courants stellaires afin de contraintre le potentiel du halo de matière noire de la Voie Lactée. Pour ce faire, le courant GD-1, long de 70 degrés, a été utilisé puisqu'il apparait sur nos cartes produites par `STREAMFINDER` (**Malhan & Ibata 2018**). Les résultats de cette analyse montrent que les solutions orbitales de GD-1 exige que la vitesse circulaire, à une distance galactique de celle du Soleil, soit de $V_{\rm circ}(R_\odot) = 244^{+6}_{-2}$ km s^{-1}, et que l'aplatissement de densité du halo a cette distance soit $q_\rho = 0.86^{+0.04}_{-0.07}$. La masse galactique correspondante, jusqu'à 14.5 kpc, c'est-à-dire la distance galactique moyenne de GD-1, est $M_{MW}(< 14.5\,{\rm kpc}) = 1.75^{+0.06}_{-0.05} \times 10^{11} M_\odot$. L'analyse ainsi que les résultats y sont discutés en détail.

La fin du manuscrit est dédiée à une discussion concernant l'utilité des courants stellaires de la Voie Lactée pour mesurer la vitesse galactique du Soleil (V_{sun}) (**Malhan & Ibata 2017**). Ce projet a été réalisé vers le début de la thèse mais il est présenté en dernier. Il y est question d'explorer la façon dont, purement sur la base de leur géométrie, les courants stellaires peuvent être exploités pour estimer V_{sun}. Cette nouvelle procédure peut être appliquées dés que quelques courants et leur astrométrie (positions, distances et vitesses) sont connues dans les données ESA/Gaia (la vitesse radiale n'est pas requise).

Abstract (EN)

The formation and evolution of the galaxies in our Universe is an enigmatic phenomenon that still remains unresolved. Several models have been prescribed to explain the formation history of our own Galaxy, but they remain under scrutiny. For e.g., it is still undetermined what fraction of the Milky Way's stellar halo population was formed *ex-situ* as a consequence of its pre-merging history, i.e., through accretion of other smaller galaxies and star clusters. This failure mostly stems from our lack of knowledge about the complete phase-space distribution of the stellar halo. Further, we are still lacking a reasonably good model of the Milky Way's gravitational potential, which plays a key role in the understanding of the dynamics of our Galaxy. This is caused majorly due to our inability to efficiently constrain the underlying dark matter distribution of the Milky Way.

Meanwhile, and only recently, *stellar streams* emerged as important Galactic archaeological tools that, to a great degree, hold the prowess to resolve the above mentioned problems. Stellar streams are orbital structures that are formed via the tidal disruption of dwarf galaxies and star clusters. Since these objects approximately delineate orbits in the underlying gravitational potential of the galaxy (Dehnen et al 2004), their dynamics can be exploited for various purposes. For example, the orbital structures of streams are sensitive tracers of the Galaxy's formation history and the underlying gravitational potential (Eyre & Binney 2009; Law & Majewski 2010), their dynamical modelling allows one to gauge the dark matter mass distribution in the Milky Way galaxy (Ibata et al. 2001; Koposov et al. 2010; Newberg et al 2010, Bovy et al. 2016), the number of stellar streams could place lower limits on the number of accretion events onto our Galaxy in the past (helping in quantifying what fraction of the stellar halo came from hierarchical merging events), and they can even probe the low mass dark matter sub-halos (Erkal et al. 2016a; Carlberg et al. 2012) predicted by ΛCDM cosmogony. Furthermore, knowing the orbits of a sample of streams can allow one to reconstruct the distribution function of halo accretions (and hence probably of the halo itself). All these analyses address directly the fundamental problems of "Galaxy formation and evolution". A few of the known streams have been subjected to dynamical modelling in the past, but the dark matter mass distribution and the Milky Way's gravitational potential still remain poorly constrained. This problem mainly arises because 1) the lack of reliable tangential velocity and distance measurements lead to systematics (Gibbons et al. 2014) and one ends up obtaining degenerate solutions of the dark matter mass distribution, and 2) the lack of a large sample of streams, probing different galactic radii, lead to the determination of the potential models that are loosely constrained. Therefore, more stream detections are essential in order to obtain better models of the dark matter halo potential which are then valid out to larger galactic radii, where the potential basically remains unconstrained by other tracers.

This PhD thesis was devoted to the detection and dynamical analysis of the stellar streams of the Milky Way galaxy. The first part of the thesis presents a novel stream detection algorithm, `STREAMFINDER`, and its application on the ESA/Gaia DR2 catalogue (Gaia collaboration 2016,

Gaia collaboration 2018). This study led to some interesting results where, for the first time, all-sky structural and kinematical maps of the stellar streams of the Milky Way halo were created. The latter part of the thesis shows the power that stream modelling holds in obtaining stringent constraints over the gravitational potential and the fundamental parameters of the Milky Way galaxy.

First, the thesis discusses the STREAMFINDER algorithm (**Malhan & Ibata 2018**), which is a new powerful algorithm that is designed especially to detect thin and dynamically cold streams in the Milky Way galaxy in the ESA/Gaia dataset. The algorithm is a generic stream dectection recipe that makes use of as much as possible of our prior knowledge about stellar streams. It can handle heterogeneous datasets that are a combination of positions and kinematics and its power lies in its performance, ability to scan the entire data set for stream structures in an automated way and its capability of detecting streams that lie along complex orbital trajectories. At its heart, STREAMFINDER shoots trial orbits using the present epoch observed phase-space values of the stars in some realistic Milky Way potential model and then performs a multidimensional calculation based on both the stellar population and the phase-space distribution of the data stars to detect groups of stars that correspond to a stream. Some initial tests were undertaken using the artificial N-body streams superimposed on the GUMS - mock Gaia catalogue (Robin et al. 2012) with kinematics degraded to Gaia - like quality. The results manifested that the algorithm, in principle, is capable of discovering ultra faint stream structures ($\Sigma_G \sim 33\,\mathrm{mag\,arcsec^{-2}}$, number of stars per stream ~ 15) in the end-of-mission ESA/Gaia catalogue. The algorithm's concept, its modus operandi and the analysis based results are described in detail.

Further, the application of the STREAMFINDER on the Pan-STARRSS1 proper motion dataset (Chambers et al 2016, Magnier et al 2016) is presented. This analysis, that was done prior to ESA/Gaia DR2, was essential in order to test the sanity and feasibility of the algorithm when applied to a realistic astrophysical dataset. The study was undertaken as a comparison between the Match Filtering technique and the STREAMFINDER algorithm by applying them both onto a magnitude limited subset of the Pan-STARRSS1 data in order to detect the previously known GD-1 stream (Grillmair & Dianatos 2006). The study resulted in a null detection for the Match Filter but a positive detection of GD-1 for STREAMFINDER (**Malhan et al 2018**). In addition, the algorithm also found the previously known PS1-E stream structure (Bernard et al. 2016) in the neighbourhood of GD-1 stream. Overall, this analysis justified the workings of the algorithm and also marked its superiority over other stream detection techniques.

The thesis further reviews the results obtained based on the application of the STREAMFINDER algorithm onto the ESA/Gaia DR2 catalogue. This was a pilot run of the algorithm that concentrated on detection of the streams in the galactic halo at heliocentric distances $> 5\,\mathrm{kpc}$, and at Galactic latitudes $|b| > 30°$. A rich network of criss-crossing streams in the halo was found, often with striking kinematic coherence (**Malhan, Ibata & Martin 2018**). In addition to the detection of several previously known streams, like Sagittarius (Ibata et al. 1994), GD-1 (Grillmair & Dianatos 2006), Orphan (Grillmair 2006), Indus and Jhelum (Shipp et al 2018), 5 new stream structures were also discovered that were named Gaia - 1, 2, 3, 4 and 5. This analysis, for the first time, produced an all-sky structural and kinematical maps of the stellar streams of the Milky Way halo. The thesis details these findings as well.

Furthermore, the thesis presents the power that streams hold in constraining the underlying potential of the dark matter halo of the Milky Way galaxy. For this, ESA/Gaia's astrometry along with SEGUE's radial velocities of 70° long GD-1 stellar stream was used as it appeared on the STREAMFINDER maps (**Malhan & Ibata 2018**). It was found that orbital solutions of GD-1 require the circular velocity at the Solar radius to be $V_{\rm circ}(R_\odot) = 244^{+6}_{-2}\,{\rm km\,s^{-1}}$, and also that the density flattening of the halo is $q_\rho = 0.86^{+0.04}_{-0.07}$. The corresponding Galactic mass within 14.5 kpc, the mean Galactocentric distance of GD-1, is $M_{MW}(< 14.5\,{\rm kpc}) = 1.75^{+0.06}_{-0.05} \times 10^{11}\,{\rm M_\odot}$. The analysis and the results have been discussed in detail.

The final Chapter demonstrates the usefulness of Milky Way streams in measuring the the Sun's galactic velocity (V_{sun}) (**Malhan & Ibata 2017**). It was explored that how stream structures can be exploited, purely on the basis of geometry, to estimate the Sun's galactic velocity V_{sun}. This novel procedure, that was tested on the basis of realistic N-body stream simulations, can be applied as soon as a few more thin streams and their astrometry (positions, distances and velocities) are identified in ESA/Gaia data (radial velocity measurement is not required).

Table of Contents

PhD Research Publications iii

Page

1 Galactic archaeology and relevant problems 1

1.1 Current Paradigm and Challenges . . . 4

1.1.1 Dark matter distribution around the Galaxies . . . 4

1.1.2 Galaxy Formation . . . 10

1.2 Killing two birds with Stellar Streams . . . 14

2 Stellar streams in the Milky Way halo 17

2.1 Stellar streams . . . 17

2.1.1 Mechanism of disruption . . . 17

2.1.2 Physical properties of stellar streams . . . 20

2.2 Significance of streams in Galactic archaeological studies . . . 22

2.3 Conventional techniques to detect stellar streams . . . 27

2.4 Sate-of-the-art tool to analyse ESA/Gaia data for streams . . . 29

3 STREAMFINDER - A new algorithm for detecting Stellar Streams 31

3.1 STREAMFINDER . . . 32

3.1.1 Stream Detection Concept . . . 32

3.1.2 Orbit Sampling in STREAMFINDER . . . 32

3.2 STREAMFINDER in action . . . 35

3.3 Luminosity function and continuity: additional STREAMFINDER criteria . . . 35

3.4 Results and Discussions . . . 37

3.5 Related Paper . . . 38

4 Application of STREAMFINDER onto Pan-STARRS1 proper motion dataset 53

4.1 Introduction . . . 54

4.2 Data . . . 54

4.3 Comparison between STREAMFINDER and Matched Filter . . . 54

4.4 Retrieving missing phase-space information for GD-1 stream . . . 57

4.5 Results and Discussions . . . 57
4.6 Related Paper . . . 58

5 Charting the Milky Way Halo's Stellar Streams with ESA/Gaia DR2 69
5.1 Data . . . 70
5.2 Contamination Model . . . 70
5.3 `STREAMFINDER` Analysis . . . 72
5.4 Results and Discussions . . . 72
5.5 Related Paper . . . 73

6 Constraining the Potential of the Milky Way galaxy with GD-1 stream 89
6.1 Introduction . . . 90
6.2 Data . . . 91
6.3 Method . . . 91
6.3.1 Logarithmic halo potential . . . 91
6.3.2 NFW halo profile . . . 92
6.4 Results and Discussions . . . 93
6.5 Related Paper . . . 95

7 Measuring Sun's velocity using Stellar Streams 107
7.1 Introduction . . . 107
7.2 Method . . . 108
7.3 Results and Discussions . . . 110
7.4 Related Paper . . . 110

8 Summary and Outlook 119
8.1 Summary . . . 119
8.2 Future prospects . . . 122

Bibliography 127

CHAPTER 1

GALACTIC ARCHAEOLOGY AND RELEVANT PROBLEMS

The world is full of mundane, meek, unconscious things materially embodying fiendishly complex pieces of mathematics- **Margaret Wertheim**

Abstract

This introductory Chapter intends to give a brief overview on the field of astrophysics - *Galactic archaeology* - around which this thesis revolved. Simply put, Galactic archaeology attemps at addressing questions pertaining to the formation and evolution of the galaxies in the Universe. The recent advents in the large astronomical surveys allowed this field to flourish; currently established as an interesting avenue, it is being explored and investigated by many astrophysicists. The past two decades saw some major groundbreaking developments in this area, both observational and theoretical, yet the field of Galactic archaeology faces some severe fundamental challenges.

For long, the Milky Way galaxy was commonly represented as comprising of only three major structural components [30]. These three components comprised of a dense spheroidal *bulge* situated at the centre of the Galaxy, a *stellar disk* lying in the plane of the Galaxy, and a sparsely populated *stellar halo* surrounding the entire Galaxy (see top panel in Figure 1.1). It took years of star mapping through innumerable surveys along with decades worth of analysis of the corresponding data, that only recently this representation of the Milky Way galaxy was revised by the artist Jon Lomberg (see bottom panel in Figure 1.1). The bulge, the disk and the stellar halo are still there in this updated representation, however the portrait now includes some

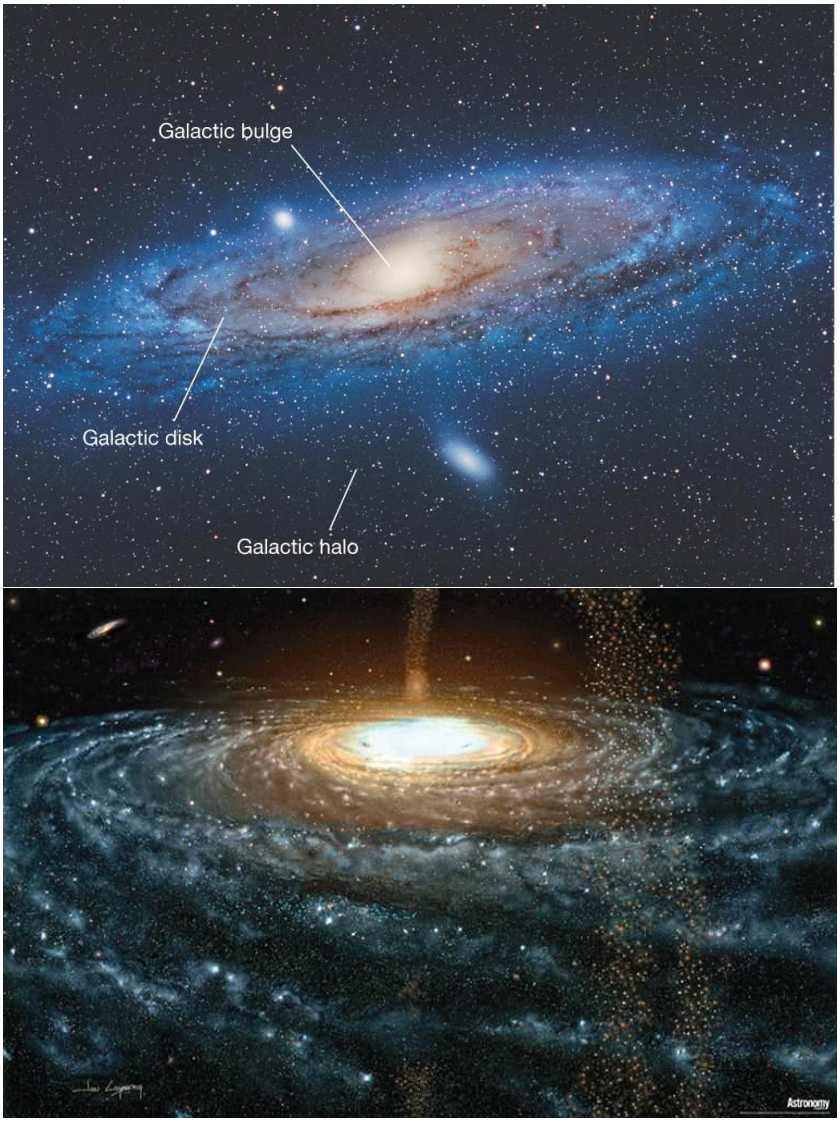

Figure 1.1: Artistic impression of the Milky Way galaxy. *Top panel* : A typical Milky Way type galaxy in the Universe consisting of a bulge, a disk and a halo (`https://pages.uoregon.edu/jimbrau/astr123/Notes/Chapter23.html`). *Lower panel* : Scientifically accurate depiction of our Milky Way galaxy and its nearest neighbours, updated from award-winning artist Jon Lomberg's original 1992 portrait of the Milky Way. It reflects our current understanding of our Galaxy's structure, based on the most recent data available (`http://astronomy.com/milkyway`)

additional features. For example, in contrast to the previous image, the spiral arms [30] in the stellar disk are now defined much more confidently. Also, some other stellar structures in the halo are now lit up much more brightly, possibly as a sign of their confirmed presence. However, the real eye-catching feature of this portrait for me was the "Sagittarius stream". One does not need to look very closely to identify a very interesting stellar structure that wraps around the Galaxy, seen to be starting from towards the observer and running all over beyond the bulge. This is the venerated Sagittarius stellar stream that was discovered in 1994 [86]. The explicit inclusion of this structure in the portrait is interesting because 1) unlike the three major components of the galaxy, this structure does not form any major constituent of the Milky Way, 2) in contrast to the depiction in the image, Sagittarius stream in reality is extremely faint in comparison to the other galactic components (the stream contributes $< 0.1\%$ by mass to the entire galactic system) and 3) there are plenty of other halo substructures, such as satellite galaxies or warps, that are luminous enough for Lomberg to have easily included in his enthralling portrait. Yet, despite all these reasons, Lomberg was somehow intrigued by this halo structure in particular and he clearly purposefully added it to his painting (by scaling up its contrast so that it becomes visible). But is his source of excitation towards Sagittarius subjective, or Sagittarius stream indeed holds some importance to our Galaxy?

Before I go any further, let me point out that Sagittarius stream is not the only *stream* structure in the Milky Way galaxy. We are aware of ~ 50 stellar streams that exist in our Galaxy (*and seemingly, there are many more lurking to be found*). Stellar streams have recently gained a lot of popularity in the field of Galactic archaeology. They serve as important tools in our understanding of the Galaxy formation history [96], in probing the gravitational potential and the mass distribution of the Galaxy [89, 111] and often prove to be useful in addressing various other relevant problems pertaining to this field [81]. Given their importance, it is not very hard to believe that this must be the reason why Lomberg was compelled to include Sagittarius in his portrait of the Milky Way. *But what is it that makes streams so important in all of these studies?*

As one said "If you don't know where you come from, how will you appreciate where you are going". For that, in order to understand the significance of streams and the prowess they hold in addressing various Galactic archaeological problems, it is first important to know the type of challenges that the astrophysicists are currently facing in this field. So now I shall restrain myself from rambling about the stellar streams (I would continue that in Chapter 2) and would take a detour to present the current scenario in the field of Galactic archaeology, with the Milky Way galaxy in context, and some of the principal challenges that it poses.

1.1 Current Paradigm and Challenges

Galactic archaeology aims at studying the structure and evolution of our Galaxy by measuring and analysing ages, chemical compositions and dynamical properties of stellar populations in different parts of the Milky Way. In general, one of the key questions that Galactic archaeology attempts at answering is the structure and galaxy formation in the Universe. Currently, the overall scenario of the structure formation in the Universe is understood as follows. In modern cosmological models, ~ 5/6th of the mass in the Universe is made of dark matter [147]. This dark matter forms the underlying soil on which galaxies form, evolve, and dynamically interact. In the context of this well established model, fluctuations in the matter distribution were created in the first fraction of a second during an inflationary period [75]. Gravitational instability grew these fluctuations over time. Gas and dark matter were initially well mixed; and as the Universe evolved, gas dissipated and fell to the centres of dark matter halos. For massive dark matter halos, gas cooled down and formed stars, and formed a *protogalaxy* [193]. The power spectrum of matter indicates that small objects should form first, and halos should grow and merge over time becoming more massive and bigger in size. Galaxies within these halos then continued forming stars (in-situ) as well as grew through merging (ex-situ), because their dark matter halos merge. This phenomenon is famously known as *hierarchical merging scenario of the Galaxies*.

This is merely our theoretical understanding of the formation and evolution of the galaxies. This understanding comes primarily through studies based on computer simulations, and although is also observationally motivated, but has yet not been completely accepted. This impairment comes majorly because we are unaquainted about the knowledge of the dark matter and its distribution around the galaxies. This in turn poses two principal challenges to the field of Galactic archaeology that are disussed below.

1.1.1 Dark matter distribution around the Galaxies

The mass density profile and spatial distribution of the dark matter halo around the Milky Way galaxy are of great astrophysical and cosmological importance. Yet, despite decades of intense efforts, our best estimates differ by more than their uncertainties [14].

Soon after the ubiquitous existence of the dark matter in the Universe was confirmed through various observational means (for e.g., analysis of the dynamics of the solar neighbourhood [3, 144], flat rotation curves of the galaxies [15, 154, 157, 159–162], power spectrum of the *CMB* [147], X-rays emission by hot gas [54, 158, 167], gravitational lensing and observations of the extra-galactic systems [41, 170]), the ingredients were in place for detailed calculations of the evolution of the structure of the Universe from its initial generation until the formation of first nonlinear structures. This was carried out using the famous Λ Cold Dark matter (ΛCDM) N-body simulations [68, 146, 183, 194]. To some extent, ΛCDM results confirmed our intuition about the nonlinear structure formation in an expanding Universe, but in many ways it rendered new

insights about the galaxy formation and global properties of the dark matter halos in which galaxies form and evolve. A new picture of hierarchically merging population of dark matter halos formed the basis for the galaxy formation scenario [195], that provided the gravitational potential wells within which gas cools and condenses to form galaxies. These simulations suggested that both the dark matter mass of a galaxy and its mass distribution are intrinsically linked to the formation and growth of structure in the Universe [31]. This gave dark matter halos a special status in cosmological context. So it was deemed that accurate determination of these parameters (dark matter mass distribution, its velocity profile and sub-structureness) for the Milky Way should give us a clearer understanding of where our Galaxy sits in a cosmological context [56].

The cosmological simulations that model Milky Way like halo (e.g., `Via Lactea` or `Aquarius` [43, 113]) were taken under investigation in order to estimate the dark matter density and its velocity distribution. Many studies found that dark matter halos in dark-matter-only simulations (where baryons are absent) are generally strongly triaxial [32, 45, 58, 94, 188] and appear to be well modelled by Navarro-Frenk-White (*NFW*) profile [137, 138]:

$$\rho_{\rm NFW}(r) = \frac{\rho_o}{(r/r_s)(1+r/r_s)^2}, \tag{1.1}$$

where r_s and ρ_o are characteristic radius and density, respectively. Einasto profile [48] is another dark matter profile that frequently appears in the literature and is again favoured by dark-matter-only simulations:

$$\rho_{\rm Ein}(r) = \rho_o \exp\left[-\frac{2}{\gamma}\left(\left(\frac{r}{r_s}\right)^{\gamma} - 1\right)\right], \tag{1.2}$$

where γ is a free parameter that sets the sharpness of the slope of the dark matter density profile. These two density functions suggest that halo density profiles are "cuspy", i.e., the density diverges towards the centre with a logarithmic slope. On the other hand, it may be possible that the inner profile is more "cored" (e.g. , has a flatter slope, like observed in some of the dwarf galaxies, [187]) than the NFW or Einasto profiles. The Burkert profile [23] is one such example:

$$\rho_{\rm Burk}(r) = \frac{\rho_o}{(1+r/r_s)(1+(r/r_s)^2)},, \tag{1.3}$$

where r_s is the core radius. A comparison of the NFW, Einasto, and Burkert profiles is shown in Figure 1.2. Among these dark matter density profiles, NFW profile is understood as an approximately universal dark matter halo shape, which is cosmologically motivated, but its physical origin is not well understood [40, 178]. However, such a halo profile reflects formation through the anisotropic collapse of ellipsoidal over-densities in the initial mass distribution, and subsequent growth by accretion and mergers.

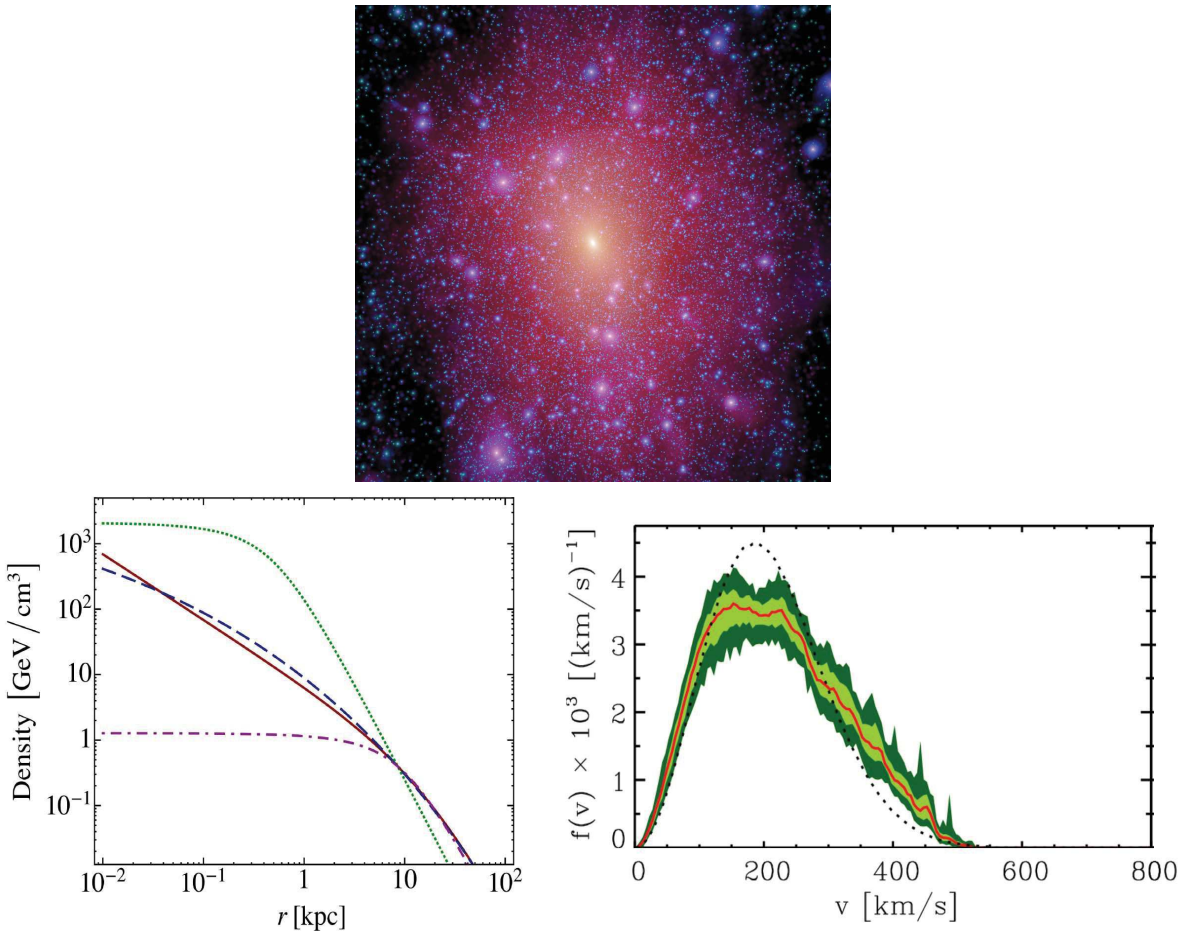

Figure 1.2: Dark matter density profiles motivated by cosmological simulations. *Top panel* : `Aquarius` Milky Way like halo simulated in full cosmological context (assuming the concordance ΛCDM cosmology), showing dark matter subhalos and substructures [196]. The image shows the projected dark matter density at z=0, in a box of side 1.07 Mpc. *Bottom left panel* : A comparison of the NFW (solid red), Einasto (dashed blue) and Burkert with $r_s = 0.5$ (dotted green) and 10 kpc (dot-dashed purple) profiles. *Bottom right panel*: The expected velocity distribution from the `Via Lactea` simulation (solid red), with the 68% scatter and the minimum/maximum values shown by the light and dark green shaded regions, respectively. For comparison, the best-fit Maxwell-Boltzmann distribution is shown in dotted black. Notice the localised spikes in the tail of velocity distribution, which are associated with recent mergers, debris inflow and streams.

N-body simulations also find evidence for substructure in the dark matter phase-space distribution. This includes localized features that arise from minor mergers between the Milky Way and other galaxies. When another dark matter subhalo falls into an orbit about the centre of the Milky Way, tidal effects strip dark matter (and possibly stars) along its orbit. This 'debris' eventually virializes with the other particles in the Milky Way's halo. However, at any given time, there is likely to be some fraction of this debris that has not come into equilibrium and which exhibits unique features that may get reflected in the observations. Examples of such substructures include clumps, stellar streams and debris flow. The bottom right panel of Figure 1.2 shows localised spikes in the tail of velocity distribution, which are assocaited with streams in `Via Lactea` [43]. These debris infall in turn also affect the density distribution of the dark matter in the host galaxy.

Anyhow, the reasons for the origin of the NFW dark matter density profile and the velocity chracteristics of the dark matter halos are only ΛCDM simulations based semi-analytical prediction that require validation through analogous observational studies.

1.1.1.1 Problem: the shape and mass of the dark matter halo

The problem is that estimates of the Milky Way's mass, that comes from the data analysis, is very sensitive to assumptions made in the modelling, and typically range from as low as $\sim 0.5\times10^{12}\,M_\odot$ [189] to as high as $2-3\times10^{12}\,M_\odot$ [20, 184]. This seemingly unimportant uncertainty in the determination of the Milky Way's mass leads to a major difference in the efficiency of conversion of baryons into stars, puts the Milky Way's companions - Large Magellanic Cloud and the Leo I dwarf spheroidal - on unbound (if light halo) or bound (if heavy halo) orbits and can or cannot solve the Too-Big-to-Fail problem[1] ([179], one of the challenges faced by ΛCDM framework). Accurate determination of the mass profile of the Milky Way also has implications for the understanding of the dynamical history our Galaxy, of the Local Group [184] and the Milky Way's satellite population, particularly the Sagittarius dwarf spheroidal and its impressive tidal stream [53], and the Magellanic Clouds [101]. The masses of the baryonic components of the Milky Way (the central nucleus that harbours a supermassive black hole at its heart [64], the bulge and the disk) are reasonably well determined [14, 92]. Its the halo that is dominated by dark matter that requires accurate mass measurement (only a few percent of the mass of the halo is baryonic [81]).

1.1.1.2 Current constraints on the dark matter distribution in our Galaxy

Figure 1.3 represents a dark matter halo surrounding the Milky Way galaxy that is triaxial in shape - the most generic form of the dark matter halo. The shape of the dark halo, in general, is determined by its 1) radial profile - how the dark matter density varies with the galacto-

[1]The problem is that while the number of massive sub-halos in dark-matter-only simulations matches the number of classical dwarf satellites observed, the central densities of these simulated dwarfs are higher than the central densities observed in the real galaxies.

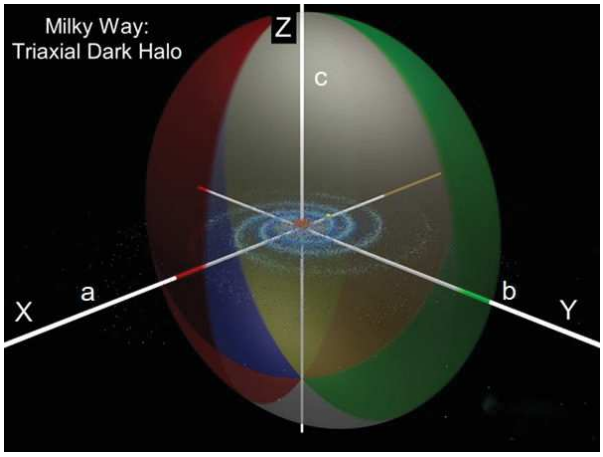

Figure 1.3: This illustration shows a "beachball" representation of the dark matter halo surrounding the Milky Way galaxy (flattened blue spiral; the colors of the beachball were chosen arbitrarily). The location of the Sun in this image is indicated by the yellow dot; white 'XYZ' coordinate axes are drawn for reference.

centric distance, and 2) extent that it can be described as triaxial based on the axis ratios b/a (intermediate-to-long) and c/a (short-to-long). Most of the studies indicate that dark halos are only mildly triaxial and oblate ($b \approx a, c/a < 1$,[111]), with the equatorial plane of the dark halo nearly coinciding with that of the stellar body (for example, galactic disk). Also, dark halos appear to be extended to at least ~ 50 kpc with total enclosed masses that rise linearly with the galactocentric radius [164]. Whether this behaviour can be extrapolated to distances as large as 200 kpc and beyond is controversial as results at this radius are model-dependent.

It is our inability to detect the dark matter directly that gives rise to such an uncertainty in Milky Way's mass. However, the total gravitational potential of galaxies - its extent, radial density profile, flattening, and triviality - strongly affects the motions and morphology of associated stellar and gaseous components. And therefore, we can infer dark matter's presence by its influence on its surroundings. Typically, this is the purview of dynamical studies. Any mass distribution gives rise to a gravitational potential that causes objects to move; and by studying measurements of the motions of the objects, we can recover the underlying gravitational potential and, thus, the underlying mass distribution. Listed below are several observational techniques that are used to infer the shape of the Milky Way's dark matter halo. While each method holds its own significance, many of their results are model-dependent; some are in apparent conflict with others.

1. **Rotation curve**

   Primary constraint on the gravitational potential in the Milky Way and external galaxies alike has been the rotation curve. This analysis requires to know our distance from the Galactic centre ($R_\odot$), the local circular velocity at the Sun's position ($V_{\rm circ}$) and the peculiar velocity of the Sun with respect to this circular velocity ($V_{p\odot}$). Estimates of $R_\odot$ can vary, at

the very extremes, from $\sim 6.5\,\mathrm{kpc}$ to $\sim 9.5\,\mathrm{kpc}$, while associated measurements of the local circular velocity vary from $\sim 180\,\mathrm{km\,s^{-1}}$ to $300\,\mathrm{km\,s^{-1}}$, all these values again being heavily model-dependent [128].

But rotation curves are hardly sensitive to the detailed three-dimensional shape of a mass distribution, and hence precise measurements of the shapes of galactic dark-matter halos are close to non-existent. This is an unfortunate situation because, as pointed out before, numerical simulations of the formation of dark-matter halos make strong predictions for their three-dimensional shapes.

2. **Stellar dynamical models**

   With current large astrometric and kinematic surveys, such as ESA/Gaia [34, 61, 62], RAVE [173], APOGEE [1] and GALAH [57], one way forward to determine the dark matter distribution is to construct equilibrium dynamical models, using Jeans theorem [19, 114]. In principle, one can iterate the fits with different Galactic potentials until the best-fitting potential is found, giving access to the underlying mass distribution of the dark matter.

   Estimates of the shape of the inner halo ($r< 20\,\mathrm{kpc}$) from these measurements remain undetermined ranging from strongly oblate ($c/a \sim 0.4$, [114]) to prolate [19]. Nevertheless, the main caveat is the possible effects that non-axisymmetries in the Galaxy (bar, spiral arms or perturbation from the Magellanic Clouds) might have on the resulting estimates.

3. **Milky Way's mass from hypervelocity stars**

   The trajectories of hypervelocity stars are also sensitive to the shape of the force field and are useful in obtaining an upper limit on the Milky Way's mass [67]. The recent studies performed based on Gaia data suggest that the Milky Way's virial mass is beginning to converge to specific values ($\sim M_{200} = 1.2 - 1.6 \times 10^{12}\,\mathrm{M_\odot}$ [78, 130]), however these values must be cross-checked with the mass estimates obtained from other methods. Also, the shape of the dark matter halo is not usefully constrained by this principal technique.

4. **Globular clusters and dwarf galaxies as tracers**

   Most dynamical methods work by using tracer objects to probe the properties of the whole system, and can only estimate the mass over the distance range for which tracer data are available. Thus different families of tracers provide crucial information at different points depending on the range they cover. This is particularly crucial in the Milky Way where globular clusters tend to probe the inner regions of the halo, while satellite galaxies offer better coverage further out.

   One key problem with the mass estimation via kinematics of tracer objects is that we need to know the total velocity of each tracer, but we are seldom fortunate enough to have all 3 components of motion for a large sample of tracers. Typically, we only have 1D

line-of-sight velocities (v_{los}) and offer virtually no information about the Galactocentric tangential motions of the tracers. With only one componenet of the velocities, the masses we estimate depend very strongly on what assumptions we make for the tangential motions: the well-known *mass-anisotropy degeneracy*.

This, however, now seems to change with the Gaia catalogue in our hands as Gaia has delivered proper motions for ~ 1.3 billion stars in our Galaxy using which tangential motions of these tracer objects can be derived. Recent studies, based on this technique, seemingly suggest that the Milky Way's mass within 20 kpc lie between the values $M(< 20\,\mathrm{kpc}) = 1.91 - 2.2 \times 10^{11}\,\mathrm{M}_\odot$ [148, 191].

5. **Constraints from ΛCDM simulations**

   Dark-matter-only simulations do not take into account the effects of baryons (stars and gases) in the galaxies and therefore are insensitive to the ramifications that might be invoked due to the star formation processes, AGN feedbacks and growth of the stellar disk.

   However, it has been observed that the growth of a galactic baryonic disk modifies the density profile and shape of the halo causing the halos to become more axisymmetric and aligned with the disk (in contrast to the NFW profile that is triaxial in shape), but the minor-to-major axis ratio c/a changes only by a few tenths to c/a~ $0.7 - 0.8$ [36, 44, 74]. The amount of sphericalization depends on the mass of the baryonic component [103]. Given the generic overview of CDM halo properties as seen in the simulations, there are large halo-to-halo variations in most of the properties of the halos and their sub-halo populations. But these regularities are of fundamental importance and prove to be useful for studies of galaxy formation.

1.1.2 Galaxy Formation

The theory of the formation of galaxies is one of the great outstanding problems of astrophysics and is critical in obtaining a full picture of the evolution of the Universe. Yet, we are really just starting to understand this, and the corresponding uncertainties in our measurements remain large.

Broadly, there are two main galaxy formation scenarios. Under the first scenario, given in 1962 by Eggen [47], the metal-poor stars reside in a halo that was created during the rapid collapse of a relatively uniform, isolated protogalactic cloud shortly after it decoupled from the universal expansion. This *smooth monolithic collapse* of the protocloud happened at a timescale of order 10^8 years. Another scenario, that is slightly contradictory to this one that was proposed in 1978, suggested that Milky Way halo is built up over an extended period from independent fragments with masses of $\sim 10^8\,\mathrm{M}_\odot$ through hierarchical merging and accretion of mass systems [169]. This meant that the halo instead formed in a *rapid free-fall collapse*. However, one thing

that both these scenarios advocate for is that it should be possible to understand the formation of our Galaxy through studies based on the stellar abundances and stellar dynamics.

The current paradigm, where the observations argue for a halo that has built up over a long period from infalling debris, is a topic of debate [81].

1.1.2.1 Problem : Galaxy formation and evolution scenario

The stellar halo is arguably the Galactic component that contains the most useful information about the evolutionary history of our Galaxy. This is because the most metal-poor stars, and possibly the oldest ones, in the Galaxy are found here that keep the potential to provide us with a picture of the Milky Way in its early stages of evolution. These halo stars are thus fossils whose chemical abundance and motions contain information of their sites of origin. Also, the dynamical times of the halo objects are longer compared to the age of the galaxy and hence knowledge of the present energy and momenta of individual objects tells us something of the initial dynamic conditions under which they were formed.

Despite its crucial importance, our knowledge of the stellar halo is fragmentary. What we seek is a detailed physical understanding of the sequence of events which led to its formation.

1.1.2.2 Current constraints

The assembly process of a galaxy leaves imprints in the spatial, kinematical, age and chemical distribution of its stars. By studying these properties of the stellar components cumulatively, we should be able to probe the galaxy formation scenarios.

1. **Spatial structure of the halo : star counts, density profile and shape**

   The structure of the stellar halo is intimately linked to how the Galaxy formed [56]. Different galaxy formation scenarios predict different halo shapes, stellar distribution and correlations with properties such as age and metallicity. In the simplest case, the structure of the stellar halo could also give us insights into the structure of the dark matter halo[2].

   In the early 1980s, astronomers began constructing Milky Way galaxy models using star counts [4], based on which they proposed a power density law ($\rho \propto r^n$, n<0) for the Milky Way's stellar halo [76, 133]. Typically RR Lyrae and blue horizontal branch stars (BHBs) are used as tracers of the halo population in order to study the stellar density of the halo because such stars are relatively bright and so they can be observed with modest telescopes upto a distance of 100 kpc from galactic centre. The density profile of the stellar halo is often parametrized in a principal axis cartesian coordinate system as :

[2] However, in ΛCDM cosmological models, it is now clear that the structure of the stellar and dark halo do not necessarily follow one another.

$$\rho(x,y,z) = \rho_o \left(\frac{x^2 + \frac{y^2}{p^2} + \frac{z^2}{q^2} + a^2}{r_o^n} \right) \tag{1.4}$$

where $n(<0)$ is the power-law exponent, and q and p are the minor-to-major and intermediate-to-major axis ratios (in the axisymmetric case, $p = 1$) and a is the scale radius [81]. ρ_o is the stellar halo density at a given radius r_o , which is generally taken to be the solar radius for obvious reasons (and referred to as the local normalization).

Over the years, different studies have led to different stellar halo profiles that yet largely remains unconstrained. These parameters have been measured as $n = -2.3/2.5$ and $q = 0.6/0.5$ (values depending on the local normalization of the halo, [28]) based on the SDSS data [199]; $n = -3.2 \pm 0.3$ and $q = 0.65$ [199]; $n = -3.1 \pm 0.1$, but q varying with radius [186] from RR Lyraes based on QUEST survey.

Wide field surveys such as SDSS [201], Pan-STARRS1 [100], DES [180] have imaged $\sim 10,000 - 30,000\,\mathrm{deg}^2$ of Milky Way sky down to $r_{\mathrm{band}} \sim 22 - 24$, yielding a truly panoramic view of the Galaxy. However, instead of simplifying the picture and providing definitive answers, they have shown that the halo is far more complex than was traditionally envisioned ([12, 99, 141, 171, 198], see Chapter 2). These observations in complimentary to velocity surveys, such as Gaia or RAVE survey, should ultimately reveal the structure of the stellar halo.

2. **Kinematics of the halo**

Velocity profile of the halo, in accompaniment of the spatial distribution, constructs a complete distribution function DF(x,v) of the stellar halo. This is truly of vital importance to understand the formation history of our Galaxy. Moreover, the use of integrals, such as energy and angular momentum, which are conserved under some conditions as the Galaxy evolves, can be a powerful tool for identifying stars with common origin and understanding their merging history [29, 82, 96, 116].

Various studies have been done on the basis of kinematic information in order to understand the kinematical properties of the Milky Way halo. For example, local samples of halo stars show a small amount of prograde rotation $V_\phi \sim 30 - 50\,\mathrm{km\,s^{-1}}$ [25, 112, 134]. In some cases, the velocity ellipsoid is found to be roughly aligned with a cylindrical coordinate system, having dispersions of $(\sigma_R, \sigma_\phi, \sigma_z) = (141 \pm 11, 106 \pm 10, 94 \pm 8)\,\mathrm{km\,s^{-1}}$ [29] and in other cases it was found in cartesian coordinates as $(\sigma_U, \sigma_V, \sigma_W) = (168 \pm 13, 102 \pm 8, 97 \pm 7)\,\mathrm{km\,s^{-1}}$. This, for example, meant that the stellar halo is supported by random motions and is slightly flattened along z axis.

Until now, the catalogues that possessed relatively accurate 3D kinematics had paucity of halo stars (most of these catalogues were constructed using Hipparcos's proper motions

and radial velocities from other surveys sampling stars that typically lied within few kpc around the Sun). This impariment to a greater extent is now resolved with latest velocity surveys such as Gaia, APOGEE, RAVE and GALAH.

3. **Substructure-ness**

   One of the most fundamental prediction of the ΛCDM cosmological model is that galaxies grow via mergers where a stellar halo is easily built up via the superposition of disrupted satellites [21, 22, 96, 177] (see left panel of Figure 1.4). Therefore, perhaps the most direct way of testing this paradigm is by quantifying the amount of mergers that galaxies have experienced over their lifetime. This implies finding the traces of those merger events as mergers are expected to have left large amounts of debris in the present-day components of galaxies.

   This prediction became even stronger once the deeper astronomical surveys started to reveal the substructure-ness in the Milky Way halo and various studies were able to discover the evidences of disrupted dwarf galaxies and globular clusters [6, 82, 86, 199], conforming the hierarchical cosmologies (see right panels of Figure 1.4).

   These results have further boosted the search for substructure in the halo of our Galaxy in recent years. If ΛCDM cosmological model is indeed the right framework, then one expects to find more of these substructures in the volume of the Milky Way halo. This again should become possible with the Gaia data. However, verified by both theoretical models and observations, such a scenario invokes challenging problem of quantification of the amount of stars in the Milky Way halo which are a result of these minor and major merging events [6, 21].

4. **Ages and chemical abundances of halo stars**

   Element abundances of metal-poor stars, along with their age estimates [55], is useful in constraining the formation history of our Galaxy. Currently, the local halo metallicity distribution peaks at a value [Fe/H] ~ -1.6 dex, and extends well below [Fe/H] ~ -3 dex [163]. Based on SDSS data, the idea that the halo may be described by two broadly overlapping components was revived [26]. It was estimated that the inner halo peaks at [Fe/H] ~ -1.6 dex, is flattened and slightly prograde, while the outer halo would peak around [Fe/H] ~ -2.2 dex, is rounder and in net retrograde rotation.

   The current high-resolution spectroscopic surveys, such as APOGEE [1], Gaia-ESO [66], RAVE [173] and the GALAH survey [57], complement each other in their scientific objectives, target selection, and spectral coverage. Together, they will obtain high-resolution spectra for over a million stars - an unprecedented volume of spectral data in astronomy. With these data, the chemical evolution of our Galaxy can be unravelled. Moreover, it may be possible to chemically tag individual stars as remnants of individual proto-galaxy

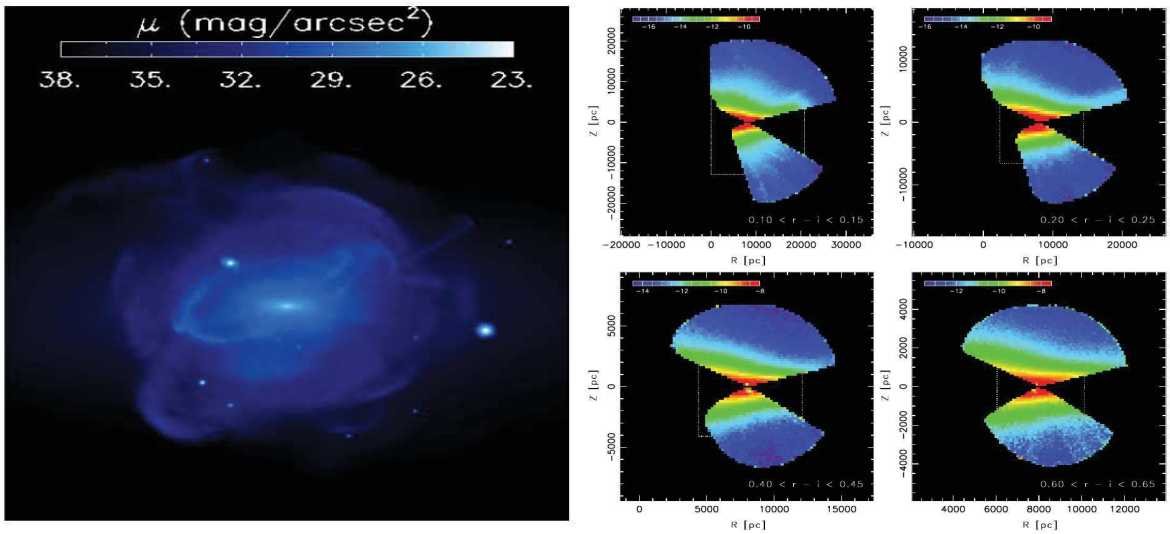

Figure 1.4: Substructure-ness in the Milky Way galaxy. *Left panel* : A simulated stellar halo built up from accreted satellites [21]. The color scale indicates surface brightness. *Right panels* : Stellar number density as a function of (R, z) for different $r-i$ bins using SDSS photometric parallaxes (the distance scale greatly varies from panel to panel) [99]. Note the large overdensities in different regions of the sky.

fragments. Along with Gaia's position, distances and proper motion, this would allow the reconstruction of merger history of the Milky Way in extremely fine detail. However, the crux of these interpretations will rely on the homogeneity of their spectral analyses. To infer minute chemical differences throughout the Galaxy, a homogenous analysis is essential.

1.2 Killing two birds with Stellar Streams

By all means, our own Galaxy is the best laboratory to ask and address these Galactic archaeological problems. Milky Way is a benchmark for understanding the disk galaxies, providing a unique opportunity to measure the shape of the dark matter halo, the mass of the Galaxy and its formation and evolutionary history. This is because Milky Way is the only Galaxy for which we will always be equipped with the maximum stellar information in terms of the phase-space distribution of stars and their chemistry [35].

Now coming back to the same point from where we started this Chapter, the significance of stellar streams lie in their promise to address many of the above mentioned problems. *Thats right*. And it is simply this realisation because of which streams have recently gained tremendous popularity in the astrophysical community. As described in Chapter 2, stellar streams come across as extremely useful Galactic archaeological tools in estimating the mass of the Milky Way, in probing the underlying dark matter density distribution and the gravitational potential,

in studying the merging and the pre-merging history of our Galaxy, in quantification of the substructure-ness in the halo, and also in reconstructing the DF(x,v) of the halo accretions and possibly of the halo itself.

CHAPTER 2

STELLAR STREAMS IN THE MILKY WAY HALO

When you catch a glimpse of a potential in something, that is when passion is born- **Zig Ziglar**

Abstract

The Chapter aims at giving a brief review on stellar stream structures, their physical properties, their conventional modes of detection and their importance in probing the dark matter distribution and in the studies of the formation and evolution of the Galactic halo.

2.1 Stellar streams

Figure 2.1 presents the Pal 5 stream structure [143]. This ~ 15° long stellar arc is a consequence of the tidal disruption of the Pal 5 globular cluster [76], that can be seen to be sitting at [R.A., Dec] = [229.018°, −0.124°] along the arc, and lies at a distance of ~ 23.5 kpc from the Sun [90]. Pal 5 stream is a typical example of the class of stellar structures that fall under the category of *tidal stellar streams*.

2.1.1 Mechanism of disruption

Stellar streams are stellar structures that are formed via tidal disruption of star clusters or satellite galaxies as they orbit around the host galaxy. Satellite bodies that come too close to the host's centre suffer tidal disruption - the differential gravitational force between one side of the

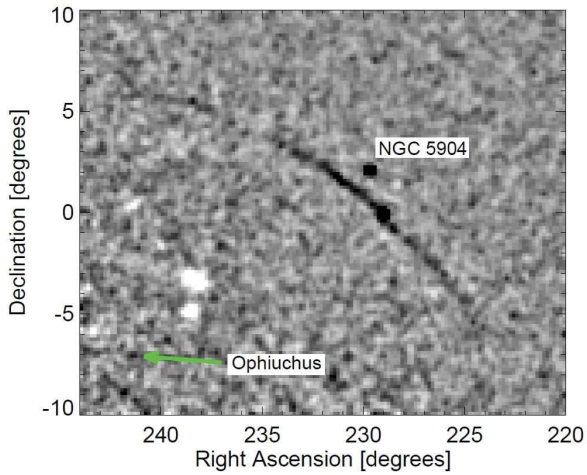

Figure 2.1: Close-up view of the area around Pal 5 stream [12] obtained via Match Filtering technique to the Pan-STARRS1 dataset.

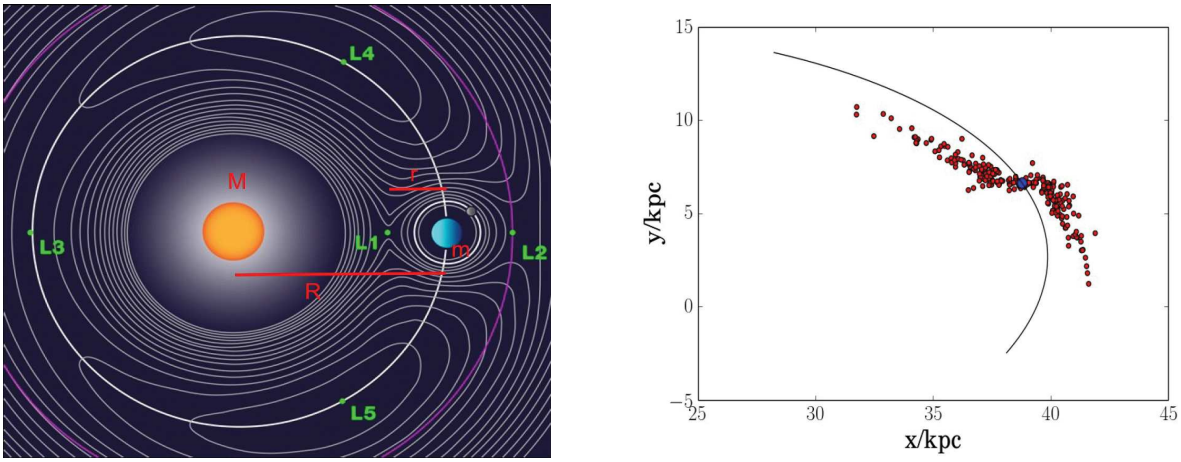

Figure 2.2: Disruption mechanism of a star cluster into stream. *Left panel* : Lagrange points in a 2 body system, where $m << M$, r_t is the tidal radius of the body 'm' and R is the separation distance. The lagrange points are labelled as $L1, L2, L3, L4, L5$. *Right panel* : A snapshot of an N-body simulation of stream where stars can be seen escaping the potential well of the cluster from $L1$ and $L2$ points as the cluster orbits around the host system [18].

star system and the other - that rips out some of the stars from the progenitor system which then begin to orbit the host galaxy along with their progenitor. Tidal forces on stars in dwarf galaxies and star clusters pull them out of their progenitor from Lagrange points $L1$ and $L2$ (see Figure 2.2). The Lagrangian points are positions in an orbital configuration of two large bodies (say M and m, where $M >> m$, Figure 2.2) where a small test particle can maintain its position fixed relative to the two large bodies. These L points mark positions where the combined gravitational pull of the two masses provides precisely the centripetal force required to orbit the test particle with them. This means that this test particle placed at either of these L points will have the same time period as that of the mass m. There are five such points in a two body system, labeled from $L1-L5$ in Figure 2.2, and all of them lie in the orbital plane of the two large bodies. Our focus for current discussion is only $L1$ and $L2$ - points from where the stars escape the progenitor cluster.

If M and m were stationary with respect to each other separated by the distance R, the L point would be a position where gravity between the two bodies are balanced. Such a point would lie somewhere between the masses M and m and would require

$$\frac{GM}{(R-r_t)^2} = \frac{Gm}{r_t^2}, \tag{2.1}$$

r_t being the $L1$ point. Knowing the masses M and m and the separation distance R would easily allow one to calculate r_t. However, situation becomes complicated when one of the bodies m is orbiting around the other mass M, because of the centrifugal force that comes into the picture. The balancing equation then gets additional terms that takes into account the centrifugal force as well. The centripetal force on the particle, in this case, would be equal to the net gravitational force coming due to both the masses M and m,

$$\frac{m_p v_p^2}{r_t} = \frac{Gm_pM}{(R-r_t)^2} - \frac{Gm_pm}{r_t^2} \tag{2.2}$$

The time period for this particle would be

$$T = \frac{2\pi(R-r_t)}{v_p}, \tag{2.3}$$

substituting above equation back into the main equation gives

$$\frac{4\pi^2(R-r_t)^2}{T^2 r_t} = \frac{GM}{(R-r_t)^2} - \frac{Gm}{r_t^2} \tag{2.4}$$

Now since $v_m = 2\pi R/T$ but also $v_m^2 = GM/R$, substituting v_m in LHS term gives

$$\frac{GM(1-\frac{r_t}{R})^2}{Rr_t} = \frac{GM}{(R-r_t)^2} - \frac{Gm}{r_t^2} \tag{2.5}$$

and now doing a binomial expansion upto first order (as $r << R$) on both the sides gives

$$\frac{GM}{Rr_t} + \frac{2GMr_t}{R^2 r_t} = \frac{Gm}{R^2} + \frac{2GMr_t}{R^3} - \frac{Gm}{r_t^2} \tag{2.6}$$

solving which gives

$$r_t = \left(\frac{m}{3M}\right)^{1/3} R \tag{2.7}$$

Considering mass M to be the mass of the Galaxy within the separation distance R and m to be the mass of the star cluster, then r_t basically sets the *tidal radius* of the progenitor cluster. This means, that the stellar particles lying at a distance greater than this r_t value lie beyond the trap of the potential well of the cluster and will be stripped off. Consider Milky Way's mass in the inner 20 kpc to be $M_{MW}(< 20\,\text{kpc}) \sim 2 \times 10^{11}\,\text{M}_\odot$ [119], mass of some progenitor cluster situated at $R = 20\,\text{kpc}$ to be $m = 6 \times 10^5\,\text{M}_\odot$, then this sets $r_t = 0.2\,\text{kpc}$.

Note that r_t is not a constant for any given cluster. The value of $R(\equiv R(t))$ is a function of time as it changes with the orbital trajectory of the cluster (unless the cluster system is on a circular orbit). Further, $M \equiv M(R)$, also evolves according to the progenitor's orbit. Also, $m \equiv m(t)$ - because as the stars strip from the cluster, cluster's mass decreases over time.

The stellar particles that are tidally stripped from the outer $L2$ point of the progenitor cluster (point farther from the galactic centre) receive higher energy values and higher angular momenta and form the *trailing arm* of the stream in comparison to the particles that are stripped from $L1$ point (point closer from the galactic centre) that form the *leading arm* of the stream. At this point when the stars are no longer trapped by the gravity of the star cluster, they begin to orbit the Milky Way however maintaining a similar orbit as that of the progenitor cluster. As the stars escaping the potential well of the cluster get launched into orbits with slightly lower and higher energies, their orbits do not exactly align along the orbit of the progenitor cluster, and therefore the leading and trailing arms of the stream do not delineate an orbit as that of the progenitor (see right panel of Figure 2.2). As the orbital period of Milky Way's satellites are ~ 1 Gyr [96], the timescale over which tidal streams evolve is also Gyrs.

2.1.2 Physical properties of stellar streams

Past couple of decades saw a spate of stream discoveries in the halo of the Milky Way [71]. The structural, kinematical and chemical properties of many of these streams have been studied and now we have a general idea about what type of halo substructures qualify to be stellar streams.

1. **Structural characteristic**

   Stellar streams are orbital structures and therefore they appear as elongated arc-like features in the configuration space. As described previously, the elongation is a consequence of the tidal stripping of the progenitor cluster that forms the tidal arms. But different streams can have different physical lengths. The lengths of the tidal tails depend on the

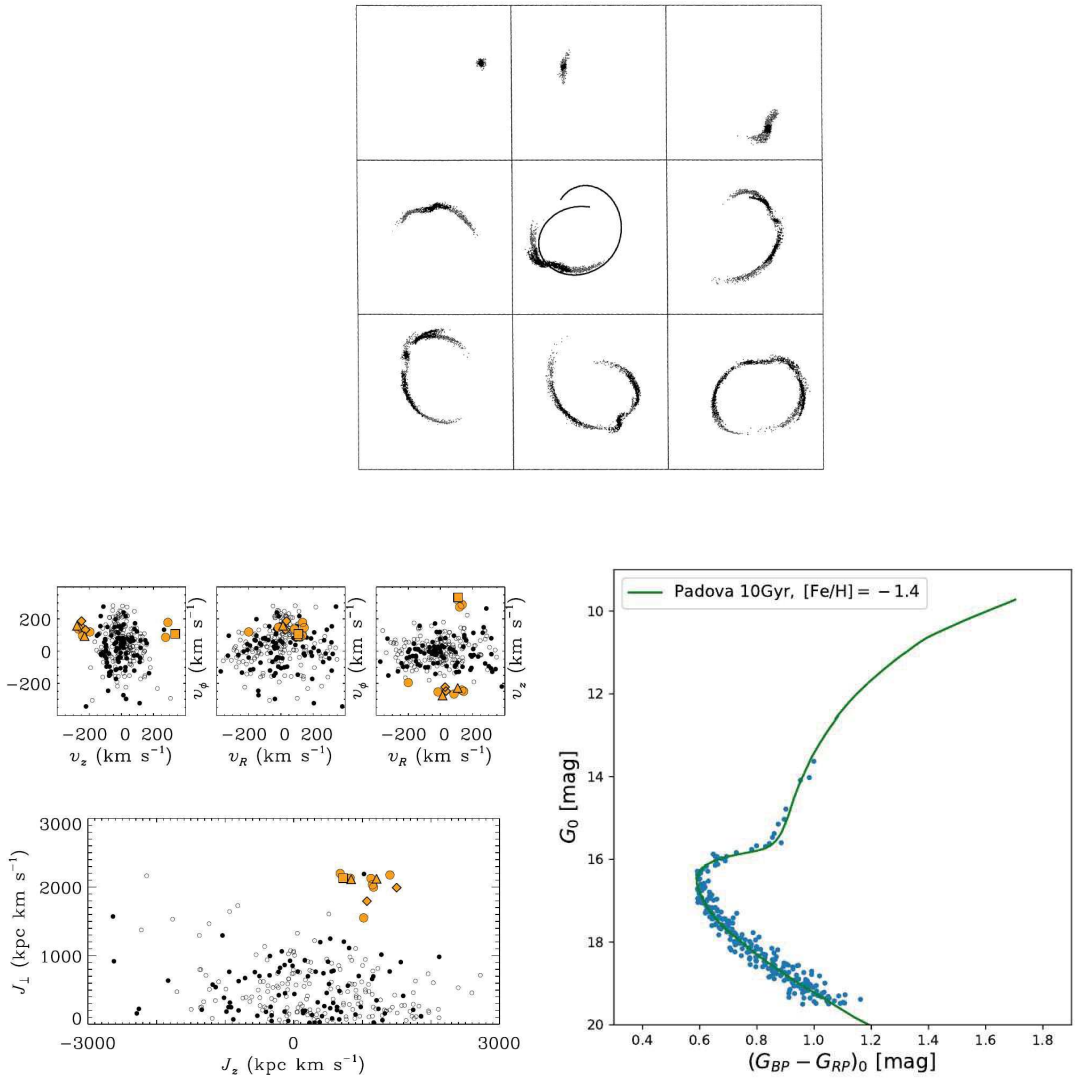

Figure 2.3: Physical properties of stellar streams. *Top panel* : The simulated evolution of a dwarf satellite as it disrupts going around the Milky Way [95]. The boxes are 175 kpc on a side. The frames are equally spaced over 4.5 Gyrs. The orbit of the progenitor cluster is overlaid in solid curve in the middle box. The Figure shows that streams are elongated in the configuration space. Notice that the leading and the trailing tails of the stream do not delineate along the orbit of the progenitor system. *Bottom left panel* : The discovery of the Helmi stream [82] based on the analysis of the kinematics of the stars from the Hipparcos mission. The upper panels show the kinematics of the stars and the lower panel shows the distribution in angular momentum space ($J \equiv L$ in their notation). Since streams are orbital structures that have long dynamical times, they maintain coherence in the velocity space for several Gyrs. *Bottom right panel* : The color-magnitude diagram of the recently discovered Phlegethon stream [91]. Since stars in the tidal tails of a stream were once a member of the progenitor cluster, cummulatively they follow the same isochrone trend and chemical properties as that of their progenitor cluster.

mass and the scale radius of the progenitor system (that determines how easy it will be to strip the stars), their orbital path around the Milky Way (since the tidal forces on a cluster are stronger closer to galactic centre when the system is at its pericentric passage than when it is at its apocentre), and the time duration the satellite/cluster had been orbiting the Milky Way (more time duration allows stripping of more number of stars and hence longer are the tidal tails). See Figure 2.3 for descriptive understanding.

Also, observed tidal streams could have a known progenitor which still survives, despite the fact that some of its stars have been removed (for example, the Pal 5 stream [143], the Eridanus and Palomar 15 streams [135]). A stream might also have no associated progenitor either because the progenitor from which it formed has been completely disrupted into tidal arms, or because it has yet to be discovered (for example, it is believed that the progenitor of GD-1, if it still survived, might be lying behind the Galactic disk).

2. **Velocity space coherence**

   Since stellar streams are orbit-like structures, the member stars are expected to remain coherent in the configuration as well as in the velocity space for several Gyrs. Therefore, member stars of a stream are often found with similar velocity values and they tend to occupy a tiny volume in the phase-space (see Figure 2.3). If one assumes an axisymmetric potential for the Milky Way galaxy (which is a good zeroth order approximation, see [106, 107, 119]), where energy E and z-component of angular momentum L_z are conserved, then due to its orbital property the entire stream would appear as a *dot* in the $E - L_z$ space.

3. **Photometric description**

   Star clusters have for long been known to follow a characteristic *color-magnitude diagram (CMD)* curve [109]. This isochrone curve depends on the Age and metallicty ([Fe/H]) of the stellar population. The stars that are in the tidal tails of the cluster, that were once members of the progenitor cluster, are also expected to follow the same isochrone trend (see Figure 2.3) which is another identifiable characteristic of stellar streams.

It is these physical properties of stellar streams that make them excellent tools in addressing various current problems of Galactic archaeology.

2.2 Significance of streams in Galactic archaeological studies

Stellar streams are remnants of the satellite galaxies or star clusters that were accreted by the Milky Way. Therefore, they hold important place in galactic formation and evolution. Also, since these structures orbit in the underlying potential of the galaxy, their orbital properties tend to be sensitive to the gravitational potential and the mass distribution of the host galaxy.

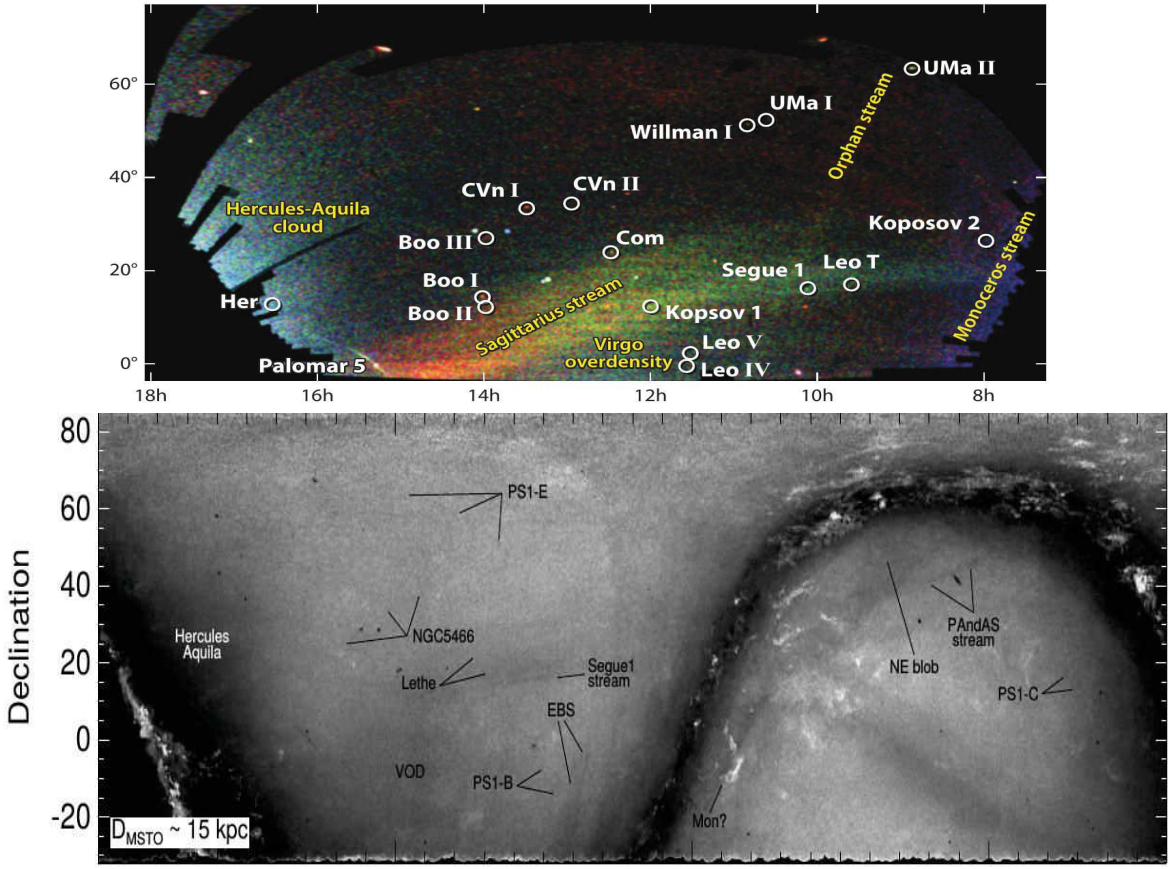

Figure 2.4: Substructure-ness in the Milky Way halo. *Top panel* : "Field of Streams" stellar map created using the SDSS data [92]. The circle represent Milky Way companions, most of which are dwarf galaxies and globular clusters. Five substructures are shown in yellow, including Sagittarius stream. *Bottom panel* : Matched-filtered stellar density maps of the whole Pan-STARRS1 footprint at a distance of $D_{MSTO} \sim 15\,\text{kpc}$ [12]. The darker areas indicate higher surface densities; a few black patches are due to missing data. The main substructures are labeled.

1. **Galaxy formation : origin of the stellar halo and substructure-ness**

   As explained in Chapter 1, simulations based on ΛCDM cosmogony find that the dark matter halos are not smooth and vast numbers of self-bound susbtructures ("sub-halos") swarm within them [65, 131]. This supports the idea that a large fraction of the stellar halo formed through the accretion and disruption of low mass star groups (satellites and globular clusters) onto the host galaxy. *Substructure-ness is not a sufficient but a necessary condition for hierarchical structure formation framework to be a valid theory.* So if we go by this framework, the halo of the Milky Way should have been made of all of these accreted bodies. This means that if we could establish (observationally) that in fact halo is a playground of accreted structures, then this would greatly confirm the hierarchical

framework of structure galaxy formation.

In the past, SDSS data has shown that the substructure comprises 30% of the inner halo and increases with larger galactocentric radii, showing that accretion has occured throughout the history [6] and that accretion was in fact the dominant mechanism to build up the stellar halo. But such a global quantification would also be affected by the total number of streams in the halo. These streams may individually contribute insignificantly to the total accreted halo fraction, but the summation over all the stream structures might be non-negligible.

Various wide field astrophysical surveys have revealed a wealth of stellar streams in the Milky Way halo [10–12, 70, 72, 73, 85, 93, 105, 124, 136, 143, 171, 196], that display different morphologies (see Figure 2.4) and contribute to the substructure-ness of the stellar halo. Not only do these tidally disrupted streams confirm and advocate for a hierarchical merging scenario of the Galactic stellar halo, but their orbits can be retro-engineered in order to reconstruct the pre-merging history of our Galaxy to understand its origin and its formation history.

2. **DF(x,v) of the halo substructures using conserved quantities**

   We lack the knowledge about the complete DF(x,v) for our stellar halo that is of extreme importance in order to understand its origin and evolution, and in probing the underlying gravitational potential of the halo. DF(x,v) plays crucial role in associating the accreted stars to a single progenitor system (as accreted stars might appear unassociated in the configuration space, but are strongly correlated in the 6D phases-space or (E, L_z) space). Once the members of the associated groups are confirmed, their origin and accretion history could then be verified.

   Knowledge of the complete phase-space information of the halo stars would not come even with the Gaia data[1]. However, since streams are orbital structures, their orbits can be used for creating complete 6D phase-space maps of the stream stars even in the cases where one or more phase-space information is missing [122]. Therefore, with the quality of the data that Gaia provides, it is indeed possible to obtain a reasonably well estimated complete DF(x,v) of the stars of the Milky Way that are associated with streams.

3. **Constraining the dark matter mass distribution of the Milky Way**

   The mass density profile and the spatial distribution of the dark matter halo around the Milky Way galaxy are of great astrophysical and cosmological importance, and until now remains poorly constrained. Access to good potential model is needed also to understand the dynamical evolution of our Galaxy.

[1] Although Gaia provides 5D astrometric solutions (2D positions, 2D proper motions and paralalxes) for all the observed stars, but it delivers radial velocities for only brighter stars for which $G_{Gaia} < 12$.

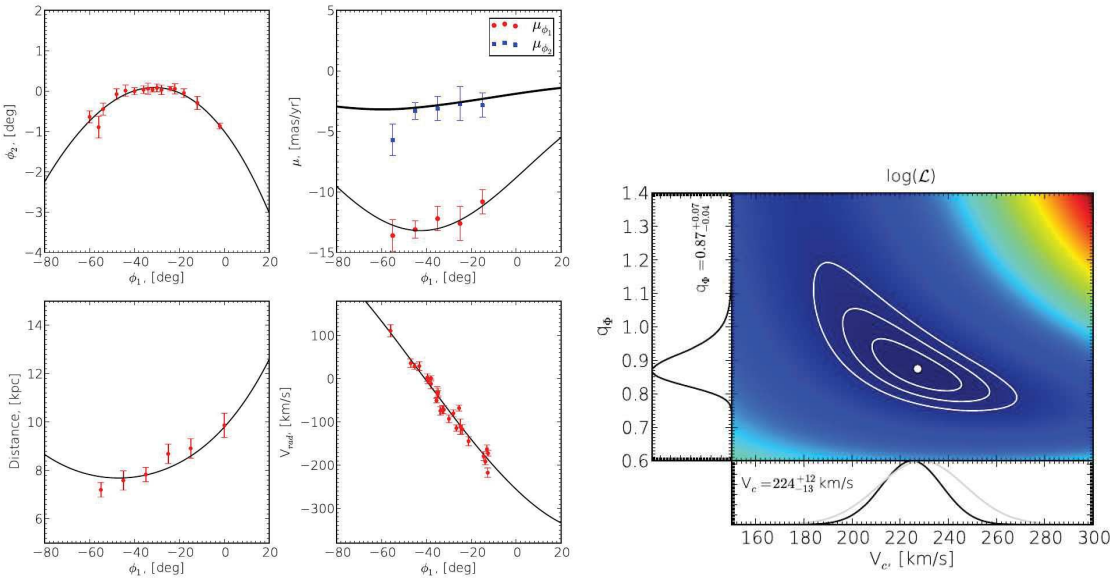

Figure 2.5: Constraining Milky Way potential via orbit-fitting of GD-1 stream [106]. *Left panels* : The data-to-model comparison for the best-fit orbit through the GD-1 stream, where the orbit is shown with black curves while the data is represented by colored points accompanied with the associated error bars. *Right panel* : The contours of the log-likelihood space of the potential's parameters $(V_{\rm circ}(R_\odot), q_\Phi)$ obtained from the corresponding analysis.

As pointed out in Chapter 1, various methods are often employed to constrain the mass distribution of the Milky Way galaxy. These include analyses based on the rotation curve of the Galaxy [175], Jeans analyses that assume dynamical equilibrium of some tracer population to constrain the gravitational force field [19, 42, 114, 150], orbital analyses of satellites [59, 192], and distribution function analyses [148]. However, many recent studies have turned to using stellar streams as dynamical probes [17, 79, 85, 106, 107, 111, 119] (see Figure 2.5). This is because orbits in a gravitational potential are powerful tracers of the matter distribution. Tidal streams in the halo have the added advantage of being far enough from the bright galactic components that the fitting is unaffected by small errors in the disk and bulge models [185].

Most attempts of inferring the Milky Way's potential through stream's dynamical analysis, to date, have focused on the Sagittarius stream [80, 85, 111] due to its length and the quality of available data. Recently, some other streams have also been employed for dynamical analysis [17, 106, 107, 140]. However, results from stream analysis, altogether, have consistently defied attempts to build a unified potential model [80, 85, 97, 110, 111]. Analyses based on Sagittarius stream favour a mildly triaxial potential with potential flattening $(c/a)_\Phi \sim 0.72$ in the disc plane and $(b/a)_\Phi \sim 0.99$ aligned with the symmetry axis

of the Galactic disc [111]. However, such a model is dynamically unstable [37], suggesting unmodelled stream complexity or incomplete data. A very recent study based on the GD-1 and the Pal 5 stream estimated the overall potential flattening as $(c/a)_\Phi = 0.95 \pm 0.04$ at the location of GD–1 ($[R,Z] \approx [12.5, 6.7]$kpc) and 0.94 ± 0.05 at the position of Pal 5 ($[R,Z] \approx [8.4, 16.8]$kpc) suggesting a highly spherical halo [17]. However, this estimate is in tension with the numerical simulations that suggest a strongly triaxial halo (see Chapter 1). It is expected that the quality of the velocity measurements that Gaia has now provided should improve our resulting estimates.

4. **Studying lumpiness in dark matter distribution from stream gaps**

   ΛCDM models predict two orders of magnitude more dark matter halos (lumps with masses $> 10^7\,M_\odot$) than satellites observed around the Milky Way [104, 132]. Solutions to this problem include self-interacting dark matter [176], truncated power spectra [102] and the restriction of gas accretion to the lowest mass dark matter halos before the epoch of reionization [22]. The first two solutions would get rid of the smallest dark matter halos entirely, while the latter would predict that only one percent of the satellite halos actually contain stars, and the others only contain dark matter - resulting into *dark matter sub-halos*.

   Density variations along the tidal tails of stellar streams could very well be induced due to its interaction with a perturber, such as sub-halos. This provides observational means to infer the presence of the dark matter sub-halos by investigating the possible source of perturbation. The effect of the interaction of a stream with a sub-halo would be reflected in the dynamics of the ejection of stars from the progenitor or the tidal arms, and compression and expansion of a stream around an orbit (see Figure 2.6). These signatures can be used to guide us towards the physical properties of the sub-halo such as its mass and density profile [49]. Further, the quantitative analysis of the number of gaps in all the streams in the Milky Way can help in creating a global consensus of the number of dark matter sub-halos streaming the halo [24]. Stellar streams lying outer in the Galactic halo are much more trustworthy for such analysis because closely lying streams can get response from the interaction with the Galactic disk, bar and spiral arms [121, 145].

5. **Measuring Sun's Galactic velocity with stellar streams**

   Not only streams are useful in constraining the parameters of the gravitational potential (for e.g., the potential flattening q_Φ, or the mass), but also in constraining the fundamental parameters of the Galaxy. Exploitation of the geometry of the stream structures can be used in order to gauge the Sun's galactic velocity ($\mathbf{V}_\odot$) [118]. This idea, that employs a simplistic procedure, is detailed in Chapter 7.

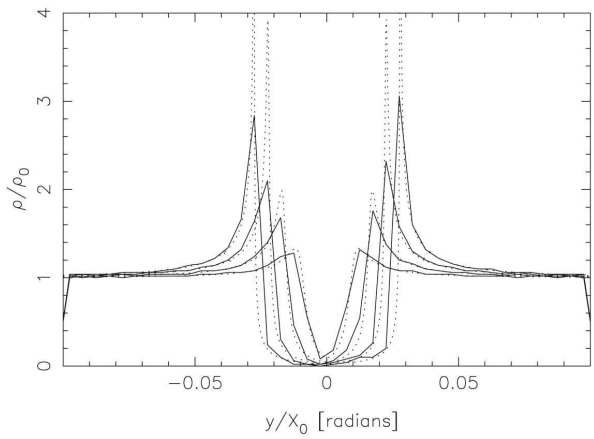

Figure 2.6: Figure illustrating development of a density gap in a cold stream after an encounter with a $10^6 M_\odot$ sub-halo [24]. The Y axis shows the relative density of stars against the angular coordinate on the X axis. The plot is shown at dimensionless times 20, 40, 60, and 80, where the rotation period is 2π. The dotted lines show the predicted relation at different times.

In contrast to the analysis based on the other tracer objects (listed in Chapter 1), dynamical analysis of streams appear to put relatively tight constraints on the matter distribution of our Galaxy and other relevant galactic parameters. However, the solutions yet do not converge at definite values. The disparities have persisted in part due to the lack of good quality tangential velocity measurements and distance estimates of halo tracer stars. This situation now looks set to change with the excellent Gaia data along with various other velocity surveys such as APOGEE [1], GALAH [57] and RAVE [173].

But still, in order to significantly improve our estimates, more stream detections are required both in the inner and the outer halo of the galaxy in order to obtain a global solution on the Galactic mass distribution that is then valid upto to outer galatic radii. More stream detections are also needed in order to quantify the number of halo stars that are a result of the accretion events.

2.3 Conventional techniques to detect stellar streams

There exist some effective stream detection methods that have been successful in detecting the known Milky Way streams. These techniques essentially exploit the same physical properties of the stream structures that were discussed in Section 2.1.2. Discussed below are some of these conventional stream detection techniques (also summarised in Figure 2.7) and their shortcomings.

1. **Detection of stream as an overdensity in the halo**

   The most straightforward technique to identify tidal streams, or any halo substructure for that matter, is to determine 3D positions of the halo stars and then look for localised

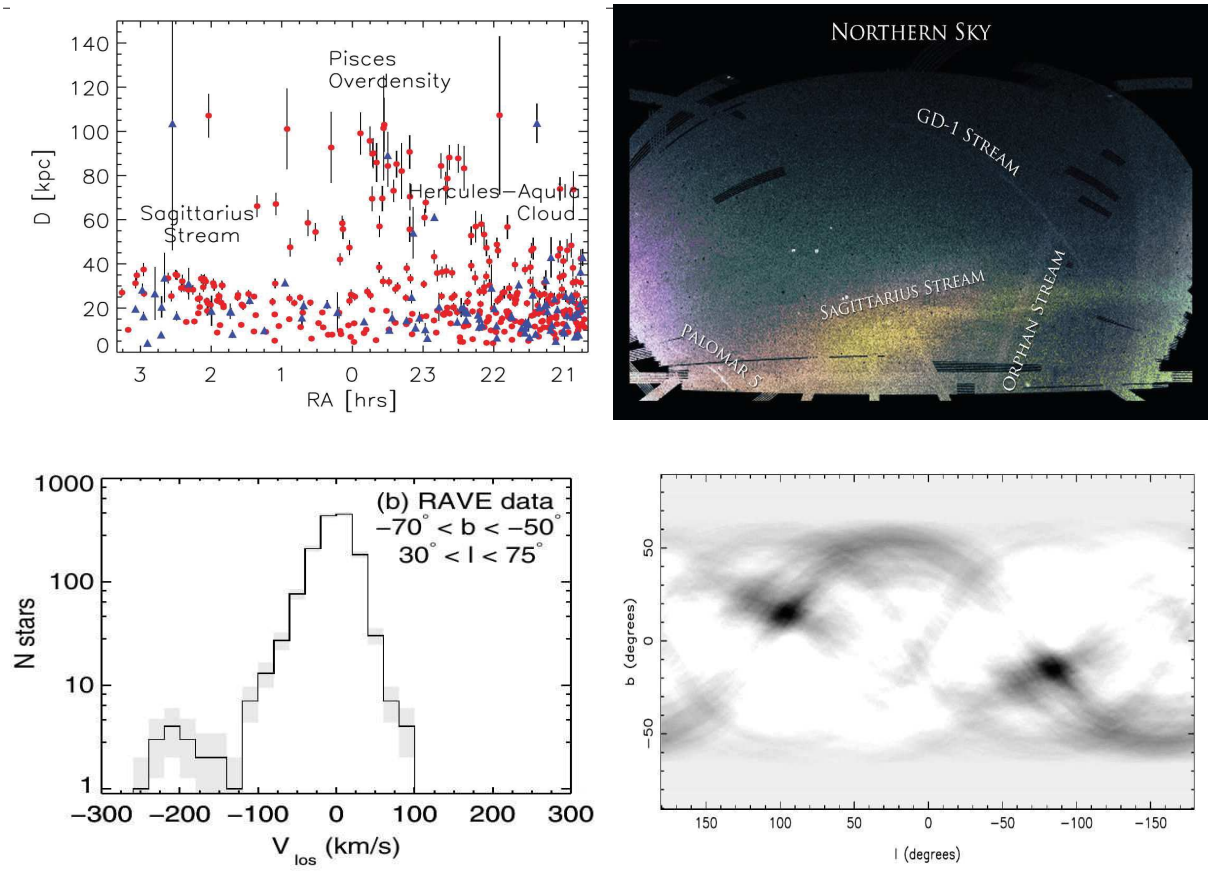

Figure 2.7: Conventional techniques to detect stellar streams. *Top left* : The spatial distribution of the ab-type (red circles) and the c-type (blue triangles) RR Lyraes [190]. *Top right* : The matched filter density map of the northern footprint of the SDSS survey [10]. Many stream structures are visible and are labelled. *Bottom left* : Overdensity of stars in V_{los} in RAVE data identified as the Aquarius stream [197] (see the region $-250 < V_{los} < -150\,\mathrm{km\,s^{-1}}$). *Bottom right* : The working of the pole-count procedure shown by revealing the location of the pole ($\ell = 95°, b = 13°$) of the orbit of the Sagittarius dwarf galaxy stream, implying detection of the stream [88].

overdensities. As this method requires the distance measurements, the stars with known absolute magnitudes (standard candles - RR Lyraes, Blue Horizontal Branch stars (BHBs) in general) must be selected (see Figure 2.7). The Sagittarius stream [7, 8, 84, 86], the Monoceros ring [142], the Pisces overdensity [190] were all discovered and identified using this technique.

However, note that such a technique would work only for the detection of very high contrast streams that are high enough in number density to stand out significantly from the contaminating background population. Streams that are remnants of low mass progenitors would be hard to nail down using such a simplistic procedure.

2. **Matched filtering technique**

The matched filter technique [5, 156] incorporates colour-magnitude weighting of stars to find structures that belong to a specific Single Stellar Population (SSP) model. It is this technique that must be thanked for rendering detections of most of the streams in the Milky Way halo. The Pal 5 stream [143], GD-1 [72], Orphan [69], Lethe, Cocytos, and Styx [70], the Eridanus and Palomar 15 streams [136], PS1-A,PS1-B, PS1-C, PS1-D, PS1-E and Ophiuchus streams [11, 12], Indus and Jhelum streams [171], and many others were all found using the matched filtering technique.

Although, the number of streams detections justify the advantage of this method, the shortcoming of this procedure is that it does not incorporate kinematics of the stars. This means that such a procedure could also have tendency of rendering some false positives. Also, its performance is expected to drop significantly if the structure possesses a significant distance gradient.

3. **Detection of co-moving groups of stars**

   Several halo substructures were initially identified as groups of stars of similar type (e.g. RR Lyrae, Blue Horizontal Branch Stars) that are contained within a small phase-space volume possessing similar velocities. Several streams in the Milky Way have been detected this way (for e.g., the Aquarius stream [197], the Arcturus structure [2] and the Virgo stream [46]). See, for example, the bottom left panel of Figure 2.7 that shows the detection of the Aquarius co-moving group in the line-of-sight velocity space based on RAVE survey.

4. **Pole counts**

   The Pole Count technique [96] works by looking for overdensity of stars along the great circular paths of the Milky Way galaxy and then assigning the corresponding weight to the associated pole value. Therefore, this technique works well for identifying substructures that are on great circle paths around the Milky Way and are also of high contrast. For example, it was useful in reproducing the Sagittarius stream [88]. This method can be further improved by supplying the algorithm the available kinematic information [125].

   Nevertheless, the method is expected to reveal only those streams that lie almost along great circular paths on the sky, and the streams on rather complex orbits can go undetected.

2.4 Sate-of-the-art tool to analyse ESA/Gaia data for streams

Figure 2.8 summarises all the Milky Way stellar streams that were prior to Gaia DR2. There are >40 streams that are visible on this map that were a result of the application of the detection mechanisms that were mentioned before.

Prior to Gaia DR2, the kinematics of majority of these streams were unknown. Even with Gaia in our hands, velocities of many of these structures might remain unaccessible due to the shallow-ness of Gaia's coverage ($G_{\mathrm{Gaia\,limit}} \sim 20.5$). Therefore, along with estimating the

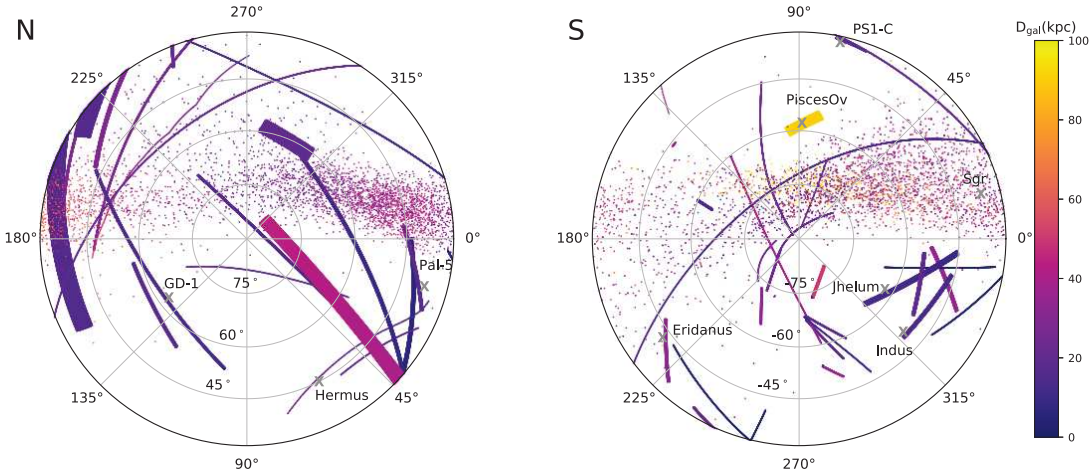

Figure 2.8: Schematic stellar stream map of the Milky Way sky prior to Gaia DR2. Here is shown the Milky Way stellar stream map (minus some stellar clouds) that was created using the GALSTREAMS package [125], transformed into polar Zenith Equal Area projections [122]. The colour represents the Galacto-centric distances to these structures. The left and right panels show, respectively, the projection from the North and South Galactic poles. The names of a few streams are labelled to help the reader's orientation in this coordinate system. Galactic longitude increases clockwise in the north panel and counter-clockwise in the south panel, while Galactic latitude changes radially as shown.

kinematics of the known streams that can be accessed in the Gaia data (that can then be used for various Galactic archaeological studies), more stream detections are needed for which we are then equipped with the complete phase-space information.

Therefore, in light of the revolutionary dataset that Gaia was to deliver, construction of a stream detection algorithm was desired that is able to use all the prior knowledge of stellar streams and as much as possible information from Gaia data in order to maximise the detection efficiency. For this, a state-of-the-art tool was built as a part of this thesis that was used to analyse Gaia for the detection of the stellar streams in the Milky Way halo. This algorithm was named - the STREAMFINDER.

CHAPTER 3

STREAMFINDER - A NEW ALGORITHM FOR DETECTING STELLAR STREAMS

The beginning is the most important part of the work- **Plato**

Related paper : **STREAMFINDER I - A new algorithm for detecting Stellar Streams**, 2018, Khyati Malhan & Rodrigo Ibata, published in *MNRAS* (ADS entry)

Abstract

A new powerful algorithm was designed to detect stellar streams in an automated and systematic way. The STREAMFINDER algorithm is well suited for finding dynamically cold and thin stream structures that may lie along any simple or complex orbits in Galactic stellar surveys containing any combination of positional and kinematic information. This Chapter introduces the STREAMFINDER algorithm, lays out the ideas behind it, explains the methodology that it adapts to detect streams and details its workings by showing the results that were obtained by running it on a suite of simulations of mock Galactic survey data of similar quality to that expected from the ESA/Gaia end-of-mission survey. The results that were obtained showed that the algorithm is capable of detecting even ultra-faint stream features lying well below previous detection limits. Numerical tests revealed that STREAMFINDER should be able to detect distant halo stream structures $> 10°$ long containing as few as ~ 15 members ($\Sigma_G \sim 33.6\,\mathrm{mag\,arcsec^{-2}}$) in the final Gaia dataset.

3.1 STREAMFINDER

With ESA/Gaia data [60–63] in sight, development of a generic stream finding algorithm was desired that superseded the previously existing stream detecting algorithms in terms of performances, in its capability of handling heterogenous datasets containing any useful combination of positions and kinematics and the sort of surveys that have partial sky coverage and incomplete information on some parameters, so as to make the most of the available surveys. Since the most massive streams in the Milky Way have probably already been discovered, the STREAMFINDER algorithm was primarily designed to detect narrow low-mass tidal streams, that are also ideal for constraining the Galactic potential and for probing the Galactic dark matter distribution [115].

3.1.1 Stream Detection Concept

Consider an ideal scenario where we have a segment of an orbit (see Figure 3.1a). The red dots represent the positions of the stars (members of a hypothetical stream that perfectly delineates this orbit) along their orbital structure in 6D phase-space. Suppose we have access to perfect 6D position and velocity values ($\mathbf{x}$, $\mathbf{v}$) for all these stream stars and that we also know the underlying gravitational potential. Then, if one integrates a *trial orbit* (blue-dashed curve) using the given 6D phase-space value ($\mathbf{x_i}$, $\mathbf{v_i}$) of one of these stream stars, then this trial orbit would sew through the remaining stars in the 6D phase-space, revealing the entire stream structure.

In reality, streams do not delineate perfect orbits (Figure 3.1b). Stars in a tidal stream have slightly different (E, L_z) values, and therefore lie along slightly different orbits [52]. The slight differences in energies and orbital trajectories of the stream stars as they are lost from their progenitor lead to a finite structural stream width in real space and velocity dispersion in velocity space.

The prescribed stream detecting method made use of the realisation that the members of a stream can be contained within a 6D hyper-dimensional tube (or *hypertube*) in phase-space, with width in real and velocity space similar to the size and velocity dispersion of the progenitor cluster. This meant that a way to detect streams is to construct 6D hypertubes, with plausible phase-space width and length, and then count the number of stars that are encapsulated within them. This scenario is depicted in Figure 3.1(b) where red dots represent the stream stars, and the black cylinder is the hypertube surrounding the trial orbit (blue dashed curve).

Such an analysis exploits the coherence of the stream structure by analysing the data in spatial and kinematics space (6D phase-space) simultaneously.

3.1.2 Orbit Sampling in STREAMFINDER

Building onto this conception of stream detection, it meant that the task at the disposal was simply to integrate orbits for every star in the catalogue and compare these *trial orbits* with the data in order to find coherently associated star groups that behave like stream structures.

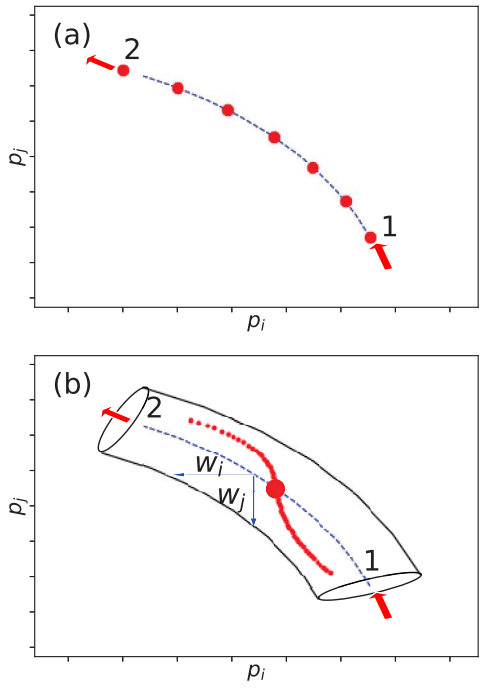

Figure 3.1: The STREAMFINDER concept. (a) The red dots represent schematically the spatial positions along a segment of an orbit, part of a stream that we are interested in detecting. The dots labelled '1' and '2' mark, respectively, the beginning and the end of this orbit segment. The blue dashed curve represents the orbit integrated using the 6D phase-space value of stellar point '1' as initial conditions. This *trial orbit* passes close to other stream members, allowing them to be associated with the structure. (b) The red dots now represent a more realistic scenario of a stellar stream where the tidal arms and the progenitor possess slightly different energies and hence lie along different orbits. Therefore, the trial orbit (blue-dashed curve) calculated using the phase-space measurement of some stream star corresponding to some (E, L_z) value fails to fit the entire stream structure. But if the same 6D orbit is upgraded to a 6D *hyper-dimensional-tube* (black cylinder), then the stream becomes circumscribed within it.

Now, the integration of an orbit requires a precise 6D phase-space value - the initial condition which can be integrated into a trajectory. However 1) Gaia lacks radial velocity measurements for all the stars for which G > 12, and 2) the proper motions and the parallaxes have associated errors that further causes impediment in pin-pointing a specific phase-space location of every star. This issue was circumvented by forcing STREAMFINDER to sample orbits, choosing parameter initial positions in the coordinates of the observables that are consistent with the corresponding uncertainty distributions.

For every star, the on-sky 2D position measurements (say ℓ, b) are extremely accurate and hence are kept fixed. The algorithm uses a trial Single Stellar Population (SSP) model of single age and metallicity to calculate the possible distance (D_i) that renders at most three possible distance values (see Subsection 3.1.1 of the paper attached). Furthermore, every star has two

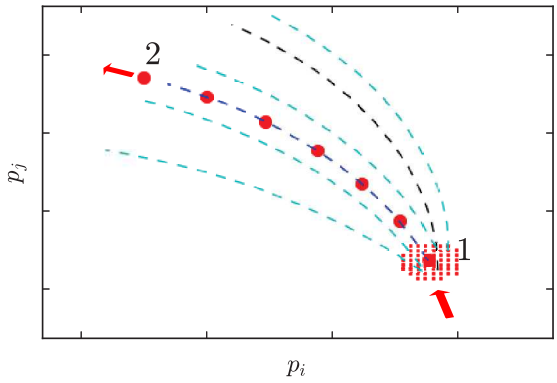

Figure 3.2: Orbit sampling. Due to measurement uncertainties and the missing phase-space information of the stars, their current 6D phase-space position cannot be pinned down precisely. This uncertainty in information is illustrated here as tiny red dots around star '1' which are also the sampled phase-space positions of this star. Using these sampled phase-space positions, STREAMFINDER integrates trial orbits (cyan dashed curves) along which the streams (large red dots) are searched for in the dataset. If one uses the "observed" phase-space values directly for orbit-integration, instead of sampling phase-space, that might launch an orbit that is mis-aligned with the true trajectory of the star (black dashed curve) and hence may not yield a detection.

proper motion components in Gaia (say μ_l, μ_b). The corresponding measurement uncertainties forces the algorithm to sample values from the proper motion space as well. So for a given (ℓ, b, D_i) combination, the algorithm samples proper motion values between $[-3\sigma_\mu, +3\sigma_\mu]$ independently for the two proper motion components. Finally, the algorithm samples linearly over radial velocity with a certain resolution (say of $10\,\mathrm{km\,s^{-1}}$) in such a way that the total velocity covers the range $[-v_{\rm esc}, +v_{\rm esc}]$.

In this way for every data point STREAMFINDER obtains $\sim 30{,}000$ sampled values ($n_D(\sim 3) \times n_{\mu_l}(\sim 10) \times n_{\mu_b}(\sim 10) \times n_{v_r}(\sim 100)$). Thus the uncertainty associated with the astrometric and photometric measurements, as well as the essentially completely unconstrained radial velocity, is reflected as 30,000 possible 6D positions where a given star could lie in 6D phase-space. To check if a given data point has other associated coherent members that share a similar orbital path, all of the 30,000 sampled initial conditions are integrated into orbits and then compared with the data. The procedure is sketched in Figure 3.2.

For a given star, different trial orbits encapuslate different number of stars based on which different log-likleihood values $L_{\rm k}$ ('k' for *kinematics coherence test*) are calculated. The trial orbit with the highest value of $L_{\rm k}$ is considered to be the best orbit, and both the corresponding $L_{\rm k}$ value and the orbital trajectory are then assigned to that datum. In this way, every data points gets assigned a log-likelihood value, $L_{\rm k}$, based on *how well that datum is able to coherently associate itself with the other data stars along one of the provided sampled orbits*. In this way, the

stars in the data that correspond to a stream receive higher $L_{\rm k}$ values, in contrast to the field stars that have zero or very small number of coherently associated star members.

3.2 STREAMFINDER in action

Different scenarios of stream detection were analysed and studied in order to get convinced with the working of the algorithm (see the paper attached). For each case study, a perfect stream model was simulated in a realistic Galactic potential model. This stream model was then degraded in observational measurements consistent with what is expected from end-of-mission Gaia survey and the radial velocity information was entirely omitted. This stream model was then added into a realistic mock dataset for Gaia (for which the Gaia Universe Model Snapshot, or GUMS [155], was used) and only 5D astromteric solution was retained for the entire dataset. This data served as the input data for the STREAMFINDER algorithm that was then processed to find the underlying stream from the stellar contamination. One of the studies is highlighted in Figure 3.3.

After processing all the data stars in the manner described previously, the output of the algorithm gets summarized in a density plot such as that shown in Figure 3.3(g), where the input stream model can be clearly seen.

3.3 Luminosity function and continuity: additional STREAMFINDER criteria

The algorithm aims to find thin and cold stream structures. These structures are expected to be remnants of a globular cluster that are formed by their disruption and dissolution. The member stars of most star clusters follow closely stellar evolutionary models of a single age and metallicity, and although now totally disrupted, the stream stars share similar age and metallicity as that of the progenitor and hence must follow a similar isochrone track. This concept was also incorporated into the algorithm, thus making use of the photometric information of each candidate group of stars identified by it.

For this, a G-band cumulative luminosity function of the same SSP model is used as a template, that is also used to derive the distance solution during orbit sampling. For each candidate group of stars that gets encapsulated by the hypertube, STREAMFINDER calculates the Kolmogorov-Smirnoff Test probability ($P_{\rm KS,LF}$) that the stars are drawn from this model luminosity function.

We further expect that stellar streams are extended structures, yet so far the criteria that have been described do not allow us to distinguish an extended stream from a small-scale localized over-density. To remedy this, an additional criterion was incorporated into the algorithm to calculate the Kolmogorov-Smirnoff Test probability ($P_{\rm KS,continuous}$) that the member stars of a

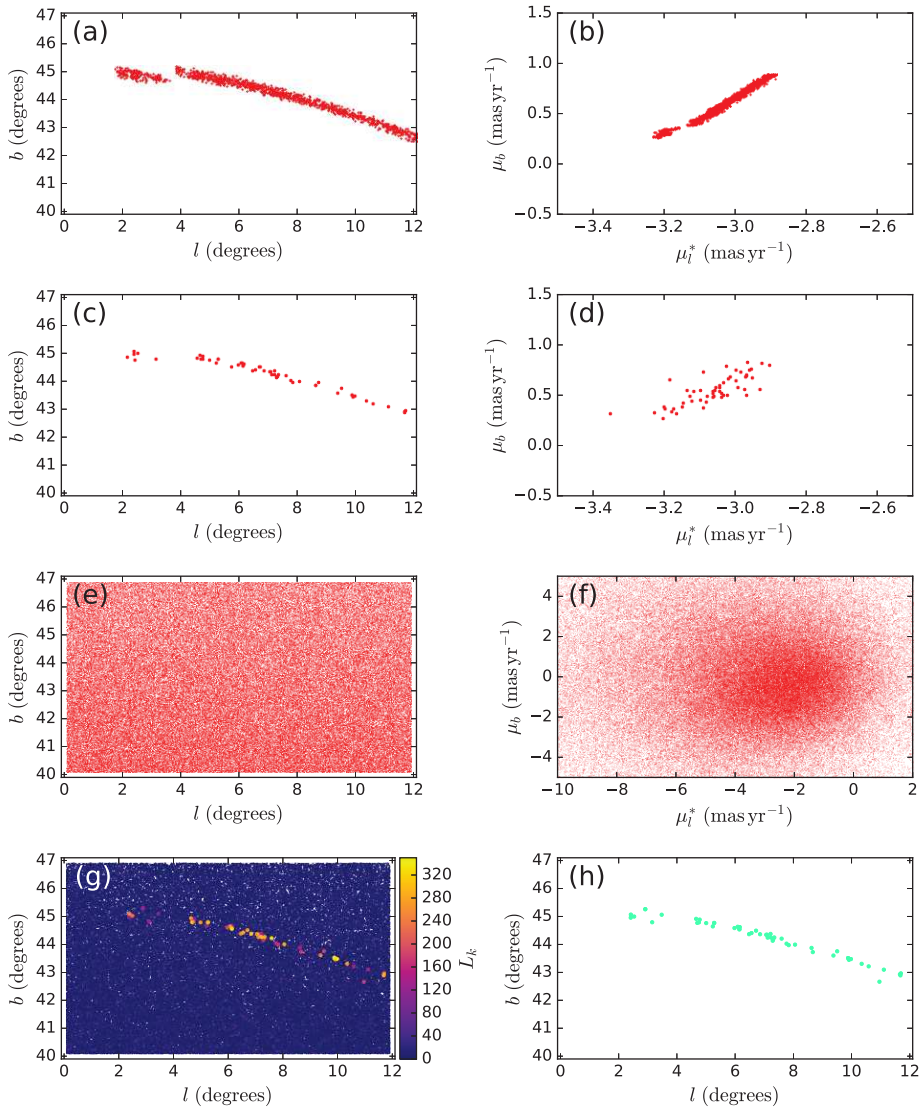

Figure 3.3: STREAMFINDER inputs and outputs. (a) and (b) present the simulated stream model constructed in a realistic Galactic potential. (c) and (d) show the stars that were actually retained from the perfectly simulated stream model convolved with Gaia-like errors. (e) and (f) show the total dataset obtained by plunging the degraded version of the stream model with the degraded version of the GUMS dataset. This served as the input catalogue to the STREAMFINDER algorithm. (g) and (h) present the STREAMFINDER output received after data processing, where (g) shows the easy recovery of the simulated stream in a Log-Likelihood density plot and (h) shows the corresponding highest likelihood stars.

candidate structure are uniformly distributed along the orbit segment contained within the sky window under study.

The final statistic for every star, based on the kinematics ($L_{\rm K}$), luminosity function and continuity criteria, is expressed as:

$$L = L_k + \ln\left(P_{\rm KS,LF}\right) + \ln\left(P_{\rm KS,continuous}\right). \tag{3.1}$$

and can be presented in a likelihood density plot (see Section 6 in the paper attached). Inclusion of the terms $P_{\rm KS,LF}$ and $P_{\rm KS,continuous}$ in the final statistic further improves the likelihood values of the stream stars.

3.4 Results and Discussions

To some extent, `STREAMFINDER` can be regarded as a very efficient stream detection algorithm. This is because not only the algorithm essentially incorporates all the ideas that lie behind the previously existing stream finding techniques, but also 1) unlike any other previous stream detection techniques, the algorithm detects streams along orbital trajectories which is a rather much more physically motivated means of finding streams, and 2) the simultaneous multidimensional analysis based on phase-space-color-magnitude allows one to find extremely faint stream structures as well.

Various tests, based on realistic simulation study, advocated that very faint stream structures with number of stars as few as ~ 15 (and an equivalent surface brightness of $\Sigma_{\rm G} \sim 33.6\,{\rm mag\,arcsec^{-2}}$) can be detected using the algorithm[1]. This was very promising and meant that the application of `STREAMFINDER` onto the actual Gaia dataset could reveal the presence of ultra-faint streams.

The design of the algorithm is such that along with the stream detection, it renders other useful insights about the detected candidate structures that can be used for further analysis:

1. The primary by-product that the algorithm delivers is the orbital trajectory along which the stream lies. Radial velocities and distance information of the stars is missing for the great majority of halo stars in the Gaia DR2 catalogues, and in the subsequent Gaia data realeases. However, since the algorithm gives the possible orbital solutions for a given stream structure, it therefore provides a means to complete the 6D phase-space solutions that are possible for a given stream star.

2. The algorithm delivers a complete 6D phase-space distribution of possible orbital solutions that a given stream might be on. When executed over the entire sky, the end product would be the distribution function of stream stars in the Galactic halo. This solution could be

[1] Recently we discovered a much fainter stream structure, Phlegethon, with the equivalent surface brightness of $\Sigma_G \sim 34.6\,{\rm mag\,arcsec^{-2}}$ in the Gaia DR2 catalogue ([91], ADS entry).

extremely useful for re-creating the pre-merging history of the Milky Way, or to perform Schwarzschild modelling to constrain the dark matter distribution in the Galaxy.

3. The length of the structure, that can be calculated along the orbital trajctory.

4. Since the algorithm offers orbital solutions for every stream, one can easily calculate simple orbital properties of the stream structure such as the eccentricity or energy of the streams.

3.5 Related Paper

Monthly Notices of the ROYAL ASTRONOMICAL SOCIETY

MNRAS **477,** 4063–4076 (2018) doi:10.1093/mnras/sty912
Advance Access publication 2018 April 12

STREAMFINDER – I. A new algorithm for detecting stellar streams

Khyati Malhan★ and Rodrigo A. Ibata
Observatoire Astronomique de Strasbourg, CNRS, Université de Strasbourg, UMR 7550, F-67000 Strasbourg, France

Accepted 2018 April 9. Received 2018 April 4; in original form 2018 February 19

ABSTRACT

We have designed a powerful new algorithm to detect stellar streams in an automated and systematic way. The algorithm, which we call the STREAMFINDER, is well suited for finding dynamically cold and thin stream structures that may lie along any simple or complex orbits in Galactic stellar surveys containing any combination of positional and kinematic information. In the present contribution, we introduce the algorithm, lay out the ideas behind it, explain the methodology adopted to detect streams, and detail its workings by running it on a suite of simulations of mock Galactic survey data of similar quality to that expected from the European Space Agency/*Gaia* mission. We show that our algorithm is able to detect even ultra-faint stream features lying well below previous detection limits. Tests show that our algorithm will be able to detect distant halo stream structures $>10^{\circ}$ long containing as few as $\sim$15 members ($\Sigma_{\rm G} \sim 33.6\,{\rm mag\,arcsec^{-2}}$) in the *Gaia* data set.

Key words: stars: kinematics and dynamics – Galaxy: halo – Galaxy: kinematics and dynamics – Galaxy: structure.

1 INTRODUCTION

Stellar streams around galaxies are of great importance as their orbital structures are sensitive tracers of galaxy formation history and the underlying gravitational potential (Eyre & Binney 2009; Law & Majewski 2010). The number of streams in principle places a lower limit on the number of past accretion events, allowing one to quantify the number of stars that are a result of hierarchical merging events. Moreover, in the case of the Milky Way, where we can obtain a full phase space picture, knowing the orbits of a sample of streams can shed light on the distribution function of halo accretions (and hence probably of the halo itself). Dynamical modelling of such stellar streams is a promising avenue to constrain the dark matter distribution of the Milky Way and measure the lumpiness in its distribution (Dalal & Kochanek 2002; Ibata et al. 2002a; Johnston, Spergel & Haydn 2002; Carlberg, Grillmair & Hetherington 2012; Erkal et al. 2016; Sanders, Bovy & Erkal 2016).

Streams that are a result of tidal disruption of low-mass progenitors tend to be dynamically cold and thin and are in particular of great interest for probing the dark matter. Dynamical modelling of their well-defined and simple orbital structures is one of the best ways to constrain the dark matter distribution in the Galaxy (Koposov, Rix & Hogg 2010; Ngan & Carlberg 2014; Bovy et al. 2016). However, the general lack of reliable tangential velocities and distance measurements of the stream stars can be consistent with multiple (degenerate) solutions (see e.g. Varghese, Ibata & Lewis 2011). Dynamical modelling of the known streams using the quality of velocity information that will soon be made available in the second data release (DR2, scheduled for April 2018) of the European Space Agency's *Gaia* mission (de Bruijne 2012; *Gaia* Collaboration et al. 2016) can be used in combination with distance estimates (derived from *Gaia* photometry or other surveys like the Canada–France Imaging Survey, Ibata et al. 2017) to resolve this degeneracy to some extent. But, in order to significantly improve the estimates of the Galactic mass distribution and the distribution function of the halo out to large Galactic radii, where the potential is basically unconstrained by other tracers, more stream detections are required. The present contribution aims to construct an optimized algorithm to detect stream structures.

There already exist some effective stream detection methods that have been successful in detecting the streams that we know of so far in the Milky Way. These include:

(i) Matched filter: The matched filter technique (Rockosi et al. 2002; Balbinot et al. 2011) incorporates colour–magnitude weighting of stars to find structures that belong to a specific Single Stellar Population (SSP) model. The Palomar 5 stream (Odenkirchen et al. 2001), GD-1 (Grillmair & Dionatos 2006), Orphan (Belokurov et al. 2006), Lethe, Cocytos, and Styx (Grillmair 2016), and most recently the Eridanus and Palomar 15 streams (Myeong et al. 2017) and the 11 new streams detected in the Dark Energy Survey (DES, Shipp et al. 2018) were all found with this technique. However, the drawback of this method is that it does not incorporate kinematics and its performance is expected to drop significantly if the structure possesses a significant distance gradient.

(ii) Detection of comoving groups of stars: Several halo substructures were initially identified as groups of stars of similar type

★ E-mail: kmalhan07@gmail.com

(e.g. RR Lyrae, Blue Horizontal Branch Stars) that are contained within a small phase space volume. Several streams in the Milky Way have been detected by employing this or a variation of this technique (Aquarius by Williams et al. 2011, Arcturus by Arifyanto & Fuchs 2006 and the Virgo stream by Duffau et al. 2006). The drawback of this approach lies in the fact that it requires the stars to have complete kinematic information. This requirement will not be completely fulfilled in the Galactic halo (where the streams of interest for dark matter studies lie) even in *Gaia* DR2.

(iii) Pole counts: The Pole Count technique (Johnston, Hernquist & Bolte 1996) works well for identifying substructures that are on great circle paths around the Milky Way and are of high contrast (it was useful in detecting structures like the Sagittarius stream; Ibata et al. 2002b). This method can be further improved by supplying the algorithm the available kinematic information (Mateu, Read & Kawata 2017). The method is expected to reveal only those streams that lie almost along great circular paths on the sky, and the streams on rather complex orbits can again go undetected.

However, in light of the revolutionary data set that *Gaia* will deliver, we desired to build an algorithm that is able to use as much as possible of our prior knowledge of stellar streams to maximize the detection efficiency. In this paper, we introduce the STREAMFINDER algorithm that we have built, explain the physical motivation behind it, and demonstrate its workings by running a suite of test simulations. We find that our algorithm can detect very faint stream features in the data set of the quality that will soon be delivered by *Gaia* DR2.

This paper is arranged as follows. In Section 2, we present the motivation and the basic idea behind the workings of our algorithm. Section 3 gives a proof of concept of our method through the detection of a simplistic orbital stream model. Section 4 presents the success of our technique by demonstrating the detection of an *N*-body tidal stream structure. Section 5 exhibits the ability to detect multiple streams criss-crossing each other in a given patch of sky. In Section 6, we detail additional criteria incorporated into the algorithm that improve the contrast of the streams. We test the detection limit of our algorithm in finding extremely faint stream structures in Section 7. In Section 8, we study the effect of assuming a wrong Galactic mass model. Finally, in Section 9 we discuss the implications of our study.

2 STREAMFINDER

Different surveys of the Milky Way cover different sky regions, probe different depths of the sky, and deliver different combinations of phase space measurements. We sought to develop a generic algorithm that would work with any mix of data sets containing any combination of positions and kinematics. We also desired the algorithm to have the property of being able to handle data sets with partial sky coverage and incomplete information on some parameters, so as to make the most of the available surveys.

Since we suspect that the most massive star streams in the Milky Way have already been discovered, we decided to design the STREAMFINDER algorithm to detect primarily narrow low-mass tidal streams, and we expect these faint structures to lie hidden under a dominant 'background' of contaminants (in most cases the contaminants will actually be in the foreground).

2.1 Stream detection concept

The tidal disruption of low-mass progenitors leads to the formation of thin and dynamically cold streams. These streams closely delineate orbits in the underlying gravitational potential of the Galaxy (Dehnen et al. 2004).

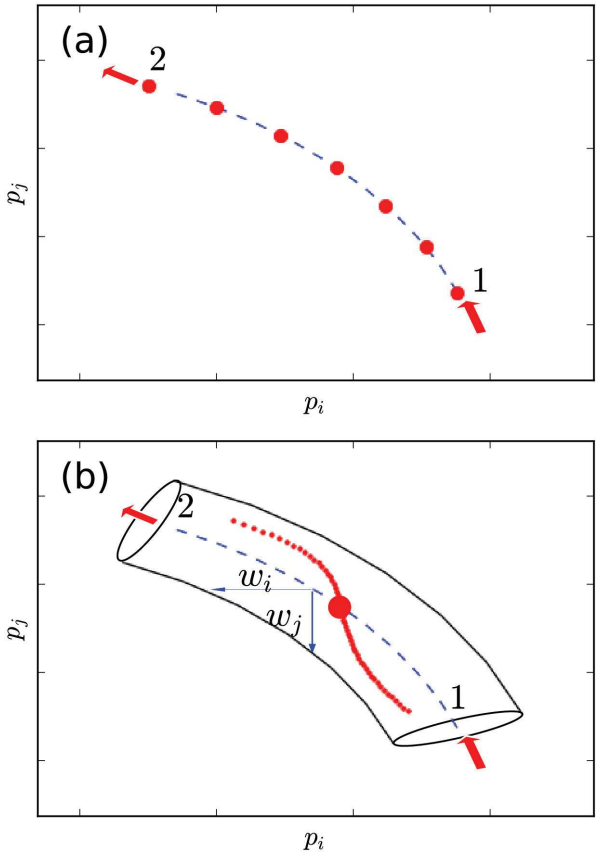

Figure 1. The STREAMFINDER concept. (a) The red dots represent schematically the spatial positions along a segment of an orbit, part of a stream that we are interested in detecting. The dots labelled '1' and '2' mark, respectively, the beginning and the end of this orbit segment. The blue-dashed curve represents the orbit integrated using the 6D phase space value of stellar point '1' as initial conditions. This *trial orbit* passes close to other stream members, allowing them to be associated with the structure. (b) The red dots now represent a more realistic scenario of a stellar stream where the tidal arms and the progenitor possess slightly different energies and hence lie along different orbits. Therefore, the trial orbit (blue-dashed curve) calculated using the phase space measurement of some stream star corresponding to some (E, L_z) value fails to fit the entire stream structure. But if the same 6D orbit is upgraded to a 6D *hyperdimensional tube* (black cylinder), then the stream becomes circumscribed within it.

Consider an ideal scenario where we have a segment of an orbit (Fig. 1a). The red dots represent the positions of the stars (members of a hypothetical stream that perfectly delineates this orbit) along their orbital structure in 6D phase space. Suppose we have access to perfect 6D position and velocity values ($\boldsymbol{x}$, $\boldsymbol{v}$) for all these stream stars and that we also know the underlying gravitational potential. Then, if one integrates a *trial orbit* (blue-dashed curve) using the given 6D phase space value ($\boldsymbol{x_i}$, $\boldsymbol{v_i}$) of one of these stream stars, then this trial orbit would sew through the remaining stars in the 6D phase space, revealing the entire stream structure.

In reality, streams do not delineate perfect orbits (Fig. 1b). Stars in a tidal stream have slightly different (E, L_z) values, and therefore lie along slightly different orbits (see e.g. Eyre & Binney 2011). The slight differences in energies and orbital trajectories of the stream stars as they are lost from their progenitor lead to a finite structural

stream width(s) in real space and velocity dispersion (σ_v) in velocity space.

Our method makes use of the realization that the members of a stream can be contained within a 6D hyperdimensional tube (or *hypertube*) in phase space, with width in real and velocity space similar to the size and velocity dispersion of the progenitor cluster. N-body disruption simulations show that the length of the stream depends on the mass distribution of the progenitor, and the orbit and time of accretion on to the host galaxy.

This suggests that a way to detect streams is to construct 6D hypertubes, with plausible phase space width and length, and then count the number of stars that are encapsulated within them. This scenario is depicted in Fig. 1b, where red dots represent the stream stars, and the black cylinder is the hypertube surrounding the trial orbit (blue-dashed curve).

3 ORBITAL STREAM MODELS

We first present the algorithm applied to an idealized situation where streams follow perfect orbits. The very low contrast streams are added into a realistic mock data set for *Gaia* (the *Gaia* Universe Model Snapshot, or GUMS, Robin et al. 2012), and then we try to detect this faint stream feature from the stellar contamination using `STREAMFINDER`.

The mock stream was modelled by degrading an orbit as follows. We selected a random 6D phase space position to give the initial conditions of the orbit. This initial condition was then integrated for $T = 0.1$ Gyr, in the realistic Galactic potential model 1 of Dehnen & Binney (1998), to form an orbit (the value of T was chosen so that the orbit appears long enough to mimic observed streams found in the SDSS). The transformation of this orbit into the heliocentric observable frame was accomplished using Sun's Galactocentric distance of 8.5 kpc and adopting the peculiar velocity of the Sun $\boldsymbol{V}_\odot = (u_\odot, v_\odot, w_\odot) = (11.1, 12.24, 7.25)\,\mathrm{km\,s^{-1}}$ (Schönrich, Binney & Dehnen 2010). The resulting orbit model is shown in Fig. 2.

To give this orbit a stream-like appearance, we need to provide a structural width and a velocity dispersion. For this, we chose $s = 50$ pc and $\sigma_v = 2\,\mathrm{km\,s^{-1}}$. These values are adopted in accordance with the values of some of the currently known dynamically cold streams (Grillmair & Carlin 2016, and references therein). To smear the data in phase space, every orbital point was then convolved with a Gaussian with dispersion equivalent to these values.

The stream stars were assigned $G_{\rm BP}-G_{\rm RP}$ colour and G magnitude in the *Gaia* bands, using a Padova SSP model (Marigo et al. 2008) of metallicity [Fe/H] $= -1.5$ and age 10 Gyr, appropriate for a typical halo globular cluster. A lower limit of $G_0 = 19$ was chosen so as to mitigate against variations in extinction in the high latitude fields of interest for halo studies, which would otherwise cause variations in survey depth. Given the assigned magnitude, we generated an uncertainty in proper motion (μ_l, μ_b) according to the 'End-of-mission' sky average[1] as shown in Fig. 2. The dependency of the proper motion errors on the G-band magnitude is shown in Fig. 4.

The detection limit for radial velocities in *Gaia* DR2 is expected to be only $G = 13$ mag, but even in the later data releases, most *Gaia* halo stars will not have measured radial velocities. Likewise, virtually no distant halo stars will have well-measured parallaxes with *Gaia*. We therefore omit both the radial velocity and distance information from our simulated streams, retaining only 4D astrometric information of the mock stream stars in the form of (ℓ, b, μ_l, μ_b) along with the stellar photometry (G, $G_{\rm BP}$, $G_{\rm RP}$) and associated observational errors (Figs 2 and 4).

The GUMS data were degraded in proper motion based on their G-band magnitudes and once again we retained only 4D phase space information of the data in the form of (ℓ, b, μ_l, μ_b) along with the photometry (G, $G_{\rm BP}$, $G_{\rm RP}$) and the observational errors.

The GUMS data with the mock stream model added in are shown in Fig. 3. This particular orbit was chosen as its position in proper motion space lies in a region of high contamination from Galactic field stars, so that it is effectively indistinguishable from Galactic field stars. The CMD and the dependency of the proper motion errors on the G-band magnitude is shown in Fig. 4. Comparing the number of Galactic stars to those in the mock stream ($n_{\rm stream}/n_{\rm data} \approx 0.015$ per cent), one can appreciate that the mock stream is an ultra-faint feature.

3.1 `STREAMFINDER` in action

The mock *Gaia* data set is fed into the algorithm to detect the ultra-faint stream model that we have introduced into the GUMS data. We now detail the steps that the algorithm takes.

Since we are interested here in identifying halo streams, we first reduce the number of disc contaminants by rejecting those sources whose parallax differs from 1/3000 arcsec at more than the 2σ level (i.e. objects that are likely to be closer than 3 kpc). This makes it natural to set 3 kpc as the lower distance limit for analysis. To avoid having to consider objects that venture arbitrarily far, we also impose an upper distance limit in our analysis of 200 kpc. These cuts removed 49 per cent of the sample.

3.1.1 Step 1: Assigning distances based on a stellar population model

The algorithm uses a trial SSP model of single age and metallicity to calculate the possible solutions to the absolute $M_{\rm G}$ magnitude value given the 'observed' $G_{\rm BP}-G_{\rm RP}$ colour. With old metal-poor isochrones, there are at most three absolute magnitude values ($M_{\rm G}$) possible for a given colour value. The algorithm then estimates the possible distance values (D_i, $i = 1, 2, 3$) of a given star based on the 'observed' apparent G magnitude value. If at least one of the possible distance values lies within the chosen distance range [$D_{\rm min}$, $D_{\rm max}$], then this particular star is retained for further study. Table 1 lists the parameter intervals that we adopted for the purpose of our analysis. By virtue of this procedure, the data that lie outside the colour range of the selected isochrone model are thrown away (in this case, leaving 42 per cent of the initial sample). We emphasize that this procedure does not follow from the matched filter technique and was applied only to reduce the number of contaminants and so boost the signal to noise of the stream detection.

The algorithm then uses the derived distances of the given star along with its proper motion value to calculate the possible tangential velocities $v_{\rm t}$ that it might have, corrected for solar reflex motion. Since we are interested in finding structures that are bound to the Galaxy, the total 3D velocity v of the member stars of the structures must be less than the escape velocity of the Milky Way ($v_{\rm esc}$), i.e.

$$\sqrt{v_{\rm t}^2 + v_{\rm r}^2} = v < v_{\rm esc}, \quad (1)$$

[1] See https://www.cosmos.esa.int/web/gaia/sp-table1

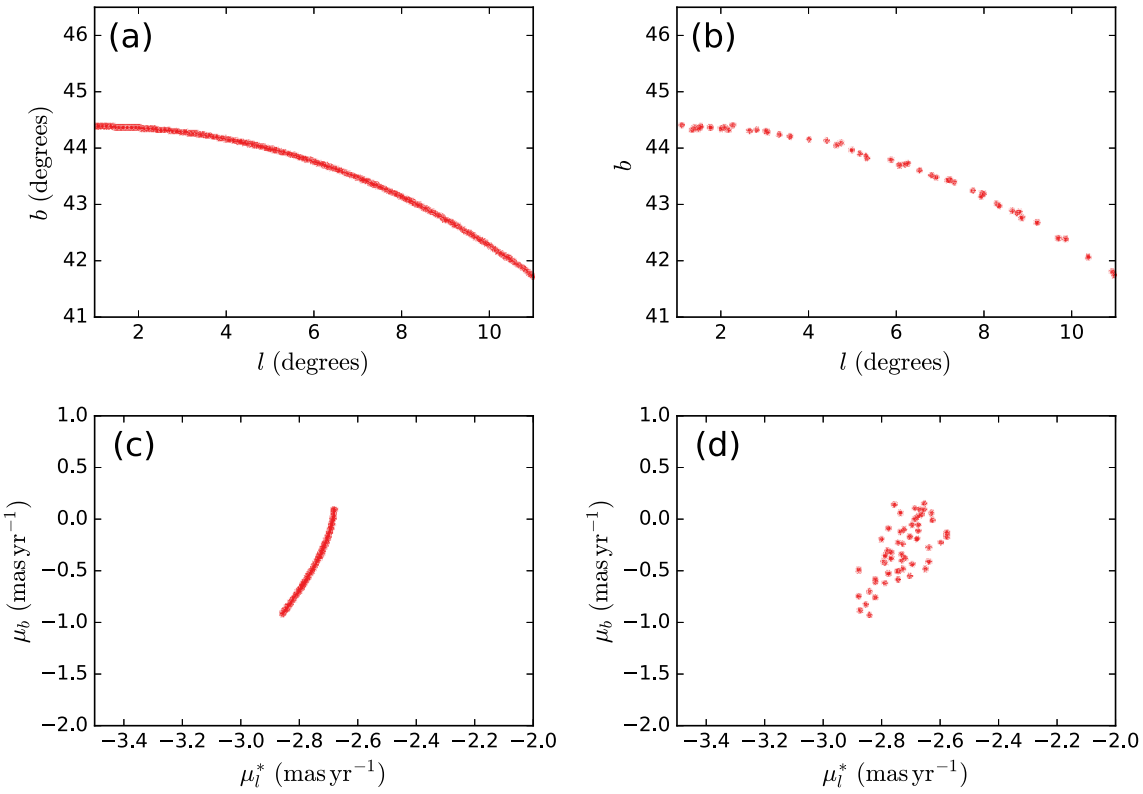

Figure 2. Orbit stream model. The left-hand panels show the perfect orbit model that we integrated, represented in position (a) and in proper motion (c) space. The right-hand panels display the same orbit smeared-out to match the properties of a typical cold stream and also convolved with errors in proper motion consistent with the expected end-of-mission *Gaia* uncertainties. We retained only ∼50 stellar points in order to obtain a low contrast structure. This structure represents the mock orbital stream model.

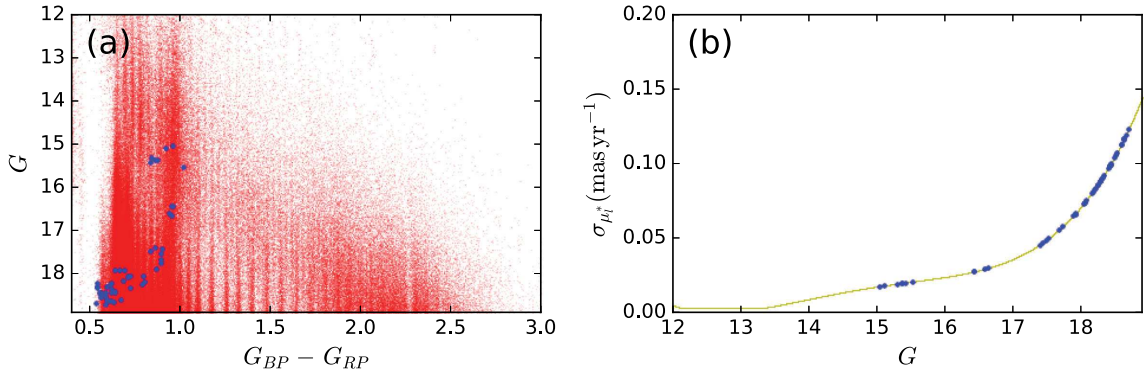

Figure 4. Mock *Gaia* data. The colour–magnitude diagram of the mock *Gaia* data set is shown in panel (a) where the stream stars are highlighted in blue. (The vertical stripes in the CMD are GUMS simulation artefacts.) Panel (b) shows the variation of the proper motion errors in σ_{μ_l} as a function of G-band magnitude (orange line). The bigger blue dots represent σ_{μ_l} for the stream stars. For the purpose of these tests, we assume that the uncertainties in σ_{μ_b} mirror those in σ_{μ_l}.

where v_r is the radial velocity of the star. Since *Gaia* will not give us access to the entire 3D velocity of halo stars, we require only that $v_t < v_{esc}$.

Then for a given star, which has already satisfied the distance criterion, if the condition $v_t < v_{esc}$ is satisfied for any distance solution D_i, then this star is retained in the sample. We adopt $v_{esc} = 600\,\mathrm{km\,s^{-1}}$, which corresponds to the upper limit derived by Smith et al. (2007).

The sample after the application of these parameter cuts is shown in Fig. 5.

3.1.2 Step 2: Orbit sampling and integration

The next task that the algorithm executes is the calculation of trial orbits for each star in the sample. Integration of trial orbits requires specifying a potential as well as the precise initial 6D phase space position. For a given star, the algorithm has access to the 4D data astrometric information (ℓ, b, μ_l, μ_b) along with the distance solutions D_i. The algorithm is not provided any radial velocity information (although we note that it would be trivial to include any v_r measurements, if they were available).

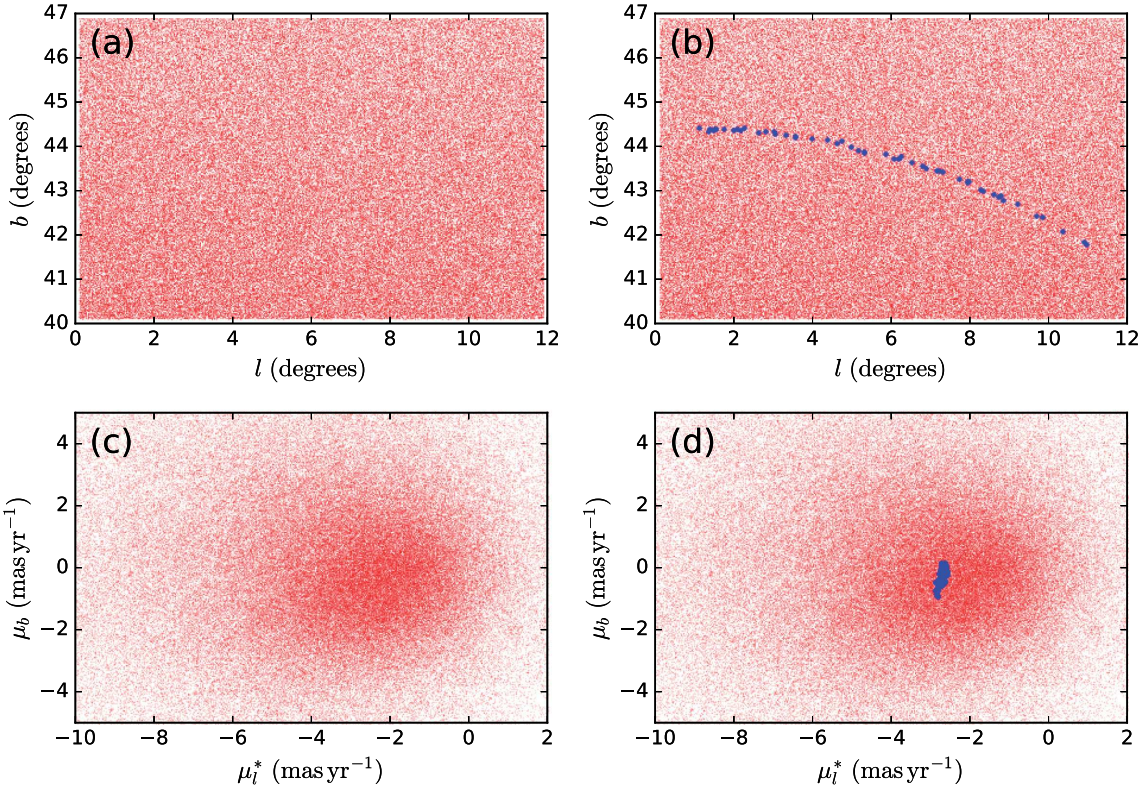

Figure 3. Mock *Gaia* data. The stream orbit model (shown in Fig. 2) was plunged into the GUMS data set. The left-hand panels represent this mock data set in (a) position and (c) proper motion space. The right-hand panels represent the same data set with the stream stars highlighted in blue. The stream is an ultra-faint feature containing only 0.015 per cent of the stars in this region of sky (the total number of stars shown is ∼330 000 stars). Given the variable extinction over the field, we trimmed the data below $G_0 = 19$ to ensure homogeneous depth.

Table 1. Parameter ranges used to integrate orbits in the Galaxy.

Parameter	Minimum	Maximum
$d_\odot$	3.0 kpc	200 kpc
$D_{\rm helio}$	3.0 kpc	200 kpc

The proper motions have associated errors and this also does not allow us to pinpoint a specific phase space location of each star. We circumvent this issue by sampling orbits choosing parameter initial positions in the coordinates of the observables that are consistent with the corresponding uncertainty distributions. The on-sky 2D position measurements (ℓ, b) are extremely accurate and hence are kept fixed. The same star has at most three possible distance values, giving three sampled distance values. Furthermore, every star has two proper motion components (μ_l, μ_b). The corresponding measurement uncertainties force us to sample values from the proper motion space as well. So, for a given (ℓ, b, D_i) combination, the algorithm samples proper motion values between $[-3\sigma_\mu, +3\sigma_\mu]$. Finally, we also sample linearly over radial velocity with a resolution of 10 km s^{-1} in such a way that the total velocity covers the range $[-v_{\rm esc}, +v_{\rm esc}]$.

In this way, for every data point we get ∼30 000 sampled values ($n_{\rm D}(\sim 3) \times n_{\mu_l}(\sim 10) \times n_{\mu_b}(\sim 10) \times n_{v_{\rm r}}(\sim 100)$). Thus, the uncertainty associated with the astrometric and photometric measurements, as well as the essentially completely unconstrained radial velocity, is reflected as 30 000 possible 6D positions where a given star could lie in 6D phase space. Although this may appear to be a crude sampling of phase space, we were surprised to find that it was adequate to detect the artificial streams we simulated. To check if this given data point has other associated coherent members that share a similar orbital path, we try all of the 30 000 orbits integrated using these sampled initial conditions. The procedure is sketched in Fig. 6.

The sampled phase space points are integrated using a symplectic leapfrog integrator. We model the acceleration field of the Milky Way with the flexible multipole expansion software of Dehnen & Binney (1998); for these particular tests, we again adopt their mass model 1.

3.1.3 *Algorithm parameters*

The algorithm is provided with some generic control parameters that allow one to tune the size of the hypertube in phase space according to the morphology of the stream structure that one aims to detect. These controls allow the algorithm to be tuned and are discussed below.

(i) *Hypertube width:* We predefine the width of the hypertubes in phase space in terms of the allowed dispersion in the velocity space (parameter σ_v) and the allowed structural width in real space (parameter σ_w). These two parameters define the morphology of the stream that the algorithm then tries to detect.
To make reasonable assumptions about σ_w and σ_v, we refer to Grillmair & Carlin (2016) and references therein, where these properties of known cold streams are listed. Based on this, we set $\sigma_w = 100$ pc and $\sigma_v = 2.0$ km s^{-1}, which are appropriate for a stream derived from a low-mass progenitor cluster. For comparison, this value of

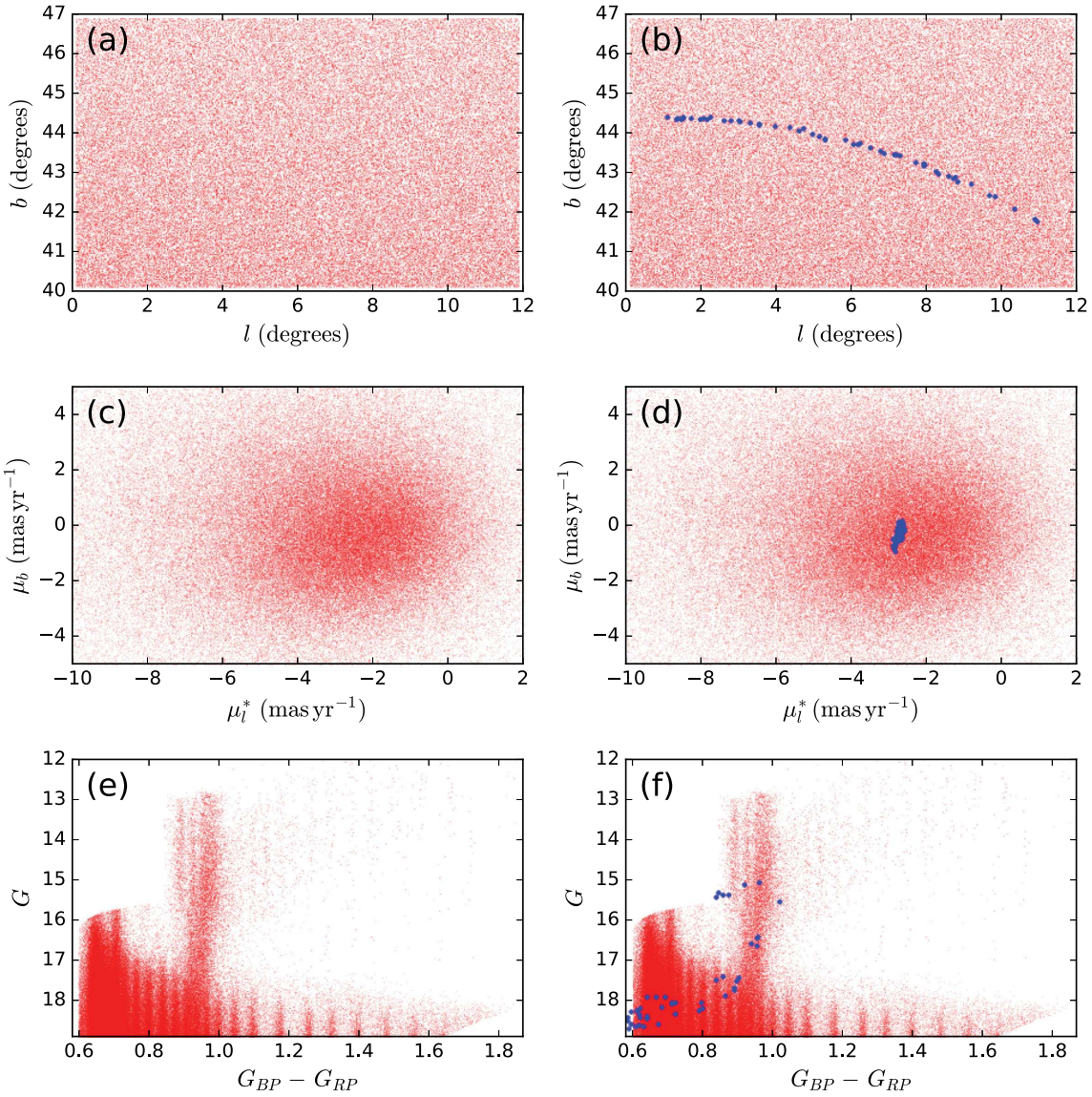

Figure 5. Data filtering. The data are first cleaned as described in the text to remove objects with high parallaxes. Next, using the adopted SSP model to derive the distance, the algorithm rejects stars with distances and tangential velocities outside of the chosen ranges. This filtering procedure allows the algorithm to diminish the contamination from field stars, making the stream search easier. In this example, the number of stars dropped from ≈330 000 to ≈140 000. Panels (a)–(d) are identical to Fig. 3, while panel (e) shows the *Gaia* CMD of the contamination and stream, with the stream highlighted in blue in panel (f).

σ_w when projected on the sky gives an angular width of the stream of 0.30° at 20 kpc. For example, the GD1 stream has an angular width of 0.5° at a distance of ∼9 kpc, implying a width of 70 pc (Carlberg & Grillmair 2013).

(ii) *Hypertube length:* Stellar streams that are detected in Milky Way surveys have different lengths that depend on the detailed structure and mass of the progenitor, its orbit, and merging history. We therefore did not fix the orbits to a particular length, but rather we integrated them until they moved out of the chosen sky window under study.

3.1.4 Step 3: Stream finding

For every trial hypertube, the algorithm tests all survey data points to establish those that are compatible with this trajectory. The orbit compatibility test is done in a 5D parameter space. Four of these dimensions come directly from the astrometry of the data in the form (ℓ, b, μ_l, μ_b). The remaining dimension is one of the distance solutions D_i, as derived from the photometry. In practice, the algorithm uses distance moduli DM to encode the distance information, in order to account easily for Gaussian uncertainties in photometry.

We model the stream as a structure that has a Gaussian distribution perpendicular to the orbit, in each of the observed dimensions of the data, and convolve this model with the corresponding observational uncertainties. For a given data point j, `STREAMFINDER` calculates the closest point k along the trial orbit as

$$\omega_{\rm sky} = \sqrt{\cos^2(b_{\rm d}^j)(\ell_{\rm d}^j - \ell_{\rm o}^k)^2 + (b_{\rm d}^j - b_{\rm o}^k)^2}, \quad (2)$$

where the ℓ and b are Galactic coordinate values and the d subscript denotes 'data', while the o subscript denotes the calculated 'orbit'. If this angular distance is greater than the chosen angular model hypertube width, then this data point is considered to be incompatible with the given orbit and deemed to be a contamination star. If the datum satisfies the angular width criteria, then for the given datum

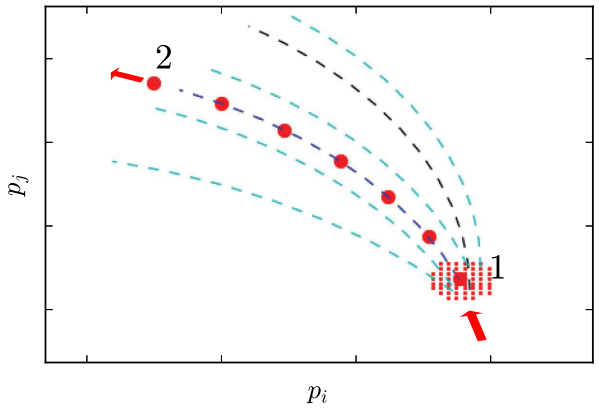

Figure 6. Orbit sampling. Due to measurement uncertainties and the missing phase space information of the stars, their current 6D phase space position cannot be pinned down precisely. This uncertainty in information is illustrated here as tiny red dots around star '1' which are also the sampled phase space positions of this star. Using these sampled phase space positions, we integrate trial orbits (cyan-dashed curves) along which the streams (large red dots) are searched for in the data set. If we had used the 'observed' phase space values directly for orbit integration, instead of sampling phase space, that might launch an orbit that is misaligned with the true trajectory of the star (black-dashed curve) and hence may not yield a detection.

j and closest orbital point k, the algorithm calculates the following statistic, based on kinematics and structure:

$$\begin{aligned}\mathcal{L}_{\rm kinematics} = &-\ln(\sigma_{\rm sky}\sigma_{\mu_l}\sigma_{\mu_b}\sigma_{\rm DM})\\ &-\frac{1}{2}\left(\frac{\omega_{\rm sky}^2}{\sigma_{\rm sky}^2}+\frac{(\mu_{l,\rm d}^j-\mu_{l,\rm o}^k)^2}{\sigma_{\mu_l}^2}\right.\\ &\left.+\frac{(\mu_{b,\rm d}^j-\mu_{b,\rm o}^k)^2}{\sigma_{\mu_b}^2}+\frac{(\mathrm{DM}_{\rm d}^j-\mathrm{DM}_{\rm o}^k)^2}{\sigma_{\rm DM}^2}\right),\end{aligned} \tag{3}$$

where $\mu_{l,\rm d}^j$, $\mu_{b,\rm d}^j$, and $\mathrm{DM}_{\rm d}^j$ are the observed proper motion and distance modulus values, and the corresponding model values are marked with the subscript o. As stated before, the Gaussian dispersions $\sigma_{\rm sky}$, σ_{μ_l}, σ_{μ_b}, $\sigma_{\rm DM}$ are the convolution of the intrinsic dispersion of the model together with the observational uncertainty of each data point.

While we have constructed our statistic deliberately to resemble the logarithm of the likelihood of a model, we stress that $\mathcal{L}_{\rm kinematics}$ is not a likelihood, as that would require one to model properly the contaminating field-star population. Such modelling would be computationally very costly and hence impractical for the present purpose of *finding* streams.

If $\mathcal{L}_{\rm kinematics}$ is found to be greater than the floor value $\mathcal{L}_{\rm kinematics,\,floor}$ (a parameter of the algorithm), then this data point j is considered to be compatible with the orbit and hence qualifies as a candidate member. The same orbit is compared to all the other stars in the data set to find all the compatible stars. If q stars out of a total of n_d in the survey are retained as members of the orbit, we derive the total statistic (based on the kinematics and structure) as

$$L_k = (n_d - q)\times\mathcal{L}_{\rm kinematics,\,floor}+\sum_q \mathcal{L}_{\rm kinematics}. \tag{4}$$

The first term on the RHS is designed to allow streams with different numbers of encapsulated stars to be compared.

This procedure is carried out for all the trial orbits through datum j. The trial orbit with the highest value of L_k is considered to be the best orbit, and is then assigned to datum j.

After processing all the data stars in this manner, the output of the algorithm can be summarized in a density plot such as that shown in Fig. 7, where the input stream model can be clearly seen. This means that despite the fact that the stream model was an ultra-faint feature, the multidimensional analysis done by STREAMFINDER allows it to detect even extremely low contrast objects. This procedure using orbital models as streams gives us a proof of concept of our algorithm.

4 *N*-BODY SIMULATED STREAM MODEL

In reality, star streams do not follow perfect orbits. So, we next test whether our hypertube search algorithm works well with more plausible structures derived from the tidal disruption of low-mass clusters. To this end, we decided to produce *N*-body models of streams for which we used the GyrafalcON *N*-body integrator (Dehnen 2000) from the NEMO software package (Teuben 1995).

Although we have tested our algorithm on various mock *N*-body streams, we decided to present here a structure on an orbit similar to that of the Palomar 5 globular cluster stream (Odenkirchen et al. 2001; Rockosi et al. 2002). This feature is a 'poster child' case (Küpper et al. 2015) of a thin cold stream of the type that STREAMFINDER aims at detecting.

The mock stream was created by choosing an initial phase space point for the progenitor cluster such that the resulting stream matches the current position, distance, and extension of the Pal 5 stream. The progenitor was built using a King model (King 1966), with mass, tidal radius, and ratio between central potential and velocity dispersion of $M_{\rm sat} = 2\times10^4\,\mathrm{M}_\odot$, $r_{\rm t} = 50$ pc, and $W_{\rm sat} = 2.5$, respectively (Thomas et al. 2016). Once the progenitor was initialized in phase space, it was then evolved forwards for 3.0 Gyr in the adopted Galactic mass model. In order to make the detection more challenging, at the end of the simulation we removed the stars within 50 pc from the progenitor remnant from the sample. Our *N*-body stream closely follows the structure and kinematics of the true Pal 5 stream, though we stress that the purpose here is not to make a quantitative comparison with the real stellar structure.

A similar procedure as before was followed to assign *Gaia*-like proper motion uncertainties and *Gaia* colour–magnitude values to the *N*-body particles. The degraded version of the simulated stream was immersed in the same degraded contamination (GUMS) model as used previously in Section 3. The simulated data with the mock *N*-body stream immersed in it is shown in Fig. 8. We chose to incorporate only 50 stream stars in this test (<4 per cent of the probable $2\times10^4\,\mathrm{M}_\odot$ progenitor of Pal 5), which amounts to 0.015 per cent of the sample. The equivalent surface brightness of the mock stream candidate is $\Sigma_{\rm G}\sim32.5\,\mathrm{mag\,arcsec}^{-2}$.

This data was then fed to the STREAMFINDER algorithm to detect this *ultra-faint* stream feature following exactly the same procedure and analysis as described in Section 3. The output of the algorithm is the map of the stream L_k statistic shown on the bottom panels of Fig. 8. The stream members can be clearly identified above the contamination in this map.

This case study demonstrates the success of our algorithm in detecting realistic and extremely faint stream features in a *Gaia*-like data set.

5 MULTIPLE STREAMS

In the hierarchical picture of galaxy formation, galaxies like the Milky Way grow by repeated merging and accretion of their satellites. Some of the disrupted satellites will have contained star clusters (Bellazzini, Ferraro & Ibata 2003), which themselves will even-

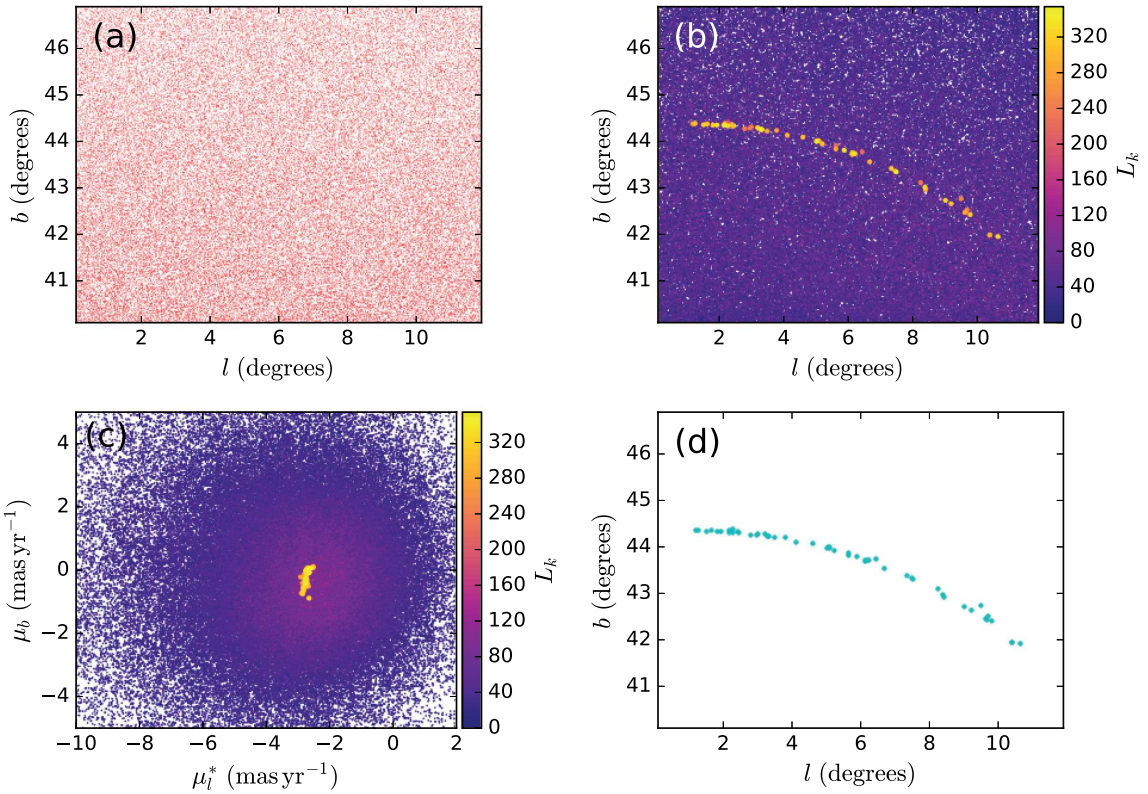

Figure 7. STREAMFINDER density plot, showing the detection of an ultra-faint mock stream feature introduced into the GUMS data. (a) The patch of sky shows no hint of the structure in density, however, it is clearly detected via the L_k statistic calculated by the STREAMFINDER algorithm (b). The colour axis marks the relative value of L_k. The corresponding proper motion distribution is shown in (c). Selecting only those stars with $L_k > L_{k,\,\mathrm{max}} - 150$ reveals the stream very clearly.

tually tidally disrupt to form long streams in the Galactic halo. The 'Field-of-Streams' image presented by Belokurov et al. (2006) and the halo substructures map created by Bernard et al. (2016) show a Galactic sky full of stream-like substructures. These images, along with the many other detections of streams over the past few years, strongly suggest that a significant fraction of the stellar halo population is a result of hierarchical merging. As the time-scales for phase mixing are extremely long, it may turn out the Milky Way halo is a patchwork of criss-crossing streams. This may be verified once *Gaia* DR2 delivers its excellent astrometric solutions for the stars over the entire sky.

Therefore, we also test the ability of our algorithm to make detections in this much more interesting case where a patch of sky contains multiple streams laid over each other. For this test, we again use the Dehnen & Binney (1998) mass model 1 and the GyrafalcOn *N*-body integrator to produce mock streams. We chose to model three such structures. We keep the same (Palomar 5-like) mock stream as previously, and add two new random streams.

The initial phase space distribution of the three progenitors of the streams was selected as follows. The initial position of each satellite was drawn at a random direction as seen from the Galactic Centre, and with a uniform probability of lying in the Galactocentric distance range of [10–30] kpc. The mean velocity of each satellite was selected randomly from an isotropic Gaussian distribution with (1D) dispersion of 100 km s^{-1} (Harris 1976). At these phase space positions, each progenitor was constructed using a King model (King 1966). The mass, tidal radius, and ratio between central potential and velocity dispersion were sampled uniformly between the ranges $M_{\mathrm{sat}} = [2\text{–}4] \times 10^4\,\mathrm{M}_\odot$, $r_{\mathrm{t}} = [20\text{–}80]$ pc, and $W_{\mathrm{sat}} = [2\text{–}4]$.

Once the progenitors were initialized in phase space, they were then evolved independently over a time period between [2–6] Gyr in the same Galactic mass model mentioned above. We resampled the initial conditions of those progenitors that did not disrupt or did not fall into the chosen sky region. Each of the three streams was assigned an SSP isochrone model of age and metallicity (10 Gyr, −1.28), (10 Gyr, −1.58), and (10 Gyr, −2.28), which cover plausible values for halo globular clusters. These streams were degraded in their astrometric measurements and were introduced into a common contamination model in the same manner as in Section 3. The data provided to the algorithm is shown in Fig. 9.

The algorithm was rerun three times with these data, each time using one of the three isochrone models to assign distances to the stream stars. Fig. 10 shows the resulting stream maps, where the first row uses the correct stellar populations model for stream m1, the middle row for stream m2, and the third row for stream m3.

This shows that the procedure needs to use the correct trial SSP model to successfully detect the input streams. With the real *Gaia* data, it will be necessary to run the algorithm over a grid in metallicity and age (our tests suggest that intervals of 0.1 dex and ∼1 Gyr are appropriate).

6 LUMINOSITY FUNCTION AND CONTINUITY: ADDITIONAL STREAMFINDER CRITERIA

So far, we have discussed searching for subgroups of stars in a sample whose kinematic and spatial properties mirror a plausible

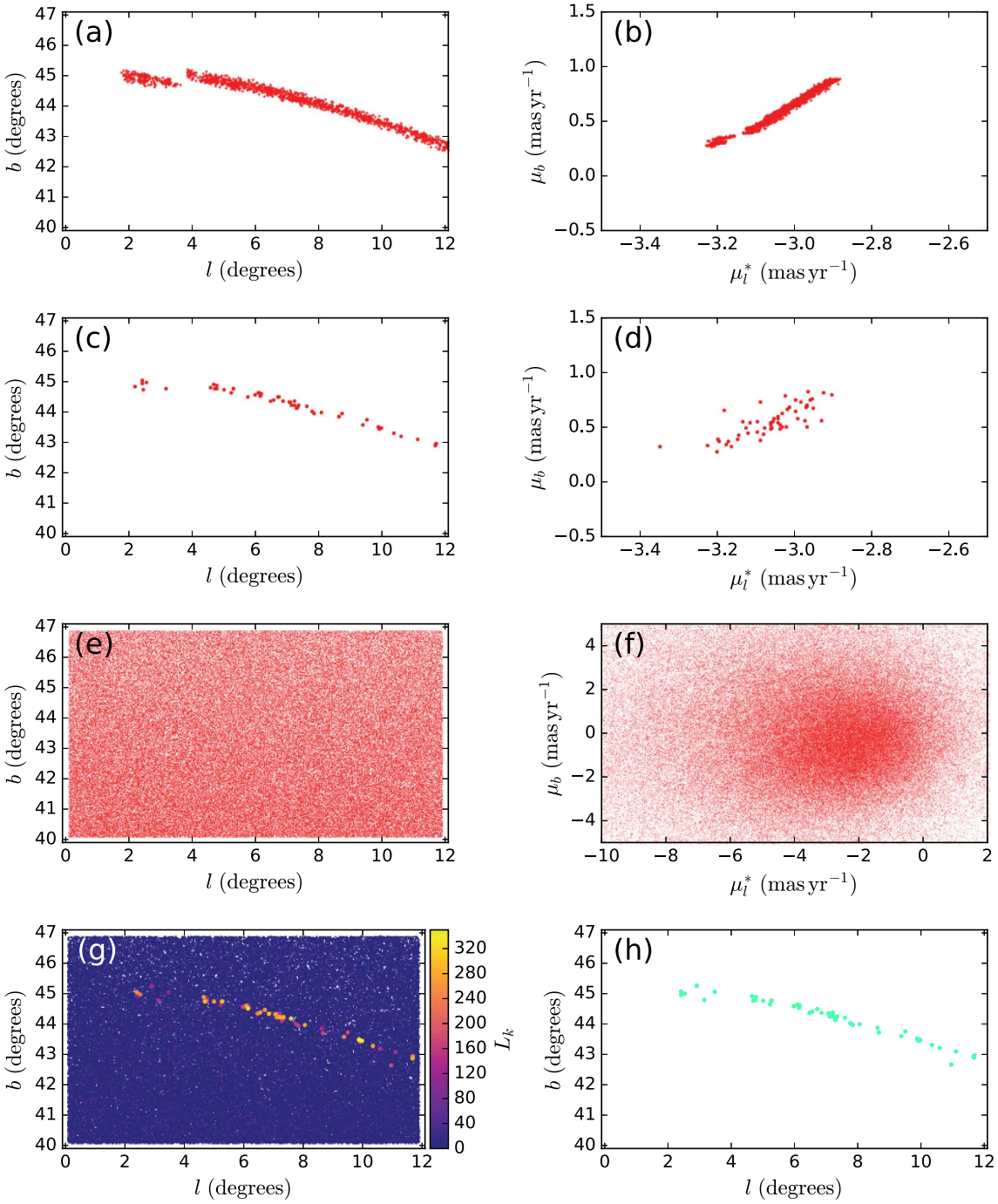

Figure 8. *N*-body stream case. The top panels (a) and (b) show the simulated stream in Galactic coordinates and proper motion space. We have purposely removed the progenitor to challenge the algorithm. (c) and (d) show the degraded version of the stream where the quality of the data is degraded in accordance to expected *Gaia* errors and only 50 data points are retained (equivalent surface brightness of $\Sigma_G \sim 32.5\,\mathrm{mag\,arcsec^{-2}}$). (e) and (f) represent the GUMS data with the mock stream superposed. There are around ∼330 000 contaminating field stars, so $n_{\mathrm{stream}}/n_{\mathrm{data}} \approx 0.015$ per cent. Panel (g) displays the relative likelihood L_k obtained from the STREAMFINDER, revealing the low contrast stream feature, while (h) represents the subsample with the highest values of L_k.

orbit. We will now also include two additional criteria that will help improve further the contrast of faint structures.

Our algorithm aims to find thin and cold stream structures. These structures are expected to be remnants of a globular cluster and are formed by their disruption and dissolution. The member stars of most star clusters follow closely stellar evolutionary models of a single age and metallicity, and although now totally disrupted, the stream stars share similar age and metallicity as that of the progenitor and hence must follow a similar isochrone track. We incorporate this concept into our algorithm, thus making use of the photometric information of each candidate group of stars identified by the algorithm.

To this end, we use as a template the *G*-band cumulative luminosity function of the same SSP model as was used to derive the distance solution with the hypertube technique. For each candidate group of stars, we calculate the Kolmogorov–Smirnoff Test prob-

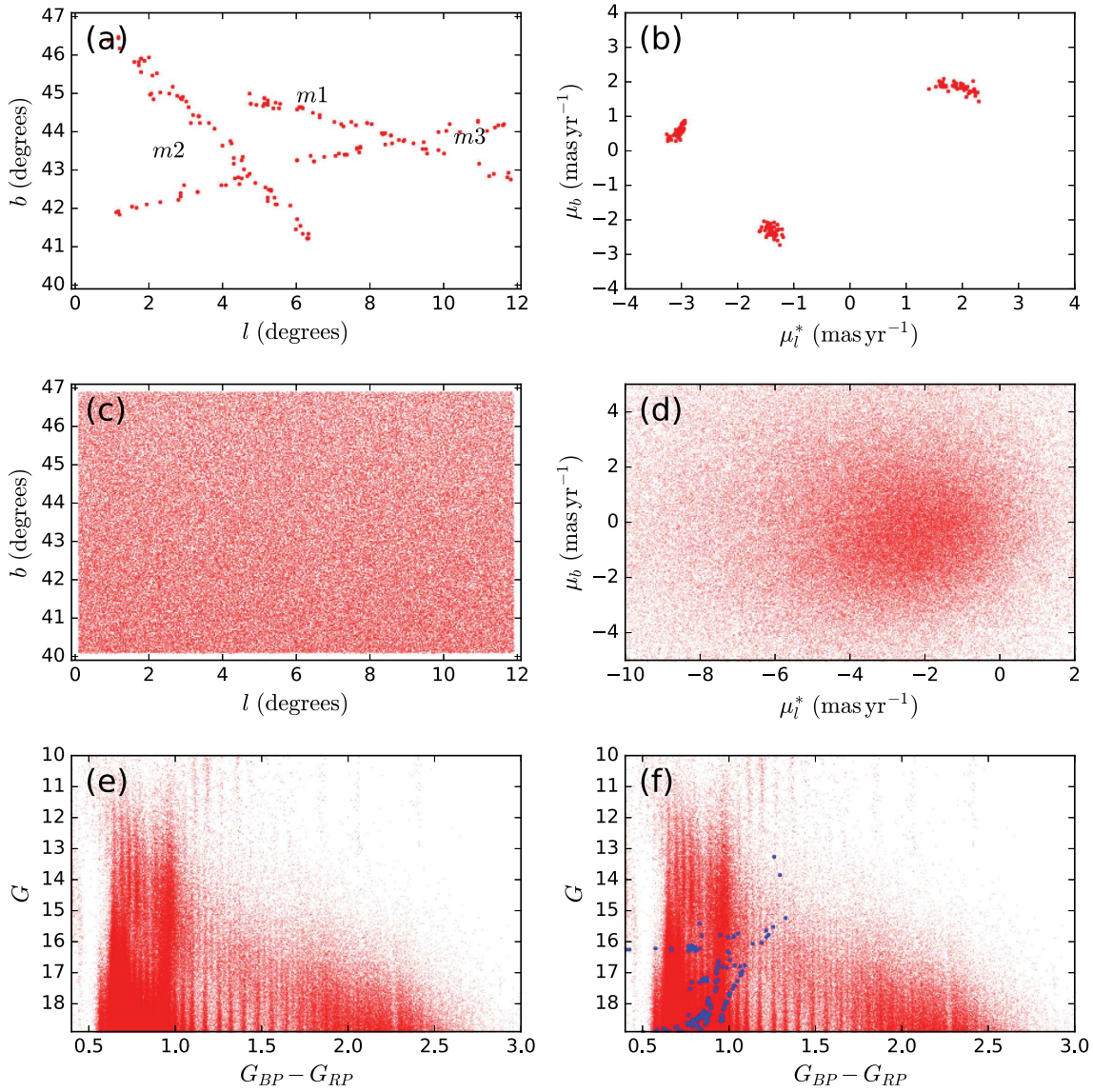

Figure 9. Multiple stream case. The top panels show the degraded version of the three *N*-body simulated streams in Galactic coordinates. The middle panels show the GUMS data with the three streams immersed. The bottom panels show the colour–magnitude distribution of these data: (e) shows the data along with the streams within it, while in (f) the stream is highlighted in blue. We chose three isochrone models appropriate for halo globular clusters with age and [Fe/H] = (10 Gyr, −1.28), (10 Gyr, −1.58), and (10 Gyr, −2.28) for, respectively, models m1, m2, and m3. Though not explicitly shown here, the streams probe distances between 10 and 28 kpc. Each stream possesses 50 stars, and has an equivalent surface brightness of $\Sigma_G \sim 32.5$ mag arcsec^{-2}.

ability $P_{\rm KS,LF}$ that the stars are drawn from this model luminosity function.

We further expect that stellar streams are extended structures, yet so far the criteria that have been described do not allow us to distinguish an extended stream from a small-scale localized overdensity. To remedy this, we incorporated an additional criterion into the algorithm to calculate the Kolmogorov–Smirnoff Test probability $P_{\rm KS,continuous}$ that the member stars of a candidate structure are uniformly distributed along the orbit segment contained within the sky window under study.

The final statistic we use is then

$$L = L_k + \ln(P_{\rm KS,LF}) + \ln(P_{\rm KS,continuous}). \quad (5)$$

Fig. 11 is an improved version of Fig. 10 after incorporating the luminosity function and the continuity criteria into the L statistic used by the algorithm. As can be seen by comparing the colour axes of the two figures, the additional criteria improve the contrast of the detection.

7 TESTING THE DETECTION LIMIT

It is useful to gauge the faintest stream structure (in terms of number of stream stars) the algorithm can detect. To this end, we reran our algorithm over the m1 mock data set, which shares the orbital properties of the Palomar 5 globular cluster. We reran the algorithm, removing one star at a time from the stream to see at what point the structure becomes lost in the noise. We found that with an initial stream containing 15 stars, 10 were recovered with values of the L statistic higher than 1 in 150 000 among the contaminating population (i.e. $\sim 4.3\sigma$). The corresponding stream has an equivalent surface brightness of $\Sigma_G \sim 33.6$ mag arcsec^{-2} over this $>10^\circ$ region, and is shown in Fig. 12. This is very promising and means

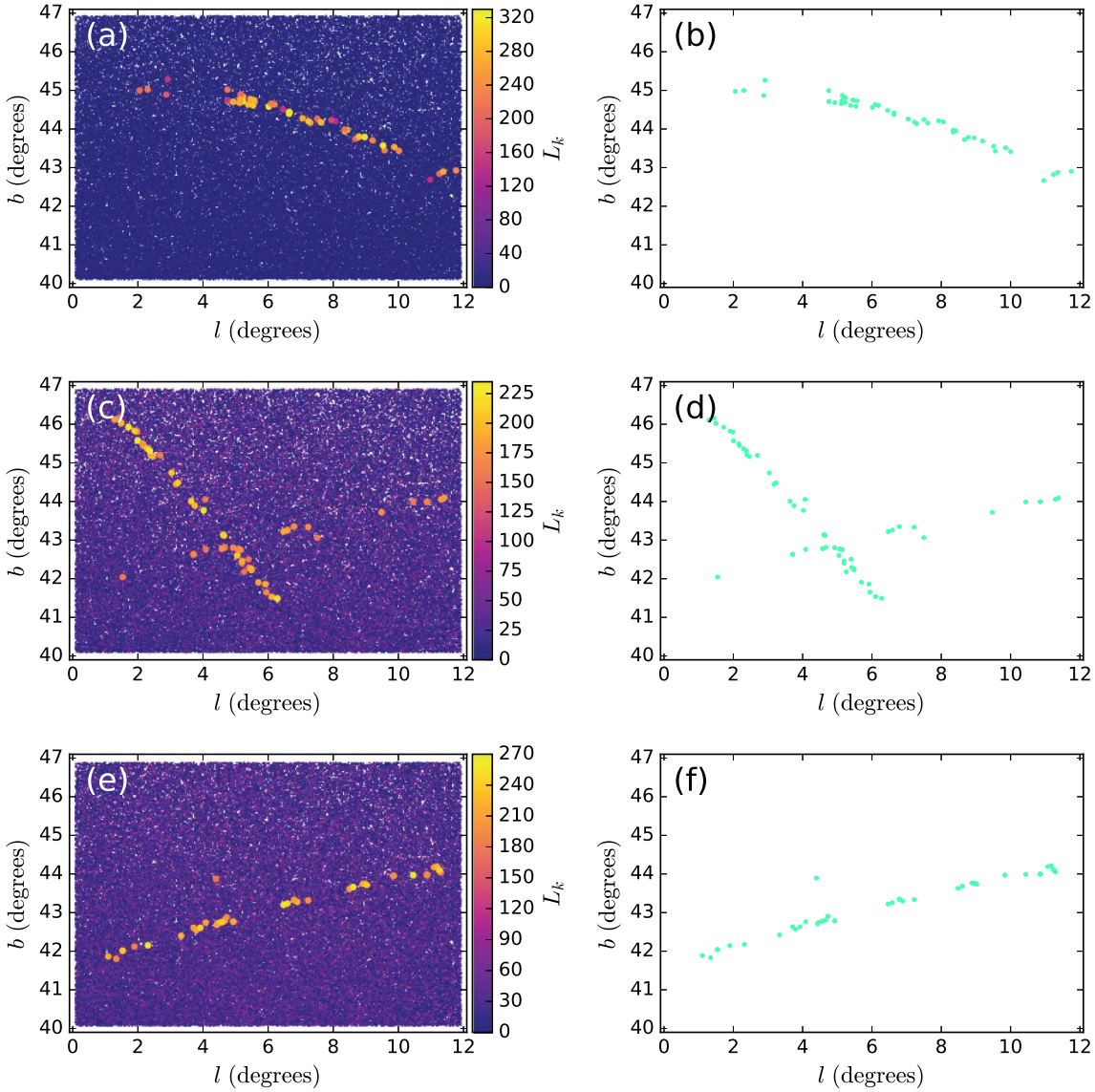

Figure 10. STREAMFINDER results for the case of multiple streams in a given patch of sky. The left-hand panels show the spatial distribution of the statistic L_k obtained using different isochrone models, and the right-hand panels show the data points with the highest L_k values. The upper, middle, and lower panels are derived using, respectively, the SSP models with age and [Fe/H] = (10 Gyr, −1.28), (10 Gyr, −1.58), and (10 Gyr, −2.28). As expected, a given isochrone model enhances the detection strength of the stream structures corresponding to that particular isochrone. (The L_k values shown here are values relative to the minimum.)

that the application of our algorithm on to the actual *Gaia* data set could reveal the presence of ultra-faint streams.

We must point out that this limit depends on the number of contaminants, the observational errors, and on the morphology of the structures that are present in the halo. However, the test case that we simulated here shares the orbit of the real Palomar 5 (albeit with a much lower surface brightness), and so we think it provides a useful preview of the detectability of a very tenuous stream at an advanced stage of tidal disruption.

8 EFFECT OF ADOPTING A WRONG GALACTIC POTENTIAL

Hitherto, we have presented test cases where the trial orbits were integrated in the same Galactic potential model in which the mock streams were originally simulated. Although the Dehnen & Binney (1998) mass model 1 we have employed here was a reasonable fit to available data in 1998, the Milky Way potential may in reality be fairly different.

To gauge the effect of adopting a wrong mass model, we reran the STREAMFINDER on exactly the same stream as shown previously in Section 4, but this time we incorporated the Dehnen & Binney (1998) mass model 4 in the detection algorithm. The resulting distribution of the statistic L is shown in Fig. 13, which can be seen to be similar to the counterpart in Fig. 8.

We suspect that by iterating over different mass models, it should be possible to find the potential that maximizes the contrast of stellar streams in the Milky Way. However, we would like to stress that the STREAMFINDER is intended as an initial detection tool. Once a sample of streams have been found, we intend to use other more accurate methods (e.g. *N*-body simulations) to model them.

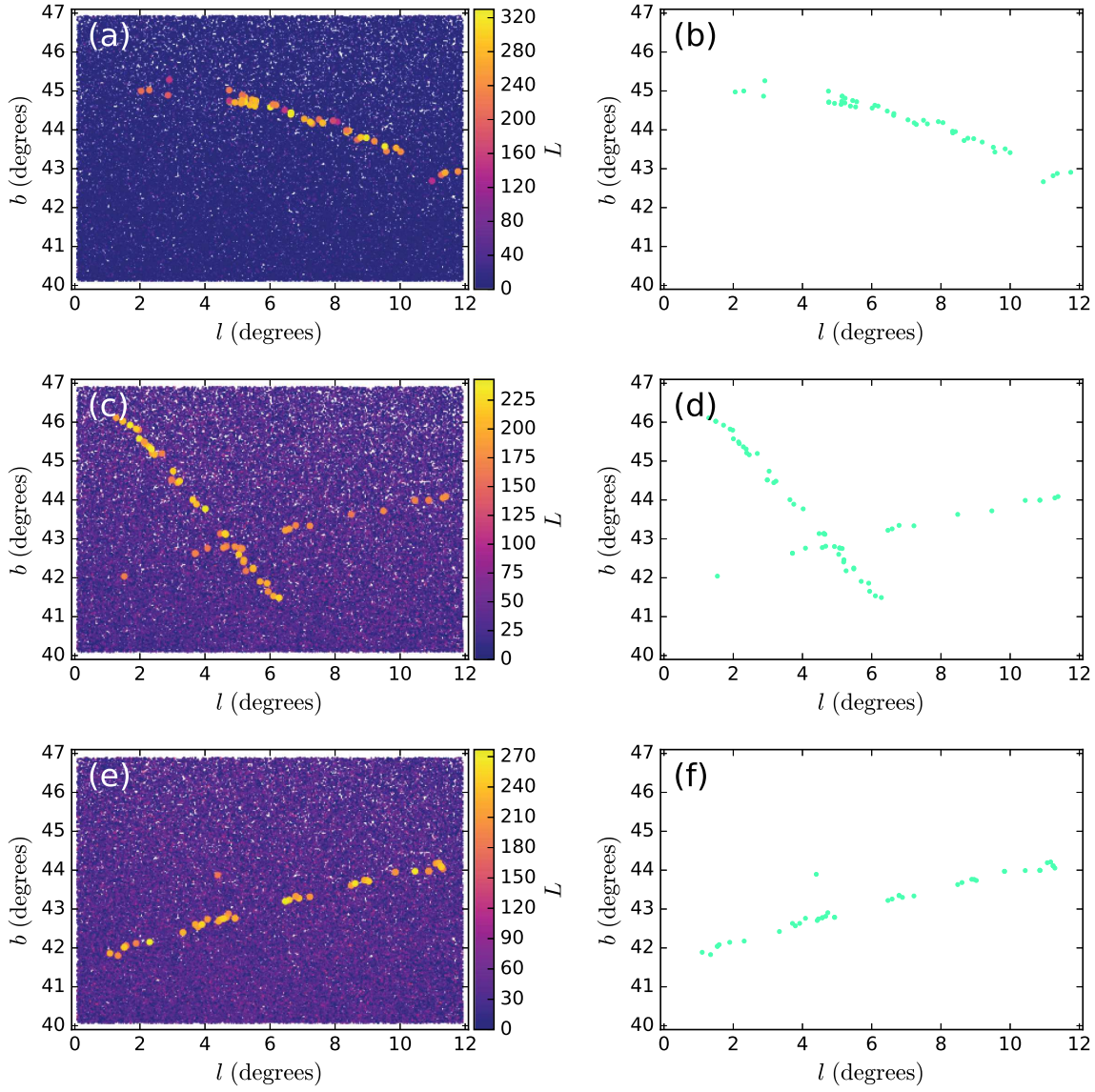

Figure 11. Luminosity function and continuity criteria. These plots are improved versions of those shown in Fig. 10, after incorporating the luminosity function and the continuity criteria in the likelihood calculation. The contrast of the streams is further improved by the additional discriminating information.

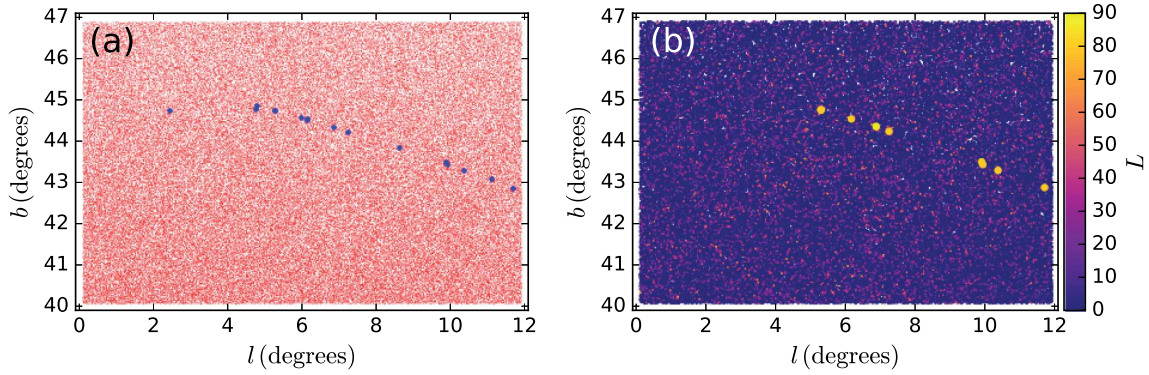

Figure 12. Detection limit test. Here, we have simulated an ultra-faint stream structure possessing only 15 stars (with $\Sigma_G \sim 33.6\,\mathrm{mag\,arcsec^{-2}}$). The spatial distribution is shown in (a) where the input stream stars are highlighted in blue, while (b) shows the corresponding L statistic: 10 stars are clearly detected above an $\sim 4.3\sigma$ threshold.

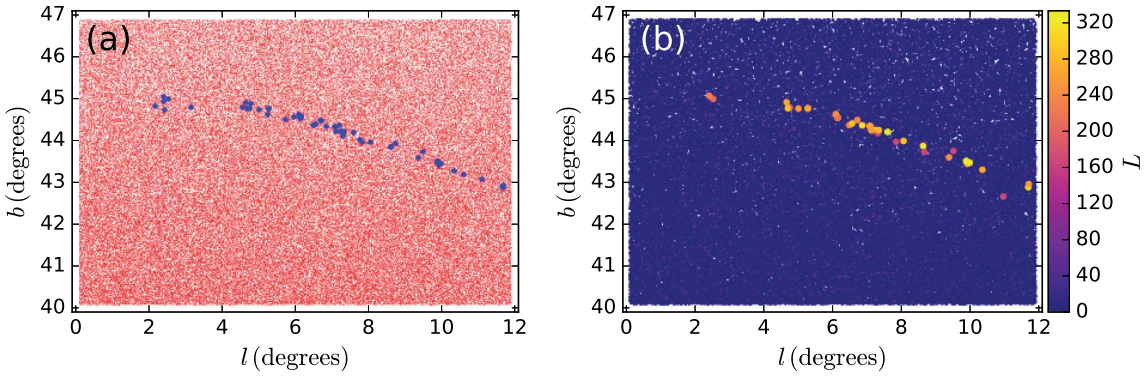

Figure 13. Galaxy mass model mismatch. (a) shows the same data and the superposed stream model as shown in Fig. 8. The stream model was simulated in DB model 1. (b) shows the corresponding L statistic obtained by using DB model 4 for integration of the trial orbits in the STREAMFINDER algorithm. It can be seen that the algorithm was easily able to detect the stream even after we forced the code to employ a wrong Galactic potential model.

9 DISCUSSION AND CONCLUSIONS

In this contribution, we have presented the STREAMFINDER, a new algorithm that aims to efficiently detect stellar stream-like features. It has been optimized to identify very faint structures using data of the quality that will soon be delivered by *Gaia* DR2. At its heart, STREAMFINDER shoots trial orbits within a realistic Galactic potential, using the astrometric and photometric measurements of the stars to select initial conditions for the orbits. These orbits are then adjusted to find the local maxima in star counts that are compatible with the trial orbit in 2D position and 2D kinematics (nevertheless, the algorithm can be easily modified to explore the full 6D phase space information available for any subsample of the data).

Every star is assigned a likelihood value based on how coherent it is with an extended stellar stream. Our tests using N-body simulated streams superimposed on the GUMS data set with kinematics degraded to *Gaia* DR2-like quality and precision show that the algorithm can detect structures lying well below previous detection limits. Because our method relies on detecting stream candidates along orbits, the algorithm can detect structures that lie along radial or other complex trajectories.

The algorithm returns a statistic that is similar to a likelihood, which must be calibrated locally to determine the structure significance, as it depends on the (varying) 'background' population. The expected distribution of the statistic in the absence of a stream structure may be estimated via the application of the STREAMFINDER to artificial data (such as the GUMS simulation) or completely empirically via the examination of the behaviour of the statistic in neighbouring regions of sky.

The design of the algorithm is such that along with the stream detection, it renders other useful insights about the detected candidate structures that can be used for further analysis.

(i) The algorithm delivers the orbital structure along which the stream lies: This is the primary by-product that the algorithm naturally returns and gives the possible set of orbital solutions that the stream might lie along. Radial velocities and distance information of the stars will be missing for the great majority of halo stars in the *Gaia* DR2 (and later) catalogues. However, since the algorithm gives the possible orbital solutions for a given stream structure, it therefore provides a means to complete the 6D phase space solutions that are possible for a given stream star.

(ii) Phase space distribution of streams: The algorithm delivers a complete 6D phase space distribution of possible orbital solutions that a given stream might be on. When executed over the entire sky, the end product would be the distribution function of stream stars in the Galactic halo. This solution could be extremely useful for recreating the pre-merging history of the Milky Way, or to perform Schwarzschild modelling to constrain the dark matter distribution in the Galaxy.

(iii) The SSP test is intrinsically incorporated into the algorithm: Most of the coherence-based detection schemes do not always take into account the best-suited stellar population model for the candidate stream structure. However, our algorithm calculates the likelihood of every stream candidate based on SSP models; thus, our approach also returns a possible set of SSP models that the stream might correspond to. This can be viewed as a low-resolution 'chemical tagging' approach, where stars can be tagged based on their age and metallicities giving an orbit–age–metallicity distribution of stars in the Milky Way halo.

(iv) Length of the structure: The algorithm also allows us to estimate the linear length of the candidate structures simply by summing along the orbit until some lower detection threshold is reached. Through subsequent modelling, this can be converted into an estimate of the minimum age since the disruption of the progenitor.

(v) Calculating orbital properties: Since the algorithm offers orbital solutions for every stream, one can easily calculate simple orbital properties of the stream structure such as the eccentricity or energy of the streams.

Motivated by these results, and to test the machinery on real data, we have applied it to the Pan-STARRS1 data set (Kaiser et al. 2002; Chambers et al. 2016a,b), the results of which will be presented in the next contribution in this series (Malhan et al. in preparation).

ACKNOWLEDGEMENTS

The authors would like to thank the anonymous referee for very useful comments that contributed to the clarity and overall improvement of the paper.

REFERENCES

Arifyanto M. I., Fuchs B., 2006, A&A, 449, 533
Balbinot E., Santiago B. X., da Costa L. N., Makler M., Maia M. A. G., 2011, MNRAS, 416, 393
Bellazzini M., Ferraro F. R., Ibata R., 2003, AJ, 125, 188
Belokurov V. et al., 2006, ApJ, 642, L137

Bernard E. J. et al., 2016, MNRAS, 463, 1759
Bovy J., Bahmanyar A., Fritz T. K., Kallivayalil N., 2016, ApJ, 833, 31
Carlberg R. G., Grillmair C. J., 2013, ApJ, 768, 171
Carlberg R. G., Grillmair C. J., Hetherington N., 2012, ApJ, 760, 75
Chambers K. C. et al., 2016a, preprint (arXiv:1612.05560)
Chambers K. C. et al., 2016b, preprint (arXiv:1612.05560)
Dalal N., Kochanek C. S., 2002, ApJ, 572, 25
de Bruijne J. H. J., 2012, Ap&SS, 341, 31
Dehnen W., 2000, ApJ, 536, L39
Dehnen W., Binney J., 1998, MNRAS, 294, 429
Dehnen W., Odenkirchen M., Grebel E. K., Rix H.-W., 2004, AJ, 127, 2753
Duffau S., Zinn R., Vivas A. K., Carraro G., Méndez R. A., Winnick R., Gallart C., 2006, ApJ, 636, L97
Erkal D., Belokurov V., Bovy J., Sanders J. L., 2016, MNRAS, 463, 102
Eyre A., Binney J., 2009, MNRAS, 400, 548
Eyre A., Binney J., 2011, MNRAS, 413, 1852
Gaia Collaboration et al., 2016, A&A, 595, A2
Grillmair C. J., 2016, Astrophysics and Space Science Library, Vol. 420, Tidal Streams in the Local Group and Beyond. Springer International Publishing, Cham
Grillmair C. J., Carlin J. L., 2016, in Newberg H. J., Carlin J. L., eds, Astrophysics and Space Science Library, Vol. 420, Tidal Streams in the Local Group and Beyond. Springer International Publishing, Switzerland. p. 87
Grillmair C. J., Dionatos O., 2006, ApJ, 643, L17
Harris W. E., 1976, AJ, 81, 1095
Ibata R. A., Lewis G. F., Irwin M. J., Quinn T., 2002a, MNRAS, 332, 915
Ibata R. A., Lewis G. F., Irwin M. J., Cambrésy L., 2002b, MNRAS, 332, 921
Ibata R. A. et al., 2017, ApJ, 848, 128
Johnston K. V., Hernquist L., Bolte M., 1996, ApJ, 465, 278
Johnston K. V., Spergel D. N., Haydn C., 2002, ApJ, 570, 656
Kaiser N. et al., 2002, in Tyson J. A., Wolff S., eds, Proc. SPIE Conf. Ser. Vol. 4836, Survey and Other Telescope Technologies and Discoveries, SPIE, Bellingham, p. 154
King I. R., 1966, AJ, 71, 64
Koposov S. E., Rix H.-W., Hogg D. W., 2010, ApJ, 712, 260
Küpper A. H. W., Balbinot E., Bonaca A., Johnston K. V., Hogg D. W., Kroupa P., Santiago B. X., 2015, ApJ, 803, 80
Law D. R., Majewski S. R., 2010, ApJ, 714, 229
Marigo P., Girardi L., Bressan A., Groenewegen M. A. T., Silva L., Granato G. L., 2008, A&A, 482, 883
Mateu C., Read J. I., Kawata D., 2017, MNRAS, preprint (arXiv:1711.03967)
Myeong G. C., Jerjen H., Mackey D., Da Costa G. S., 2017, ApJ, preprint, (arXiv:1704.07690)
Ngan W. H. W., Carlberg R. G., 2014, ApJ, 788, 181
Odenkirchen M. et al., 2001, ApJ, 548, L165
Robin A. C. et al., 2012, A&A, 543, A100
Rockosi C. M. et al., 2002, AJ, 124, 349
Sanders J. L., Bovy J., Erkal D., 2016, MNRAS, 457, 3817
Schönrich R., Binney J., Dehnen W., 2010, MNRAS, 403, 1829
Shipp N. et al., 2018, ApJ, preprint, (arXiv:1801.03097)
Smith M. C. et al., 2007, MNRAS, 379, 755
Teuben P., 1995, in Shaw R. A., Payne H. E., Hayes J. J. E., eds, ASP Conf. Ser., Vol. 77, Astronomical Data Analysis Software and Systems IV, Astron. Soc. Pac, San Francisco, p. 398
Thomas G. F., Ibata R., Famaey B., Martin N. F., Lewis G. F., 2016, MNRAS, 460, 2711
Varghese A., Ibata R., Lewis G. F., 2011, MNRAS, 417, 198
Williams M. E. K. et al., 2011, ApJ, 728, 102

This paper has been typeset from a TEX/LATEX file prepared by the author.

CHAPTER 4

APPLICATION OF STREAMFINDER ONTO PAN-STARRS1 PROPER MOTION DATASET

It is wrong always, everywhere, and for anyone to believe anything upon insufficient evidence- **William K. Clifford**

Related paper : **STREAMFINDER II: A possible fanning structure parallel to the GD-1 stream in Pan-STARRS1**, 2018, Malhan et al , published in *MNRAS* (ADS entry)

Abstract

The workings of the STREAMFINDER algorithm was tested with real proper motion data from the Pan-STARRS1 survey. By selecting targets down to $r_{P1} = 18.5$ mag, it was showed that the software is easily able to detect the GD-1 stellar stream, whereas the same structure remains below a useful detection limit when using a Matched Filter technique, demonstrating the power of the algorithm. Also, the radial velocity solutions provided by the STREAMFINDER for GD-1 candidate members were found to be in good agreement with the spectroscopic observations. Furthermore, the algorithm also detected a $\sim 40°$ long structure[1] approximately parallel to GD-1, and which fans out from it, possibly a sign of stream-fanning due to the triaxiality of the Galactic potential. This analysis validated the STREAMFINDER algorithm and showcased the promise it held for detecting and analysing stellar streams in the Gaia DR2 catalogue.

[1] It was later brought to our attention that the parallel sequence to GD-1 was previously reported as PS1-E stream [12].

4.1 Introduction

Motivated by the stream detection results obtained from the studies based on simulations (presented in Chapter 3), and to test the reliability of the STREAMFINDER's machinery on a real dataset, the algorithm was applied to the Pan-STARRS1 survey. For this, the algorithm was applied to the region containing the so called "GD-1" stream. The GD-1 stream [72] is a quintessential example of a dynamically cold and narrow stream structure that extends over 80° in length over the sky [149] and is devoid of any significant internal velocity dispersion or distortions [119]. Therefore, GD-1 stream served as a perfect example of the class of stream structure that STREAMFINDER was constructed to find.

4.2 Data

Prior to Gaia DR2, the Pan-STARRS1 (PS1) proper motion dataset [27, 100, 117, 182] was the only astrophysical dataset that provided proper motion measurements (along with the positions and the photometry) of the stars for a major volume of the Galactic halo down to $r_{P1} \sim 22.0$ mag. Therefore, this dataset provided the test bed to verify the implementation of the algorithm onto a realistic astrophysical catalogue.

For this, a rectangular patch of PS1 sky with $130° < \alpha < 220°$ and $15° < \delta < 70°$ was selected. This region corresponded to the region where GD-1 stream lies (shown in Figure 4.1).

4.3 Comparison between STREAMFINDER and Matched Filter

It was deemed most useful to compare the STREAMFINDER algorithm with the Matched Filtering (MF) technique [5, 156]. The major reason for challenging MF was that most of the known Milky Way streams, like the Pal-5 stream [143], the NGC 5466 structure [73], the Orphan stream [10, 69], Lethe, Cocytos, and Styx [70], Indus, Ravi, Jhelum, Chenab [172] and others, along with GD-1 itself, were detected via through MF technique, that shows the power it holds over other stream detection methods.

For this comparison making, only those stars in the PS1 dataset were selected that were brighter than $r_{P1} = 18.5$ and followed the criterion $0.15 < g_{P1} - r_{P1} < 0.30$. The magnitude cut was done both to challenge the MF algorithm (explained in the paper attached) and in order to retain stars with useful proper motion information (as shown in Figure 4.1, uncertainties in PS1 proper motions become substantially large from 19 mag onwards). The colour-cut was done in order to discard the local M dwarfs of the disk [106].

First, the MF technique was executed. GD-1 did not appear with a very strong detection significance, a nearly non-detection with a significance of $\approx 2.5\sigma$ (see upper panel in Figure 4.2). This was not surprising as most of the stars which lied at the *Main Sequence Turn Off* and below in GD-1, the CMD region where the power of the MF lies, were discarded while making

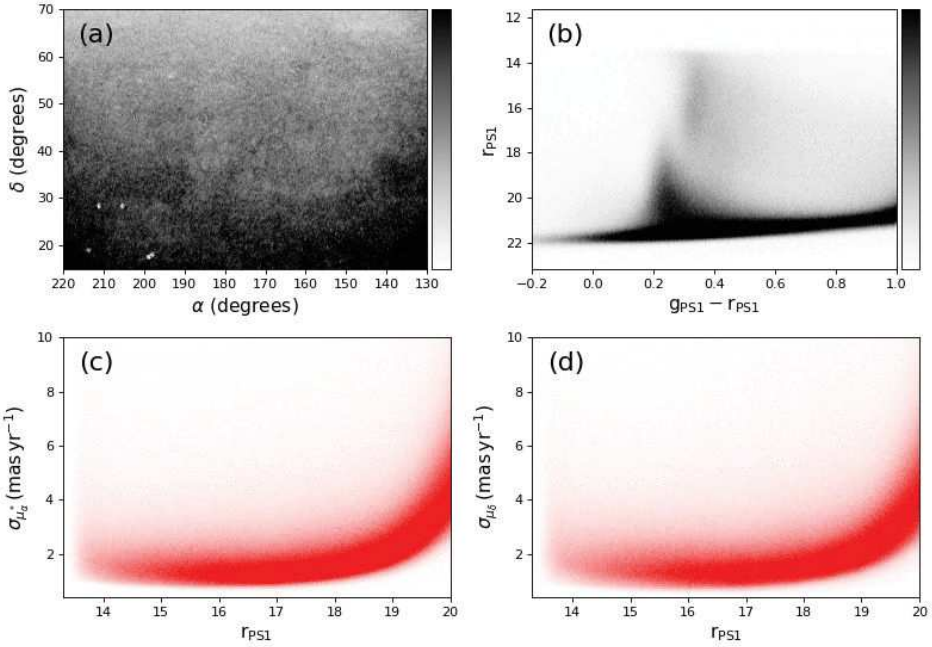

Figure 4.1: PS1 proper motion dataset. (a) Raw density map of stars in the given patch of the sky obtained using the PS1 catalogue. The darker regions imply higher density regions. The GD-1 stream lies in this particular area of the sky. (b) Colour-magnitude Hess-Diagram of the same patch of sky. The stars on the red side of $g_{P1} - r_{P1} = 1.0$ consists mostly of local M dwarfs of the disk and were not used in the analysis. Panels (c) and (d) show the behaviour of the proper motion uncertainties with respect to r_{P1}. These uncertainties become very large for $r_{P1} > 20$.

the magnitude selection in the dataset. The stars that received higher weights based on the MF weighting scheme were thence less in number and the contrast of the GD-1 structure in the density plot was much diminished.

For the STREAMFINDER case, a similar analysis was followed as presented in Chapter 3. The orbits were integrated within a realistic Galactic potential model [38], and these orbits were then projected into the heliocentric frame of observables. Moreover, the algorithm used a pre-selected isochrone model with metallicity [Fe/H] = −1.4 and Age = 9 Gyr, that essentially corresponded to the proposed SSP of the GD-1 stream[2]. The output of the STREAMFINDER algorithm was summarised in density plots that are displayed in the lower panels of Figure 4.2. Unlike MF, the simultaneous kinematical, spatial and photometric analysis of the data points allowed the algorithm to detect GD-1 stream. Along with it, another stream alongside GD-1 also gets detected. Significance of this structure was found to be comparable to that of GD-1, appearing at a detection level of $> 4.4\sigma$. This parallel sequence to GD-1 was PS1-E stream [12].

[2]However, Chapter 6 shows that $[Fe/H]_{GD1} = -2.25 \pm 0.04$ [119]

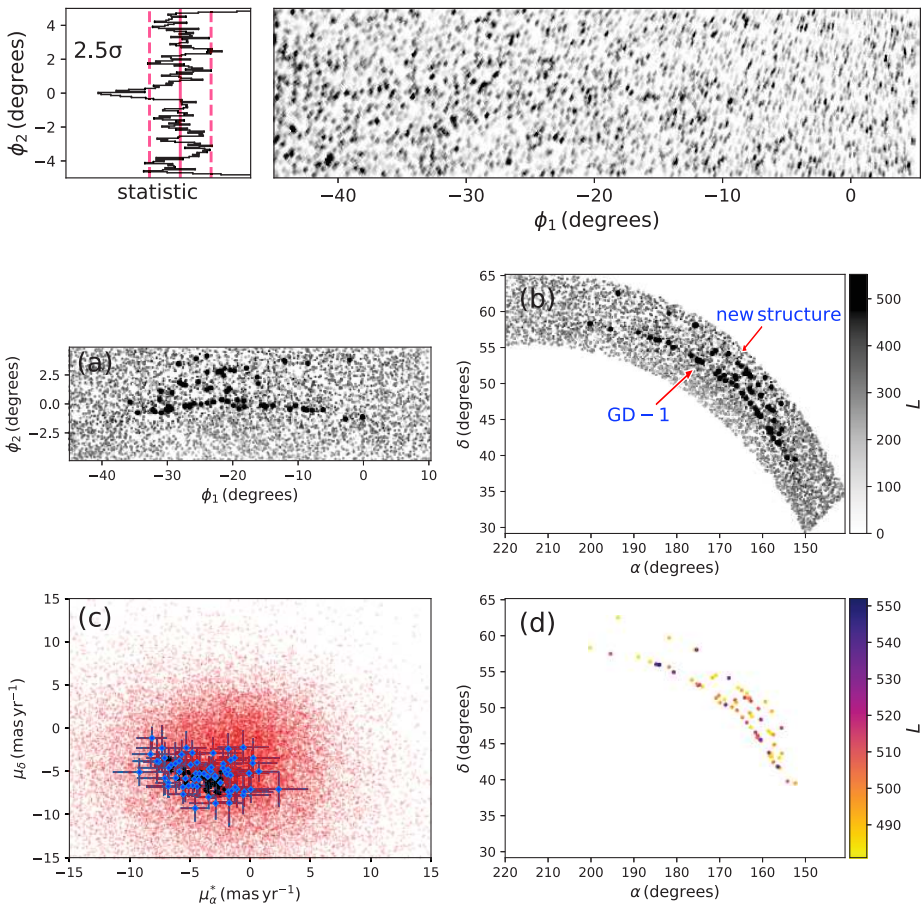

Figure 4.2: Comparison between MF and STREAMFINDER. *Top panel* : Non-detection of GD-1 using the MF technique. The GD-1 stream appears with only $\approx 2.5\sigma$ detection significance, due to the absence of stars fainter than $r_{P1} = 18.5$. *Lower panels*: Detection of GD-1 with the STREAMFINDER. (a) The algorithm after processing the given patch of sky returns a density plot that is shown here in the rotated coordinate system that aligns with the GD-1 stream. The highest likelihood stars (0.2% of the sample) are marked in large black dots that immediately reveal the GD-1 structure along $\phi_2 \sim 0$. Along with GD-1, STREAMFINDER revealed PS1-E stream towards the north. (b) The same as (a) but in equatorial coordinates. (c) The proper motions of the stars of the data are shown in red. The highest likelihood stars are marked with blue dots together with their error bars. The black coloured dots show the expected proper motion values of these highest likelihood stars, a by-product of STREAMFINDER. (d) The highest likelihood stars are shown in equatorial coordinates, revealing the two distinct structures that are detected at comparable significance. Based on the statistics of the contamination, STREAMFINDER detected both stream structures at a $> 4.4\sigma$ level of confidence.

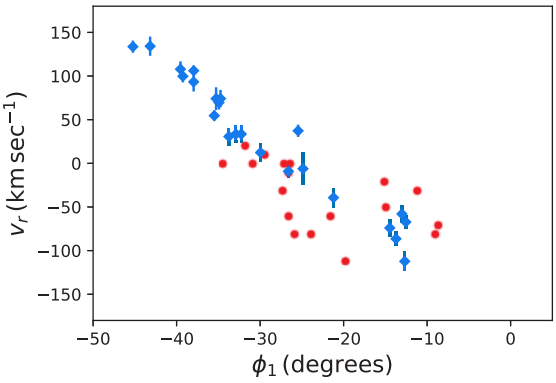

Figure 4.3: Retrieving the missing phase-space information of streams stars with STREAMFINDER. The red dots represent the radial velocity solutions of the GD-1 signal stars that are derived as a by-product of the application of the algorithm. The blue markers are the observed radial velocities of GD-1 stars [106], corrected for the radial component of the Solar reflex motion (taking $V_{\rm circ} = 220\,{\rm km\,s^{-1}}$). The agreement of the orbital solutions with the observations illustrates the power of the STREAMFINDER algorithm in predicting the missing phase-space information of stream stars.

4.4 Retrieving missing phase-space information for GD-1 stream

As STREAMFINDER integrates orbits in order to detect stream structures, the primary by-product that the algorithm naturally returns are the possible set of orbital solutions along which the stream might lie. The power of this by-product was also highlighted by comparing the possible set of radial velocity solutions of the highest likelihood GD-1 stars with the observations. This comparison is shown in Figure 4.3 that displays the agreement between the predicted and the observed radial velocity measurements. This analysis showed that the algorithm has potential not only for detecting streams, but also for predicting the missing phase-space information of the stream stars.

Radial velocity and distance information will be missing for the great majority of halo stars in the Gaia DR2 (and successive Gaia catalogues). However, since the algorithm gives the possible orbital solutions for the detected stream structures, it therefore provides a means to complete the 6D phase-space solutions that are possible for a given stream star.

4.5 Results and Discussions

The detection of the GD-1 and PS1-E streams in the PS1 proper motion catalogue validated the workings of the STREAMFINDER algorithm. Their positive detection suggested that other similar structures in Gaia DR2 should also be detected, as the proper motion uncertainties of stars were to be a factor of ~ 5 better in each proper motion dimension (yielding a ~ 25 times better-resolved

phase-space volume).

Although GD-1 and PS1-E appeared as clearly-distinguishable stream-like structures on the sky, interestingly, their orbits seemed to overlap in distance and velocity space (see Figure 6 in the paper attached with this Chapter). At the distance of GD-1, the PS1 proper motion uncertainties correspond to a typical uncertainty on the transverse motion of $> 50\,\mathrm{km\,s^{-1}}$. This, together with the absence of radial velocity measurements, made it hard to speculate on the orbital properties of the system at that stage. It should be interesting to compare the metallicity of GD-1 and PS1-E, and to study their orbits in detail with proper motions from Gaia DR2 together with accurate radial velocities.

The algorithm naturally delivers the possible set of orbital solutions of the detected stream structures. The analysis showed good agreement between the radial velocities of the GD-1 stars obtained as a by-product from STREAMFINDER and from spectroscopic observations. This missing phase-space information that the algorithm provides can be used to estimate the 6D distribution function of Milky Way streams to some extent, and hence probe the nature and formation history of these star streams and the Galactic halo that together they span.

4.6 Related Paper

Monthly Notices
of the
ROYAL ASTRONOMICAL SOCIETY

MNRAS **478,** 3862–3870 (2018)
Advance Access publication 2018 May 18

doi:10.1093/mnras/sty1338

STREAMFINDER II: A possible fanning structure parallel to the GD-1 stream in Pan-STARRS1

Khyati Malhan,[1]★ Rodrigo A. Ibata,[1] Bertrand Goldman,[1,2] Nicolas F. Martin,[1,2] Eugene Magnier[3] and Kenneth Chambers[3]

[1]*Université de Strasbourg, CNRS, Observatoire Astronomique de Strasbourg, UMR 7550, F-67000 Strasbourg, France*
[2]*Max-Planck-Institut fur Astronomie, Königstuhl 17, D-69117 Heidelberg, Germany*
[3]*Institute of Astronomy, University of Hawaii, 2680 Woodlawn Drive, Honolulu, Hawaii 96822, USA*

Accepted 2018 May 16. Received 2018 May 16; in original form 2018 April 9

ABSTRACT

STREAMFINDER is a new algorithm that we have built to detect stellar streams in an automated and systematic way in astrophysical datasets that possess any combination of positional and kinematic information. In Paper I, we introduced the methodology and the workings of our algorithm and showed that it is capable of detecting *ultra-faint* and distant halo stream structures containing as few as ∼15 members ($\Sigma_G \sim 33.6$ mag arcsec^{-2}) in the Gaia dataset. Here, we test the method with real proper motion data from the Pan-STARRS1 survey, and by selecting targets down to $r_0 = 18.5$ mag we show that it is able to detect the GD-1 stellar stream, whereas the structure remains below a useful detection limit when using a Matched Filter technique. The radial velocity solutions provided by STREAMFINDER for GD-1 candidate members are found to be in good agreement with observations. Furthermore, our algorithm detects a ∼40° long structure approximately parallel to GD-1, and which fans out from it, possibly a sign of stream-fanning due to the triaxiality of the Galactic potential. This analysis shows the promise of this method for detecting and analysing stellar streams in the upcoming Gaia DR2 catalogue.

Key words: stars: kinematics and dynamics – Galaxy: evolution – Galaxy: formation – Galaxy: halo – Galaxy: kinematics and dynamics – Galaxy: structure.

1 INTRODUCTION

Stellar streams hold great promise for Galactic Archaeology (Freeman & Bland-Hawthorn 2002). Their orbital structures are sensitive tracers of galaxy formation history, the underlying Galactic potential (Johnston, Hernquist & Bolte 1996; Eyre & Binney 2009; Law & Majewski 2010) and the lumpiness in the dark matter distribution (Ibata et al. 2002a; Johnston, Spergel & Haydn 2002; Carlberg, Grillmair & Hetherington 2012; Erkal et al. 2016; Sanders, Bovy & Erkal 2016). Therefore, both stream-detection and stream dynamical analysis are currently hot fields of astrophysics and small-scale cosmology.

In the past two decades, several stellar streams have been detected around the Milky Way galaxy (Ibata et al. 2001; Odenkirchen et al. 2001; Belokurov et al. 2006; Grillmair & Dionatos 2006; Grillmair & Johnson 2006; Grillmair 2009; Williams et al. 2011a; Bernard et al. 2014; Koposov et al. 2014; Martin et al. 2014; Bernard et al. 2016; Grillmair 2017; Helmi et al. 2017; Jethwa et al. 2017; Li et al. 2017; Mateu, Read & Kawata 2017; Myeong et al. 2017a,b; Shipp et al. 2018a; see also Grillmair & Carlin (2016) and Smith (2016) for recent reviews). Most streams were detected in large area surveys such as SDSS (York et al. 2000), Pan-STARRS1 (Chambers et al. 2016; Kaiser et al. 2002), and DES (Shipp et al. 2018a), and a few by radial velocity surveys like RAVE (Steinmetz et al. 2006) and TGAS (Gaia Collaboration et al. 2016; Lindegren et al. 2016). The much larger number of streams found in the photometric surveys is simply a consequence of much better statistics. However, this handicap of the kinematic surveys will soon be overcome because of the ESA/Gaia mission (de Bruijne 2012; Gaia Collaboration et al. 2016, 2018), whose second data release (DR2) is scheduled for the 2018 April 25.[1] It is likely that the Milky Way contains a large number of hitherto undetected stellar streams. With the exceptional quality of the data expected in Gaia DR2, it is clearly worthwhile to devote effort to design new and better stream detection schemes.

Existing stream detection techniques employ data analysis methodologies that exploit only a subset of the information that we will soon have on large numbers of stars in the Milky Way. For

★ E-mail: kmalhan07@gmail.com

[1]Gaia DR2 shall deliver parallaxes and proper motions for all stars down to $G_0 \sim 21$, and radial velocities for stars brighter than $G_0 \sim 13$

example, the Pole Count technique (Johnston et al. 1996; Ibata et al. 2002b) utilizes only the positions of the stars, whereas the Matched-Filter technique (Rockosi et al. 2002; Balbinot et al. 2011) employs only the positions and the photometry of the stars. Most of the detections of co-moving groups have been made on the basis of structural coherence by looking for clumping of stars only in velocity space (Duffau et al. 2006; Williams et al. 2011b; Helmi et al. 2017). Stream detection techniques engaging all the stellar information (positions, kinematics, and photometry) simultaneously should definitely improve the scope and the significance of stream detection. It has been long suggested that the right set of coordinates to identify substructures is the space of the integrals of motion, but that requires complete knowledge of the 6D phase-space distribution of the stars, something that even Gaia will only deliver for bright and nearby objects (a very small subset of the full Gaia sample, see Ibata et al. 2017). Therefore, stream search methods using integrals of motion will not be very useful for detecting streams that exist in the distant halo of the Milky Way.

Given the quality of the data that shall soon become available from Gaia DR2, and what we perceived as the shortcomings of the existing stream detection techniques, we decided to build a new stream detecting algorithm (the STREAMFINDER; Malhan & Ibata 2018, hereafter Paper I). The main purpose of STREAMFINDER is to detect cold and narrow tidal stellar streams of the type produced by the tidal disruption of globular clusters or very low-mass galaxies. The algorithm incorporates our prior knowledge of stellar streams and analyses data in position, kinematics, and photometry space simultaneously to maximize the stream detection efficiency. Our algorithm makes use of the realization that the members of a stream can be contained within a 6D hyper-dimensional tube (or hypertube) that coils much like an orbit in phase-space, with width in real and velocity space similar to the size and velocity dispersion of the progenitor cluster. For each star (with acceptable proper motion measurements), the algorithm shoots orbits using the phase-space information of the data, as observed today, in a realistic Milky Way potential. These orbits are transformed into hypertubes within the algorithm, with plausible phase-space width and length. The number of stars that get encapsulated within these hypertubes are then counted. After processing all the survey stars in this manner, the output of the algorithm can be summarized in a density plot where the likelihood of every star corresponds to how well a star is coherently compatible with other stars in the data to form a stream like structure (see fig. 7 of Paper I).

In Paper I, we introduced the STREAMFINDER algorithm that we have built, explained the physical motivation behind it and demonstrated its workings. Our analysis, based on a mock dataset of the quality Gaia will deliver, suggested that the algorithm is capable of detecting even ultra-faint stream features lying well below previous detection limits. Our tests showed that the algorithm will be able to detect distant halo stream structures $>10^{\circ}$ long containing as few as $\sim$15 members ($\Sigma_G \sim 33.6$ mag arcsec^{-2}) in the Gaia dataset.

Motivated by these results, and to test the reliability of the machinery that we have built on a real dataset, we apply it here to the Pan-STARRS1 survey, in a region containing the so-called 'GD-1' stream. The GD-1 stream is a quintessential example of a dynamically cold and narrow stream structure extending over 60° on the sky and devoid of any significant internal velocity dispersion or distortion (Grillmair & Dionatos 2006; Carlberg & Grillmair 2013). It is a perfect example of the class of stream structure STREAMFINDER is constructed to find.

This paper is arranged as follows. In Section 2 we briefly describe the data used. Section 3 shows the detection of the GD-1 stream using the Matched Filter (MF) technique. In Section 4 we make the comparison between our algorithm STREAMFINDER and the MF. In Section 5 we discuss the discovery of a new structure that we have found in the neighbourhood of GD-1. In Section 6 we present additional power that our algorithm holds in predicting the missing phase-space information of the detected stream structures. Finally, in Section 7 we discuss our results.

2 DATA ANALYSIS

We use the Pan-STARRS1 (PS1) proper motion dataset (Kaiser et al. 2002, 2010; Tonry et al. 2012; Chambers et al. 2016; Magnier et al. 2016) in all of the present analysis. In terms of astrometry, PS1 delivers 2D positions and 2D proper motions of the stars along with photometry in five bands (g_{P1}, r_{P1}, i_{P1}, z_{P1}, y_{P1}) with a 5σ single epoch depth of (23.3, 23.2, 23.1, 22.3, 21.4). At present, the PS1 survey is the only dataset that delivers proper motions for all stars with $\delta > -30^{\circ}$ down to $r_{P1} \sim 23.0$. In terms of kinematic quality, this dataset will soon be superseded by Gaia DR2 (for those stars with $G_o < 21$), nevertheless, the dataset provides us a unique opportunity to test the functionality and feasibility of our algorithm on an actual astrophysical catalogue before Gaia DR2 becomes available. But even after the Gaia release, this dataset will still remain highly useful for analysing stars fainter than the Gaia detection limit.

Each image of PS1 is calibrated against the Gaia DR1 position. To this end, the Gaia position of the astrometric reference stars are propagated back to the PS1 image epoch, using a model describing the Galactic rotation and the Solar motion and using the photometric distance to the reference stars; see Green et al. (2015) and Magnier et al. (2016), respectively. If that model were a perfect description of the motions of the Galaxy and the Sun, the resulting PS1 proper motions and parallaxes obtained by fitting the PS1, 2MASS, and Gaia (if available) positions would be inertial and extragalactic objects would have null proper motions and parallaxes. To confirm this, we first selected a sample of galaxies using both the light profiles of the objects, and their colours. Specifically, we required that the difference $m_{PSF} - m_{aperture}$ be larger than 0.2 mag on average for the four filters g, r, i, and z and be all smaller than 0.5 mag, with a signal-to-noise ratio larger than 20. In addition, we required an infrared colour of J-W1 > 1.7 mag where W1 is the WISE 3.4-μm magnitude, limited to the 12.0–15.2-mag range, and J is the UKIDSS two-arcsec-radius aperture magnitude if available ($SNR > 7$), or the 2MASS J magnitude otherwise ($SNR > 4$) (Kovács & Szapudi 2015). Finally, for each equatorial hemisphere, we calculated on a 1024x1024 grid the 3-σ-clipped mean (iterated three times) of the galaxies' proper motions over a box of 6° on a side.

Over the area of interest to this study, about 90 galaxies were used for each grid point. The corrections for μ_α and μ_δ vary smoothly from -0.5 to $+2.4$ mas yr^{-1} and from $+2.0$ to $+3.4$ mas yr^{-1}, respectively. For each catalogue entry, we subtracted the values taken at the nearest grid point from the measured proper motions to obtain inertial proper motions.

We select the rectangular patch of PS1 sky with $130^{\circ} < \alpha < 220^{\circ}$ and $15^{\circ} < \delta < 70^{\circ}$, which corresponds to the region where GD-1 stream lies. The stars in this selected part of the sky were corrected for foreground reddening using the 3D extinction map provided by Green et al. (2015) .[2] The de-reddended and proper motion corrected data is shown in Fig. 1.

[2] http://argonaut.skymaps.info/

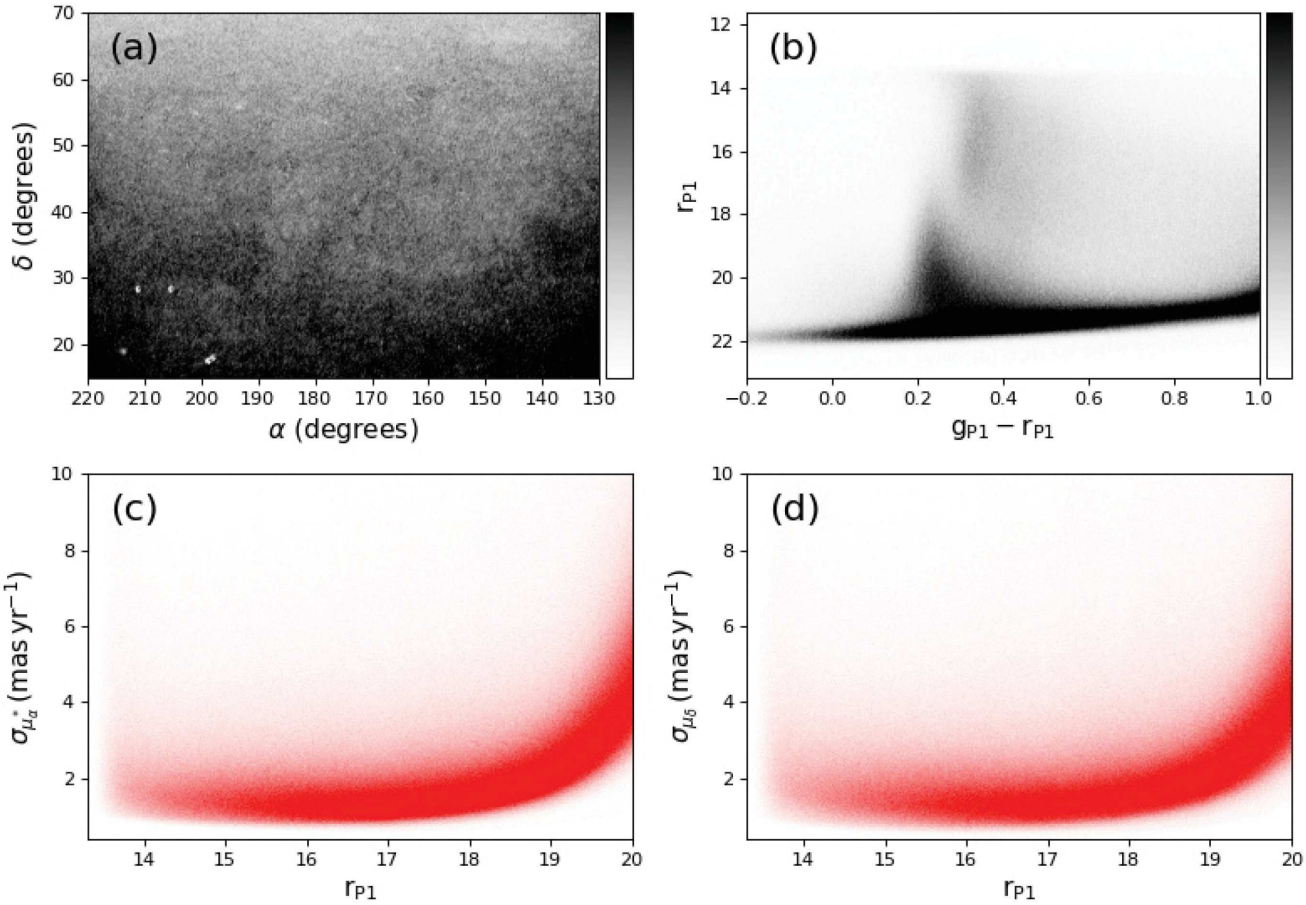

Figure 1. PS1 proper motion dataset. (a) Raw density map of stars in the given patch of the sky obtained using the PS1 catalogue. The darker regions imply higher density regions. The GD-1 stream lies in this particular area of the sky. (b) Colour–magnitude Hess-Diagram of the same patch of sky. The stars on the red side of $g_{P1} - r_{P1} = 1.0$ consists mostly of local M dwarfs of the disc and are not used in our analysis. Panels (c) and (d) show the behaviour of the proper motion uncertainties with respect to r_{P1}. These uncertainties become very large for $r_{P1} > 20$.

3 DETECTION OF GD-1 USING A MATCHED FILTER

We first present the detection of the GD-1 stream using the MF technique, the method originally used for its detection (Grillmair & Dionatos 2006). MF (Rockosi et al. 2002; Balbinot et al. 2011) is an optimal contrast adjusting technique that relies on the colour–magnitude information of the stars. The technique works by selecting a suitable colour–magnitude diagram (CMD) single stellar population (SSP) template model that represents the stellar stream members to be detected. For many halo streams the discriminating power of the MF resides mainly at the main-sequence turnoff (MSTO) and below where the stellar density rapidly increases and where it also lies blueward of the contaminating foreground population. The GD-1 stream was initially discovered in the density plot that was obtained as a result of the MF prepared using the CMD of the M13 globular cluster.

To reproduce the GD-1 detection with the MF method, we first impose CMD cuts to retain the upper main-sequence region $0.1 \leq g_{P1} - r_{P1} \leq 0.6$, and trim the data below $r_{P1} \sim 21.5$. We call the resulting subset Dataset 1.

We created an MF following the procedure described in Balbinot et al. (2011), and using the CMD of M13 globular cluster as the target template (similar to Grillmair & Dionatos 2006). We divided the CMD into bins of 0.01 mag in colour, and 0.1 in magnitude as well as 0.1° spatially on the sky. The resulting weighted image was then smoothed with a Gaussian kernel with $\sigma = 0.2°$.

The spatial density map thus obtained is shown in Fig. 2a. Since it is convenient to work in the spherical coordinate that is aligned with the GD-1 stream, we made use of the rotation matrix provided by Koposov, Rix & Hogg (2010) to make a transformation of coordinates from equatorial to these new spherical coordinates. A similar MF density plot is also shown in this new rotated spherical system in Fig. 2d. Note that the GD-1 stream is visible as a high-contrast stream feature at a detection level of $\approx 6.5\sigma$.

4 COMPARISON BETWEEN STREAMFINDER AND MATCHED FILTER

We deem it most useful to compare the STREAMFINDER to the MF technique. This is because, first of all, the GD-1 stream is too faint to be detected by a simple pole count. Secondly, the proper motion uncertainties in the PS1 dataset are too large for the GD-1 stream to be detected by using analyses that only incorporate the stellar velocity information. Moreover, most of the known Milky Way streams, such as the Pal-5 stream (Odenkirchen et al. 2001), the NGC 5466 structure (Grillmair & Johnson 2006), the Orphan stream (Grillmair 2006; Belokurov et al. 2006), Lethe, Cocytos, and Styx (Grillmair 2009), Indus, Ravi, Jhelum, Chenab (Shipp

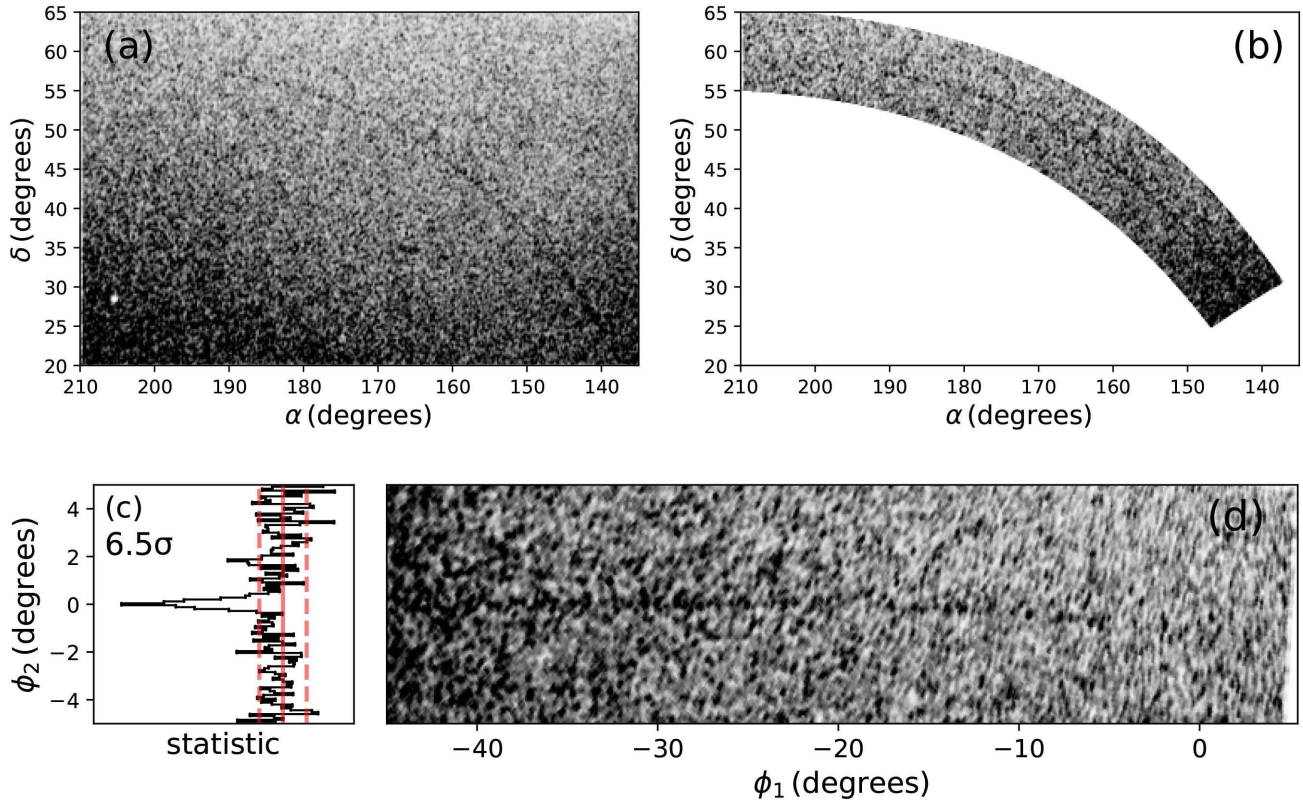

Figure 2. GD-1 stream detection using the MF technique. (a) MF density map of the chosen patch of sky in PS1, derived using the M13 globular cluster as the CMD template. The GD-1 stream can be seen as a $\sim 60^\circ$ extended structure on the sky. All stars with $14 < r_{P1} < 21.5$ and $0.1 < g_{P1} - r_{P1} < 0.6$ were used to create this density plot. (b) The same MF density plot is now shown in a particular area of the sky that runs along the GD-1 stream. (c) The MF plot is represented in the rotated spherical coordinate system aligned approximately with the GD-1 stream. The GD-1 stream can be seen to lie along $\varphi_2 \sim 0$ in this plot. (d) We estimate that the stream is detected at a significance level of $\approx 6.5\sigma$.

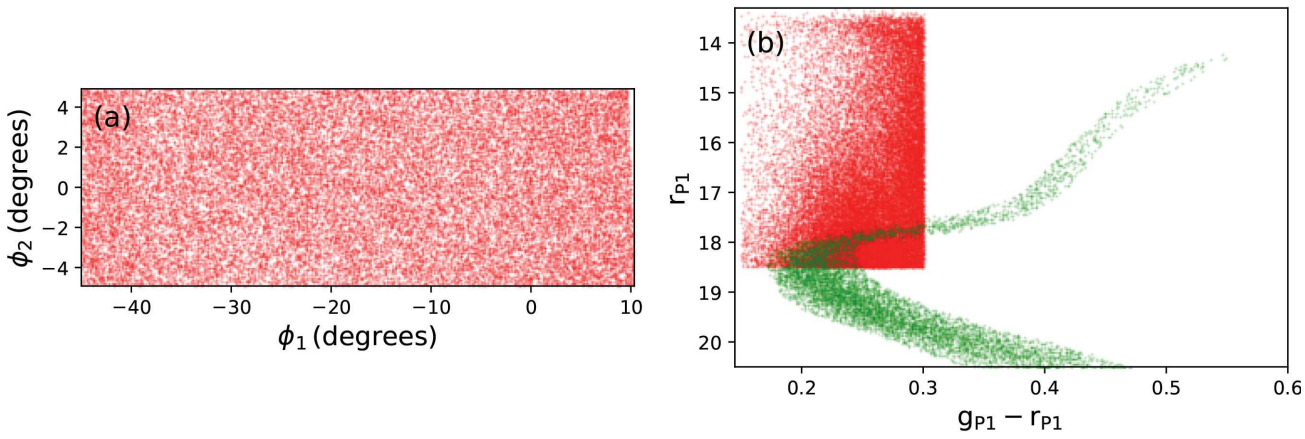

Figure 3. Dataset 2. To make a comparison between STREAMFINDER and the MF technique we take a subset of the PS1 data around GD-1, selecting stars with $r_{P1} < 18.5$ and $0.15 < g_{P1} - r_{P1} < 0.30$. (a) The subset is presented in the rotated coordinate frame. GD-1 lies at $\varphi_2 \sim 0$ in this frame. (b) Represents the CMD of this data subset. The green dots correspond to the M13 globular cluster CMD, originally used to detect the GD-1 stream. The plot shows that most of the MSTO stars in the GD-1 are lost, due to the colour–magnitude selection window.

et al. 2018b) and others, along with GD-1, were detected via an application of the MF technique, which demonstrates its power for stream detection.

The MF technique is expected to fail in detecting streams broadly in two cases, (1) if the stream happens to be elongated along the line of sight, or (2) if the stream is too low in contrast. The first case depends on the nature of the stream, however the second case is what can be examined here to compare the MF to STREAMFINDER. A stream could be observed to be low in contrast because (1) it is an ancient structure that is now very spread out spatially, or (2) it is distant in the halo and hence its MSTO, where the majority of stream stars are expected to lie, lies below the photometric limit of the survey. Indeed, there could be many faint Milky Way stellar streams that exist in the halo but that have remained undetected

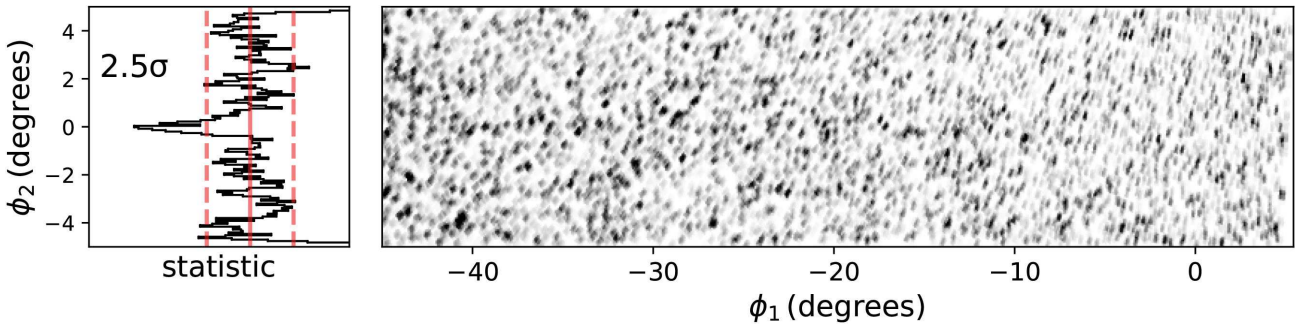

Figure 4. Non-detection of GD-1 in Dataset 2 using the MF technique. The GD-1 stream now appears with only $\approx 2.5\sigma$ detection significance, due to the absence of stars fainter than $r_{Pl} = 18.5$.

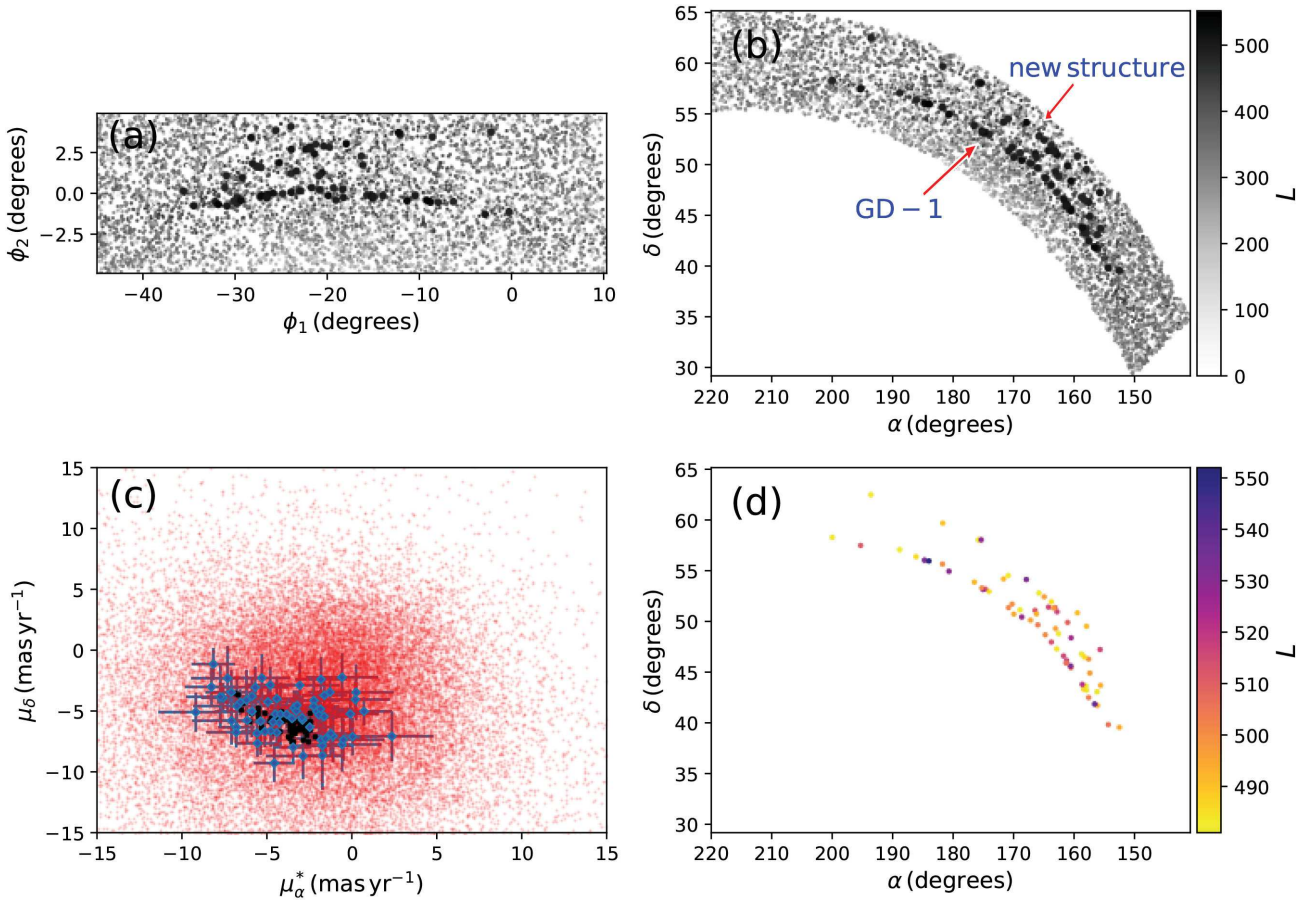

Figure 5. Detection of GD-1 with the STREAMFINDER in Dataset 2. (a) The algorithm after processing the given patch of sky returns a density plot that is shown here in the rotated coordinate system. The highest likelihood stars (0.2 per cent of the sample) are marked in large black dots that immediately reveal the GD-1 structure along $\varphi_2 \sim 0$. Along with GD-1, STREAMFINDER reveals another stream feature towards the north. (b) The same as (a) but in equatorial coordinates. (c) The proper motions of the stars of Dataset 2 are shown in red. The highest likelihood stars are marked with blue dots together with their error bars. The black coloured dots show the expected proper motion values of these highest likelihood stars, a by-product of STREAMFINDER. (d) The highest likelihood stars are shown in equatorial coordinates, revealing the two distinct structures that are detected at comparable significance. Based on the statistics of the contamination, STREAMFINDER detects both stream-like structures at a $>4.4\sigma$ level of confidence.

by MF-based weighting techniques due to the above-mentioned reasons. STREAMFINDER combats this low-density problem by performing a multidimensional analysis of the stars, incorporating all the stellar information in terms of positions, kinematics, and photometry that in turn improves the stream detection efficiency.

While we cannot alter the physical structure of GD-1, we can legitimately simulate making it harder to detect by artificially reducing the limiting magnitude of the survey. To this end, we select only those stars in Dataset 1 that are brighter than $r_{Pl} = 18.5$ and follow the criterion $0.15 < g_{Pl} - r_{Pl} < 0.30$. The colour cut follows the selection made by Koposov et al. (2010). We refer to this truncated sample as Dataset 2, which is shown in Fig. 3. While a redder colour cut would have included some GD-1 sub-giants, it would also have given rise to a greater contamination fraction, lowering the significance of the detection.

4.1 Matched Filter – once again

We execute the MF technique once again using Dataset 2. The resulting density plot is shown in Fig. 4. GD-1 does not appear with a very strong detection significance, a nearly non-detection with a significance of $\approx 2.5\sigma$. This is not surprising as most of the stars that lie at the MSTO and below in GD-1 were discarded while constructing the Dataset 2. The stars that received higher weights based on the MF weighting scheme are now less in number and the contrast of the GD-1 structure in the density plot is much diminished.

4.2 Positive detection of GD-1 in Dataset 2 with STREAMFINDER

We now feed the very same Dataset 2 to STREAMFINDER. The algorithm uses the positions and proper motions of the stars to sample orbits. For the purpose of integrating these orbits, we use only those stars for which

$$\sigma_{\mu_\alpha} < 3.0\,\mathrm{mas\,yr^{-1}} \text{ and } \sigma_{\mu_\delta} < 3.0\,\mathrm{mas\,yr^{-1}}\,, \quad (1)$$

so that the obtained orbital solutions can be trusted. A proper motion of $\sigma_\mu = 3\,\mathrm{mas\,yr^{-1}}$ at a distance of 10 kpc corresponds to an uncertainty in the transverse velocity of $\sim 150\,\mathrm{km\,s^{-1}}$, which is already a huge uncertainty compared to expected relative motion of the stream and the contaminating population. However, once the hypertubes are calculated, we use the full Dataset 2 sample to count the number of stars that lie within the hypertubes, and to calculate the corresponding likelihood values.

The orbits are integrated within the Galactic potential model 1 of Dehnen & Binney (1998), and these orbits are then projected into the heliocentric frame of observables. For this, we assume a Galactocentric distance of the Sun of 8.5 kpc and adopt the peculiar velocity of the Sun $\boldsymbol{V}_\odot = (u_\odot, v_\odot, w_\odot) = (11.1, 12.24, 7.25)\,\mathrm{km\,s^{-1}}$ (Schönrich, Binney & Dehnen 2010). Moreover, our algorithm uses a pre-selected isochrone model in order to sample orbits in distance space, as explained in Paper I. The selected isochrone model essentially corresponds to the proposed SSP of the stream. For this, we choose an isochrone with metallicity [Fe/H] = -1.4 and age 9 Gyr (Koposov et al. 2010) from the Padova stellar population models (Marigo et al. 2008). This isochrone model matches well the CMD of M13 cluster and hence that of GD-1. Other parameter ranges used to integrate orbits in the Galaxy were identical to those detailed in Paper I.

The spatial distribution of stream likelihood calculated by the STREAMFINDER is shown in Fig. 5. Unlike the MF result from the same sample (Dataset 2), one can now vividly see the GD-1 structure, which is detected at the $\approx 4.4\sigma$ level of confidence. This means that the multidimensional analysis done by STREAMFINDER easily allows it to detect stream structures that would otherwise be lost with an MF search. This detection of an extremely low-contrast stream shows the power of our algorithm over the MF and hence over many other stream-detection techniques. Moreover, our algorithm makes sure that the detected structure is in fact stream-like – spatially extended and coherent in velocity space (as can be seen in Fig. 5).

The candidate members of the GD-1 stream identified by the STREAMFINDER are listed in Table 1.

Table 1. Highest likelihood stars candidates in PS1 along the GD-1 track, as obtained by the STREAMFINDER. Columns 1 and 2 list the sky positions and columns 3 and 4 are the g_{P1} and r_{P1} magnitudes (the median of the PS1 measurements).

RA (deg)	DEC (deg)	g_{P1}	r_{P1}
154.33723	39.82138	18.44	18.18
161.73164	46.59564	18.40	18.19
157.58469	42.49022	18.47	18.21
158.63541	43.79097	18.59	18.30
160.50852	45.44162	18.50	18.25
160.56969	45.60858	18.54	18.25
161.22963	46.14118	18.38	18.13
161.25371	45.96201	18.54	18.27
161.30762	45.89013	18.16	17.87
156.59654	41.85462	18.49	18.24
163.75657	47.96208	18.31	18.04
165.99967	49.65492	18.32	18.02
168.64583	50.43288	18.32	18.08
174.67653	53.19757	18.20	17.91
175.04661	53.14976	18.45	18.20
184.73228	56.03422	18.37	18.11
184.00126	55.96127	18.42	18.19
180.68427	54.94157	18.17	17.91
195.29246	57.48671	18.38	18.09

5 PROBABLE FANNING OF THE GD-1 STREAM

The likelihood distribution plot shown in Fig. 5 reveals another stream-like feature alongside GD-1. We find that the significance of this structure is comparable to that of GD-1, appearing at a detection level of $>4.4\sigma$. Grillmair & Dionatos (2006) mention in passing that 'There may be a second, more diffuse feature with $174^\circ < \alpha < 200^\circ$ about 3° to the north of [GD-1]'. Here we confirm the detection of the feature at a level of significance sufficient to confirm its discovery. The structure appears to be extended over a length of $\sim 40^\circ$ from $155^\circ < \alpha < 195^\circ$.

In Fig. 6, we show possible orbital solutions for both GD-1 and this additional structure that we obtain as a by-product of STREAMFINDER (see Paper I). Although the two features appear as clearly distinguishable stream-like structures on the sky (Fig. 6a), interestingly, their orbits seem to overlap in distance and velocity space.

At the distance of GD-1, the PS1 proper motion uncertainties correspond to a typical uncertainty on the transverse motion of $>50\,\mathrm{km\,s^{-1}}$. This, together with the absence of radial velocity measurements, makes it hard to speculate on the orbital properties of the system at this stage. The possible candidate members of the structure parallel to GD-1 are listed in Table 2.

6 RETRIEVING MISSING PHASE-SPACE INFORMATION FROM STREAMFINDER

As STREAMFINDER integrates orbits in order to detect stream structures, the primary by-product that the algorithm naturally returns is the possible set of orbital solutions along which the stream might lie. We highlight the power of this by-product by comparing the possible set of radial velocity solutions of the highest likelihood GD-1 stars we obtain from STRAMFINDER with the radial velocities of possible GD-1 members listed in table1 of Koposov et al. (2010). The comparison is shown in Fig. 7 that displays the

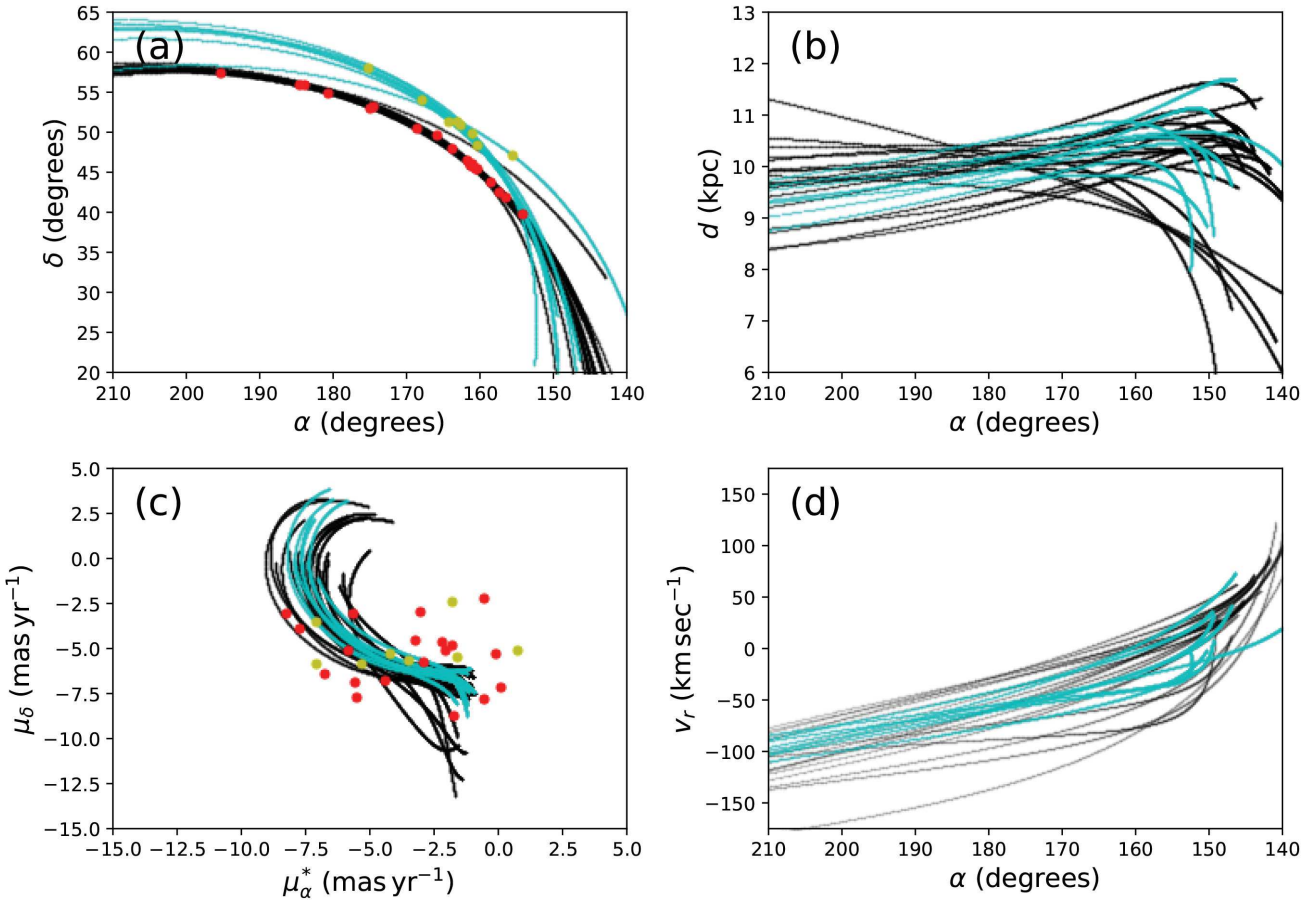

Figure 6. Orbital solutions of GD-1 and the parallel structure. The 27 stars with highest likelihood are plotted here in red dots (for GD-1) and yellow (for the feature to the north). We use their orbital solutions, obtained as a by-product from STREAMFINDER, to make a comparison with the observations. The top left (bottom left) plot compares the orbits with these data points in position (proper motion) space. The orbits obtained from GD-1 and the parallel structure candidate members are shown in black and cyan colours, respectively. The top right (bottom right) plot shows the behaviour of the orbits of the two streams in distance (radial velocity) space. Note the overlapping of the orbits at $(\alpha, \delta) \sim (152^\circ, 38^\circ)$.

Table 2. As Table 1, but for the highest likelihood stars obtained by the STREAMFINDER selected along the structure that appears parallel to GD-1.

RA (deg)	DEC (deg)	g_{P1}	r_{P1}
155.69694	47.22650	18.54	18.31
160.48647	48.38166	18.61	18.38
161.06528	49.90054	18.36	18.07
167.88944	54.13320	18.44	18.19
162.80495	50.95156	18.39	18.08
164.22409	51.40948	18.53	18.29
163.13786	51.35826	18.45	18.17
175.35981	58.04287	18.29	18.02

agreement between the predicted and the observed stellar velocity measurements. This analysis shows that our algorithm has potential not only for detecting streams, but also for predicting the missing phase-space information of the stream stars.

Radial velocity and distance information will be missing for the great majority of halo stars in the Gaia DR2 (and successive Gaia catalogues). However, since our algorithm gives the possible orbital solutions for the detected stream structures, it therefore provides a means to complete the 6D phase-space solutions that are possible for a given stream star.

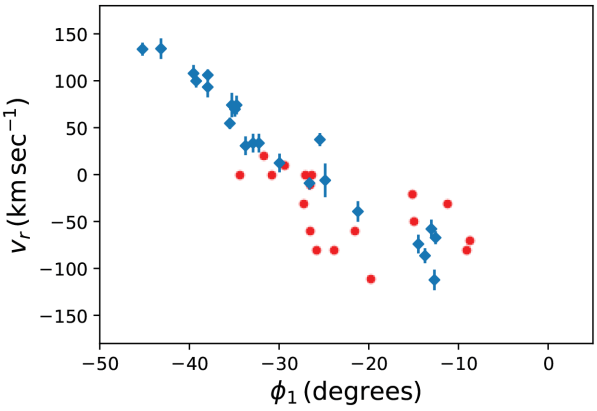

Figure 7. Retrieving the missing phase-space information of streams stars with STREAMFINDER. The red dots represent the radial velocity solutions of the GD-1 signal stars that are derived as a by-product of the application of the algorithm. The blue markers are the observed radial velocities of GD-1 stars as tabulated by Koposov et al. (2010), corrected for the radial component of the Solar reflex motion (taking $V_o = 220\,\mathrm{km\,s^{-1}}$). The STREAMFINDER sampled orbits in radial velocity space at intervals of $10\,\mathrm{km\,s^{-1}}$ (which effectively causes an uncertainty of $10\,\mathrm{km\,s^{-1}}$ on the red dots). The agreement with the observations illustrates the power of our algorithm in predicting the missing phase-space information of stream stars.

7 DISCUSSION AND CONCLUSIONS

In this contribution, we have presented the application of our STREAMFINDER algorithm onto the PS1 proper motion dataset in order to detect the GD-1 stream. We chose to analyse a magnitude-limited sample with $r_{P1} < 18.5$ which removes most of the MSTO stars of the GD-1 stream, while still containing the stars with well-measured proper motions. While this trimmed sample leads to what is effectively a non-detection with an MF search, the application of STREAMFINDER onto the very same data readily shows up the stream at a significance level of $>4.4\sigma$. This both validates our algorithm and the proper motion measurements in the PS1 catalogue.

In addition, we also confirm the presence of a parallel stream-like structure that appears in the neighbouring region of GD-1 at a significance level comparable to that of GD-1, initially suggested by Grillmair & Dionatos (2006). The similarities in the distance and kinematic properties of GD-1 and the parallel stream are striking, and indeed, they currently appear to be converging towards $\alpha \sim 154^\circ$, $\delta \sim 40^\circ$. It will be interesting to compare the metallicity of GD-1 and the parallel feature, and to study their orbits in detail with proper motions from Gaia DR2 together with accurate radial velocities.

In a very recent paper, Price-Whelan & Bonaca (2018) suggested that the progenitor of GD-1 lies at $\varphi_1 = -15^\circ$, based on the overdensity of stars that they obtain in that region (see their Figure 1). To some extent, the evidence presented here also advocates a similar position for the GD-1's progenitor (see the kink feature in Fig. 2 d and the overdensity of GD-1 stars in Fig. 5 at $\varphi_1 \sim -18^\circ$). This seems to make the stream-fanning origin for the parallel structure somewhat less plausible as the fanning is expected to cause a spreading of the tidal arms at locations along the stream away from the progenitor (Pearson et al. 2015). However in another recent study, de Boer et al. (2018) suggested that the GD-1 progenitor is located at the position of an underdensity in their MF map at $\varphi_1 = -45^\circ$ ($\alpha \sim 146^\circ$, $\delta \sim 32^\circ$, our coordinate conversion) which is surrounded by overdense stream segments on either side. If their interpretation is correct, the region displayed in Fig. 5 is fully occupied by the trailing stream. Given the similar distances, orbits, and stellar populations of GD-1 and the parallel structure, the spatial configuration shown in Fig. 5 d is therefore highly suggestive of stream-fanning (Pearson et al. 2015, cf. their Figure 4). The fanning-out of the orbits of the stream could be provoked by the triaxiality of the bar; it will be interesting in future work to simulate the dynamical evolution of the GD-1 progenitor given these new observational constraints. However, at the present time we cannot rule out the alternative possibility that the parallel structure is a new stellar stream formed from a different progenitor than that of GD-1.

The positive detection of GD-1 in this PS1 proper motion sample with the STREAMFINDER suggests that it will be possible to find other similar structures in Gaia DR2, where the proper motion uncertainties of stars will be a factor of ∼5 better in each proper motion dimension (yielding a ∼25 times better-resolved phase-space volume). Later Gaia releases are expected to further improve the astrometric accuracy by more than a factor of 5.

Our algorithm naturally delivers the possible set of orbital solutions of the detected stream structures. Our analysis here shows good agreement between the radial velocities of the GD-1 stars obtained as a by-product from STREAMFINDER and from spectroscopic observations. This missing phase-space information that the algorithm provides may be used to estimate the distribution function of Milky Way streams to some extent, and hence probe the nature and formation history of these star streams and the Galactic halo that together they span.

Note added in proof. It has been brought to our attention that the parallel sequence to GD-1 was previously reported by Bernard et al (2016), who named it PS1-E.

ACKNOWLEDGEMENTS

The Pan-STARRS1 Surveys (PS1) and the PS1 public science archive have been made possible through contributions by the Institute for Astronomy, the University of Hawaii, the Pan-STARRS Project Office, the Max-Planck Society and its participating institutes, the Max Planck Institute for Astronomy, Heidelberg and the Max Planck Institute for Extraterrestrial Physics, Garching, The Johns Hopkins University, Durham University, the University of Edinburgh, the Queen's University Belfast, the Harvard-Smithsonian Center for Astrophysics, the Las Cumbres Observatory Global Telescope Network Incorporated, the National Central University of Taiwan, the Space Telescope Science Institute, the National Aeronautics and Space Administration under Grant No. NNX08AR22G issued through the Planetary Science Division of the NASA Science Mission Directorate, the National Science Foundation Grant No. AST-1238877, the University of Maryland, Eotvos Lorand University (ELTE), the Los Alamos National Laboratory, and the Gordon and Betty Moore Foundation.

REFERENCES

Balbinot E., Santiago B. X., da Costa L. N., Makler M., Maia M. A. G., 2011, MNRAS, 416, 393
Belokurov V. et al., 2006, ApJ, 642, L137
Bernard E. J. et al., 2014, MNRAS, 443, L84
Bernard E. J. et al., 2016, MNRAS, 463, 1759
Carlberg R. G., Grillmair C. J., 2013, ApJ, 768, 171
Carlberg R. G., Grillmair C. J., Hetherington N., 2012, ApJ, 760, 75
Chambers K. C. et al., 2016, preprint (arXiv:1612.05560)
de Boer T. J. L., Belokurov V., Koposov S. E., Ferrarese L., Erkal D., Côté P., Navarro J. F., 2018, MNRAS, 477, 1893
de Bruijne J. H. J., 2012, Ap&SS, 341, 31
Dehnen W., Binney J., 1998, MNRAS, 294, 429
Duffau S., Zinn R., Vivas A. K., Carraro G., Méndez R. A., Winnick R., Gallart C., 2006, ApJ, 636, L97
Erkal D., Belokurov V., Bovy J., Sanders J. L., 2016, MNRAS, 463, 102
Eyre A., Binney J., 2009, MNRAS, 400, 548
Freeman K., Bland-Hawthorn J., 2002, ARA&A, 40, 487
Gaia Collaboration et al., 2016, A&A, 595, A2
Green G. M. et al., 2015, ApJ, 810, 25
Grillmair C. J., 2006, ApJ, 645, L37
Grillmair C. J., 2009, ApJ, 693, 1118
Grillmair C. J., 2017, ApJ, 847, 119
Grillmair C. J., Carlin J. L., 2016, in Newberg H. J., Carlin J. L., eds, 420, Tidal Streams in the Local Group and Beyond, p.87
Grillmair C. J., Dionatos O., 2006, ApJ, 643, L17
Grillmair C. J., Johnson R., 2006, ApJ, 639, L17
Gaia Collaboration Brown et al., 2018, A&A
Helmi A., Veljanoski J., Breddels M. A., Tian H., Sales L. V., 2017, A&A, 598, A58
Ibata R., Lewis G. F., Irwin M., Totten E., Quinn T., 2001, ApJ, 551, 294
Ibata R. A., Lewis G. F., Irwin M. J., Quinn T., 2002a, MNRAS, 332, 915
Ibata R. A., Lewis G. F., Irwin M. J., Cambrésy L., 2002b, MNRAS, 332, 921
Ibata R. A. et al., 2017, ApJ, 848, 128
Jethwa P. et al., 2017, preprint (arXiv:1711.09103)
Johnston K. V., Hernquist L., Bolte M., 1996, ApJ, 465, 278
Johnston K. V., Spergel D. N., Haydn C., 2002, ApJ, 570, 656
Kaiser N. et al., 2002, in Tyson J. A., Wolff S., eds, 4836, Survey and Other Telescope Technologies and Discoveries, p. 154

Kaiser N. et al., 2010, in Ground-based and Airborne Telescopes III. p. 77330E
Koposov S. E., Rix H.-W., Hogg D. W., 2010, ApJ, 712, 260
Koposov S. E., Irwin M., Belokurov V., Gonzalez-Solares E., Yoldas A. K., Lewis J., Metcalfe N., Shanks T., 2014, MNRAS, 442, L85
Kovács A., Szapudi I., 2015, MNRAS, 448, 1305
Law D. R., Majewski S. R., 2010, ApJ, 714, 229
Li G.-W. et al., 2017, Res. Astron. Astrophys., 17, 062
Lindegren L. et al., 2016, A&A, 595, A4
Magnier E. A. et al., 2016, preprint (arXiv:1612.05242)
Marigo P., Girardi L., Bressan A., Groenewegen M. A. T., Silva L., Granato G. L., 2008, A&A, 482, 883
Martin N. F. et al., 2014, ApJ, 787, 19
Mateu C., Read J. I., Kawata D., 2017, MNRAS, 474, 4112
Myeong G. C., Jerjen H., Mackey D., Da Costa G. S., 2017a, ApJ, 840, L25
Myeong G. C., Jerjen H., Mackey D., Da Costa G. S., 2017b, ApJ, 840, L25
Odenkirchen M. et al., 2001, ApJ, 548, L165
Pearson S., Küpper A. H. W., Johnston K. V., Price-Whelan A. M., 2015, ApJ, 799, 28
Price-Whelan A. M., Bonaca A., 2018, preprint (arXiv:1805.00425)
Rockosi C. M. et al., 2002, AJ, 124, 349
Sanders J. L., Bovy J., Erkal D., 2016, MNRAS, 457, 3817
Schönrich R., Binney J., Dehnen W., 2010, MNRAS, 403, 1829
Shipp N. et al., 2018a, preprint (arXiv:1801.03097)
Shipp N. et al., 2018b, preprint (arXiv:1801.03097)
Smith M. C., 2016, in Newberg H. J., Carlin J. L., eds, 420, Tidal Streams in the Local Group and Beyond, p.113
Steinmetz M. et al., 2006, AJ, 132, 1645
Tonry J. L. et al., 2012, ApJ, 750, 99
Williams M. E. K. et al., 2011a, ApJ, 728, 102
Williams M. E. K. et al., 2011b, ApJ, 728, 102
York D. G. et al., 2000, AJ, 120, 1579

This paper has been typeset from a TEX/LATEX file prepared by the author.

CHAPTER 5

CHARTING THE MILKY WAY HALO'S STELLAR STREAMS WITH ESA/GAIA DR2

For me, it is far better to grasp the Universe as it really is than to persist in delusion, however satisfying and reassuring- **Carl Sagan**

Related paper : **Ghostly Tributaries to the Milky Way: Charting the Halo's Stellar Streams with the Gaia DR2 catalogue**, 2018, Khyati Malhan, Rodrigo Ibata & Nicolas F. Martin, submitted to *MNRAS* (ADS entry)

Abstract

A panoramic map of the stellar streams of the Milky Way was created based upon astrometric and photometric measurements from the Gaia DR2 catalogue using the `STREAMFINDER`. For the pilot run of the algorithm, the concentration was made on the halo at heliocentric distances beyond 5 kpc, and at Galactic latitudes $|b| > 30°$ to detect structures along plausible orbits that were consistent with the Gaia proper motion measurements. A rich network of criss-crossing streams was found in the halo, often with striking kinematic coherence. Some of the structures that were detected were previously-known streams (GD-1, Sagittarius, Indus, Jhelum and Orphan) and several others were reported as new discoveries. This was the first time an all-sky map of the stellar streams of the Milky Way halo was made based on kinematic measurements.

5.1 Data

Gaia DR2 [62, 83] was published on 25^{th} April 2018. Along with the Gaia broad-band photometry in the G, G_{BP}, G_{RP} pass-bands, this dataset provided positions, parallaxes and proper motions (a 5D astrometric solution) for over 1.3 billion stars down to $G \sim 20.7$ in our Galaxy. The application of `STREAMFINDER` onto Gaia DR2 was the first attempt to use the Gaia dataset in order to create all-sky structural and kinematical maps of the stellar streams of the Milky Way halo.

After extensive tests of the `STREAMFINDER` using the Gaia Universe Model Snapshot (GUMS, [155]) and Pan-STARRS1 proper motion data [27, 100, 117, 182], the Gaia data sample was limited to $|b| > 30^\circ$ and $G < 19.5$. The chosen magnitude limit mitigates against the effect of completeness variations due to inhomogenous extinction, while also reducing the number of sources that need to be examined. Likewise, the Galactic latitude constraint also greatly diminishes the size of the sample. This was important as algorithm takes longer to compute high density regions of the sky where the number of field stars and the possible candidates is large. Only those sources in the catalogue were retained that had a full 5-parameter astrometric solution, along with valid magnitudes in all three photometric bands. For this pilot run of the algorithm, the concentration was directed towards the outer halo distances that lied beyond 5 kpc, as the algorithm takes longer to compute the inner regions of the sky where, again, the number of sources are large.

All the Galactic globular clusters [77] (to within their 2 tidal radii) and all the Galactic dwarf satellites [126] (to within 7 half-light radii) were omitted from the dataset. This was implemented so as to avoid creating spurious stream detections that might be caused by the presence of a compact over-density of stars in a given region of phase-space rather than an actual extended stream of stars.

5.2 Contamination Model

Though the original `STREAMFINDER` concept (described in Chapter 3) worked well at high Galactic latitudes, in regions of relatively uniform contamination; its shortcomings became evident when probing regions closer to the Galactic plane. There, the strong gradient in the background produced a large population of false positives. Therefore, the algorithm was updated to undertake a full likelihood analysis based on the Galaxy's contamination via smooth background modelling. The log-likelihood function simply becomes

$$\ln\mathscr{L} = \sum_{\text{data}} \ln(\eta\mathscr{P}_{\text{signal}}(\theta) + (1-\eta)\mathscr{P}_{\text{contamination}}), \tag{5.1}$$

where θ is the stream fitting parameters, $\mathscr{P}_{\text{signal}}$ is the most likely stream model (as presented in Chapter 3), η is the corresponding stream fraction that maximizes $\ln\mathscr{L}$ and the probability density function $\mathscr{P}_{\text{contamination}}$ is a model of the "contamiantion" from non-stream stars. By

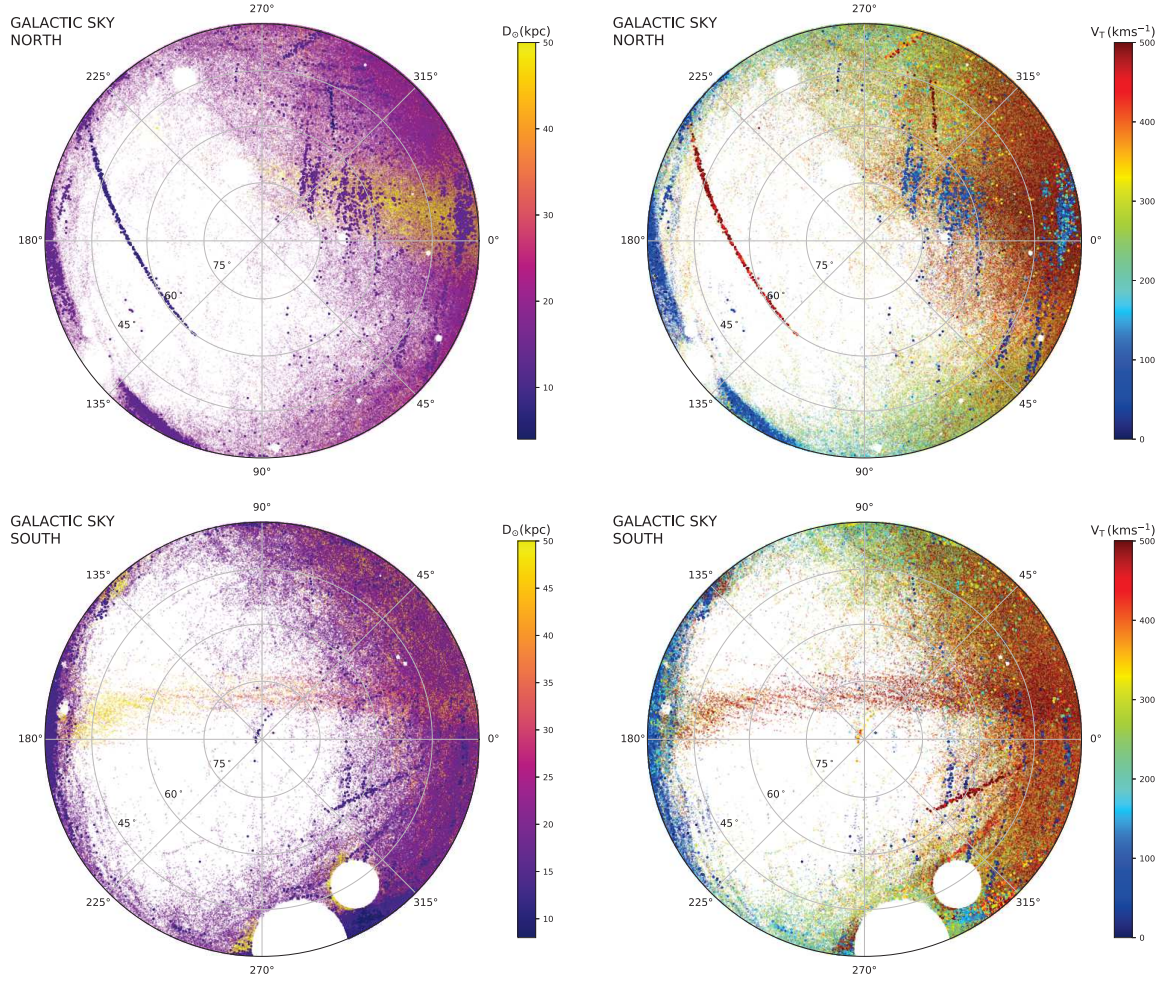

Figure 5.1: Summary diagrams of the distance ($D_\odot > 5\,\mathrm{kpc}$) and tangential velocity V_T of stream-like structures in the northern (above) and southern (below) Galactic sky. The tangential velocities are calculated based on the observed proper motion of the stars in DR2 and the corresponding distance estimates that were obtained from the algorithm.

comparing to the likelihood of the no-stream case (when $\eta = 0$), Eqn. 5.1 easily allows to measure the stream detection significance.

Such a log-likelihood definition also required to make a contamination model for the Gaia DR2 star field. For this, before running the STREAMFINDER, first an empirical smooth model of the Milky Way "contamination" was calculated (i.e. a model of the smoothly-varying population of stars that lie both in the foreground and the background of the stream-like structures of interest). This contamination model was used as a global probability density function estimate ($\mathscr{P}_{\text{contamination}}$ in equation 5.1) to calculate the likelihood function for identifying substructures. Briefly, a library of number-density maps of the Galaxy was constructed as a function of $G_{BP} - G_{RP}$ colour and G magnitude in polar Zenithal Equal Area projection with a pixel scale of $1\overset{\circ}{.}4 \times 1\overset{\circ}{.}4$, which are smoothed on a spatial scale of 2°. Furthermore, over spatial regions of $5\overset{\circ}{.}6 \times 5\overset{\circ}{.}6$ (also in polar ZEA projection), the four-dimensional distribution of $G_{BP} - G_{RP}$ colour, G magnitude, and proper motion μ_α, μ_δ, was fitted with a Gaussian Mixture Model (GMM), with 100 Gaussian components, using the Armadillo C++ library [166]. Together, the density maps and the GMM fitted maps allowed to estimate the smoothed probability of finding a star in the Galaxy in the 6-D parameter space of $\alpha, \delta, G_{BP} - G_{RP}, G, \mu_\alpha, \mu_\delta$.

5.3 STREAMFINDER Analysis

Mostly, the data-filtering and the detection scheme remained similar to as described in Chapter 3. Only this time, several Padova SSP models [123] were employed with the age 10 Gyr and metallicity values ranging between [Fe/H] = −2.2 to [Fe/H] = −1.0 (spaced at 0.2 dex intervals). These isochrone models covered plausible values for the Milky Way halo globular clusters (from which stellar streams are ultimately derived). The candidate model streams were selected to have a Gaussian width of 100pc, and to be 10° long on the sky. Other parameter ranges used to integrate orbits in the Galaxy were identical to those detailed in Chapter 3.

5.4 Results and Discussions

Several stream maps were created for different heliocentric distances, ranging from 5 – 15 kpc (inner halo), 15 – 30 kpc (intermediate halo) and 20 – 100 kpc (outer halo). Summary of these maps is shown in Figure 5.1. It was found that STREAMFINDER was succesfully able to reproduce 5 of the previously known stream structures. These streams were Sagittarius stream [86], GD-1 [72], Orphan [9], Indus and Jhelum [172]. The detection of these known streams was reassuring as it meant that the algorithm was working as desired (the positions, distance solutions and proper motions of these streams have been discussed in the paper attached).

In this first exploration, five good streams were selected from the stream maps and were named Gaia-1,2,3,4 and 5. The reason for choosing only five streams was to showcase the primary results of the algorithm's application on Gaia DR2. Many other candidates yet require careful

follow-up (positions, distances and proper motions of these new streams are also discussed in the paper attached).

5.5 Related Paper

MNRAS **000**, 1–15 (2018) Preprint 6 September 2018 Compiled using MNRAS LATEX style file v3.0

Ghostly Tributaries to the Milky Way: Charting the Halo's Stellar Streams with the Gaia DR2 catalogue

Khyati Malhan,[1⋆] Rodrigo A. Ibata,[1†] Nicolas F. Martin,[1,2‡]
[1] *Université de Strasbourg, CNRS, Observatoire Astronomique de Strasbourg, UMR 7550, F-67000 Strasbourg, France*
[2] *Max-Planck-Institut für Astronomie, Königstuhl 17, D-69117 Heidelberg, Germany*

Accepted 2018 September 05. Received 2018 August 11; in original form 2018 May 01

ABSTRACT
We present a panoramic map of the stellar streams of the Milky Way based upon astrometric and photometric measurements from the Gaia DR2 catalogue. In this first contribution, we concentrate on the halo at heliocentric distances beyond 5 kpc, and at Galactic latitudes $|b| > 30°$, using the `STREAMFINDER` algorithm to detect structures along plausible orbits that are consistent with the Gaia proper motion measurements. We find a rich network of criss-crossing streams in the halo. Some of these structures were previously-known, several are new discoveries, but others are potentially artefacts of the Gaia scanning law and will require confirmation. With these initial discoveries, we are starting to unravel the complex formation of the halo of our Galaxy.

Key words: Galaxy : halo - Galaxy: structure - stars: kinematics and dynamics - Galaxy: kinematics and dynamics

1 INTRODUCTION

The central position that stellar streams hold for Galactic Archeology studies motivates conducting a thorough census of such structures in the Milky Way. Besides testing the hierarchical merging scenario of Galaxy formation (Johnston et al. 1996; Helmi & White 1999), the number of stellar streams can, in principle, be used to put a lower limit on past accretion events into the Galactic halo, their orbital structures can be used to probe the mass distribution and shape of the Milky Way dark matter halo (Johnston et al. 1999; Ibata et al. 2001; Eyre & Binney 2009; Koposov et al. 2010; Law & Majewski 2010; Küpper et al. 2015; Bovy et al. 2016), stream-gaps can provide indirect evidence for the existence of dark matter sub-halos (Johnston et al. 2002; Carlberg et al. 2012; Erkal et al. 2016; Sanders et al. 2016), and these structures can also be used to constrain the models of the formation and evolution of globular clusters (Balbinot & Gieles 2018). Furthermore, analyses based on the quantity and the collective phase-space distribution of stellar streams hold great promise in addressing some small-scale ΛCDM problems (such as the "missing satellite problem" and the "plane-of-satellites" problem, see, e.g. Bullock & Boylan-Kolchin 2017).

Such considerations have motivated many previous studies to detect and analyse stellar streams in our Galaxy. Notable efforts in the past include the "Field-of-streams" map (Belokurov et al. 2006) of the region around the North Galactic Cap based on the SDSS DR5, which was expanded to cover both the Northern and Southern Galactic Cap regions in later SDSS releases (see, e.g. Grillmair & Carlin 2016); Bernard et al. (2014) created a panoramic map of the entire Milky Way halo north of $\delta \sim -30°$ ($\sim 30,000\,\mathrm{deg}^2$) based on the Pan-STARRS1 dataset; Mateu et al. (2018) applied a pole-counts stream-finding method to the Catalina RR-Lyrae survey revealing 14 candidate streams in the inner Galaxy; and most recently Shipp et al. (2018) discovered 11 stellar streams out to a distance of $d_\odot \sim 50$ kpc by making use of the data from the Dark Energy survey (DES). The regions of sky covered by presently-known streams have been conveniently compiled in the `GALSTREAMS` python package (Mateu et al. 2018), which we reproduce in Figure 1 for comparison to our results.

Given the arrival of all-sky data of unprecedented astrometric quality from the ESA/Gaia survey (de Bruijne 2012; Gaia Collaboration et al. 2016), we built a stream-finding algorithm (the `STREAMFINDER`, Malhan & Ibata 2018, hereafter Paper I) to make use of the kinematic information that Gaia provides. The idea that we incorporated in the `STREAMFINDER` algorithm is that stellar streams can be found more efficiently by searching along possible orbital trajectories in the underlying gravitational potential of the Galaxy. In Paper I, our tests, based on a suite of N-body simulations embedded in a mock Galactic survey, showed that

⋆ E-mail: khyati.malhan@astro.unistra.fr
† E-mail: rodrigo.ibata@astro.unistra.fr
‡ E-mail: nicolas.martin@astro.unistra.fr

the algorithm is able to detect distant halo stream structures containing as few as $\sim$ 15 members (or equivalently with a surface brightness as low as $\Sigma_{\rm G} \sim 33.6\,{\rm mag\,arcsec^{-2}}$) in the End-of-mission Gaia dataset. The detection limit depends on various factors, such as the stream structure itself and its location in phase-space with respect to the contaminating background. For instance, in Ibata et al. (2018) we reported the discovery of the (high contrast) Phlegethon stream in Gaia DR2 with a surface brightness of $\Sigma_G \sim 34.6\,{\rm mag\,arcsec^{-2}}$.

The purpose of this contribution is to present an updated stellar stream map of the halo of the Milky Way (at $D_\odot > 5\,{\rm kpc}$) obtained via the application of our `STREAMFINDER` algorithm onto the recently published Gaia Data Release 2 (DR2) (Gaia Collaboration et al. 2018; Lindegren, L. et al. 2018; Luri, Xavier et al. 2018; Evans, D. W. et al. 2018; Helmi, A. et al. 2018). In this first analysis, we restrict ourselves to analysing the outer halo at distances beyond 5 kpc as our algorithm takes longer to compute in inner regions where the density of both the field stars and the possible candidates is large (as is the case when considering closer structures or indeed in the vicinity of the Galactic Plane).

The paper is organized as follows: Section 2 details the selections made on the Gaia data; Section 3 explains how we built a model of the contaminating populations of the Milky Way; the analysis using our `STREAMFINDER` algorithm is detailed in Section 4; the results are presented in Section 5; finally we discuss these findings and draw our conclusions in Section 6.

2 DATA AND STREAM SEARCH ANALYSIS

We use the Gaia DR2 catalogue for all of our present analysis. This dataset provides positions, parallaxes and proper motions (a 5D astrometric solution) for over 1.3 billion stars down to G $\sim$ 20.7 in our Galaxy, along with the Gaia broadband photometry in the G, $\rm G_{BP}$, $\rm G_{RP}$ pass-bands. The information that is useful for our purpose are the stellar positions (α, δ), parallaxes (π), proper motions (μ_α, μ_δ), magnitudes $(\rm G, G_{BP}, G_{RP})$ and the associated observational uncertainties.

We correct all Gaia sources from extinction using the Schlegel et al. (1998) maps, assuming $A_{\rm G}/A_{\rm V} = 0.85926$, $A_{\rm BP}/A_{\rm V} = 1.06794$, $A_{\rm RP}/A_{\rm V} = 0.65199$[1]. Doing so, we naturally assume that the extinction is entirely in the foreground of the studied stars, which is likely a good assumption for the halos stars we analyse here. Henceforth, all magnitudes will refer to the extinction-corrected values.

The Gaia DR2 is based on only 22 months of observations, and not all areas of sky have been observed to uniform depth. Gaia scans the sky while spinning, and this naturally imprints great circles into the depth map. In Figure 2 we show the result of applying an unsharp-mask to all data at Galactic latitudes $|b| > 10^\circ$ and with G < 20. A large number of stripy residuals can be seen, which could in principle masquerade as streams. Any structures following this pattern are almost certainly artefacts.

[1] These extinction ratios are listed on the Padova model site http://stev.oapd.inaf.it/cgi-bin/cmd_2.8.

After extensive tests of the `STREAMFINDER` using the Gaia Universe Model Snapshot (GUMS, Robin et al. 2012), we decided to limit the sample for the present contribution to $|b| > 30^\circ$ and $G < 19.5$. The chosen magnitude limit mitigates against the effect of completeness variations due to inhomogenous extinction, while also reducing the number of sources that need to be examined. Likewise, the Galactic latitude constraint also greatly diminishes the size of the sample. We retained only those sources that had a full 5-parameter astrometric solution, along with valid magnitudes in all three photometric bands.

We further omitted all Gaia DR2 catalogue stars within two tidal radii of the Galactic globular clusters listed in the compilation by Harris (2010), as well as all the stars within 7 half-light radii around Galactic dwarf satellite galaxies (as compiled by McConnachie 2012). This was implemented so as to avoid creating spurious stream detections that might be caused by the presence of a compact over-density of stars in a given region of phase-space rather than an actual extended stream of stars.

As described in Paper I, it is convenient to reject disk contaminants based on parallax information since we are interested in finding halo structures. The number of these potential nearby contaminants was reduced by removing those sources whose parallax is greater than 1/3000 arcsec at more than the 3σ level (i.e. objects that are likely to be closer than 3 kpc).

We feed this filtered data to the `STREAMFINDER`.

3 CONTAMINATION MODEL

Before running the `STREAMFINDER`, we first calculate an empirical smooth model of the Milky Way "contamination" (i.e. a model of the smoothly-varying population of stars that lie both in the foreground and the background of the stream-like structures of interest). This contamination model is used as a global probability density function estimate to calculate the likelihood function for identifying substructures. The procedure will be more fully explained in a future contribution (Ibata et al. 2018, in prep.), but briefly, we construct a library of number-density maps of the Galaxy as a function of $\rm G_{BP} - G_{RP}$ colour and G magnitude in polar Zenithal Equal Area projection with a pixel scale of $1\overset{\circ}{.}4 \times 1\overset{\circ}{.}4$, which are smoothed on a spatial scale of 2°. Furthermore, over spatial regions of $5\overset{\circ}{.}6 \times 5\overset{\circ}{.}6$ (also in polar ZEA projection), we fit the four-dimensional distribution of $\rm G_{BP} - G_{RP}$ colour, G magnitude, and proper motion μ_α, μ_δ, with a Gaussian Mixture Model (GMM), with 100 Gaussian components, using the `Armadillo` C++ library (Sanderson & Curtin 2017). Together, the density maps and the GMM fitted maps allow one to estimate the smoothed probability of finding a star in the Galaxy in the 6-D parameter space of $\alpha, \delta, \rm G_{BP} - G_{RP}, G, \mu_\alpha, \mu_\delta$.

4 `STREAMFINDER` ANALYSIS

The `STREAMFINDER` algorithm is built to detect dynamically cold and narrow tidal stellar streams that are possible remnants of globular clusters or very low-mass galaxies. At the position of every star in the dataset, the algorithm finds the

$240\,\mathrm{km\,s^{-1}}$ and in addition we adopt the Sun's peculiar velocity to be $\boldsymbol{V}_{\odot} = (u_{\odot}, v_{\odot}, w_{\odot}) = (9.0, 15.2, 7.0)\,\mathrm{km\,s^{-1}}$ (Reid et al. 2014; Schönrich et al. 2010). As explained in Paper I, STREAMFINDER uses pre-selected isochrone models in order to sample orbits in distance space. The selected isochrone model(s) essentially correspond to the proposed Single Stellar Population (SSP) model of the stream. Here, we chose to work with Padova SSP models (Marigo et al. 2008) in the Gaia photometric system, with age 10 Gyr and with 7 metallicity values between [Fe/H] $= -2.2$ to [Fe/H] $= -1.0$ (spaced at 0.2 dex intervals). These isochrone models cover plausible values for Milky Way halo globular clusters (from which stellar streams are ultimately derived)[2]. The candidate model streams were selected to have a Gaussian width of 100 pc, and to be 10° long on the sky. Other parameter ranges used to integrate orbits in the Galaxy were identical to those detailed in Paper I.

In Paper 1, our analysis was restricted to a small and relatively high latitude patch of sky ($\sim 100\,\mathrm{deg^2}$) in which the background stellar distribution (the halo) could be approximated as a uniform distribution. In the present case, where we are analysing vast regions of sky that have a non-uniform stellar distribution, it is important to consider the background model of the Galaxy. Therefore, in contrast to Paper I, the likelihood function that we use here takes the Galaxy into consideration via the smooth contamination model discussed above. Our log-likelihood function is simply:

$$\ln\mathcal{L} = \sum_{\mathrm{data}} \ln\left(\eta\mathcal{P}_{\mathrm{signal}}(\theta) + (1-\eta)\,\mathcal{P}_{\mathrm{contamination}}\right), \qquad (1)$$

where θ are the stream fitting parameters, $\mathcal{P}_{\mathrm{contamination}}$ is the probability density function of the smooth contamination model that we obtain as explained in Section 3, and η is the fraction of the stream model compared to the contamination. The adopted stream probability density function $\mathcal{P}_{\mathrm{signal}}$ is extremely simple: we take the trial orbit under consideration and make it fuzzy by convolving it with a Gaussian in each observed dimension. The Gaussian dispersions are: σ_{sky} representing the thickness of the stream, $\sigma_{\mu_\alpha}, \sigma_{\mu_\delta}$ representing the dispersions in proper motion, and σ_{DM} representing the dispersion in distance modulus (and hence in photometry). All these dispersions are the convolution of the intrinsic Gaussian dispersion of the stream model together with the observational uncertainty on each star in the Gaia DR2 catalogue.

5 RESULTS

In Figure 3 we show, for two representative metallicity values, the spatial distribution of the stars in the processed sample that have a high-likelihood of belonging to a stream structure. These data are selected as having $\ln\mathcal{L}_{\mathrm{max}}/\ln\mathcal{L}_{\eta=0} > 15$, where $\mathcal{L}_{\eta=0}$ is the model likelihood when no stream is present, and $\mathcal{L}_{\mathrm{max}}$ is the maximum likelihood stream solution found by the algorithm. Thus, our criterion corresponds to $> 5\sigma$ when the noise distributions are Gaussian. We would like to point out that the $\ln\mathcal{L}_{\mathrm{max}}/\ln\mathcal{L}_{\eta=0}$ likelihood ratio is calculated for every star in the (filtered) catalogue, yet in the maps presented here we only show those stars where this value exceeds 15. Many other neighbouring stars may partake in a given stream structure, contributing to the high $\ln\mathcal{L}_{\mathrm{max}}/\ln\mathcal{L}_{\eta=0}$ valued-points marked in the figure, yet they may not themselves pass the criterion and so are not shown. A given stream-like structure seen in the figure is thus composed of many $> 5\sigma$ points. However, the points are not statistically independent, as by construction information is correlated over the chosen 10° trial stream length. We further stress that the aim of the STREAMFINDER algorithm is to enable the detection of streams; a complete characterization and statistical analysis of a given detection should be accomplished with other tools, for instance, by careful modelling with N-body simulations.

The left and right panels of Figure 3 show, respectively, the projection from the North and South poles. The distance solutions displayed here are the ones obtained by the algorithm and span the inner halo range $D_{\odot} = [5, 15]$ kpc. The most visible feature in the northern hemisphere is the GD-1 stellar stream (Grillmair & Dionatos 2006; de Boer et al. 2018), which appears as a $> 60^{\circ}$ stream in these spatial density maps of candidate stream members. It is possible that it continues to lower Galactic latitude, where we have not yet run the algorithm. Other notable detections are the Jhelum and Indus streams (Shipp et al. 2018) seen in the Southern hemisphere in the more metal-poor map. As a demonstration of the power of the algorithm, we display the properties of GD-1, Jhelum and Indus, as recovered by the STREAMFINDER, in Figure 4. Note that the distance solutions to these streams that we obtain from STREAMFINDER match closely the distance values that have been previously derived for these streams (as explained in Figure 4). The scatter in the distance solutions that is notably seen for individual streams could be a combination of the true intrinsic dispersion of the stream and errors from mismatches with the isochrone template model (from which the distance solutions are derived, see Paper I). We summarize some of the properties of these structures in Table 1, providing, for the first time, the proper motion values for the Jhelum and Indus streams.

The recovery of known stellar streams provides validation of our algorithm. Many other stream-like features can also be seen in this map, but these structures require detailed kinematic analysis for their confirmation (which is beyond of the scope of this paper). In the present contribution we will discuss the most obvious stream structures that not only have coherent phase-space properties (consistent with the template model and the data uncertainties) but that also stand out significantly from the background. These new streams, that are named Gaia-1,2,3,4, are shaded in grey in Figure 3 and their phase-space properties are presented in Figure 9.

Figure 5 shows the results at intermediate distances in the halo in the range $D_{\odot} = [15, 30]$ kpc (again selecting $\ln\mathcal{L}_{\mathrm{max}}/\ln\mathcal{L}_{\eta=0} > 15$). Unlike Figure 3 that exhibits clearly distinguishable stream-like strings of stars, these maps produced at intermediate distances are rather fuzzy and only seldom show thin stream-like features. Some of these stream features become apparent in the regions $|b| > 45^{\circ}$ where the density of contaminating stars is low. The most obvious

[2] In subsequent papers, we plan to run the algorithm over a fine grid in metallicity and age.

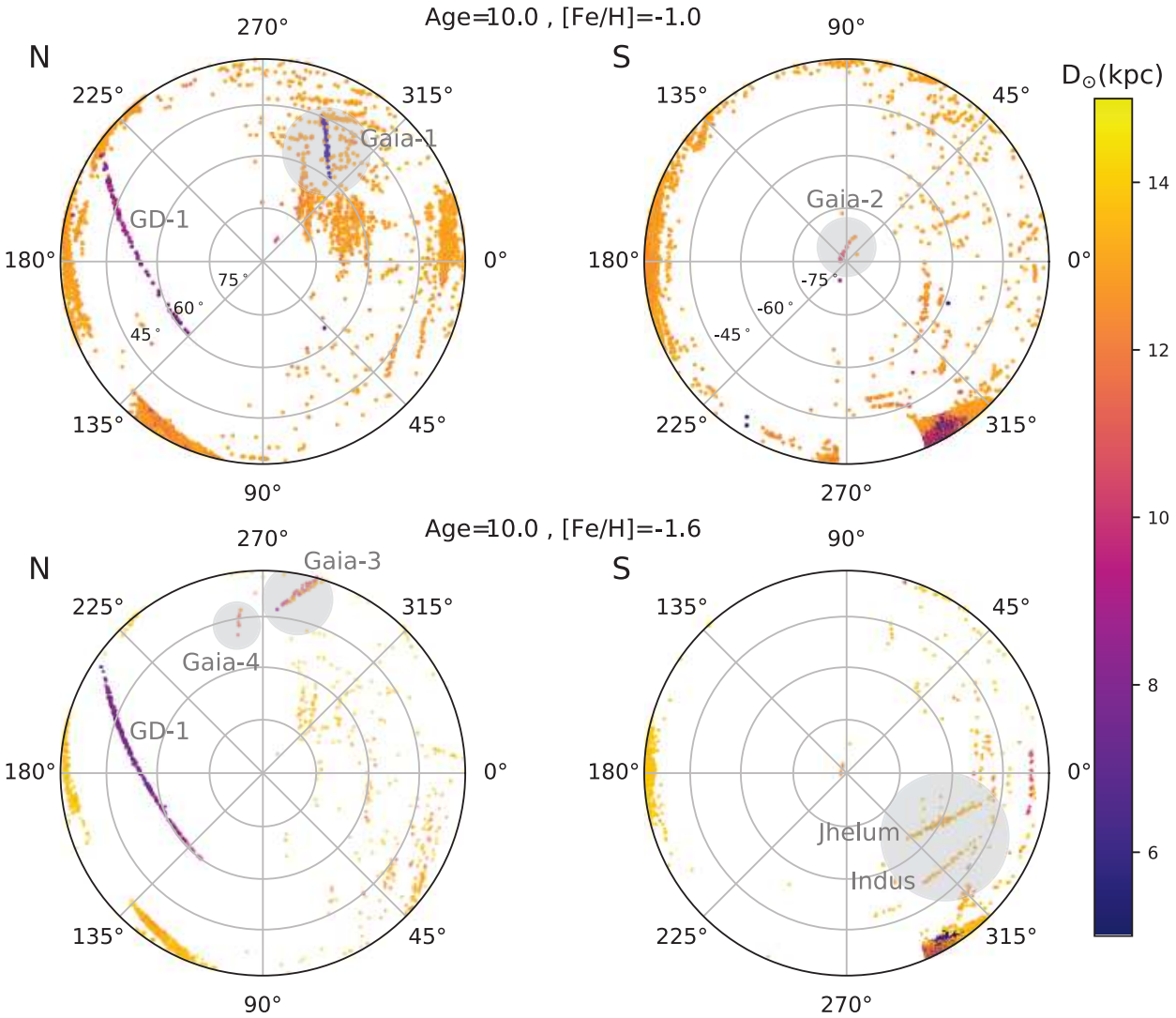

Figure 3. Potential stream stars identified by `STREAMFINDER` in the inner halo, from 5 to 15 kpc, in the same projection as Figure 1. The colour represents the distance solutions that are obtained as a by-product for these stars from the `STREAMFNIDER` analysis. The top panels show a metal-rich selection, while the lower panels show the results for intermediate metallicity. The most striking structure detected in this distance range is the GD-1 stream (Grillmair & Dionatos 2006), seen clearly towards the lower end of the distance range (coloured purple) in the Northern hemisphere (left panels). Several other streams are visible, including the Jhelum and Indus streams discovered in the DES (Shipp et al. 2018). All stream points displayed here have detection significance $> 5\sigma$. New high confidence stream detections are marked on the map, while the others will require confirmation with radial velocity measurements.

stream structure is Gaia-5, which is shaded in the grey circle in Figure 5 and its phase-space properties are presented in Figure 9.

The outer halo distribution, beyond 25 kpc is displayed in Figure 6 (again selecting $\ln\mathcal{L}_{\rm max}/\ln\mathcal{L}_{\eta=0} > 15$). The algorithm highlights a veritable deluge of stream-like structures, which are seen over a range of distances and metallicities. Comparison to Figure 1 shows that we detect the Sagittarius stream (Ibata et al. 2001; Majewski et al. 2003) over a large swathe of the outer halo. This is somewhat surprising, since we set the stream model width to 100 pc, which is appropriate for a globular cluster, but is actually a very poor template for this wide stream. We suspect that the spatial inhomogeneities in Gaia due its scanning law may partially explain the striated aspect of the Sagittarius stream in our maps (see, e.g., Figure 6). The algorithm also detected a short arc of length $\sim 10°$ of the $\sim 60°$ long Orphan stream (Grillmair 2006) in our outer halo spatial maps (again, the chosen stream width of the model was not an appropriate template for this structure, which may explain why the full length was not recovered). For the position of the arc on the sky shown in Figure 4, we find the distance solutions for the Orphan stream members to be compatible with the study by Newberg et al. (2010). Also, we find that its member stars have a tight proper motion distribution (Table 1 provides proper motion values for the Orphan stream). This map also requires follow-up with radial velocity measurements in order to test the phase-space consistency of the other possible stream like structures that are distributed on these maps (for example, see the bottom panels of Figure 6).

Careful visual inspection of these maps indicated that

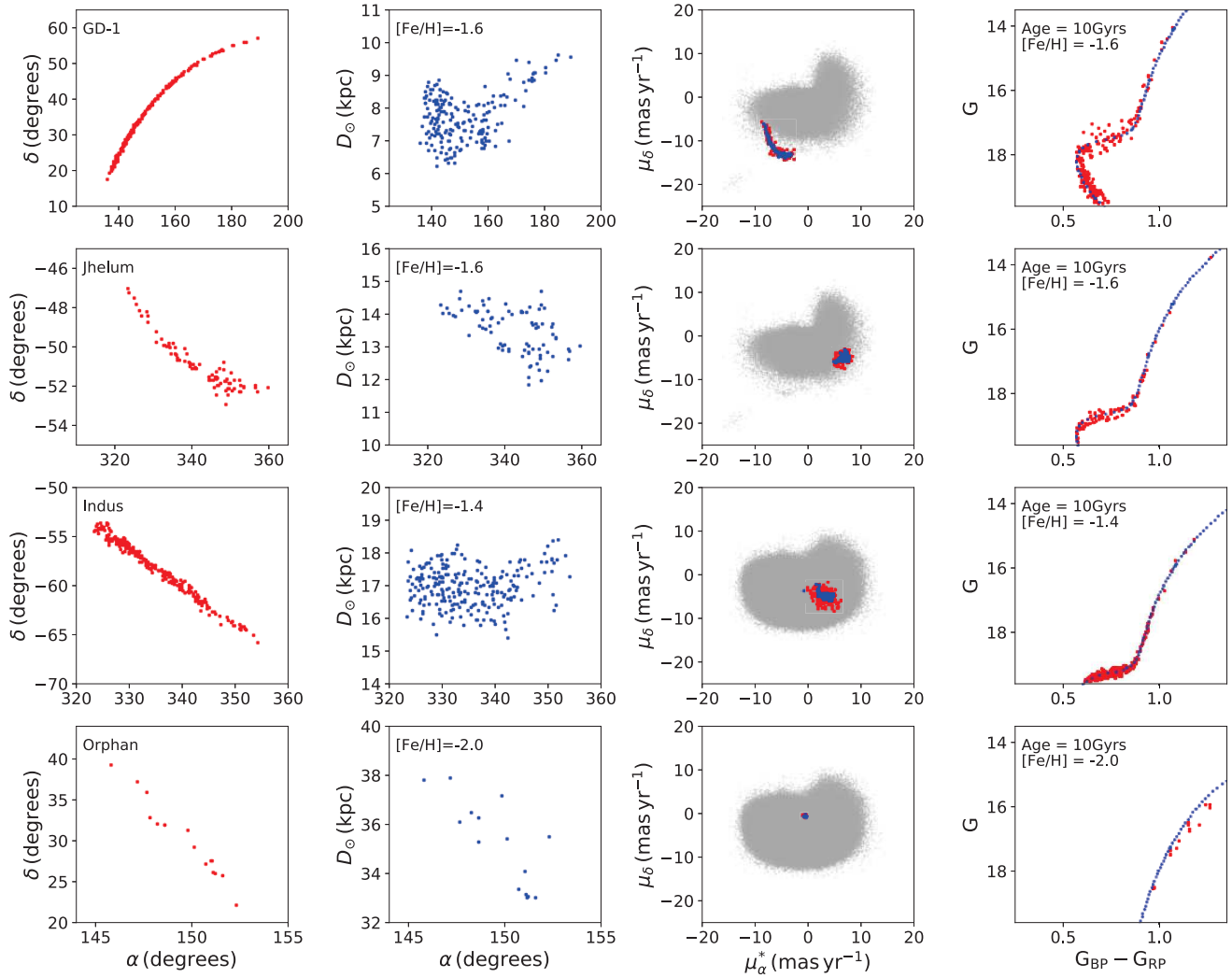

Figure 4. Properties of a sample of previously-discovered streams, as recovered by the `STREAMFINDER`. The first, second, third and fourth rows show the properties of the GD-1, Jhelum, Indus and Orphan streams, respectively. The columns reproduce, from left to right, the equatorial coordinates of the structures, the distance solutions found by the algorithm (for representative metallicity values), the proper motion distribution (with observations in red, model solutions in blue, and the full DR2 sample in grey), and the colour-magnitude distribution of the stars (with observations in red and template model in blue) selected by `STREAMFINDER`. The distance solutions found by the algorithm match closely the distance values that have been previously derived for these streams: $D_\odot \sim 8$ kpc for GD-1 (Grillmair & Dionatos 2006), $D_\odot \sim 13.2$ kpc and ~ 16.6 kpc for Jhelum and Indus, respectively (Shipp et al. 2018) and $D_\odot = [33 - 38]$ kpc for Orphan (Newberg et al. 2010). The CMD template models, shown in blue in the last column, have been plotted at the appropriate distance for the respective streams. The colour-magnitude diagram of the Orphan stream might seem peculiar, but here we only see the red-giant branch due to the trimming of the data sample below G = 19.5.

the stream-like structures recovered by the algorithm are not associated with the extinction correction. In Figures 7 and 8, we present our summary plots made by combining the distance and metallicity samples for the north and south hemispheres, respectively. The top panels of these diagrams show the estimate of the distances of these structures (provided by the algorithm), while the bottom panels show an estimate of the magnitude of the tangential velocity calculated using the measured Gaia proper motions combined with the distance estimates. Many structures are beautifully resolved in this multi-parameter space.

Our aim in this contribution is not to present a thorough or complete census of halo streams (since it would require considerable more processing time to examine the necessary parameter space), but rather to present a preview of the large-scale stream structure of our Galaxy. Nevertheless, we have selected by hand a small number of structures that appear clearly in our maps, with kinematic properties that distinguish them from the contaminating Galactic population, and that are clearly not artefacts produced by Gaia's scanning law. A large number of other stream candidates have a clearly-defined stream-like morphology, but possess proper motions distributions that are similar to that of the halo, and we deem that they require further follow-up to be confident of their nature.

The locations of the five structures we selected are

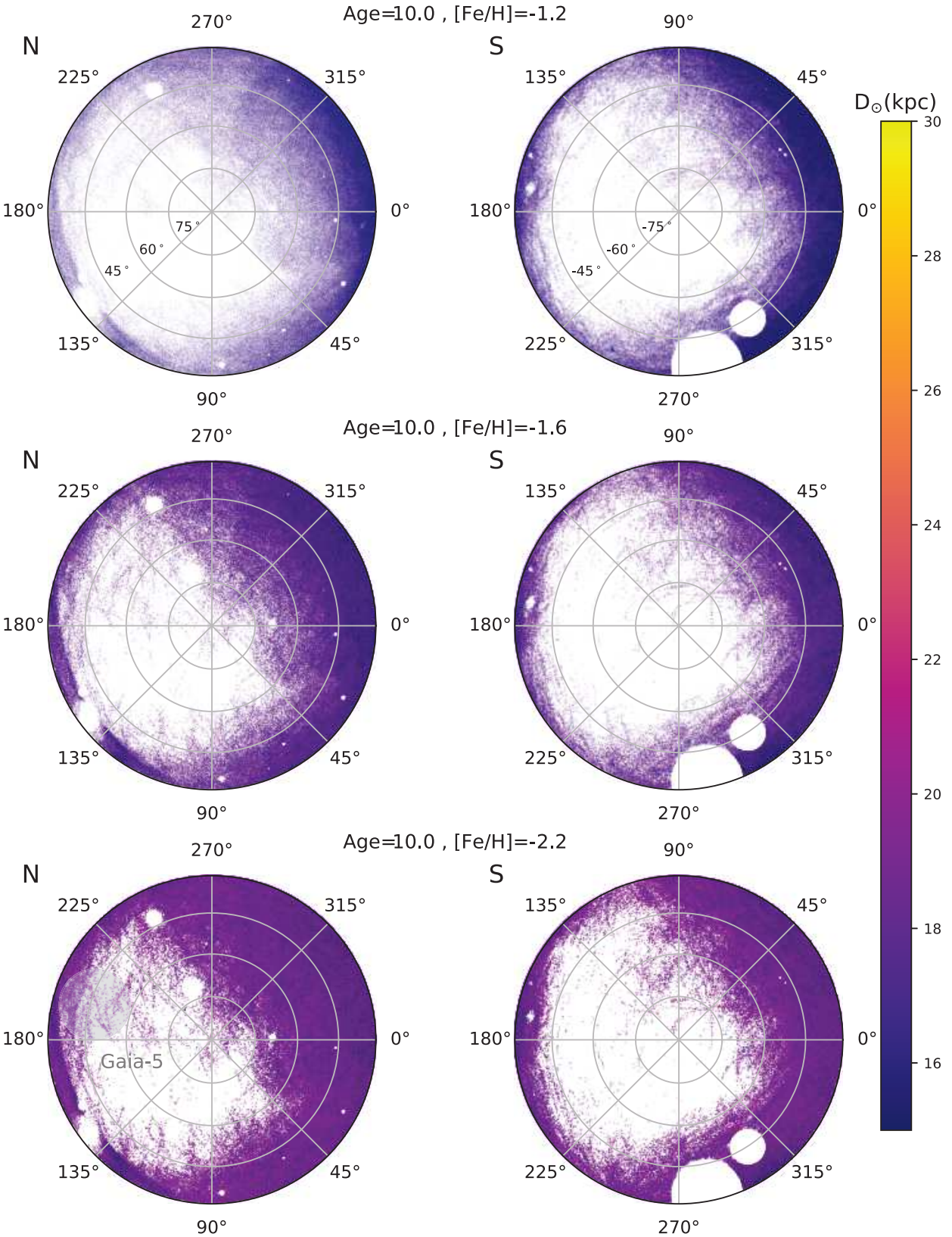

Figure 5. Spatial distribution of stream candidates at intermediate distances. Here we show the stellar stream density map as obtained from the `STREAMFINDER` based on 3 representative isochrone models. Each row corresponds to a particular isochrone model of age (in Gyr) and metallicity, as labelled. The left panels represent the North side of the ZEA projection system and the right panels represent the South. The colour scale is proportional to the heliocentric distances to the stellar members of the detected structures obtained as a by-product from the `STREAMFINDER` analysis. All streams displayed here have detection significance $> 5\sigma$. New high confidence stream detections are marked on the map.

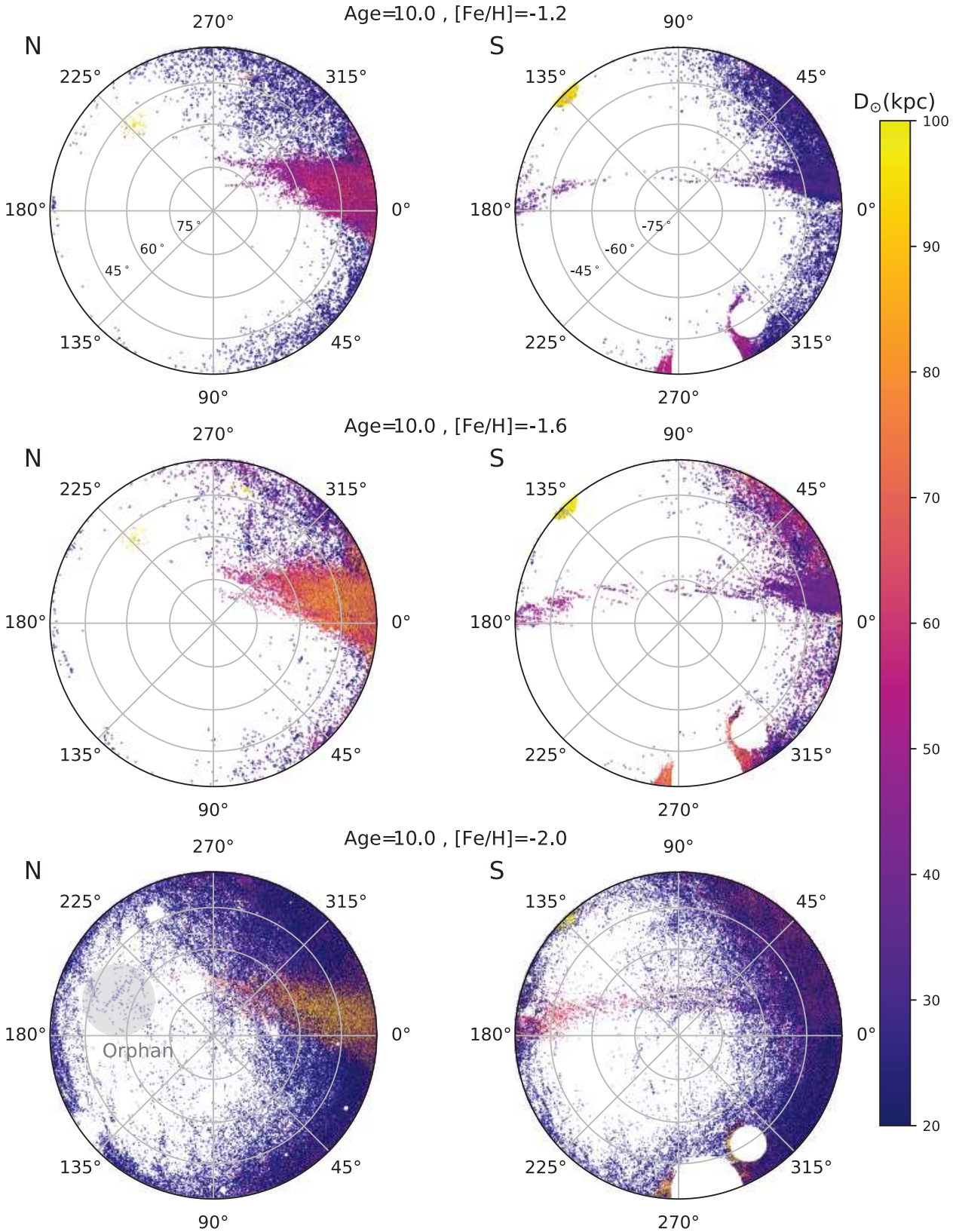

Figure 6. As Figure 5, but for the outer halo beyond 25 kpc. The dominant structure seen out to large heliocentric distances in both hemispheres is the Sagittarius stream, which is detected despite the narrowness of the stream template model that we set in our algorithm. The interesting bifurcation of this structure is seen in the top-left panel. In addition, the lower-left panel shows an overdensity of stars in the region where the Orphan stream lies (Grillmair 2006). Many other stream-like features are also detected, but most are confined to the nearer limit of the distance range shown.

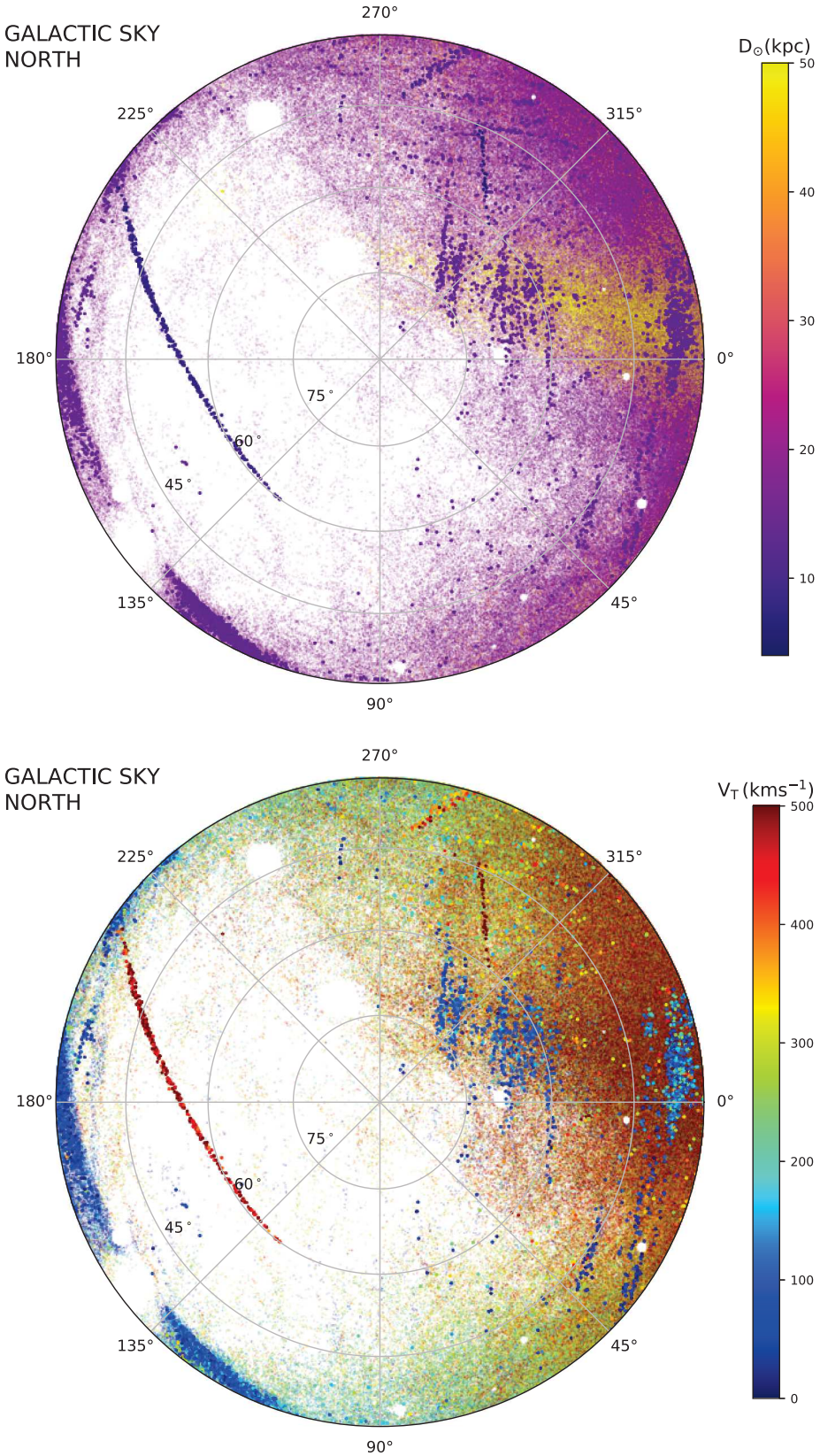

Figure 7. Summary diagrams of the distance ($D_\odot > 5\,\mathrm{kpc}$) and tangential velocity V_T of stream-like structures in the northern Galactic sky. The tangential velocities are calculated based on the observed proper motion of the stars in DR2 and the corresponding distance estimates that we obtain from the algorithm. Most of the structures that we report here are visible in these diagrams, as are many others that we intend to investigate further in future contributions.

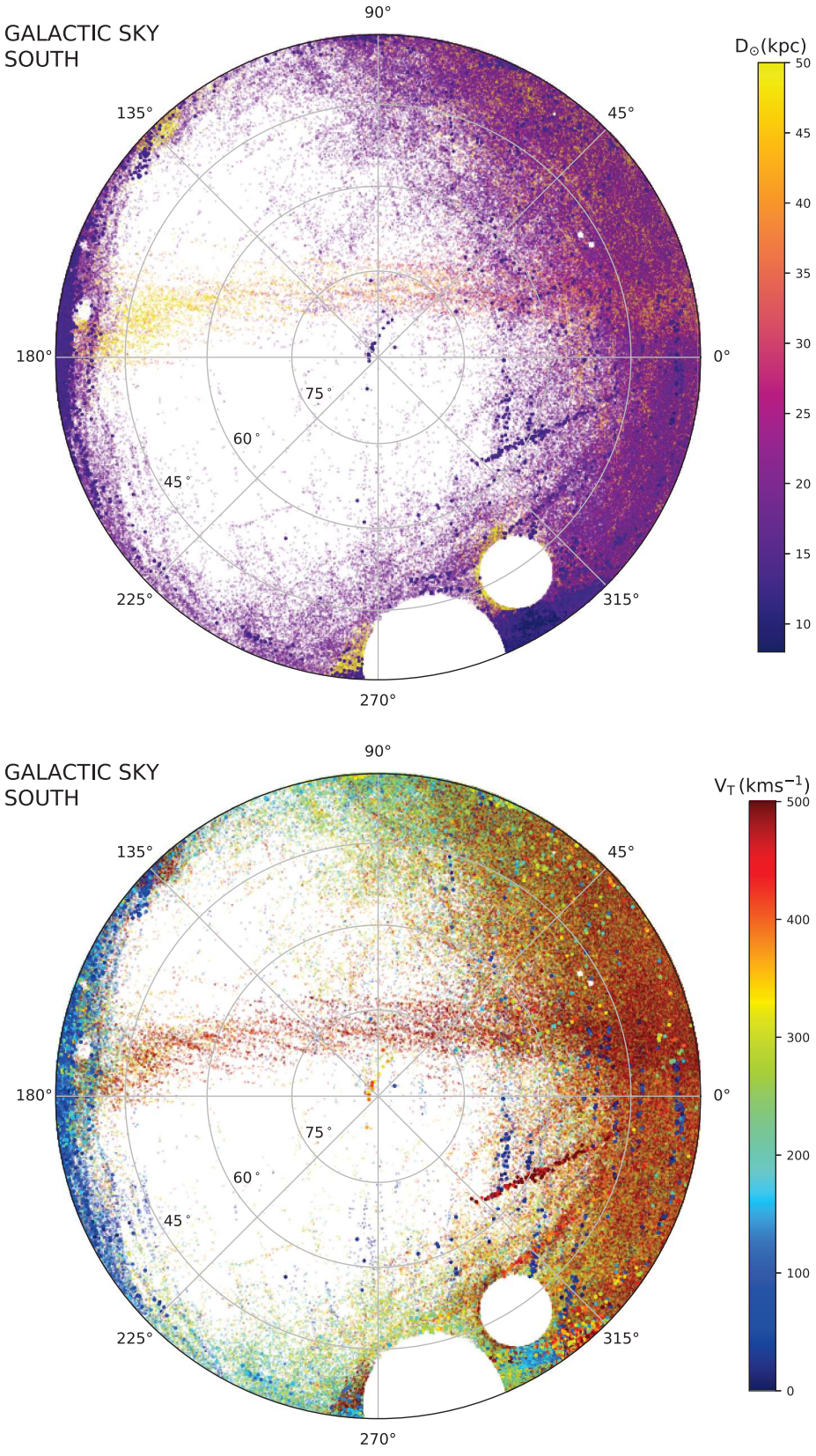

Figure 8. As Figure 7, but for the southern Galactic sky.

marked in Figures 3 and 5, and their properties are shown in Figure 9, and are also summarised in Table 1. All these structures that we find have significance $> 5\sigma$.

5.1 Gaia-1

Gaia-1 has an angular extent of $\sim 15^\circ$ and projected width of $\sim 0.5^\circ$. The orbital solutions provided by the algorithm imply that it is situated at a distance of $D_\odot \sim 5.5\,\mathrm{kpc}$, which is in reasonable agreement with the Gaia parallax measurement of $0.216 \pm 0.038\,\mathrm{mas}$ (i.e. 4.6 kpc). This means that Gaia-1 has a physical width of $\sim 40\,\mathrm{pc}$. The narrowness of the stream suggests that the progenitor likely is or was a globular cluster. Moreover, Gaia-1 has a strikingly high proper motion value of $\sim 23.5\,\mathrm{mas\,yr^{-1}}$, implying that it has a transverse motion $\gtrsim 500\,\mathrm{km\,s^{-1}}$. It will be worthwhile to measure the radial velocity of this system, as it may provide an interesting constraint on the Galactic potential simply from the requirement that the system is bound to the Milky Way.

5.2 Gaia-2

Gaia-2 turns out to be a considerably thin structure in our spatial maps. Extending over $\sim 10^\circ$ in length, we find that it possesses a distance gradient ranging from $D_\odot = [10$–$13]\,\mathrm{kpc}$. Given its narrowness and the location in the halo, we also suspect it to be a remnant of a globular cluster. We find Gaia-2 to be a highly coherent structure in proper motion space with an average proper motion magnitude of $\sim 6.5\,\mathrm{mas\,yr^{-1}}$ and proper motion dispersion of $\sim 0.75\,\mathrm{mas\,yr^{-1}}$.

5.3 Gaia-3

Gaia-3 can be easily identified as an isolated stream structure in Figure 3. In Figure 9 (third row), Gaia-3 clearly shows two distinct possible sets of distance solutions. The separation of these two different sets of solutions in position, distance and colour-magnitude distribution space, while not so much in proper motion space, suggests that what we detect here as Gaia-3 might in fact be a superposition of two streams, or a more complicated structure aligned along the line of sight. We shall describe this structure collectively here.

Gaia-3 is found to be extended over $\sim 16^\circ$ in sky with a distance range of $D_\odot = [9$–$14\,\mathrm{kpc}]$ with an average proper motion magnitude of $\sim 7.4\,\mathrm{mas\,yr^{-1}}$. Given its peculiarity, as suggested above and shown in Figure 9, it is hard to comment on its physical width or the progenitor. The distance estimate of this structure too was found to be in good agreement with the Gaia parallax measurement of $0.101 \pm 0.013\,\mathrm{mas}$ (i.e. 9.8 kpc).

5.4 Gaia-4

Gaia-4 appears to be a fine linear structure, found at a distance of $\sim D_\odot = 11\,\mathrm{kpc}$. Given its narrowness and distance, we suspect the progenitor to be a globular cluster. Although we find Gaia-4 sitting within the range of halo field stars in proper motion space with an average value of $\sim 0.36\,\mathrm{mas\,yr^{-1}}$ (and proper motion dispersion of $\sim 0.70\,\mathrm{mas\,yr^{-1}}$), the fact that it emerges as a highly coherent structure in our maps makes it a confident structure. Here, we detect it as a very cold structure in proper motion space.

5.5 Gaia-5

We include Gaia-5 here as another interesting detection (bottom row panels in Figure 9), as it is parallel to the GD-1 stream, and could easily have been confused with GD-1 without Gaia's excellent proper motion measurements. The properties of this object are shown in red for positions, observed proper motions and photometry, and in blue for distance and and proper motion orbital solutions. We also include the properties of GD-1 (in green) for comparison. The proper motions, along with the distance solutions, of Gaia-5 stars are distributed over a compact region that is very far from the region inhabited by GD-1; also the two colour-magnitude distributions (CMDs) are very different and well separated. Hence, unlike the possible bimodal stream distribution that we recognise in Gaia-3, we identify Gaia-5 as a stream unrelated to GD-1. The (error-weighted mean) parallax value we calculate for this structure would imply that it is substantially closer to the Sun than GD-1, which is both inconsistent with the model solutions of $\sim 20\,\mathrm{kpc}$, and is very difficult to reconcile with the CMD. However, our simple combination of the parallax measurements is highly susceptible to contaminants, which may explain the inconsistency.

We plan to examine these structures (and the many other stream candidates visible in Figures 7 and 8) in detail in later contributions. Careful analysis based on their astrometry and photometry, along with the mapping of these structures in deeper astrophysical catalogues (e.g. SDSS, PS1, DES), would render a fuller insight into their origin, orbits and phase-space distribution. Some of the previously-known streams and new detections appear to present spatial kinks, which is probably the effect of low-number statistics.

6 DISCUSSIONS AND CONCLUSIONS

In this contribution, we present a new stellar stream map of the Milky Way halo, obtained by the application of our `STREAMFINDER` algorithm (described in Paper I) on the recently published ESA/Gaia DR2 catalogue. This is the first time an all-sky structural and kinematic map of the stellar streams of the Milky Way halo has been constructed. Our algorithm detects numerous previously-known streams, which were discovered in much deeper photometric datasets (e.g. SDSS, PS1, DES), confirming that our method, which includes proper motion information, works as designed. Indeed, the fidelity of the GD-1 detection is striking, and reveals that the excellent Gaia proper motions provide very powerful discrimination.

In addition, we find a large number of streams and stream candidates throughout the distance range probed. In this first exploration, we selected five good streams (named here as Gaia-1,2,3,4,5), to showcase the results, but many other candidates will require careful follow-up. In particular, the fact that Gaia scans the sky along great circles, but with

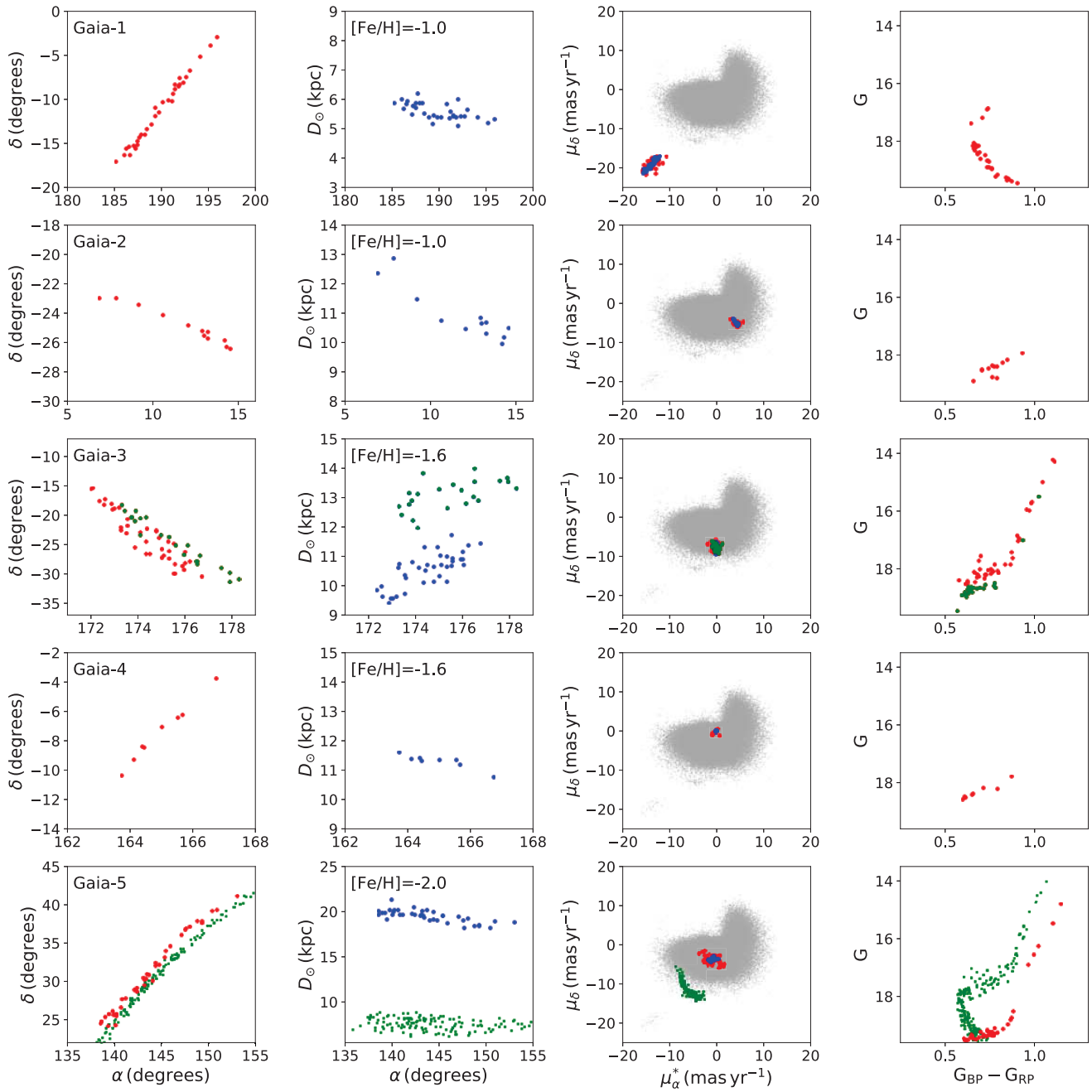

Figure 9. As Figure 4 but for the selected set of newly-discovered streams. Oddly, for Gaia-3, we found two distinct possible sets of solutions based on distance estimates that we obtained from our algorithm, as highlighted in the respective panel. The more distant stars are coloured in green, while the relatively nearby ones are shown in red. This clear distinction of these two different sets of solutions in position, distance and colour-magnitude distribution space, while not so much in proper motion space, suggests that what we detect here as Gaia-3 might in fact be a superposition of two streams, or a more complicated structure aligned along the line of sight. The bottom row shows the properties of Gaia-5, which is found to lie parallel, but slightly offset, to GD-1 (shown on this bottom row in green). Nevertheless, it is very distinct from GD-1 both in its proper motion distribution and in its colour-magnitude distribution.

an inhomogeneous number of visits, causes density inhomogeneities that appear like great circle streaks on the sky. This could cause some spurious stream detections (although the kinematics test in the `STREAMFINDER` algorithm should allow us to reject most such fake streams). Nevertheless, these spatial inhomogeneities in the Gaia DR2 necessarily make the survey noise properties very complex, invalidating the assumptions behind our $\ln\mathcal{L}_{\rm max}/\ln\mathcal{L}_{\eta=0} > 15$ selection criterion. This means, unfortunately, that the effective stream detection threshold is not uniform in our sky maps, and the significance of the detections is lower in regions where the Gaia inhomogeneities are more pronounced.

Table 1. Parameters of the stellar streams. The "Position" column gives the extent of these structures, '$D_\odot$' is the approximate range of the distance solution as obtained by our algorithm, while column 4 lists the range of observed proper motion of the structure in the 2D proper motion space. The parallax π is an uncertainty-weighted average of the Gaia measurements; for those objects where the parallax uncertainty is less than 33% of the parallax, we also provide the corresponding distance. The discrepancy between the model distances and mean parallax measurement for the cases of Indus and Gaia-5 may be due to contaminants in the samples affecting the simple weighted average parallax reported here.

Name	Position (extent)	$D_\odot$ (model) (kpc)	$(\mu^*_\alpha, \mu_\delta)$ (mas yr^{-1})	π (mas)	$\frac{1}{\pi}$ (kpc)
GD-1	$135° < \alpha < 190°$ $17° < \delta < 58°$	$6.5 - 10$	$([-9.0, -3.0], [-14.0, -6.0])$	0.107 ± 0.010	9.3
Jhelum	$320° < \alpha < 360°$ $-53° < \delta < -47°$	$11.7 - 15$	$([5.0, 8.0], [-7.0, -3.0])$	0.086 ± 0.013	11.6
Indus	$320° < \alpha < 360°$ $-67° < \delta < -53°$	$16 - 18$	$([0.50, 6.0], [-8.0, -2.0])$	0.167 ± 0.013	6.0
Orphan	$145° < \alpha < 153°$ $20° < \delta < 40°$	$33 - 38$	$([-1.0, -0.5], [-0.7, -0.1])$	-0.006 ± 0.022	
Gaia-1	$184° < \alpha < 197°$ $-18° < \delta < -2°$	$5 - 6$	$([-16.0, -11.0], [-22.0, -17.0])$	0.216 ± 0.038	4.6
Gaia-2	$6° < \alpha < 15°$ $-27° < \delta < -22°$	$10 - 13$	$([2.7, 5.4], [-6.0, -4.0])$	0.117 ± 0.062	
Gaia-3	$171° < \alpha < 179°$ $-32° < \delta < -15°$	$9 - 14$	$([-2.0, 1.0], [-9.3, -5.5])$	0.101 ± 0.013	9.9
Gaia-4	$163° < \alpha < 167°$ $-11° < \delta < -3°$	$10.7 - 11.5$	$([-1.1, 0.5], [-1.1, 0.6])$	0.006 ± 0.105	
Gaia-5	$137° < \alpha < 154°$ $23° < \delta < 42°$	$18.5 - 20.5$	$([-4.0, 1.5], [-5.7, -1.5])$	0.156 ± 0.031	6.4

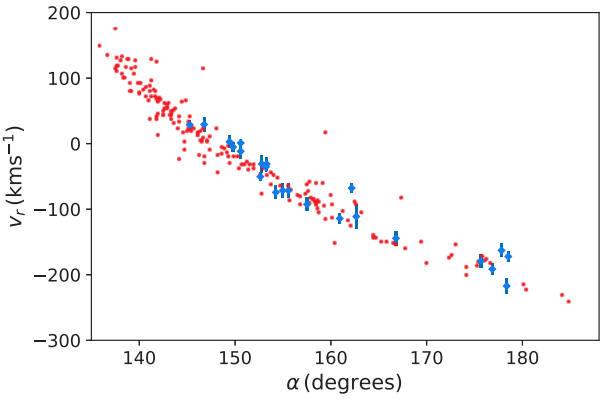

Figure 10. Predicting the missing phase-space information of streams stars with `STREAMFINDER`. The red dots represent the radial velocity solutions of the GD-1 stars that are derived as a by-product of the application of the algorithm, whereas the blue markers are the observed radial velocities of GD-1 stars as tabulated by Koposov et al. (2010). The `STREAMFINDER` sampled orbits in radial velocity space at intervals of 10 km s^{-1} (which effectively causes an uncertainty of 10 km s^{-1} on the red dots). The good agreement with the observations illustrates the power of our algorithm in predicting the missing phase-space information of stream stars.

A further caveat relates to the model distances we report. These distances are calculated by the algorithm based on an assumption of the metallicity of the stream stars. We expect that we do, in fact, have some ability to estimate the metallicity of the candidate streams with our procedure, since using the correct metallicity model should enhance the contrast of the streams. This is borne out, for instance, for the case of GD-1, where we recover the largest number of stream stars when using the model corresponding to the actual metallicity of the system. Nevertheless, this is a poor substitute for actual metallicity measurements. Ongoing sky surveys, such as the Canada-France Imaging Survey (CFIS; Ibata et al. 2017a,b), or future large photometric surveys such as LSST (LSST Dark Energy Science Collaboration 2012), can help overcome this issue by providing good photometric metallicities that will break the distance degeneracy (and improve stream detection). The third Gaia data release (DR3), currently planned for 2020, will provide low-resolution prism spectra, also allowing metallicity measurements for the brighter stars.

As we showed in Paper I, our algorithm naturally delivers the possible set of orbital solutions of the detected stream structures. This means that the algorithm predicts both the radial velocities and the distances of the stream stars. In Figure 10 we use the orbital solutions to the GD-1 stream to demonstrate that this works very well: the predicted `STREAMFINDER` radial velocities match the stream velocities measured by Koposov et al. (2010). Furthermore, our parallax measurement of 0.107 ± 0.010 mas for GD-1, based on the sample we obtain with the `STREAMFINDER`, also matches well the distance range of the orbital solutions shown in Figure 4 (these are not independent measurements, however the algorithm "sees" the potential stream stars diluted in a gigantic Galactic contaminating population). This success gives us confidence that we will be able to use the

predicted STREAMFINDER radial velocities to probe the orbital properties of the stellar stream population as a whole.

Several more streams have been reported within 40 kpc than the five that we recover here (see Figure 1). The reason for this is likely to be due, in part, to the specific parameter choices we adopted in the algorithm (for instance we chose a model width of 100 pc throughout, and we examined only a narrow range of stellar population template models). In subsequent contributions, we intend to relax these constraints allowing for a more complete census to be established. Additionally, we intend to examine different models of the Galactic potential; presumably our stream detection method should reveal the highest contrast for long stellar streams when using the correct potential. However, another reason that we did not recover all known streams within 40 kpc is simply that Gaia's photometry is not as deep as existing sky surveys; note that for a stellar population of metallicity $[\mathrm{Fe/H}] = -1.5$, the distance at which the proper motion uncertainties in Gaia DR2 at the main sequence turnoff are $50\,\mathrm{km\,s^{-1}}$ (i.e. approximately half the dispersion of the contaminating halo) is 14.0 kpc. Hence it is not very surprising that photometric surveys that are much deeper than Gaia remain competitive for finding low-mass stellar streams at distances $\gtrsim 15$ kpc.

Thanks to the amazingly rich phase-space information provided by the Gaia spacecraft and consortium, we are now starting to unravel the very fine details of galaxy formation in action. While the results presented here are but a first step in the comprehensive mapping of the Milky Way's stellar halo and accretion events, they already show the promises borne out by the deep, multi-dimensional space unveiled in DR2. The harvest of previously unknown thin stellar streams, likely stemming from the tidal disruption of globular clusters, opens up exciting times as these are powerful probes of the distribution of dark matter sub-halos in our surroundings (Johnston et al. 2002; Ibata et al. 2002; Carlberg et al. 2012; Bovy 2016), they can provide an independent inference of the location of the Sun in phase space (Malhan & Ibata 2017), and they can be used as sensitive seismographs to constrain the shape and depth of the Milky Way potential (Ibata et al. 2013; Bonaca & Hogg 2018). The combination of Gaia DR2 and detections provided by STREAMFINDER places us in a unique position to disentangle the numerous detections accretion events in the Milky Way halo and open the most exciting Galactic archaeology playground to date.

ACKNOWLEDGEMENTS

We thank the anonymous referee very much for their helpful comments.

This work has made use of data from the European Space Agency (ESA) mission *Gaia* (https://www.cosmos.esa.int/gaia), processed by the *Gaia* Data Processing and Analysis Consortium (DPAC, https://www.cosmos.esa.int/web/gaia/dpac/consortium). Funding for the DPAC has been provided by national institutions, in particular the institutions participating in the *Gaia* Multilateral Agreement.

The authors would like to thank Michel Ringenbach of the HPC centre of the Université de Strasbourg for his kind support. We also acknowledge support by the Programme National Cosmology et Galaxies (PNCG) of CNRS/INSU with INP and IN2P3, co-funded by CEA and CNES. N. F. Martin gratefully acknowledges the Kavli Institute for Theoretical Physics in Santa Barbara and the organizers of the "Cold Dark Matter 2018" program, during which some of this work was performed. This research was supported in part by the National Science Foundation under Grant No. NSF PHY11-25915

REFERENCES

Balbinot E., Gieles M., 2018, MNRAS, 474, 2479
Belokurov V., et al., 2006, ApJ, 642, L137
Bernard E. J., et al., 2014, MNRAS, 443, L84
Bonaca A., Hogg D. W., 2018, preprint, (arXiv:1804.06854)
Bovy J., 2016, Physical Review Letters, 116, 121301
Bovy J., Bahmanyar A., Fritz T. K., Kallivayalil N., 2016, ApJ, 833, 31
Bullock J. S., Boylan-Kolchin M., 2017, ARA&A, 55, 343
Carlberg R. G., Grillmair C. J., Hetherington N., 2012, ApJ, 760, 75
Dehnen W., Binney J., 1998, MNRAS, 294, 429
Erkal D., Belokurov V., Bovy J., Sanders J. L., 2016, MNRAS, 463, 102
Evans, D. W. et al., 2018, A&A
Eyre A., Binney J., 2009, MNRAS, 400, 548
Gaia Collaboration et al., 2016, A&A, 595, A2
Gaia Collaboration Brown, A. G. A. Vallenari, A. Prusti, T. de Bruijne, J. H. J. et al. 2018, A&A
Grillmair C. J., 2006, ApJ, 645, L37
Grillmair C. J., Carlin J. L., 2016, in Newberg H. J., Carlin J. L., eds, Astrophysics and Space Science Library Vol. 420, Tidal Streams in the Local Group and Beyond. p. 87 (arXiv:1603.08936), doi:10.1007/978-3-319-19336-6˙4
Grillmair C. J., Dionatos O., 2006, ApJ, 643, L17
Harris W. E., 2010, preprint, (arXiv:1012.3224)
Helmi A., White S. D. M., 1999, in Gibson B. K., Axelrod R. S., Putman M. E., eds, Astronomical Society of the Pacific Conference Series Vol. 165, The Third Stromlo Symposium: The Galactic Halo. p. 89 (arXiv:astro-ph/9811108)
Helmi, A. van Leeuwen, F. McMillan, P. DPAC 2018, A&A
Ibata R., Lewis G. F., Irwin M., Totten E., Quinn T., 2001, ApJ, 551, 294
Ibata R. A., Lewis G. F., Irwin M. J., Quinn T., 2002, Monthly Notices of the Royal Astronomical Society, 332, 915
Ibata R., Lewis G. F., Martin N. F., Bellazzini M., Correnti M., 2013, ApJ, 765, L15
Ibata R. A., et al., 2017a, ApJ, 848, 128
Ibata R. A., et al., 2017b, ApJ, 848, 129
Ibata R. A., Malhan K., Martin N. F., Starkenburg E., 2018, preprint, (arXiv:1806.01195)
Johnston K. V., Hernquist L., Bolte M., 1996, ApJ, 465, 278
Johnston K. V., Zhao H., Spergel D. N., Hernquist L., 1999, ApJ, 512, L109
Johnston K. V., Spergel D. N., Haydn C., 2002, ApJ, 570, 656
Karim M. T., Mamajek E. E., 2017, MNRAS, 465, 472
Koposov S. E., Rix H.-W., Hogg D. W., 2010, ApJ, 712, 260
Küpper A. H. W., Balbinot E., Bonaca A., Johnston K. V., Hogg D. W., Kroupa P., Santiago B. X., 2015, ApJ, 803, 80
LSST Dark Energy Science Collaboration 2012, preprint, (arXiv:1211.0310)
Law D. R., Majewski S. R., 2010, ApJ, 714, 229
Lindegren, L. Hernandez, J. Bombrun, A. Klioner, S. Bastian, U. Ramos-Lerate, M. 2018, A&A
Luri, Xavier et al., 2018, A&A

Majewski S. R., Skrutskie M. F., Weinberg M. D., Ostheimer J. C., 2003, ApJ, 599, 1082
Malhan K., Ibata R. A., 2017, MNRAS, 471, 1005
Malhan K., Ibata R. A., 2018, MNRAS,
Marigo P., Girardi L., Bressan A., Groenewegen M. A. T., Silva L., Granato G. L., 2008, A&A, 482, 883
Mateu C., Read J. I., Kawata D., 2018, MNRAS, 474, 4112
McConnachie A. W., 2012, AJ, 144, 4
Newberg H. J., Willett B. A., Yanny B., Xu Y., 2010, ApJ, 711, 32
Reid M. J., et al., 2014, ApJ, 783, 130
Robin A. C., et al., 2012, A&A, 543, A100
Sanders J. L., Bovy J., Erkal D., 2016, MNRAS, 457, 3817
Sanderson C., Curtin R., 2017, Journal of Open Source Software, 2
Schlegel D. J., Finkbeiner D. P., Davis M., 1998, ApJ, 500, 525
Schönrich R., Binney J., Dehnen W., 2010, MNRAS, 403, 1829
Shipp N., et al., 2018, preprint, (arXiv:1801.03097)
de Boer T. J. L., Belokurov V., Koposov S. E., Ferrarese L., Erkal D., Cote P., Navarro J. F., 2018, preprint, (arXiv:1801.08948)
de Bruijne J. H. J., 2012, Ap&SS, 341, 31

This paper has been typeset from a TEX/LATEX file prepared by the author.

CHAPTER 6

CONSTRAINING THE POTENTIAL OF THE MILKY WAY GALAXY WITH GD-1 STREAM

There are no facts, only interpretations- **Friedrich Wilhelm Nietzsche**

Related paper : **Constraining the Milky Way Halo Potential with the GD-1 stellar stream**, 2018, Khyati Malhan & Rodrigo Ibata, submitted to *MNRAS* (ADS entry)

Abstract

ESA/Gaia astrometry together with SEGUE measurements of the 70° long GD-1 stellar stream were used to explore the improvement on the Galactic gravitational potential that the new Gaia data provided. Assuming a realistic universal model for the halo together with reasonable models of the baryonic components, it was found that the GD-1's orbital solutions require the circular velocity at the Solar radius to be $V_{\rm circ}(R_\odot) = 244^{+6}_{-2}\,{\rm km\,s^{-1}}$, and also that the density flattening of the halo is $q_\rho = 0.86^{+0.04}_{-0.07}$. The corresponding Galactic mass within 14.5 kpc, the mean Galactocentric distance of GD-1, was found to be $M_{MW}(< 14.5\,{\rm kpc}) = 1.75^{+0.06}_{-0.05} \times 10^{11}\,{\rm M_\odot}$. Moreover, Gaia's excellent proper motions also allowed estimation of the velocity dispersion of the GD-1 stream in the direction tangential to the line of sight to be $< 1.25\,{\rm km\,s^{-1}}$ (90% confidence limit), confirming the extremely cold dynamical nature of this system.

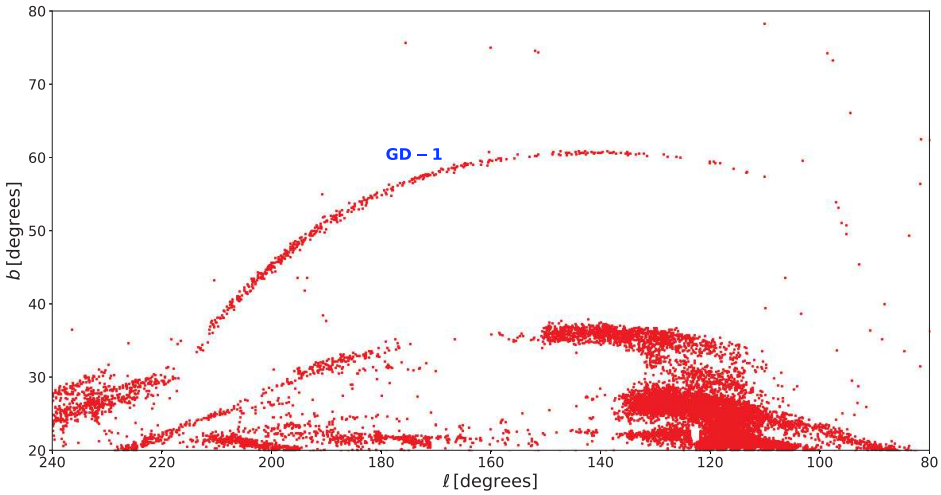

Figure 6.1: GD-1 stream in the STREAMFINDER density map. The figure shows the stream detection density plot that was obtained from the STREAMFINDER algorithm after its application on Gaia DR2 dataset (see Chapter 5). The map corresponds to the Stellar Population template model of ([Fe/H], Age) = $(-2.2, 10\,\mathrm{Gyr})$, and shows stars with detection significance $> 5\sigma$. The $\sim 70°$ long GD-1 stream stands out strikingly in this plot, which provides the basis for the sample that was used in present analysis.

6.1 Introduction

Stellar streams of low mass progenitors closely follow orbits [39, 52] and hence their orbital properties are often exploited to constrain the underlying gravitational potential. Different methods of stream dynamical analyses have been developed, including 1) the *orbit-fitting procedure* where orbits are integrated in different potential models and are then compared to stream data [106, 140], 2) the *N-body simulation procedure* where N-body simulated particles are compared with the data [111, 181], 3) the *particle-spray modelling* that models stellar tidal streams with mass-less particles [108, 185], and 4) *action-angle methods* that make use of the properties of streams in action-angle space rather than in the conventional 6D phase-space [17, 51].

In the cases where stellar streams vividly exhibit two tidal arms emerging out of the progenitor cluster at slightly different energies and angular momenta (like the Palomar 5 stream [90, 156]), it is ideal to undertake a particle-spray approach or N-body simulation to allow for more realistic modelling [107, 181]. However, GD-1 is observed to be a narrow linear stream structure that lacks any obvious twin tidal arm features, and to date suggestions of the location of the progenitor's remnant are not completely convincing [33, 121, 149]. Therefore, given the narrow and simple structure of GD-1 (see Figure 6.1), this stream was chosen to be modelled with an orbit fitting procedure.

6.2 Data

The selection of the sample of GD-1 member stars was extracted from the output of the `STREAMFINDER` algorithm [120–122], obtained from processing the Gaia DR2 dataset [60, 62, 63], after adopting a Single Stellar population (SSP) template model of ([Fe/H], Age) = (−2.2, 10 Gyr). The corresponding stream map is shown in Figure 6.1, where all sources have a significance of $> 5\sigma$ of belonging to a stellar stream, as estimated by the algorithm. In this map, the 70° long GD-1 stream stands out strikingly from the background contaminating stars.

This GD-1 sample was then cross-matched with the SDSS/SEGUE dataset [200] in order to obtain their line-of-sight (los) velocities ($v_{\rm los}$) that were missing in Gaia DR2[1], for which only a tiny fraction of positive matches were found. After rejecting the outliers, the resulting sample consisted of 403 high confidence GD-1 stars in which all the stars possessed 5D astrometric measurements and only 31 had additional $v_{\rm los}$ measurements. For the stars without SEGUE measurements, they were assigned $v_{\rm los} = 0$ and respective uncertainties of $\delta v_{\rm los} = 600\,{\rm km\,s^{-1}}$ were assumed (equivalent to the escape velocity from the Milky Way [174]).

6.3 Method

`galpy` module[2] [16] was used for the purpose of setting the Galactic potential models and for the orbit calculations. Two Milky Way potential models were studied, both of them consisting of a bulge, a disk and a dark-matter halo. Such a 3 component parameterization reproduces the main mass components of the Milky Way, that also has been a common choice in previous stream dynamical studies done on the Sagittarius, GD-1 and Pal-5 streams [106, 107, 111]. The two parameters of the potential that were explored in both the cases were the circular velocity at the solar radius $V_{\rm circ}(R_\odot)$ and z-flattening parameter of the dark matter halo q_ρ.

6.3.1 Logarithmic halo potential

In this first case, the bulge was represented by a Hernquist potential, the disk by a Miyamoto-Nagai potential [129] and the dark-matter halo model, that was intended to be studied, by a logarithmic potential given as :

$$\Phi_h(x,y,z) = \frac{V_h^2}{2}\ln\left(x^2 + y^2 + \frac{z^2}{q_\Phi^2} + d^2\right), \tag{6.1}$$

with V_h as the circular velocity of the halo in the limit $r >> d$ and q_Φ as the z-flattening of the potential. The total Galactic potential $\Phi(x,y,z)$ sets the value of the circular velocity at the solar radius $V_{\rm circ}(R_\odot)$.

[1] Gaia DR provides line of sight velocities only for stars with G < 12

[2] `http://github.com/jobovy/galpy`

The scheme used for the orbit fitting and parameter exploration was straightforward. The $(V_{\rm circ}(R_\odot), q_\Phi)$ parameter space was first gridded in bins of $4\,{\rm km\,s^{-1}} \times 0.04$. The orbit fitting for a given value of $(V_{\rm circ}(R_\odot), q_\Phi)$ was done as follows. A 6D phase-space starting point is required to integrate an orbit. Without loss of generality, $\delta = 39°$ was fixed as a starting point of the orbit (the $\delta = 39°$ line passes close to the mid point of the GD-1 stream), and $\alpha, \varpi, \mu_\alpha, \mu_\delta, v_{\rm los}$ were left as free parameters to be explored by a Markov Chain Monte Carlo (MCMC) algorithm. Every starting 6-D phase-space point was integrated into an orbit, that was then compared with the data in the 6D observable space $(\alpha, \delta, \pi, \mu_\alpha, \mu_\delta, v_{\rm los})$ in order to find the best orbit corresponding to the highest log-likelihood value for the given set of $(V_{\rm circ}(R_\odot), q_\Phi)$. For every potential $\Phi(x, y, z | V_{\rm circ}(R_\odot), q_\Phi)$, the best fit orbit was found and the corresponding log-likelihood was assigned to the $(V_{\rm circ}(R_\odot), q_\Phi)$ bin.

For this case, the likelihood surface was found to be well behaved and peaked at the value $(V_{\rm circ}(R_\odot), q_\Phi) = (238^{+14}_{-4}\,{\rm km\,s^{-1}}, 0.89^{+0.05}_{-0.03})$ (see Figure 3 in the paper attached). Using the approximation $1 - q_\rho \approx 3(1 - q_\Phi)$ [13], that is valid for moderate flattening, the best value corresponded to the parameter set $(V_{\rm circ}(R_\odot), q_\rho) = (238^{+14}_{-4}\,{\rm km\,s^{-1}}, 0.67^{+0.04}_{-0.02})$. This resulting value of $V_{\rm circ}(R_\odot) = 238^{+14}_{-4}\,{\rm km\,s^{-1}}$ was found to be consistent with various previous independent studies [106, 107, 127, 152]. However, the resulting rotation curve severely overestimated the Milky Way's mass at large radius.

6.3.2 NFW halo profile

To overcome the limitations of the simple logarithmic halo model, the previous analysis was repeated but this time using a Navarro-Frenk-White (NFW) halo model [139], which was also motivated by cosmological simulations (as also pointed out in Chapter 1).

To this end, the bulge was modelled as a power-law density profile, the disk by a Miyamoto-Nagai potential and the dark-matter halo model by an axisymmetric NFW profile given as:

$$\rho_h(x, y, z) = \frac{M_{vir}}{4\pi r_s^3} \frac{1}{(m/r_s)(1 + m/r_s)^2}, \tag{6.2}$$

where

$$m = x^2 + \frac{y^2}{(b_h/a_h)^2} + \frac{z^2}{(c_h/a_h)^2}\,. \tag{6.3}$$

An axisymmetric NFW profile was modelled by setting $a_h, b_h = 1$, and c_h ($\equiv q_\rho$, i.e. the z-flattening of the density) along with $V_{\rm circ}(R_\odot)$ parameters were explored.

Figure 6.2 presents the resulting contour plot of the parameter exploration and the comparison between the data and the best-fit orbit. This time, the best values were obtained as $(V_{\rm circ}(R_\odot), q_\rho) = (244^{+6}_{-2}\,{\rm km\,s^{-1}}, 0.86^{+0.04}_{-0.07})$, thereby placing tight constraints on the circular velocity at the Solar radius and the shape of the dark matter halo assuming this model potential. It was also noted that this halo flattening was significantly different to the one that was obtained with the logarithmic

halo model. Using the same approximation as before, it was found that $q_\Phi = 0.95^{+0.04}_{-0.08}$. The resulting Milky Way rotation curve also matched the expectations for the circular velocity in the outer regions of the Galaxy reasonably well.

6.4 Results and Discussions

Two different Galactic potential models were studied by employing dynamical analysis of the GD-1 stream. Both of these potential models were 3 component models comprising a bulge, a disk and a dark matter halo.

In the first case, the bulge, disk and halo were modelled with Hernquist, Miyamoto-Nagai and logarithmic profiles respectively. In this case, the potential parameter values were estimated as $(V_{\rm circ}(R_\odot), q_\rho) = (238^{+14}_{-4}\,{\rm km\,s^{-1}}, 0.67^{+0.04}_{-0.02})$. While providing a useful comparison to some previous studies (for e.g., [106]), this model was disfavoured as it was not motivated by cosmological simulations.

The second potential model that was then examined comprised a bulge, a disk and a halo, modelled with a power-law, Miyamoto-Nagai and axisymmetric NFW profile respectively. This time, the parameter values were measured as $(V_{\rm circ}(R_\odot), q_\rho) = (244^{+6}_{-2}\,{\rm km\,s^{-1}}, 0.86^{+0.04}_{-0.07})$. This estimate of the $V_{\rm circ}(R_\odot)$ value was found to be in excellent agreement with those obtained by other authors based on different [127, 152] and similar [107] approaches. As for q_ρ result, it was found to be consistent with one of the previous results that also employed dynamical analysis of the GD-1 stream [17], however being in tensions with another one [106]. Also, this q_ρ result was found to be inconsistent with a recent measurement where a prolate halo solutions with $q_\rho = 1.3 \pm 0.25$ was favoured based on analysis of globular clusters [148].

With this second model, the mass of the Milky Way in the inner 14.5 kpc, the mean Galactocentric distance of GD-1, was estimated to be $M_{MW}(< 14.5\,{\rm kpc}) = 1.75^{+0.06}_{-0.05} \times 10^{11}\,{\rm M_\odot}$. Extrapolating out slightly to $R = 20\,{\rm kpc}$, it was found that $M_{MW}(< 20\,{\rm kpc}) = 2.14 \pm 0.07 \times 10^{11}\,{\rm M_\odot}$. This value was found to be consistent with those obtained based on analysis of globular clusters based on Gaia DR2 kinematics [148, 191], and also with previous studies of Pal 5 stream [107]. The agreement between these studies with different approaches and different dynamical tracers suggests that the mass in the inner regions of the halo is beginning to be understood. However, these results are dependent on the models and associated parameters that have been assumed in the various studies, and in particular the corresponding uncertainties have to be interpreted with care.

Gaia's well measured proper motions were also used in order to measure, for the first time, the internal velocity dispersion of the GD-1 stream stars. Although, no useful constraints could be put on the line of sight dispersion component due to the large uncertainties in the SEGUE radial velocity measurements, but strong limits on the tangential (2D) velocity dispersion were placed that was found as $\sigma_{v_T\,int} < 1.25\,{\rm km\,s^{-1}}$ at the 90% confidence level. In addition to indicating that GD-1 is an extremely dynamically cold system and indeed the remnant of a globular cluster, such

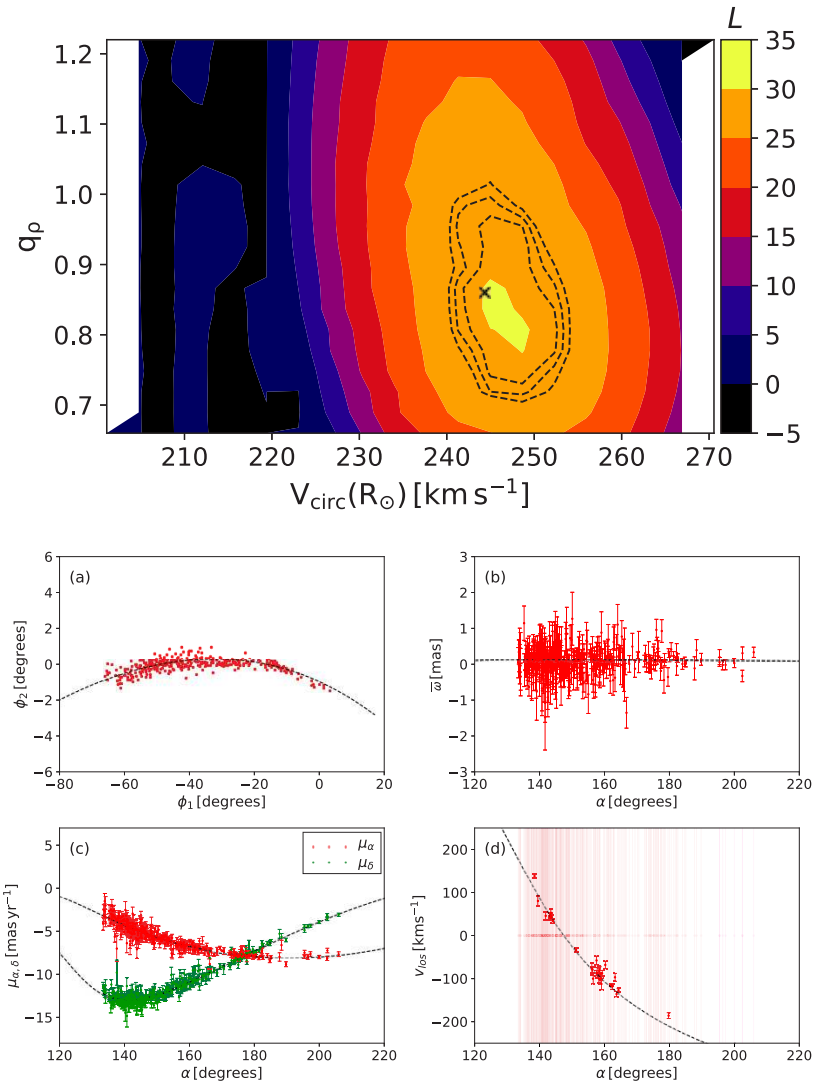

Figure 6.2: Orbit-fitting for the NFW halo potential. *Top panel* : The contours of log-likelihood. The tuple of best-fit parameters $(V_{\rm circ}(R_\odot), q_\rho) = (244^{+6}_{-2}\,{\rm km\,s^{-1}}, 0.86^{+0.04}_{-0.07})$ is marked with a cross, while the black dashed contours show the $1\sigma, 2\sigma, 3\sigma$ confidence regions. *Lower panels* : The data-model comparison for the best-fit orbit, which is shown with black dashed curves while the data is represented by colored points accompanied with the associated error bars. The light colored vertical red streaks in the los velocity plot correspond to data points that were missing v_{los} measurements.

a low velocity dispersion also suggests that so far GD-1 has not suffered significant external heating, due to interactions with the disk, bar, or any halo substructures in the Milky Way.

6.5 Related Paper

MNRAS **000**, 1–11 (2018) Preprint 15 July 2018 Compiled using MNRAS LATEX style file v3.0

Constraining the Milky Way Halo Potential with the GD-1 stellar stream

Khyati Malhan,[1⋆] Rodrigo A. Ibata,[1†]
[1] *Université de Strasbourg, CNRS, Observatoire Astronomique de Strasbourg, UMR 7550, F-67000 Strasbourg, France*

Accepted XXX. Received YYY; in original form ZZZ

ABSTRACT

We use ESA/Gaia astrometry together with SEGUE measurements of the 70° long GD-1 stellar stream to explore the improvement on the Galactic gravitational potential that these new data provide. Assuming a realistic universal model for the halo together with reasonable models of the baryonic components, we find that orbital solutions require the circular velocity at the Solar radius to be $V_{\rm circ}(R_\odot) = 244^{+6}_{-2}\,{\rm km\,s^{-1}}$, and also that the density flattening of the halo is $q_\rho = 0.86^{+0.04}_{-0.07}$. The corresponding Galactic mass within 14.5 kpc, the mean Galactocentric distance of GD-1, is $M_{\rm MW}(< 14.5\,{\rm kpc}) = 1.75^{+0.06}_{-0.05} \times 10^{11}\,{\rm M}_\odot$. Moreover, Gaia's excellent proper motions also allowed us to measure the velocity dispersion of the GD-1 stream in the direction tangential to the line of sight to be $< 1.25\,{\rm km\,s^{-1}}$ (90% confidence limit), confirming the extremely cold dynamical nature of this system.

Key words: Galaxy : halo - Galaxy: structure - stars: kinematics and dynamics - Galaxy: fundamental parameters

1 INTRODUCTION

The mass density profile and spatial distribution of the dark matter halo around the Milky Way galaxy are of great astrophysical and cosmological importance, but observationally they have been very hard to pin down. In recent years a wide range of solutions for the shape of the dark matter halo have been found, from close to spherical (Ibata et al. 2001; Küpper et al. 2015), oblate or prolate (Law et al. 2005; Helmi 2004), to triaxial (Law & Majewski 2010). The disparities have persisted in part due to a lack of good quality tangential velocity measurements and distance estimates of halo tracer stars. This situation now looks set to change thanks to the excellent ESA/Gaia data that has recently been made available to the astronomical community (Gaia Collaboration et al. 2016, 2018a,b,c).

Various methods have been employed to constrain the mass distribution of the Milky Way galaxy. These include analyses based on the rotation curve of the Galaxy (Sofue 2012), Jeans analyses that assume dynamical equilibrium of some tracer population to constrain the gravitational force field (Loebman et al. 2014; Bowden et al. 2016; Diakogiannis et al. 2017; Read & Steger 2017), orbital analyses of satellites (Watkins et al. 2018a; Fritz et al. 2018), and distribution function analyses (Posti & Helmi 2018). However, many recent studies have turned to using stellar streams as dynamical probes (Ibata et al. 2001; Helmi 2004; Koposov et al. 2010; Law & Majewski 2010; Küpper et al. 2015; Bovy et al. 2016).

Stellar streams are structures that are formed via the tidal disruption of globular clusters or dwarf galaxies as they orbit around their host galaxy (Johnston 1998; Helmi & White 1999). In the low mass limit, the track traced by a stream closely delineates an orbit (Dehnen et al. 2004; Eyre & Binney 2011), and this orbital property can be exploited to constrain the underlying gravitational potential and the dark matter distribution, especially in the Milky Way where accurate measurements of the kinematic and distances of stars are available (Ibata et al. 2001; Koposov et al. 2010; Newberg et al. 2010; Varghese et al. 2011; Küpper et al. 2015; Bovy et al. 2016). Now with the arrival of the second data release (DR2) of the ESA/Gaia mission (de Bruijne 2012; Gaia Collaboration et al. 2018a; Lindegren, L. et al. 2018), which has provided a huge leap in the quality of phase-space information of streams in the Milky Way, we may re-appraise the constraints provided by these structures.

In this contribution we make use of the GD-1 stellar stream (discovered by Grillmair & Dionatos 2006) to probe the the Milky Way's gravitational potential. The GD-1 stream has been used before for a similar purpose (Koposov et al. 2010; Bovy et al. 2016). Situated at an intermediate halo distance ($d_\odot \sim 8\,{\rm kpc}$), this vastly extended pen-

⋆ E-mail: khyati.malhan@astro.unistra.fr
† E-mail: rodrigo.ibata@astro.unistra.fr

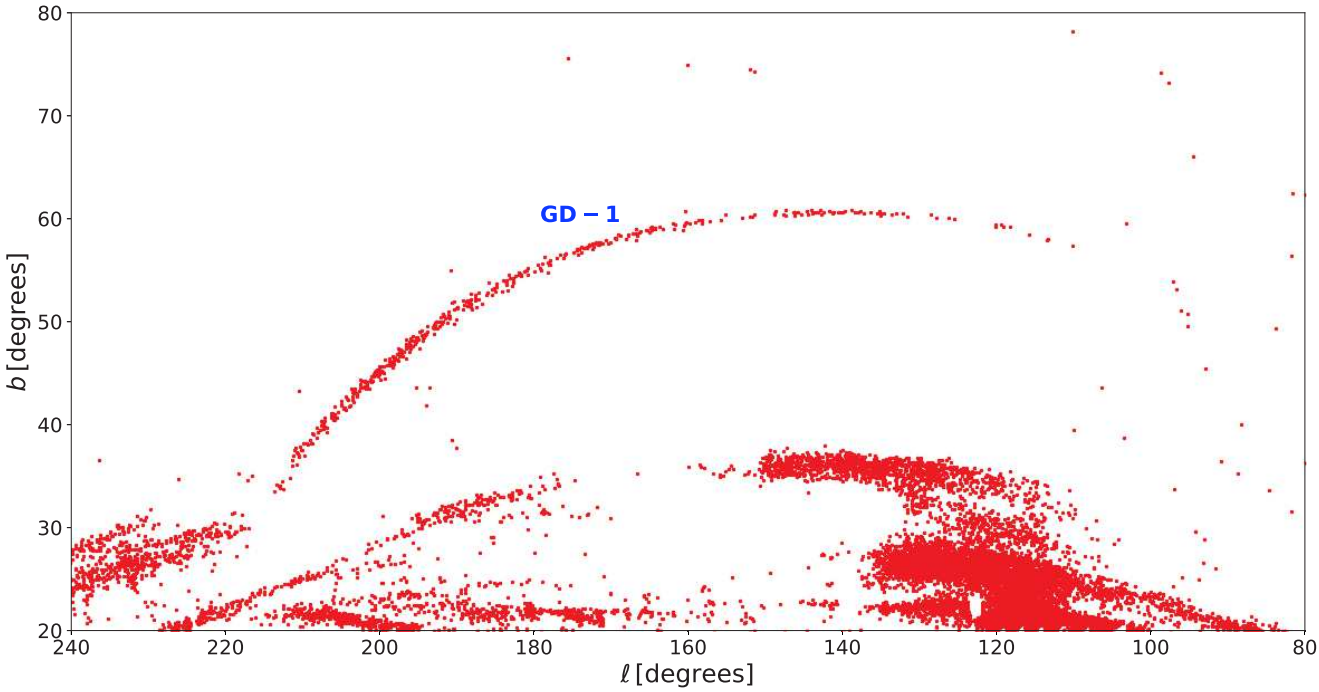

Figure 1. GD-1 stream in the STREAMFINDER density map. The figure shows the stream detection density plot that we obtained from the STREAMFINDER algorithm after its application on Gaia DR2 dataset. The map corresponds to the Stellar Population template model of ([Fe/H], Age) = $(-2.2, 10\,\mathrm{Gyr})$, and shows stars with detection significance $> 5\sigma$. The $\sim 70^\circ$ long GD-1 stream stands out strikingly in this plot, which provides the basis for the sample used in our analysis.

cil line structure ($\sim 80^\circ$ in angular length, Price-Whelan & Bonaca 2018) is among the highest contrast streams in the Gaia dataset, making it a useful case study to assess the improvement provided by the excellent proper motions in Gaia DR2.

This paper is arranged as follows. In Section 2 we describe the selection criteria that were applied to the original Gaia data in order to select the GD-1 stream stars. Section 3 details the different potential models that we employ in our analysis and the resulting parametric constraints. In Section 4 we measure the internal velocity dispersion of the GD-1 stream. Finally in Section 5 we discuss our results and draw our conclusions.

2 DATA

The selection of our sample of GD-1 member stars was extracted from the output of the STREAMFINDER algorithm (Malhan & Ibata 2018; Malhan et al. 2018a,b), obtained from processing the Gaia DR2 dataset (Gaia Collaboration et al. 2018a; Luri, Xavier et al. 2018), after adopting a Single Stellar population (SSP) template model of ([Fe/H], Age) = $(-2.2, 10\,\mathrm{Gyr})$. The corresponding stream map is shown in Figure 1, where all sources have a significance of $> 5\sigma$ of belonging to a stellar stream, as estimated by the algorithm. In addition to several stream structures detected around the Galactic anti-centre region (and which will be discussed in a future contribution), the algorithm detects the GD-1 stream which stands out strikingly from the background contaminating stars. Here, our algorithm detected the GD-1 stream as a $\sim 70^\circ$ long structure (but see Price-Whelan & Bonaca 2018 where they report it to be $\sim 80^\circ$ in length). Although the STREAMFINDER detects streams by looking along orbits integrated in an assumed Galactic potential model, we have shown (Malhan & Ibata 2018) that the stream detection itself is rather independent of the potential model, as long as a reasonably realistic Galactic mass model is used.

We then drew a generous $\sim 5^\circ$ wide irregular polygon around the GD-1 structure in this map. This selection yielded 438 potential GD-1 stars that appear highly coherent in position, proper motion and color-magnitude space. These stars were cross-matched with the SDSS/SEGUE dataset (Yanny et al. 2009) in order to obtain their line-of-sight (los) velocities ($v_{\rm los}$) that are missing in Gaia DR2[1]. A total of 60 GD-1 candidate members yielded positive cross-matches with SEGUE, from which we obtained $v_{\rm los}$ and metallicity ([Fe/H]) measurements. For the stars without SEGUE measurements, we assign $v_{\rm los} = 0$, and [Fe/H] = 0, and assume respective uncertainties of $\delta v_{\rm los} = 600\,\mathrm{km\,s^{-1}}$ (equivalent to the escape velocity from the Milky Way, Smith et al. 2007) and $\delta[Fe/H] = 10$ dex.

The dataset was cleaned by rejecting 3σ outliers in parallax and [Fe/H]. To reject the outliers in parallax, we used the STREAMFINDER distance solutions as the distance model values[2] that match quite well with the photometric distance

[1] Gaia DR provides line of sight velocities only for stars with G < 12

[2] As explained in Malhan & Ibata (2018), STREAMFINDER obtains

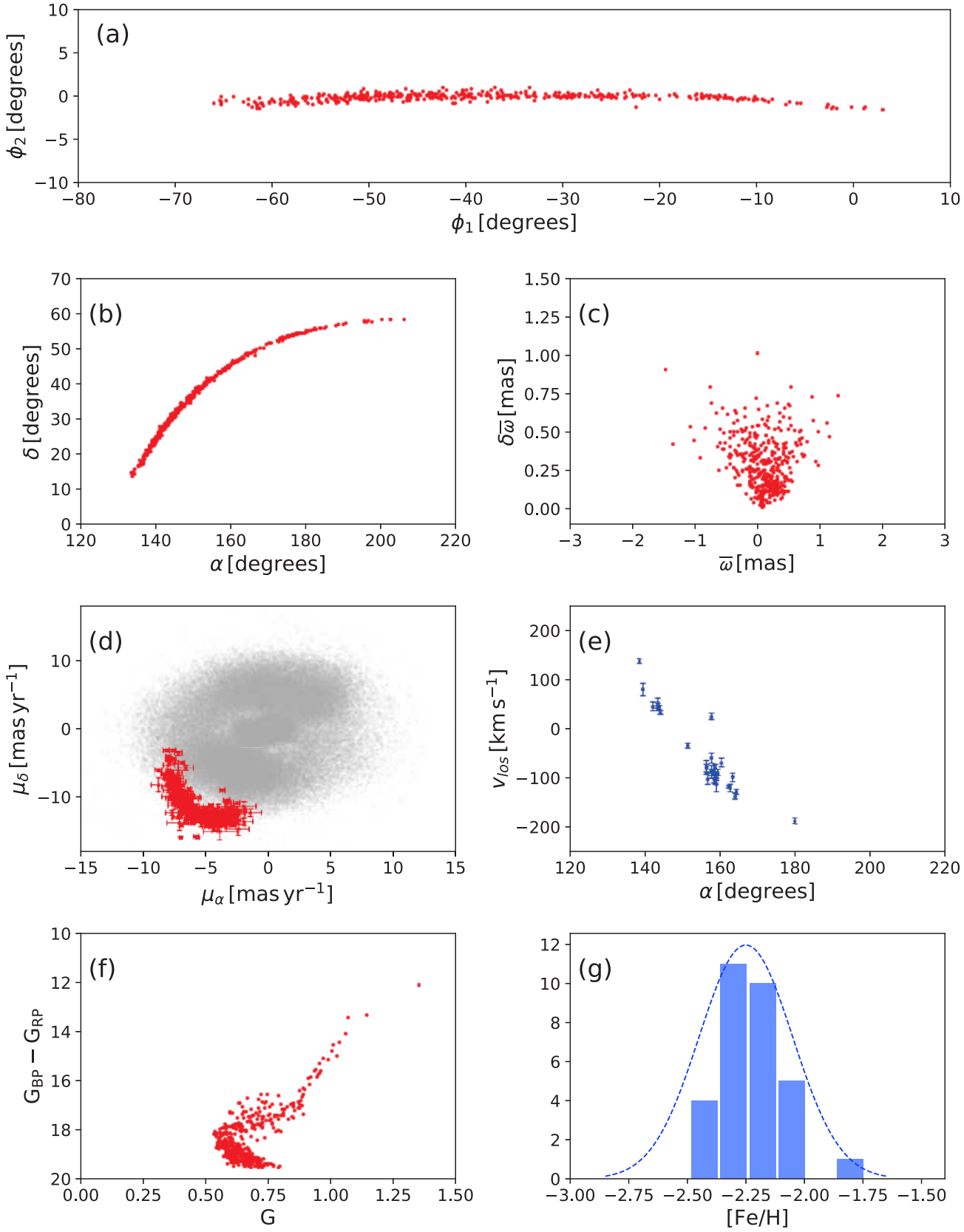

Figure 2. GD-1 stream phase-space map and chemistry. We extracted a $\sim 5°$ wide region around the GD-1 stream in Figure 1 yielding 438 stars. This sample was cleaned for contamination by implementing a sigma clipping procedure to reject the 3σ outliers in parallax and metallicity, resulting in a sample containing 403 potential GD-1 members. The position, parallax, proper motion, radial velocity, color-magnitude and metallicity distribution of these stars are shown here. The red points represent all the 403 stars in the sample observed by Gaia, while the 31 blue points show the cross-matches that we found in the SDSS/SEGUE dataset. The gray stars in the proper motion space are the remaining `STREAMFINDER` processed stars.

values that have been previously reported for GD-1 stars (Grillmair & Dionatos 2006; Koposov et al. 2010). The iterative 3σ clipping in [Fe/H] converged on a mean value of $[\mathrm{Fe/H}]_o = -2.25$. After rejecting the outliers, the resulting sample consisted of 403 high confidence GD-1 stars in which all the stars possessed 5D astrometric measurements and only 31 had additional $v_{\rm los}$ and [Fe/H] values. This GD-1 sample is represented in Figure 2. We find the GD-1 stream to be an extremely metal poor halo substructure, having a mean metallicity of $[\mathrm{Fe/H}] = -2.25 \pm 0.04$, consistent with previous studies (Li et al. 2017; Huang et al. 2018). The spatial, kinematical and chemical properties of the GD-1 stream are tabulated in Table 1. We refer to this GD-1 sample as sample-1.

3 CONSTRAINING THE MILKY WAY HALO POTENTIAL

Stellar streams of low mass progenitors closely follow orbits (Dehnen et al. 2004; Eyre & Binney 2011) and hence their orbital properties are often exploited to constrain the underlying gravitational potential. Different methods of stream dynamical analysis have been developed, including (1) the *orbit-fitting procedure* where orbits are integrated in different potential models and are then compared to stream data (Koposov et al. 2010; Newberg et al. 2010), (2) the *N-body simulation procedure* where N-body simulation particles are compared with the data (Law & Majewski 2010; Thomas et al. 2016), (3) the *particle-spray modelling* that models stellar tidal streams with massless particles (Varghese et al. 2011; Küpper et al. 2012), and (4) *action-angle methods* that make use of the properties of streams in action-angle space rather than in the conventional 6D phase-space (Eyre & Binney 2009; Bovy et al. 2016).

In the cases where stellar streams vividly exhibit 2 tidal arms emerging out of the progenitor cluster at slightly different energies and angular momenta (like the Palomar 5 stream, Rockosi et al. 2002; Ibata et al. 2016), it is ideal to undertake a particle-spray approach or N-body simulation to allow for more realistic modelling (Küpper et al. 2015; Thomas et al. 2016). However, GD-1 is observed to be a narrow linear stream structure that lacks any obvious twin tidal arm features, and to date suggestions of the location of the progenitor's remnant are not completely convincing (de Boer et al. 2018; Malhan et al. 2018a; Price-Whelan & Bonaca 2018). Therefore, given the narrow and simple structure of GD-1 (as can be seen in Figure 2a), we chose to model this stream with an orbit fitting procedure.

We make use of the `galpy` module[3] (Bovy 2015) for the purpose of setting the Galactic potential models and for the orbit calculations. We discuss two Milky Way potential models, both of them consisting of a bulge, a disk and a dark-matter halo. Such a 3 component parameterization reproduces the main mass components of the Milky Way, and has been a common choice in previous stream dynamical studies done by Law & Majewski (2010), Koposov et al. (2010) and Küpper et al. (2015) on the Sagittarius, GD-1 and Pal-5 streams respectively.

3.1 Logarithmic Halo Potential

In this first case, we represent the bulge by a Hernquist potential that is initialized as `HernquistPotential` in `galpy` and is expressed as:

$$\rho_b(r) = \frac{1}{4\pi a^3}\frac{GM_b}{(r/a)(1+r/a)^3}\,, \tag{1}$$

the disk is represented by a Miyamoto-Nagai potential (Miyamoto & Nagai 1975) initialized by `MiyamotoNagaiPotential` and expressed as:

$$\Phi_d(R,z) = -\frac{GM_d}{\sqrt{R^2+(b+\sqrt{z^2+c^2})^2}}\,, \tag{2}$$

and the dark-matter halo model, that we intend to study here, was represented by a logarithmic potential (`LogarithmicHaloPotential`) given by:

$$\Phi_h(x,y,z) = \frac{V_h^2}{2}\ln\left(x^2+y^2+\frac{z^2}{q_\Phi^2}+d^2\right), \tag{3}$$

with $M_b = 3.4\times10^{10}\,\mathrm{M}_\odot$, $a = 0.70\,\mathrm{kpc}$, $M_d = 1\times10^{11}\,\mathrm{M}_\odot$, $b = 6.50\,\mathrm{kpc}$, $c = 0.26\,\mathrm{kpc}$, $d = 12\,\mathrm{kpc}$. The M_d value was taken from Küpper et al. (2015) and the values for the remaining parameters were taken from Koposov et al. (2010). This leaves (V_h, q_Φ) as the free parameters of the halo and hence of the total gravitational potential model of the Galaxy. V_h is the circular velocity of the halo in the limit $r >> d$ and q_Φ is the z-flattening parameter of the potential that defines the ellipticity (i.e. oblateness or prolateness) of the dark-matter halo. Logarithmic potentials are simplistic potential models that exhibit some of the dynamical properties of the halos of disk galaxies (in particular, their approximately flat rotation curves). Therefore, in this first case we chose to work with this simple model that was also previously employed in the kinematic modelling of GD-1 by Koposov et al. (2010).

The scheme used for the orbit fitting and parameter exploration is straightforward. We first grid the (V_h, q_Φ) parameter space ranging from $V_h = [180, 360]\,\mathrm{km\,s^{-1}}$ and $q_\Phi = [0.65, 1.25]$. V_h is a parameter associated only with the halo component. In the plots below we decided to show instead the corresponding circular velocity at the Solar radius, $V_{\rm circ}(R_\odot)$, which is a directly-measurable quantity that emerges from the total Galactic potential. We grid our parameter space in bins of $4\,\mathrm{km\,s^{-1}}\times 0.04$.

The orbit fitting for a given value of $(V_{\rm circ}(R_\odot), q_\Phi)$ was done as follows. A 6D phase-space starting point is required to integrate an orbit. Without loss of generality, we fixed $\delta = 39^\circ$ as a starting point of the orbit (the $\delta = 39^\circ$ line passes close to the mid point of the GD-1 stream), and left $\alpha, \varpi, \mu_\alpha, \mu_\delta, v_{\rm los}$ as free parameters to be explored by a Markov Chain Monte Carlo (MCMC) algorithm. Every starting 6-D phase-space point was integrated into an orbit that was then compared with the data, defined as sample-1 in Section 2, in the 6D observable space $(\alpha, \delta, \varpi, \mu_\alpha, \mu_\delta, v_{\rm los})$ in order to find the best orbit corresponding to the highest log-likelihood value for the given set of $(V_{\rm circ}(R_\odot), q_\Phi)$.

To account for possible contamination in sample-1,

distance solutions for every processed star based on the chosen SSP model.

[3] `http://github.com/jobovy/galpy`

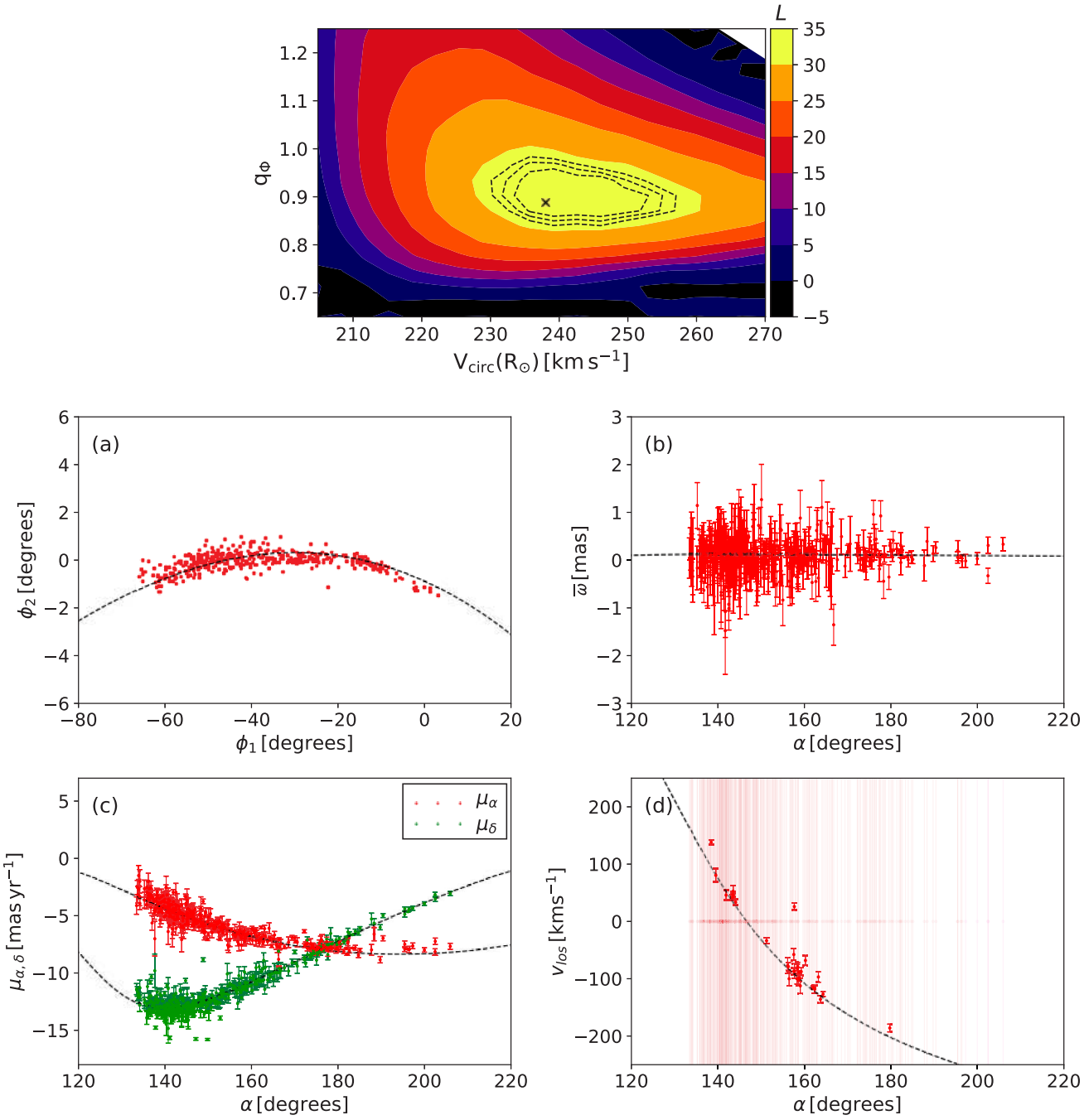

Figure 3. Orbit-fitting for the Logarithmic halo potential. The topmost panel represents the contours of log-likelihood obtained from our analysis presented in Section 3.1. The tuple of best-fit parameters $(V_{\rm circ}(R_\odot), q_\Phi) = (238^{+14}_{-4}\,{\rm km\,s^{-1}}, 0.89^{+0.05}_{-0.03})$ is marked with a cross, while the black dashed contours show the $1\sigma, 2\sigma, 3\sigma$ confidence regions. The lower four panels show the data-model comparison for the best-fit orbit, which is shown with black dashed curves while the data is represented by colored points accompanied with the associated error bars. The light colored vertical red streaks in the radial velocity plot correspond to data points that were missing radial velocity measurements.

we adopted the "conservative formulation" of Sivia (1996) which involves a modification of the log-likelihood equation that lowers the contribution from outliers to the likelihood. The log-likelihood for each datum i is given by:

$$\ln \mathcal{L}_i = -\ln\Big((2\pi)^{5/2}\sigma_{\rm sky}\sigma_{\mu_l}\sigma_{\mu_b}\sigma_{\varpi}\sigma_{v_{\rm los}}\Big) + \ln N - \ln D, \quad (4)$$

where

$$
\begin{aligned}
N &= \prod_{j=1}^{5}(1-e^{-R_j^2/2})\,,\\
D &= \prod_{j=1}^{5} R_j^2\,,\\
R_1^2 &= \frac{\omega_{\rm sky}^2}{\sigma_{\rm sky}^2}\,,\\
R_2^2 &= \frac{(\mu_{l,d}-\mu_{l,o})^2}{\sigma_{\mu_l}^2}\,,\\
R_3^3 &= \frac{(\mu_{b,d}-\mu_{b,o})^2}{\sigma_{\mu_b}^2}\,,\\
R_4^4 &= \frac{(\varpi_d-\varpi_o)^2}{\sigma_{\varpi}^2}\,,\\
R_5^2 &= \frac{(v_{los,d}-v_{los,o})^2}{\sigma_{v_{\rm los}}^2}\,.
\end{aligned}
\tag{5}
$$

Here, $\omega_{\rm sky}$ is the angular difference between the orbit and the data point, $\mu_{l,d}, \mu_{b,d}, \varpi_d$ and $v_{los,d}$ are the observed proper motion, parallaxes and los velocities, and the corresponding orbital model values are marked with the subscript 'o'. The Gaussian dispersions $\sigma_{\rm sky}, \sigma_{\mu_l}, \sigma_{\mu_b}, \sigma_{\varpi}, \sigma_{v_{\rm los}}$ are the convolution of the intrinsic dispersion of the model together with the observational uncertainty of each data point. The products N and D are over the 5 terms as written in the above equation for every phase-space dimension. Finally, the full log-likelihood used in the comparison of the model to the data is then:

$$
\ln \mathcal{L} = \sum_i \ln \mathcal{L}_i\,. \tag{6}
$$

Conversion from Galactocentric coordinates to Heliocentric observables was done by assuming that the Sun is situated at a distance of $R_\odot = 8.20\,$kpc from the Galactic centre, and we set the Sun's peculiar velocity to be $(9.0, 15.2, 7.0)\,{\rm km\,s^{-1}}$ (Schönrich et al. 2010; Reid et al. 2014).

For every potential $\Phi(x, y, z|V_{\rm circ}(R_\odot), q_\Phi)$, the best fit orbit was found and the corresponding log-likelihood was assigned to the $(V_{\rm circ}(R_\odot), q_\Phi)$ bin. Figure 3 presents the resulting contour plot of the parameter exploration and the comparison between the data and the best fit orbit. We find that the likelihood surface is well behaved and peaks at the value $(V_{\rm circ}(R_\odot), q_\Phi) = (238^{+14}_{-4}\,{\rm km\,s^{-1}}, 0.89^{+0.05}_{-0.03})$. Using the approximation $1-q_\rho \approx 3(1-q_\Phi)$ (Binney & Tremaine 2008), that is valid for moderate flattening, the best value corresponds to the parameter set $(V_{\rm circ}(R_\odot), q_\rho) = (238^{+14}_{-4}\,{\rm km\,s^{-1}}, 0.67^{+0.04}_{-0.02})$.

The resulting value of $V_{\rm circ}(R_\odot) = 238^{+14}_{-4}\,{\rm km\,s^{-1}}$ is consistent with various previous independent studies (McMillan 2011; Reid et al. 2014; Küpper et al. 2015; Koposov et al. 2010). However, the resulting rotation curve (shown in Figure 4 with the black dashed curve) severely overestimates the mass at large radius (see Figure 13 of Küpper et al. 2015 and references therein for comparison).

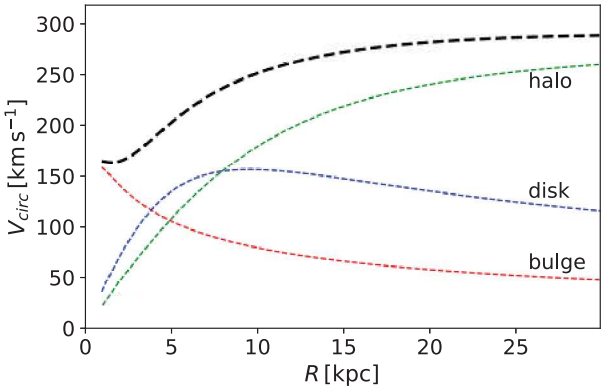

Figure 4. Velocity curve of the Galaxy model discussed in Section 3.1 incorporating a logarithmic halo potential. The red, blue and green curves correspond to the independent velocity curves due to the Hernquist bulge profile, the Miyamoto-Nagai disk profile and the logarithmic halo. The combined circular velocity curve of the Galaxy is plotted in black. We emphasize that although the rotation curve lies in the reasonable range around $R_\odot = 8.2\,$kpc, it exceeds current estimates by a great margin at large radius (for comparison see Figure 13 of Küpper et al. 2015 and references therein).

3.2 NFW Halo Profile

To overcome the limitations of the simple logarithmic halo model, we decided to repeat the previous analysis but now using a Navarro-Frenk-White (NFW) halo model, which is motivated by cosmological simulations (Navarro et al. 1997). To this end, we chose to use the `MWPotential2014` Galactic potential model of Bovy (2015), but with a slightly different halo component.

We model the bulge and the disk exactly as they are prescribed in `MWPotential2014` (Bovy 2015). The bulge is modelled as a power-law density profile (with an exponential cut-off) and is expressed as:

$$
\rho_b(r) = \rho_{bo}\left(\frac{r_1}{r}\right)^{\alpha} e^{-(r/r_c)^2}, \tag{7}
$$

with power-law exponent $\alpha = -1.8$ and cut-off radius $r_c = 1.9\,$kpc. The disk is modelled by a Miyamoto-Nagai disk potential, just like in the previous case, only this time setting b and c to the values 3.0 kpc and 0.28 kpc respectively. We describe the dark-matter halo by an axisymmetric NFW profile, instead of a simple spherical NFW profile that is used in `MWPotential2014`, given by:

$$
\rho_h(x, y, z) = \frac{M_{vir}}{4\pi r_s^3}\frac{1}{(m/r_s)(1+m/r_s)^2}, \tag{8}
$$

where

$$
m = x^2 + \frac{y^2}{(b_h/a_h)^2} + \frac{z^2}{(c_h/a_h)^2}\,. \tag{9}
$$

The ratios between a_h, b_h, c_h set the triaxiality of the dark matter halo. For the NFW halo we adopted the default values for $r_s = 16.0\,$kpc, as described in Bovy (2015), and set $a_h, b_h = 1$ forcing the halo to be axisymmetric, and aligned with the symmetry axis of the disk. We henceforth explore c_h ($\equiv q_\rho$, i.e. the z-flattening of the density) and the circular velocity at the Solar radius $V_{\rm circ}(R_\odot)$. `MWPotential2014`

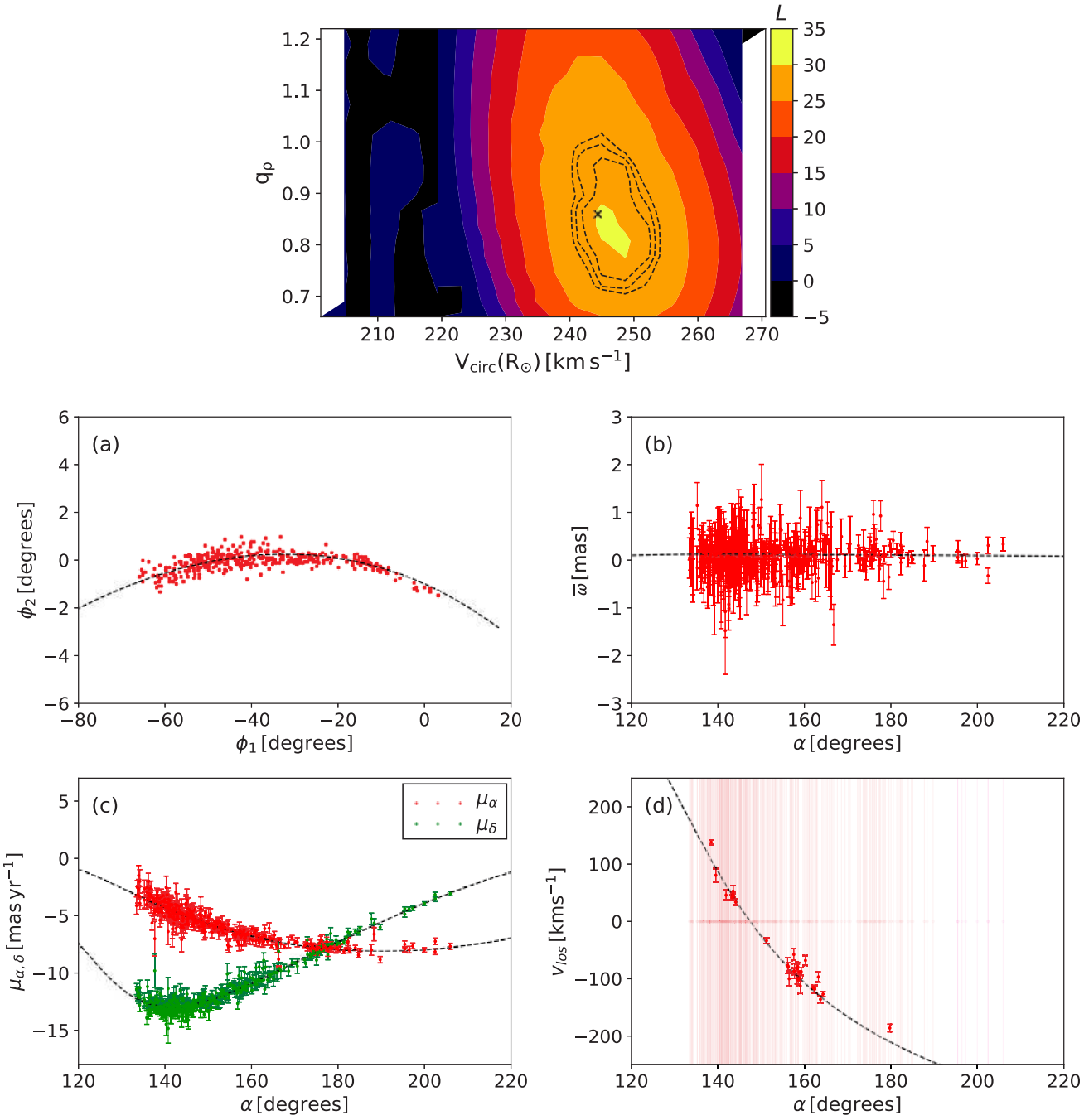

Figure 5. As Figure 3, but for the Galactic potential model discussed in Section 3.2. This time we obtained the best parameter values as $(V_{\rm circ}(R_\odot), q_\rho) = (244^{+6}_{-2}\,{\rm km\,s^{-1}}, 0.86^{+0.04}_{-0.07})$ as represented in the contour plot shown on the top panel.

sets the relative contribution from the bulge, the disk and the halo as $(f_b, f_d, f_h) = (0.05, 0.60, 0.35)$ that internally normalizes the $V_{\rm circ}(R_\odot = 8\,{\rm kpc})$ to $220\,{\rm km\,s^{-1}}$, and hence sets M_{vir} (as well as the total masses of the bulge and disk). As we probe different $V_{\rm circ}(R_\odot)$ values, we vary the three components in lock-step so as to maintain the same relative fractions of $0.05, 0.60, 0.35$ for the bulge, the disk and the halo respectively.

We make use of the previous analysis with the logarithmic halo model from Section 3.1 to improve the sample selection. This was done by rejecting those stars that lie beyond 5σ from the best orbit model in any of the observed parameters. In this way we retained 372 out of the 403 stars from sample-1 and we refer to this data set as sample-2. Now that we hold highly probable GD-1 stars, we employ the usual likelihood function, which for each datum i is ex-

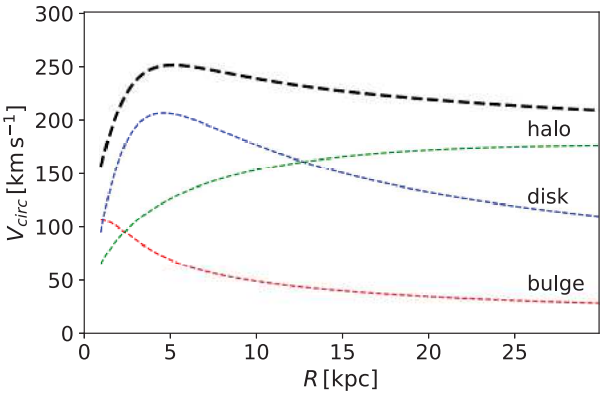

Figure 6. As Figure 4, but for a Galactic potential containing an NFW halo. The overall velocity curve of the galaxy (black) corresponding to $(V_{\rm circ}(R_\odot), q_\rho) = (244\,{\rm km\,s^{-1}}, 0.86)$, is able to both reproduce reasonable $V_{\rm circ}$ at $R_\odot$ and the expected outer rotation curve shape of the Milky Way.

pressed as:

$$\ln \mathcal{L}_i = -\ln(\sigma_{\rm sky}\sigma_{\mu_l}\sigma_{\mu_b}\sigma_{\varpi}\sigma_{v_r}) - \frac{1}{2}\Big(\frac{\omega^2_{\rm sky}}{\sigma^2_{\rm sky}} + \frac{(\mu_{l,d}-\mu_{l,o})^2}{\sigma^2_{\mu_l}} + \frac{(\mu_{b,d}-\mu_{b,o})^2}{\sigma^2_{\mu_b}} + \frac{(\varpi_d-\varpi_o)^2}{\sigma^2_{\varpi}} + \frac{(v_{los,d}-v_{los,o})^2}{\sigma^2_{v_{\rm los}}}\Big), \quad (10)$$

where the terms hold the same meaning as previously defined.

Figure 5 presents the resulting contour plot of the parameter exploration and the comparison between the data and the best-fit orbit. Here, we obtain as best values $(V_{\rm circ}(R_\odot), q_\rho) = (244^{+6}_{-2}\,{\rm km\,s^{-1}}, 0.86^{+0.04}_{-0.07})$, thereby placing tight constraints on the circular velocity at the Solar radius and the shape of the dark matter halo assuming this model potential. However, note that the halo flattening is significantly different to that obtained previously with the logarithmic halo model. Using the same approximation as before, we find $q_\Phi = 0.95^{+0.04}_{-0.08}$. This value of the potential flattening matches exactly the value found by Bovy et al. (2016) at the location of the GD-1 stream.

The resulting Milky Way rotation curve corresponding to $(V_{\rm circ}(R_\odot), q_\rho) = (244\,{\rm km\,s^{-1}}, 0.86)$ is shown in Figure 6, which matches expectations for the circular velocity in the outer regions of the Galaxy reasonably well (see Figure 13 of Küpper et al. 2015 and references therein). The corresponding mass inside of 14.5 kpc, the mean Galactocentric distance of our GD-1 sample, is $M_{\rm MW}(R < 14.5\,{\rm kpc}) = 1.75^{+0.06}_{-0.05} \times 10^{11}\,{\rm M_\odot}$.

The orbital trajectory of the best-fit orbit is shown in Figure 7, integrated over a period of 3 Gyr in the best-fit potential model. The orbit of GD-1 appears to be loop-like and is strongly retrograde, possessing an apocenter at $r_{\rm apo} = 26.7\,{\rm kpc}$, a pericenter at $r_{peri} = 14.2\,{\rm kpc}$, a maximum height from the Galactic plane of $z_{\rm max} = 16.8\,{\rm kpc}$ and an eccentricity of $e = 0.3$ (these values are also tabulated in Table 1).

4 VELOCITY DISPERSION OF THE GD-1 STREAM

We took advantage of the excellent proper motion measurements in Gaia to estimate, for the first time, the internal velocity dispersion of the GD-1 stream. The very fine pencil-line track of the GD-1 structure extending $\gtrsim 70^\circ$ over the sky suggests that the stream must be dynamically cold and hence is possibly a remnant of some globular cluster. We test this hypothesis here.

For an isotropic system, the internal velocity dispersion $\sigma_{\rm int}$ can be expressed as sum of its components as:

$$\sigma^2_{\rm int} = \sigma^2_{v_T\,{\rm int}} + \sigma^2_{v_{\rm los}\,{\rm int}}\,, \quad (11)$$

where $\sigma_{v_T\,{\rm int}}$ and $\sigma_{v_{\rm los}\,{\rm int}}$ are, respectively, the tangential and the radial components of the velocity dispersion. Had we possessed the 3D velocities for all the stars in our GD-1 sample, equation 11 would have served for the estimation of the velocity dispersion. However, as was pointed out previously, all the stars in the dataset contain proper motion measurements, but only a small fraction of them additionally possess los velocity measurements. So in order to maximise the statistics, we decided to estimate the $\sigma_{v_T\,{\rm int}}$ and $\sigma_{v_{\rm los}\,{\rm int}}$ independently. We use sample-2 and the best-fit orbit (obtained in Section 3.2) as our model. The log-likelihood functions are taken to be:

$$\ln \mathcal{L}_1 = \sum_{\rm data} -\ln(\sigma_{v_T\,{\rm obs}}) - \frac{1}{2}\Big(\frac{v^m_T - v^d_T}{\sigma_{v_T\,{\rm obs}}}\Big)^2$$
$$\ln \mathcal{L}_2 = \sum_{\rm data} -\ln(\sigma_{v_{\rm los}\,{\rm obs}}) - \frac{1}{2}\Big(\frac{v^m_{\rm los} - v^d_{\rm los}}{\sigma_{v_{\rm los}\,{\rm obs}}}\Big)^2\,, \quad (12)$$

where v^d_T is the observed tangential velocity of the data calculated by multiplying the orbit model distance with the proper motion measurement, and $v^d_{\rm los}$ is the observed radial velocity. The corresponding orbital model values are marked with superscript 'm'. The Gaussian dispersions $\sigma_{v_T\,{\rm obs}}$ and $\sigma_{v_{\rm los}\,{\rm obs}}$ are the convolution of the intrinsic dispersion of the model together with the observational uncertainty of each data point ($\sigma^2_{obs} = \sigma^2_{\rm int} + \delta^2_i$, with δ_i being the measured uncertainty of the data).

A Markov chain Monte Carlo algorithm was used to survey the parameter space of $\sigma_{v_T\,{\rm int}}$ and $\sigma_{v_{\rm los}\,{\rm int}}$. The resulting distribution is shown in Figure 8. In the direction tangential to the line of sight, we find $\sigma_{v_T\,{\rm int}} < 1.25\,{\rm km\,s^{-1}}$ (at the 90% confidence level), whereas in the line of sight direction, we obtain $\sigma_{v_{\rm los}\,{\rm int}} = 15.08^{+2.25}_{-1.90}\,{\rm km\,s^{-1}}$.

The value of $\sigma_{v_T\,{\rm int}}$ clearly shows that the GD-1 stream system is dynamically extremely cold and is a remnant of some very low mass system (such as a globular cluster). The much higher value of $\sigma_{v_{\rm los}\,{\rm int}}$ suggests that the observational uncertainties of these stars in the SEGUE survey are underestimated, but note that the average velocity uncertainty of $8\,{\rm km\,s^{-1}}$ greatly exceeds the internal velocity dispersion (assuming that in reality the intrinsic line of sight and tangential velocity dispersions have similar value).

5 DISCUSSION AND CONCLUSIONS

In this contribution we probe the underlying gravitational potential of the Milky Way by fitting the orbital path of the GD-1 stream (Grillmair & Dionatos 2006) in different

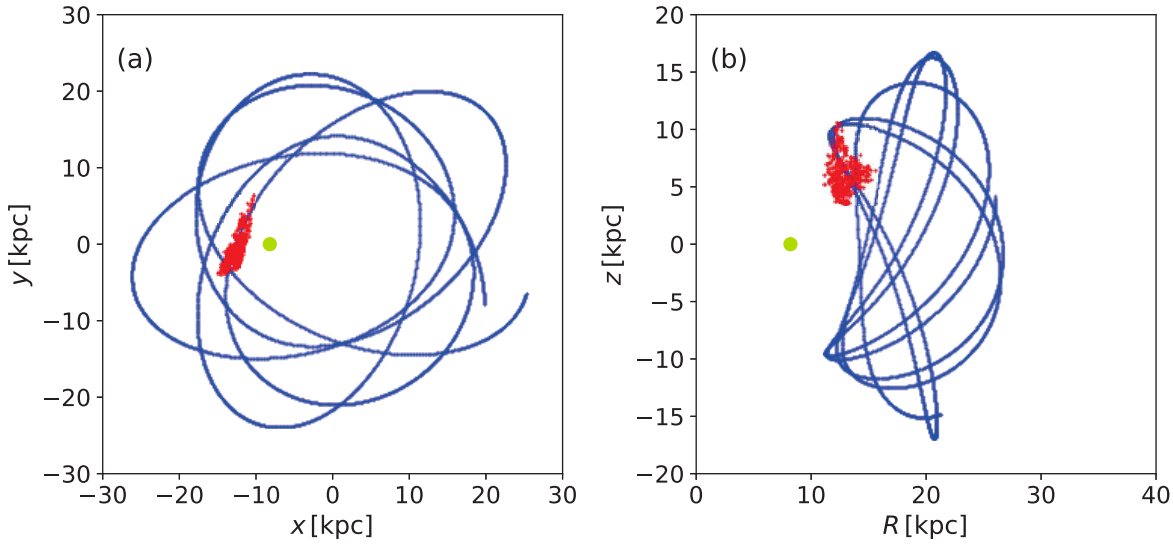

Figure 7. The orbital trajectory of the GD-1 stream, showing the best fit orbit obtained from the orbit-fitting procedure. (a) The orbit (blue) is presented in the Galactic $x-y$ plane; for comparison the survey stars are shown in red. In this Galactocentric Cartesian system the Galactic centre lies at the origin and the Sun (large yellow dot) is at $(x, y, z) = (-8.2, 0, 0.0)$ kpc. The orbit was integrated for 3 Gyr. (b) Same as (a) but in the Galactic $R-z$ plane. For this orbit we found $(\mathrm{r_{apo}}, \mathrm{r_{peri}}, \mathrm{eccentricity}) = (26.7\,\mathrm{kpc}, 14.2\,\mathrm{kpc}, 0.3)$. Note that GD-1 is retrograde with respect to the disk.

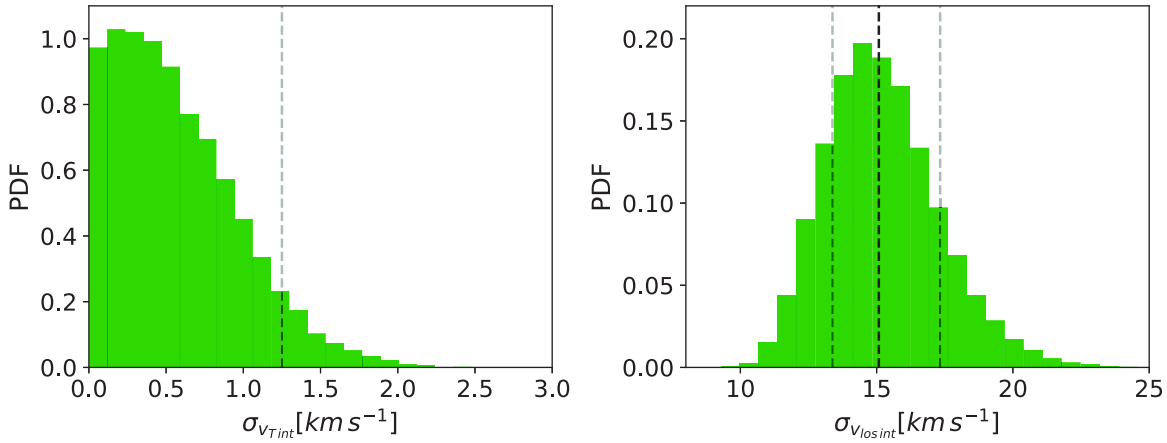

Figure 8. Velocity dispersion of the GD-1 stream along the tangential (left) and line of sight (right) directions. In the left panel the light dashed line indicates the 90% confidence upper limit on $\sigma_{v_T\,\mathrm{int}}$, whereas on the right they indicate 1σ limits.

Galaxy models, changing the circular velocity at the Solar radius ($V_{\mathrm{circ}}(R_\odot)$) and the shape of the dark matter halo (q_ρ). This 6D phase-space GD-1 map was obtained based on the 5D $(\alpha, \delta, \varpi, \mu_\alpha, \mu_\delta)$ measurements from Gaia DR2 and the 1D v_{los} from the SEGUE survey.

We study two different Galactic potential models here, both of them being 3 component models comprising a bulge, a disk and a dark matter halo. For setting up the potentials and integrating orbits, we use the `galpy` module (Bovy 2015).

We first try a Galactic potential model where we model the bulge, disk and halo with Hernquist, Miyamoto-Nagai and logarithmic profiles respectively (see Section 3.1). In this case we estimate the the parameters values as $(V_{\mathrm{circ}}(R_\odot), q_\rho) = (238^{+14}_{-4}\,\mathrm{km\,s^{-1}}, 0.67^{+0.04}_{-0.02})$ (see Figure 3). While providing a useful comparison to some previous studies (such as Koposov et al. 2010), this model is disfavoured as it is not motivated by cosmological simulations.

The second potential model that we examined comprised a bulge, a disk and a halo, modelled with a power-law, Miyamoto-Nagai and axisymmetric NFW profile respectively (see Section 3.2). This time, we measure the parameter values as $(V_{\mathrm{circ}}(R_\odot), q_\rho) = (244^{+6}_{-2}\,\mathrm{km\,s^{-1}}, 0.86^{+0.04}_{-0.07})$ (see Figure 5). This estimate of the $V_{\mathrm{circ}}(R_\odot)$ value is in excellent agreement with those obtained by other authors based on different approaches. For example, McMillan (2011) used photometric and kinematic data to fit parametrized mass models of the Milky Way and found

Table 1. Properties of the GD-1 stellar stream.

Parameter	Range/Value
R.A.	$[130°, 210°]$
Dec	$[10°, 60°]$
$d_\odot$(kpc)	$[7, 13]$
σ_w(pc)	120
μ^*_α(mas yr^{-1})	$[-9, -1]$
μ_δ(mas yr^{-1})	$[-16, -3]$
v_{los}(km s^{-1})	$[-200, 200]$
$\sigma_v(2D,$ km s^{-1})	< 1.25 (90% conf.)
[Fe/H](dex)	-2.25
$\sigma_{[Fe/H]}$(dex)	0.04
z_{max}(kpc)	16.8
r_{peri}(kpc)	14.2
r_{apo}(kpc)	26.7
e	0.30
L_z(kpc km s^{-1})	3083

$V_{\rm circ}(R_\odot = 8.29\,{\rm kpc}) = 239 \pm 5\,{\rm km\,s^{-1}}$; Reid et al. (2014) estimated $V_{\rm circ}(R_\odot = 8.34\,{\rm kpc}) = 240 \pm 8\,{\rm km\,s^{-1}}$ from studies based on the dynamics of the high-mass star forming regions in the spiral arms of the Milky Way. From a dynamical study of the Palomar 5 stream, Küpper et al. (2015) obtained $V_{\rm circ}(R_\odot = 8.30\,{\rm kpc}) = 243 \pm 16\,{\rm km\,s^{-1}}$. As for q_ρ, our result is consistent with Bovy et al. (2016), where they obtain $q_\rho = 0.86 \pm 0.04$ (our conversion from q_ϕ to q_ρ). However, there are tensions with a similar GD-1 analysis by Koposov et al. (2010), who found an oblate halo fit with $q_\rho = 0.61^{+0.05}_{-0.03}$ (our conversion from q_ϕ to q_ρ), and also with the recent measurement by Posti & Helmi (2018) who find prolate halo solutions with $q_\rho = 1.3 \pm 0.25$, based on an analysis of globular clusters.

With our model we estimate the mass of the Milky Way in the inner 14.5 kpc, the mean Galactocentric distance of GD-1, to be $M_{\rm MW}(< 14.5\,{\rm kpc}) = 1.75^{+0.06}_{-0.05} \times 10^{11}\,{\rm M_\odot}$. Extrapolating out slightly to $R = 20\,{\rm kpc}$ (which is still well within the orbit of GD-1, as shown in Figure 7), we find $M_{\rm MW}(< 20\,{\rm kpc}) = 2.14 \pm 0.07 \times 10^{11}\,{\rm M_\odot}$. This value is consistent with the recent findings of Posti & Helmi (2018) who obtain $M_{\rm MW}(< 20\,{\rm kpc}) = 1.91^{+0.17}_{-0.15} \times 10^{11}\,{\rm M_\odot}$, it is similar to the value derived from an analysis of globular cluster motions in Gaia DR2 by Watkins et al. (2018b) of $M_{\rm MW}(< 21.1\,{\rm kpc}) = 2.2^{+0.4}_{-0.3} \times 10^{11}\,{\rm M_\odot}$, and it is consistent with the analysis of Küpper et al. (2015), who find $M_{\rm MW}(< 19\,{\rm kpc}) = 2.1 \pm 0.4 \times 10^{11}\,{\rm M_\odot}$ from the phase-space structure of the Palomar 5 stream. The agreement between these studies with different approaches and different dynamical tracers suggests that the mass in the inner regions of the halo is beginning to be understood, although the extra-planar distribution (i.e. what is often modelled as an ellipsoidal "flattening") is still quite uncertain. Nevertheless, these results are dependent on the models and associated parameters that have been assumed in the various studies, and in particular the corresponding uncertainties have to be interpreted with care.

We used the well-measured Gaia proper motions in order to measure, for the first time, the internal velocity dispersion of the GD-1 stream stars. Although we could not put useful constraints on the line of sight dispersion component due to the large uncertainties in the SEGUE radial velocity measurements, we could place strong limits on the tangential (2D) velocity dispersion, which we find to be $\sigma_{v_T\,\rm int} < 1.25\,{\rm km\,s^{-1}}$ at the 90% confidence level. In addition to indicating that GD-1 is an extremely dynamically cold system and indeed the remnant of a globular cluster, such a low velocity dispersion also suggests that so far GD-1 has not suffered significant external heating, due to interactions with the disk, bar, or any halo substructures in the Milky Way.

Thanks to Gaia's remarkably precise proper motion measurements, we were able to obtain tight constraints on the Milky Way's $(V_{\rm circ}(R_\odot), q_\rho)$ parameters by analysing only a single stream structure. However, the solutions are model-dependent, and so it will be useful to readdress this problem with improved Milky Way models once the mass distribution in the disk and bulge are better constrained from future Gaia studies. A further caveat is that our analysis is based on the assumption that GD-1 perfectly delineates an orbit through the Galaxy; this is only an approximation, and the influence of the assumption should be reassessed with N-body simulations once the position of the progenitor remnant is securely known. It is likely that armed with Gaia's unprecedentedly accurate proper motions, performing similar analyses with an ensemble of streams will ultimately unleash the full power of tidal streams, possibly providing much improved constraints on the underlying potential and dark matter density of the Milky Way halo, that can then be extrapolated out to larger Galactic radii with more confidence.

ACKNOWLEDGEMENTS

The authors would like to thank Nicolas F. Martin for helpful comments and discussions.

This work has made extensive use of `galpy` module (Bovy 2015) for setting up the different galactic potential models, discussed in the paper and for the purpose of orbit integration.

This work has made use of data from the European Space Agency (ESA) mission *Gaia* (https://www.cosmos.esa.int/gaia), processed by the *Gaia* Data Processing and Analysis Consortium (DPAC, https://www.cosmos.esa.int/web/gaia/dpac/consortium). Funding for the DPAC has been provided by national institutions, in particular the institutions participating in the *Gaia* Multilateral Agreement.

The SDSS is managed by the Astrophysical Research Consortium for the Participating Institutions. The Participating Institutions are the American Museum of Natural History, Astrophysical Institute Potsdam, University of Basel, University of Cambridge, Case Western Reserve University, University of Chicago, Drexel University, Fermilab, the Institute for Advanced Study, the Japan Participation Group, Johns Hopkins University, the Joint Institute for Nuclear Astrophysics, the Kavli Institute for Particle Astrophysics and Cosmology, the Korean Scientist Group, the Chinese Academy of Sciences (LAMOST), Los Alamos National Laboratory, the Max-Planck-Institute for Astronomy (MPIA), the Max-Planck-Institute for Astrophysics (MPA), New Mexico State University, Ohio State University, University of Pittsburgh, University of Portsmouth, Princeton

University, the United States Naval Observatory, and the University of Washington.

REFERENCES

Binney J., Tremaine S., 2008, Galactic Dynamics: Second Edition. Princeton University Press
Bovy J., 2015, ApJS, 216, 29
Bovy J., Bahmanyar A., Fritz T. K., Kallivayalil N., 2016, ApJ, 833, 31
Bowden A., Evans N. W., Williams A. A., 2016, MNRAS, 460, 329
Dehnen W., Odenkirchen M., Grebel E. K., Rix H.-W., 2004, AJ, 127, 2753
Diakogiannis F. I., Lewis G. F., Ibata R. A., Guglielmo M., Kafle P. R., Wilkinson M. I., Power C., 2017, MNRAS, 470, 2034
Eyre A., Binney J., 2009, MNRAS, 400, 548
Eyre A., Binney J., 2011, MNRAS, 413, 1852
Fritz T. K., Battaglia G., Pawlowski M. S., Kallivayalil N., van der Marel R., Sohn T. S., Brook C., Besla G., 2018, preprint, (arXiv:1805.00908)
Gaia Collaboration et al., 2016, A&A, 595, A2
Gaia Collaboration et al., 2018c, preprint, (arXiv:1804.09381)
Gaia Collaboration et al., 2018b, preprint, (arXiv:1804.09378)
Gaia Collaboration Brown, A. G. A. Vallenari, A. Prusti, T. de Bruijne, J. H. J. et al. 2018a, A&A
Grillmair C. J., Dionatos O., 2006, ApJ, 643, L17
Helmi A., 2004, MNRAS, 351, 643
Helmi A., White S. D. M., 1999, MNRAS, 307, 495
Huang Y., Liu X., Chen B., Zhang H., Yuan H., Xiang M., Wang C., Tian Z., 2018, preprint, (arXiv:1806.03748)
Ibata R., Lewis G. F., Irwin M., Totten E., Quinn T., 2001, ApJ, 551, 294
Ibata R. A., Lewis G. F., Martin N. F., 2016, ApJ, 819, 1
Johnston K. V., 1998, ApJ, 495, 297
Koposov S. E., Rix H.-W., Hogg D. W., 2010, ApJ, 712, 260
Küpper A. H. W., Lane R. R., Heggie D. C., 2012, MNRAS, 420, 2700
Küpper A. H. W., Balbinot E., Bonaca A., Johnston K. V., Hogg D. W., Kroupa P., Santiago B. X., 2015, ApJ, 803, 80
Law D. R., Majewski S. R., 2010, ApJ, 714, 229
Law D. R., Johnston K. V., Majewski S. R., 2005, ApJ, 619, 807
Li G.-W., et al., 2017, Research in Astronomy and Astrophysics, 17, 062
Lindegren, L. Hernandez, J. Bombrun, A. Klioner, S. Bastian, U. Ramos-Lerate, M. 2018, A&A
Loebman S. R., et al., 2014, ApJ, 794, 151
Luri, Xavier et al., 2018, A&A
Malhan K., Ibata R. A., 2018, MNRAS,
Malhan K., Ibata R. A., Martin N. F., 2018b, preprint, (arXiv:1804.11339)
Malhan K., Ibata R. A., Goldman B., Martin N. F., Magnier E., Chambers K., 2018a, MNRAS,
McMillan P. J., 2011, MNRAS, 414, 2446
Miyamoto M., Nagai R., 1975, PASJ, 27, 533
Navarro J. F., Frenk C. S., White S. D. M., 1997, ApJ, 490, 493
Newberg H. J., Willett B. A., Yanny B., Xu Y., 2010, ApJ, 711, 32
Posti L., Helmi A., 2018, preprint, (arXiv:1805.01408)
Price-Whelan A. M., Bonaca A., 2018, preprint, (arXiv:1805.00425)
Read J. I., Steger P., 2017, MNRAS, 471, 4541
Reid M. J., et al., 2014, ApJ, 783, 130
Rockosi C. M., et al., 2002, AJ, 124, 349
Schönrich R., Binney J., Dehnen W., 2010, MNRAS, 403, 1829
Sivia D., 1996, Data Analysis: A Bayesian Tutorial. Oxford science publications, Clarendon Press, https://books.google.fr/books?id=wR5yljKasLsC
Smith M. C., et al., 2007, MNRAS, 379, 755
Sofue Y., 2012, PASJ, 64, 75
Thomas G. F., Ibata R., Famaey B., Martin N. F., Lewis G. F., 2016, MNRAS, 460, 2711
Varghese A., Ibata R., Lewis G. F., 2011, MNRAS, 417, 198
Watkins L. L., van der Marel R. P., Sohn S. T., Evans N. W., 2018a, preprint, (arXiv:1804.11348)
Watkins L. L., van der Marel R. P., Sohn S. T., Evans N. W., 2018b, preprint, (arXiv:1804.11348)
Yanny B., et al., 2009, AJ, 137, 4377
de Boer T. J. L., Belokurov V., Koposov S. E., Ferrarese L., Erkal D., Côté P., Navarro J. F., 2018, MNRAS, 477, 1893
de Bruijne J. H. J., 2012, Ap&SS, 341, 31

This paper has been typeset from a TEX/LATEX file prepared by the author.

CHAPTER 7

MEASURING SUN'S VELOCITY USING STELLAR STREAMS

It is all relative-**anonymous**

Related paper : **Measuring Sun's Velocity with Stellar Streams**, 2017, Khyati Malhan & Rodrigo Ibata, published in *MNRAS* (ADS entry)

Abstract

A novel method for measuring the Sun's motion ($\mathbf{V}_\odot$) using the proper motions of Galactic halo star streams was formulated. The method relies on the fact that the motion of the stars perpendicular to a stream from a low-mass progenitor is close to zero when viewed from a non-rotating frame at rest with respect to the Galaxy, and that the deviation from zero is due to the reflex motion of the observer. Such a procedure of measuring Sun's velocity has the advantage of being independent of the Galactic mass distribution. Suite of simulations were made to run to test the algorithm that was developed, and the input Solar motion was found to be recoverable to good accuracy with data of the quality that ESA/Gaia mission has provided.

7.1 Introduction

Apart from constraining the potential of the Milky Way, orbital structures of stellar streams can be exploited even to constrain the fundamental parameters of the Galaxy. This is something that was explored as well as a part of this thesis work.

Since all the astronomical and cosmological observations are taken from the Sun's frame of reference (heliocentric frame), it is fundamentally important to obtain best estimates of Sun's

galactocentric distance $R_\odot$ and the Galactic velocity $\mathbf{V}_\odot (= V_{\rm circ}\hat{\mathbf{y}} + \mathbf{V}_{p\odot}; \mathbf{V}_{p\odot}$ is the Sun's peculiar velocity vector). The knowledge of $\mathbf{V}_\odot$ is required to transform any observed heliocentric velocity into the Galactic frame. This is necessary, for instance, for scientific interpretation when studying Galactic dynamics or for correcting the motion of many extragalactic systems (see, e.g., [165]). Moreover, the circular velocity at the Solar radius $V_{\rm circ} (\equiv V_{\rm circ}(R_\odot))$ also serves as a crucial constraint on the mass models of the Milky Way (as demonstrated in Chapter 6). Therefore, the determination of $\mathbf{V}_\odot$ is a crucial task of Galactic astronomy.

There exist various ways for measuring the Sun's parameters [151, 153, 168]. However, the conventional techniques of measuring Sun's motion are often accompanied by some conspicuous complications or caveats (see the Introduction section of the paper attached for detailed discussion). Nevertheless, it is also always useful to have different mechanisms to measure the same physical parameter(s) so that the resulting parameteric values, evaluated through different techniques, can be cross checked for consistency.

This new technqiue to gauge the Sun's Galactic velocity $\mathbf{V}_\odot$, that is described here, is a simplistic geometrical procedure that successfully works without involving any extensive chemo-dynamical modeling of our Galaxy, saves one from analysing highly dust obscured measurements coming from the Galactic centre and does not rely on the Galaxy's gravitational potential or its mass distribition. The given approach exploits a very basic behaviour of any low-mass stellar stream structure: *the proper motion vectors of the stream stars should be aligned along the stream structure in the rest frame of the Galaxy*. This approximation is reasonably good as stars in a stellar stream, that is derived from a low mass progenitor system where velocity dispersion is very low, closely delineate an orbit [39]. This means that the velocity vectors of each star must align along the stream structure itself. In such a case, any perpendicular motion of the stream stars then must arise primarily due to the reflex motion of the observer, the Sun. This is the central hypothesis around which this algorithm was constructed.

7.2 Method

Given approach makes use of the assumption that for a thin stream (originating from a low mass progenitor) all the stars lie close to a single test-particle orbit (see, e.g. [39]). In general, the stars in a tidal stream have different energies, but the approximation that stream stars trace the same orbit is admissible for thin streams that are remanants of low-mass progenitor systems, such as globular clusters, where velocity dispersions are fairly low (such as the GD-1 stream, as also explained in Chapter 6).

Consider a small segment of an orbit on the Galactic sky (as shown in Figure 7.1). The red points represent the orbital positions along this orbital structure. These points can also be viewed as different time positions for a given orbit. Let us define a tangent vector $\mathbf{v}_d$ which locally gives the direction of motion of that orbital point on this 2D Galactic sky. This vector is generated by

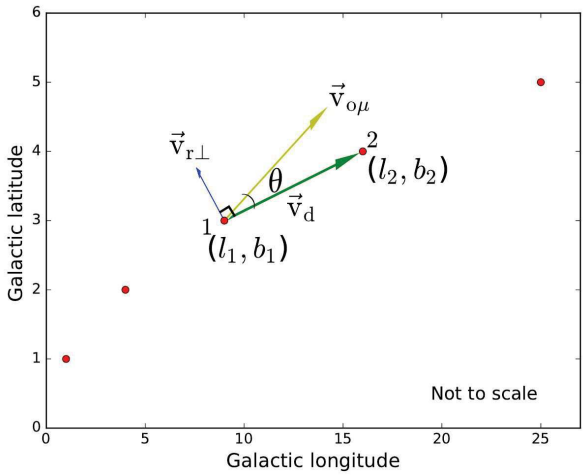

Figure 7.1: Vector diagram. Red dots represent the positions at successive (equal interval) timesteps along a tiny segment of an orbit. $\mathbf{v}_d$ is the vector that measures the path along the orbit. The proper motion vector $\mathbf{v}_{o\mu}$ that gets measured in observations should lie along $\mathbf{v}_d$ in a non-rotating frame in the Galaxy. But due to the reflex motion of the Sun, the perpendicular vector $\mathbf{v}_{r\perp}$ emerges, causing the deviation of $\mathbf{v}_{o\mu}$ from vector $\mathbf{v}_d$.

connecting position at time '1' to position at time '2', along the direction of motion of the orbit and is given by:

$$\mathbf{v}_d = \cos(b_1)(\ell_2 - \ell_1)\hat{\ell} + (b_2 - b_1)\hat{\mathbf{b}}, \tag{7.1}$$

where $\hat{\ell}$ is the unit Galactic longitude vector and $\hat{\mathbf{b}}$ is the unit Galactic latitude vector.

The assumption that the constituent stars of stellar streams follow an orbit means that the path depicted in Figure 7.1 can be recovered from the position of the stream stars on the sky. This means that the two time intervals '1' and '2' along the orbital path can be equivalently thought of as two stars '1' and '2' along a stream structure.

With this assumption, in the Galaxy's rest frame, the observed proper motion vector of star '1' (see Figure 7.1) should align along the vector $\mathbf{v}_d$, since '1' must practically trace out the orbit of the succeeding star '2' (by the definition of an orbit). But in the heliocentric frame, the observed proper motion vector ($\mathbf{v}_{o\mu}$) is different in direction and magnitude due to the motion of the Sun. The observed proper motion vector $\mathbf{v}_{o\mu}$ can be written as:

$$\mathbf{v}_{o\mu} = \mu_{l_1}\cos(b_1)\hat{\ell} + \mu_{b_1}\hat{\mathbf{b}}. \tag{7.2}$$

In such a case, the perpendicular component (lets call it $\mathbf{v}_{r\perp}$) of vector $\mathbf{v}_{o\mu}$ to $\mathbf{v}_d$ emerges totally due to the reflex motion of the Sun as seen at position '1' and is given by:

$$\mathbf{v}_{r\perp} = (|\mathbf{v}_{o\mu}|\sin\theta)\hat{\mathbf{v}}_{\mathbf{r}\perp}, \tag{7.3}$$

where θ is the angle between $\mathbf{v}_d$ and $\mathbf{v}_{o\mu}$ and $\hat{\mathbf{v}}_{r\perp}$ is the unit vector normal to $\mathbf{v}_d$. It is this $\mathbf{v}_{r\perp}$ vector that decides the vector the magnitude and direction of the vector $\mathbf{V}_\odot$.

This effect is not correlated with the $R_\odot$ value and depends only on the Sun's total velocity vector $\mathbf{V}_\odot$. The procedure that was then followed to gauge $\mathbf{V}_\odot$ was to sample different values of the Sun's three-dimensional velocity $\mathbf{V}_\odot = (u_\odot, v_\odot, w_\odot)$ using a Markov Chain Monte Carlo algorithm. The apparent stream motion was calculated as the reflex motion vector $\mathbf{v}_{r\perp}$ and was compared against $\mathbf{v}_{r\perp}$ obtained from data. The adopted figure of merit was the likelihood of the data given the stream model.

At first, an analysis based on the *perfect orbit models* was performed to both test and demonstrate the workings of the algorithm in an ideal case scenario (Section 3.1 of the paper). After that, a realistic case study was made by employing *N-body simulated stream models* that were degraded in the proper motions (with Gaia-like uncertainties) and in the distances (10% uncertainty errors in distance measurements as expected from photometric parallaxes derivation). It was found that the input Solar motion can be recovered to good accuracy even with such realistic measurements errors in the observed astrometric values (Section 3.2 of the paper).

7.3 Results and Discussions

Such a method does not assume any Galactic mass model, which must be viewed as a strength of the technique. Also, it must be noted that such an analysis ends up determining the Sun's velocity with respect to a sample of streams (instead of with respect to the Galactic centre, for example) in the Galactic halo, and this velocity might turn out to be different from the velocity measured with respect to the Galactic centre or with respect to the LSR for a variety of interesting astrophysical reasons. This could happen, for instance, if Sgr A^* is not at rest with respect to the Galaxy, or if the disk possesses significant non-circular motions, or if there is a bulk motion of the streams with respect to the disk (as might happen if there is a substantial ongoing accretion: e.g., the LMC or the Sgr dwarf). Using two independent measurement techniques might give us some insight about the relative motion between the dynamical centres of the inner Milky Way and the outer Milky Way (around which the streams actually orbit).

The reason for asserting the usage of low-mass streams for constraining the Solar motion using this method is simple. The high-mass (thick) streams like the Sagittarius stream, formed from the disruption of dwarf galaxies, are highly dispersed in phase space [89, 98]. Although their broad trajectory could be curve fitted (or modelled using an orbit), the dispersion in the stream track would result in higher uncertainties in the measured Solar motion values.

7.4 Related Paper

Monthly Notices of the ROYAL ASTRONOMICAL SOCIETY

MNRAS **471,** 1005–1011 (2017) doi:10.1093/mnras/stx1618
Advance Access publication 2017 July 4

Measuring the Sun's motion with stellar streams

Khyati Malhan★ and Rodrigo A. Ibata
Université de Strasbourg, CNRS, Observatoire astronomique de Strasbourg, UMR 7550, F-67000 Strasbourg, France

Accepted 2017 June 23. Received 2017 June 23; in original form 2017 March 13

ABSTRACT

We present a method for measuring the Sun's motion using the proper motions of Galactic halo star streams. The method relies on the fact that the motion of the stars perpendicular to a stream from a low-mass progenitor is close to zero when viewed from a non-rotating frame at rest with respect to the Galaxy, and that the deviation from zero is due to the reflex motion of the observer. The procedure we implement here has the advantage of being independent of the Galactic mass distribution. We run a suite of simulations to test the algorithm we have developed, and find that we can recover the input solar motion to good accuracy with data of the quality that will soon become available from the ESA/*Gaia* mission.

Key words: Sun: fundamental parameters – stars: kinematics and dynamics – Galaxy: fundamental parameters – Galaxy: halo – Galaxy: structure.

1 INTRODUCTION

In physics, it is always of fundamental importance to know the properties of the frame from which measurements are being made. Observations of astrophysical or cosmological systems, using satellites or ground-based telescopes, can be corrected into the Heliocentric frame with ease. However, knowledge of the Sun's Galactic velocity $\mathbf{V}_{\odot}$ is required to transform any observed Heliocentric velocity into the Galactic frame. This is necessary, for instance, for scientific interpretation when studying Galactic dynamics or for correcting the motion of many extragalactic systems (see e.g. Salomon et al. 2016). Moreover, the related circular velocity at the solar radius ($v_{\rm circ\odot} \equiv v_{\rm circ}(\mathrm{R}_{\odot})$) also serves as a crucial constraint on the mass models of the Milky Way (e.g. Dehnen & Binney 1998a). Therefore, the determination of $\mathrm{V}_{\odot}$ is a crucial task of Galactic astronomy.

It is important to realize that the Sun's Galactic velocity $\mathrm{V}_{\odot}$ needs to be measured with respect to some other reference or tracer. A conceptually straightforward way to measure $\mathrm{V}_{\odot}$ is to determine the Sun's motion with respect to a presumed motionless object with respect to the Galaxy. Such measurements are derived from the observed proper motion of Sgr A^* (Reid & Brunthaler 2004). But such an approach requires an accurate measurement of $\mathrm{R}_{\odot}$ and a critical assessment of measurements coming from the dense region at the Galactic Centre, with its complex dynamical mix of gas, dust, stars and central black hole.

Alternatively, analyses can be based on local tracers, where one assumes that the solar motion can be decomposed into a circular motion of the local standard of rest (LSR) plus the so-called peculiar motion of the Sun with respect to the LSR: $\mathrm{V}_{\odot} = \mathrm{V}_{\rm circ\odot} + \mathrm{V}_{\rm p\odot}$. Such a study was presented by Dehnen & Binney (1998b), who applied the Strömberg relation (Strömberg 1946) in their method to a sample of ∼15 000 main-sequence stars from the Hipparcos catalogue. They determined the peculiar velocity to be $\mathrm{V}_{\rm p\odot} = (10.0 \pm 0.36, 5.25 \pm 0.62, 7.17 \pm 0.38)\,\mathrm{km\,s^{-1}}$ (in the conventional U, V, W directions, respectively). However, Schönrich, Binney & Dehnen (2010) caution against this employment of Strömberg's Relation and illustrate, using their chemodynamical model of the Galaxy, that the metallicity gradient of the disc population causes a systematic shift in the estimation of the kinematics of the Sun. They describe an alternative method to determine the Sun's velocity with respect to the LSR from the velocity offset that optimizes their model fit to the observed velocity distribution. Using their chemodynamical evolution model of the Galaxy, described in Schönrich & Binney (2009), they find the Sun's peculiar motion to be $\mathrm{V}_{\rm p\odot} = (11.1^{+0.69}_{0.75}, 12.24^{+0.47}_{0.47}, 7.25^{+0.37}_{0.36}\,\mathrm{km\,s^{-1}})$ and estimate roughly the systematic uncertainties as $(1.0, 2.0, 0.5)\,\mathrm{km\,s^{-1}}$. However, their approach has the disadvantage being based on an extensive modelling of the Milky Way, and hence of being sensitive to the adopted approximations in dynamics and chemistry.

Once the Sun's peculiar velocity is known, one still needs to add the velocity of the LSR to obtain the Sun's velocity with respect to the Galaxy. It is interesting in this context to examine what it is currently possible to measure with respect to nearby tracers. In a recent contribution, Bobylev (2013) determined the solar Galactocentric distance $\mathrm{R}_{\odot}$ and Galactic rotational velocity $v_{\rm circ\odot}$, as modified by Sofue et al. (2011), using data of star-forming regions and young Cepheids near the solar circle. Based on a sample of 14 long-period Cepheids with *Hipparcos* proper motions they obtained $\mathrm{R}_{\odot} = 7.66 \pm 0.36\,\mathrm{kpc}$ and $v_{\rm circ\odot} = 267 \pm 17\,\mathrm{km\,s^{-1}}$. However, with a sample of 18 Cepheids with UCAC4 proper motions (among which two were taken from *Hipparcos*) they found $\mathrm{R}_{\odot} = 7.64 \pm 0.32\,\mathrm{kpc}$ and $v_{\rm circ\odot} = 217 \pm 11\,\mathrm{km\,s^{-1}}$. The difference in the derived $v_{\rm circ\odot}$ values highlights the difficulty of such measurements, and their sensitivity to the adopted tracers and data. Masers located in regions of massive star formation have

★ E-mail: kmalhan07@gmail.com

also yielded estimates of the LSR motion ($254 \pm 16\,\mathrm{km\,s^{-1}}$, Reid et al. 2009; $236 \pm 11\,\mathrm{km\,s^{-1}}$, Bovy, Hogg & Rix 2009), though these results are derived from a small number of sources (18) and require knowledge of the velocity lag of the masers with respect to circular motions (Rygl et al. 2010).

Here, we will examine the power that streams hold to constrain the solar velocity with respect to the Galaxy. A growing number of stellar streams have been detected in recent years from the Sloan Digital Sky Survey and Pan-STARRS (Odenkirchen et al. 2001; Grillmair & Dionatos 2006; Bernard et al. 2014; Bernard et al. 2016). The most recent contributions come from the ATLAS survey and surveys with CTIO/DECam (the Atlas stream in Koposov et al. 2014, and the Eridanus and Palomar 15 streams in Myeong et al. 2017). The kinematics of these structures will soon be revealed in the second data release of the *Gaia* mission survey (Gaia Collaboration et al. 2016). *Gaia* would possibly also uncover many new low-contrast star streams that are currently below detection limits in star-count surveys.

The key insight about streams that we exploit here is that stream stars move approximately along their orbits, not perpendicular to them. That is, the velocity vector of a stream star in the Galaxy's rest frame must be a tangent vector to the orbit of this extended structure at that stellar position. Thus, if we measure any motion perpendicular to the orbital path of the stream at this position, we must reconcile it with the apparent (reflex) motion that emerges due to the motion of the observer's frame (from the Sun). Hence, by measuring this perpendicular motion vector for the stars in the streams, we can constrain the Sun's velocity in the Galaxy. This is not an entirely new insight. Several studies made in the past that have examined the kinematics of stellar streams have had to include (implicitly or explicitly) the solar motion or the circular velocity of the LSR as a nuisance parameter to fit the stream in kinematics space (Ibata et al. 2001; Koposov, Rix & Hogg 2010; Küpper et al. 2015; Bovy et al. 2016). Although, Dehnen et al. (2004) comment on the fact that in their modelling of the tidal dissolution of the Palomar 5 globular cluster, the ensuing stream actually deviates slightly from the path of the orbit (rather than not at all, as would be naively expected). Such an offset of the stream structure from the underlying orbit could, in principle, create a bias in the solar velocity measurements using the method proposed in this contribution. However, we show that by analysing multiple streams on different orbits the bias is largely eliminated.

A similar, but less general version of the idea presented here, was explored in Majewski et al. (2006). They suggest measuring the Sun's reflex motion using the Sagittarius (Sgr) stream (Ibata et al. 2001; Majewski et al. 2003), making use of the fact that the orbital plane of the Sgr stream is polar and that the Sun lies close to this plane. Thus, the V motions of the stars in the Sgr stream are almost entirely due to the solar reflex motion. Since the method requires fitting the Sgr stream to spatial and velocity data to predict its 6D phase-space configuration, it relies heavily on the shape of the Galactic potential, which also involves the value of the Galactocentric radius of the Sun ($\mathrm{R}_\odot$). Moreover, the method only constrains the V component of the Sun's motion. They estimate being able to recover the solar velocity to within $10\,\mathrm{km\,s^{-1}}$ (using data of the quality that was expected from NASA's former *Space Interferometry Mission project*, Unwin et al. 2008, which aimed to measure trigonometric parallaxes to an accuracy of 4 μas).

In contrast to these previous studies, here we do not attempt to present physical models of one or more of the Galaxy's stellar streams, but rather, we develop an algorithm that is based entirely on simple geometry, and that can be applied to a sample of streams. The new alternative method to measure the Sun's motion that we present in this paper is not correlated with the value of $\mathrm{R}_\odot$, it saves us from having to analyse observations of densely populated regions in the centre of the Galaxy, it requires only 5D phase-space information about stream stars (radial velocity constraints are not needed) and does not invoke the need to model the gravitational potential of the Milky Way or the stellar populations of the disc.

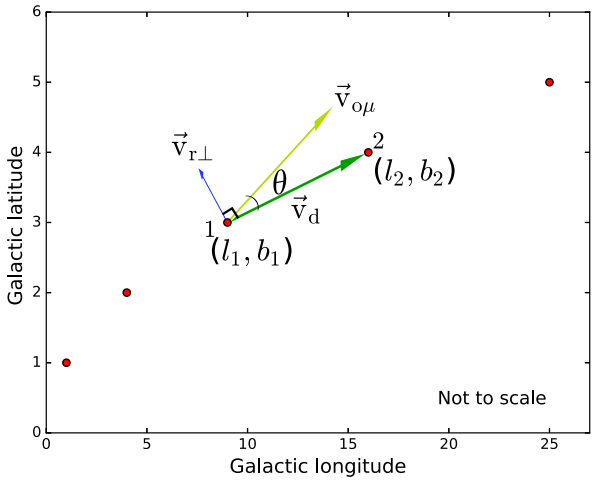

Figure 1. Vector diagram. Red dots represent the positions at successive (equal interval) time-steps along a tiny segment of an orbit. $\boldsymbol{v}_\mathrm{d}$ is the vector that measures the path along the orbit. The proper motion vector $\boldsymbol{v}_{\mathrm{o}\mu}$ that gets measured in observations should lie along $\boldsymbol{v}_\mathrm{d}$ in a non-rotating frame in the Galaxy. But due to the reflex motion of the Sun, the perpendicular vector $\boldsymbol{v}_{\mathrm{r}\perp}$ emerges, causing the deviation of $\boldsymbol{v}_{\mathrm{o}\mu}$ from vector $\boldsymbol{v}_\mathrm{d}$.

The outline of this paper is as follows. In Section 2, we present the method employed in our study. Section 3 presents our methodology to measure the Sun's velocity using (Section 3.1) perfect orbits and (Section 3.2) *N*-body tidal stellar stream models, demonstrating the success of the method. Section 3.3 discusses the deviation of Sun's velocity from its true value given by a systematic bias in distance measurements of stream stars. Finally, in Section 4, we present the conclusion of this study.

2 METHOD

Our approach makes use of the assumption that for a thin stream (originating from a low mass progenitor) all the stars lie close to a single test-particle orbit (see e.g. Dehnen et al. 2004). In general, the stars in a tidal stream have different energies, but the approximation that stream stars trace the same orbit is admissible for thin streams from low-mass progenitors.

Consider a small segment of an orbit on the Galactic sky (as shown in Fig. 1). The red points represent the positions of the stars (members of some stream) along their orbital structure. These points can also be viewed as different time positions for a given orbit. We define a tangent vector $\boldsymbol{v}_\mathrm{d}$, which locally gives the direction of motion of the star's orbit on this 2D Galactic sky. This vector is generated by connecting position at time '1' to position at time '2', along the direction of motion of the orbit. Vector $\boldsymbol{v}_\mathrm{d}$ is then given by

$$\boldsymbol{v}_\mathrm{d} = \cos(b_1)(\ell_2 - \ell_1)\hat{\boldsymbol{\ell}} + (b_2 - b_1)\hat{\boldsymbol{b}}\,, \tag{1}$$

where $\hat{\boldsymbol{\ell}}$ is the unit Galactic longitude vector and $\hat{\boldsymbol{b}}$ is the unit Galactic latitude vector.

Our assumption that stellar streams follow the orbit of the constituent stars means that the path depicted in Fig. 1 can be recovered from the position of the stream on the sky, so that the two time intervals '1' and '2' along the path can be equivalently thought of as two stars '1' and '2' along the orbit.

With this assumption, in the Galaxy's non-rotating frame, the observed proper motion vector of star '1' (see Fig. 1) should align along the vector $\boldsymbol{v}_{\rm d}$, since '1' must practically trace out the orbit of the succeeding star '2' (by the definition of an orbit). But due to the motion of the observer's frame in the Galaxy, the observed proper motion vector is different in direction and magnitude. We define this observed proper motion vector $\boldsymbol{v}_{{\rm o}\mu}$ as

$$\boldsymbol{v}_{{\rm o}\mu} = \mu_{l_1} \cos(b_1)\hat{\boldsymbol{\ell}} + \mu_{b_1}\hat{\boldsymbol{b}}\,. \tag{2}$$

Therefore, the perpendicular component (which we call $\boldsymbol{v}_{{\rm r}\perp}$) of vector $\boldsymbol{v}_{{\rm o}\mu}$ to $\boldsymbol{v}_{\rm d}$ emerges totally due to the reflex motion of the Sun as seen at position '1' and is given by

$$\boldsymbol{v}_{{\rm r}\perp} = (|\boldsymbol{v}_{{\rm o}\mu}|\,\sin\theta)\hat{\boldsymbol{v}}_{{\rm r}\perp}, \tag{3}$$

where θ is the angle between $\boldsymbol{v}_{\rm d}$ and $\boldsymbol{v}_{{\rm o}\mu}$, and $\hat{\boldsymbol{v}}_{{\rm r}\perp}$ is the unit vector normal to $\boldsymbol{v}_{\rm d}$.

However, even for a simple orbit, the precession of the orbital plane in the Galaxy will also contribute to the vector $\boldsymbol{v}_{{\rm r}\perp}$. We can estimate approximately the contribution of precession to $\boldsymbol{v}_{{\rm r}\perp}$, using the analytic approximation of Steiman-Cameron & Durisen (1990). Their formula is valid for a very simple case assuming a circular orbit evolving in a spheroidal potential in which the reference frame is not tumbling. The precession rate is then

$$\dot{\Omega}_{\rm p} = -\frac{3\Phi_2(r)}{2\,r\,v_{{\rm circ}\odot}}\cos\,i\,, \tag{4}$$

where

$$\Phi_2(r) = \frac{v^2_{{\rm circ}\odot}}{2}\left(\frac{1-q_\phi^2}{q_\phi^2+\frac{1}{2}}\right)\,. \tag{5}$$

Here, $\Omega_{\rm p}$ is the longitude of the ascending node of an orbit, i is the inclination of the orbital plane, $\Phi_2(r)$ is one of the components of the expansion of the scale-free logarithmic potential function $\Phi(r)$ and q_ϕ is the (spheroidal) flattening of the potential. Taking an orbit at a typical radius of $r = 30$ kpc in a potential with density flattening of $q_\rho = 0.8$ and with circular velocity of $v_{{\rm circ}\odot} = 200\,{\rm km\,s^{-1}}$, yields $|\,\dot{\Omega}_{\rm p}\,| = 0.11\cos\,i$ mas yr^{-1}. The component along the vector $\boldsymbol{v}_{{\rm r}\perp}$ then becomes $\boldsymbol{v}'_{{\rm r}\perp} = 0.055\cos(2i-90)$ mas yr^{-1}, i.e. with a maximum at $i = 45^\circ$ of $|\,\dot{\Omega}_{\rm p}\,| = 0.055$ mas yr^{-1}. This corresponds to a maximum of 4 per cent of the proper motion of the corresponding circular orbit. This estimate shows that the effect of precession should be relatively small. Note also that if we consider multiple streams that are on different orbits, then they will also have different orbital plane inclinations i. Hence, the precession corrections will tend to cancel out on average.

The procedure we follow is to sample different values of the Sun's 3D velocity $\mathrm{V}_\odot = (u_\odot, v_\odot, w_\odot)$ using a Markov chain Monte Carlo (MCMC) algorithm. The apparent stream motion is calculated as the reflex motion vector $\boldsymbol{v}_{{\rm r}\perp}$ and is compared against $\boldsymbol{v}_{{\rm r}\perp}$ obtained from data. The figure of merit we adopt is the likelihood of the data, given the stream model. In Section 3.1, we investigate first the results given a set of perfect orbit streams, while in Section 3.2, we will take the more realistic case of an N-body stream due to tidally disrupted satellites.

For these calculations, we will make use of the realistic Galactic potential model of Dehnen & Binney (1998a) (their model 1), which contains a bulge, thin disc, thick disc, interstellar medium and a halo component. We stress that this potential model is only used to set up the artificial stream realizations, and is in no way used to deduce the solar velocity vector. The method we present here is independent of any models of the Galactic potential.

3 ESTIMATION OF THE SUN'S VELOCITY USING STREAM MODELS

3.1 Employing perfect orbit models

In order to be completely assured of our method, we first demonstrate a proof of concept, using perfect orbit models (which, in principle, can be considered as an ideal stream case). Since orbits are infinitely thin curves, the Sun's velocity $\mathrm{V}_\odot$ should be perfectly recovered to within the biasses created by the orbital precession.

To achieve this, we selected three 6D phase-space positions drawn randomly to give the orbits' initial conditions. Each of these initial conditions was then integrated for $T = 0.06$ Gyr in the Galactic potential model described above to form an orbit (the value of T was chosen, somewhat arbitrarily, just so that the orbits appear long enough to mimic observed streams found in the SDSS). Since we need to constrain three components of the Sun's velocity, we either need a single stream that probes different regions of the sky in such a way that each component of the reflex motion dominates, or we need a minimum collection of three stream segments that again explore the sky so that the corresponding reflex motion components are significant. The latter possibility is considered here, since all low-mass globular cluster streams currently known are approximately great-circle segments, at most a few tens of degrees long. Once integrated, the complete phase-space information of these three orbits was then transformed from the Galactocentric Cartesian frame to a Heliocentric (observable) frame using the Sun's parameters (that we refer to as the *true* parameters) as $(\mathrm{R}_\odot, \mathrm{V}_\odot) = (\mathrm{R}_{\odot,\mathrm{T}}, u_{\odot,\mathrm{T}}, v_{\odot,\mathrm{T}}, w_{\odot,\mathrm{T}})$ $= (8.34\,{\rm kpc}, 9.0\,{\rm km\,s^{-1}}, 255.20\,{\rm km\,s^{-1}}, 7.0\,{\rm km\,s^{-1}})$. However, only 5D information was retained in the form of $(\ell, b, d_\odot, \mu_\ell, \mu_b)$. The resulting spatial projection of the randomly-chosen orbits is shown in Fig. 2.

An MCMC algorithm is used to survey the parameter space of solar velocity components $(u_\odot, v_\odot, w_\odot)$, where the model likelihood is taken to be

$$L[u_\odot, v_\odot, w_\odot] = \sum_{\rm Data} -\ln(\sigma_\ell\,\sigma_b) - \left(\frac{\mu^{\rm data}_{\perp,\ell} - \mu_{\perp,\ell}{}^{\rm model}}{\sqrt{2}\sigma_\ell}\right)^2 - \left(\frac{\mu^{\rm data}_{\perp,b} - \mu^{\rm model}_{\perp,b}}{\sqrt{2}\sigma_b}\right)^2, \tag{6}$$

where $\mu^{\rm data}_{\perp,\ell}$ and $\mu^{\rm data}_{\perp,b}$ are the observed ℓ, b components of $\boldsymbol{v}_{{\rm r}\perp}$, and $\mu^{\rm model}_{\perp,\ell}$ and $\mu^{\rm model}_{\perp,b}$ are the corresponding model predictions. In Section 3.2 , σ_l and σ_b will represent proper motion uncertainties of the stream stars in, respectively, the Galactic longitude and latitude directions. However, for the perfect orbit model tests, we allow the MCMC algorithm to fit a global value for these two dispersion parameters (in this situation, they can be considered as model mismatch errors).

Fig. 3 shows the resulting distribution of solar velocity components explored by the MCMC algorithm in 1.5×10^6 iterations in the form of a triangular correlation diagram. The most likely values are found to be $(u_\odot, v_\odot, w_\odot) = (9.03, 255.26, 7.001)$ km s^{-1}, which shifts the measured values from the true values by $(u_\odot - u_{\odot,\mathrm{T}}, v_\odot - v_{\odot,\mathrm{T}}, w_\odot - w_{\odot,\mathrm{T}}) = (0.03, 0.06, 0.001)$ km s^{-1}, and the corresponding uncertainties $(\sigma_u, \sigma_v, \sigma_w) = (0.11, 0.68, 0.13)$ km s^{-1}. Thus, the results from this idealized example

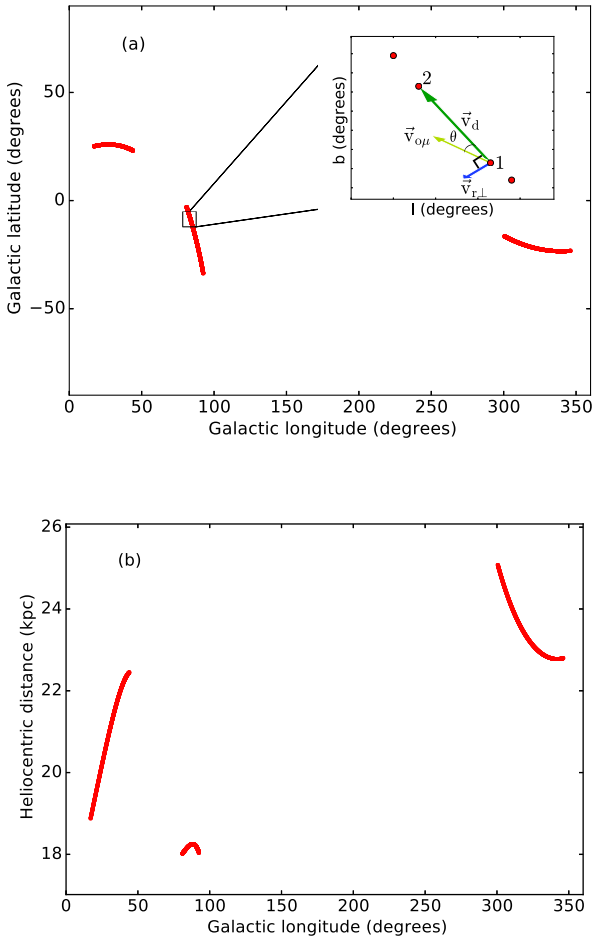

Figure 2. Sky view of the perfect orbits. (a) shows the path of the orbits on the Galactic sky and (b) represents the Heliocentric distances that these orbits span. The orbits were integrated in the Galactic potential model 1 of Dehnen & Binney (1998a). The zoomed-in panel in (a) represents a small segment of the orbit detailing the geometry of our procedure. It is the vector $\boldsymbol{v}_{r\perp}$ that our model is compared against.

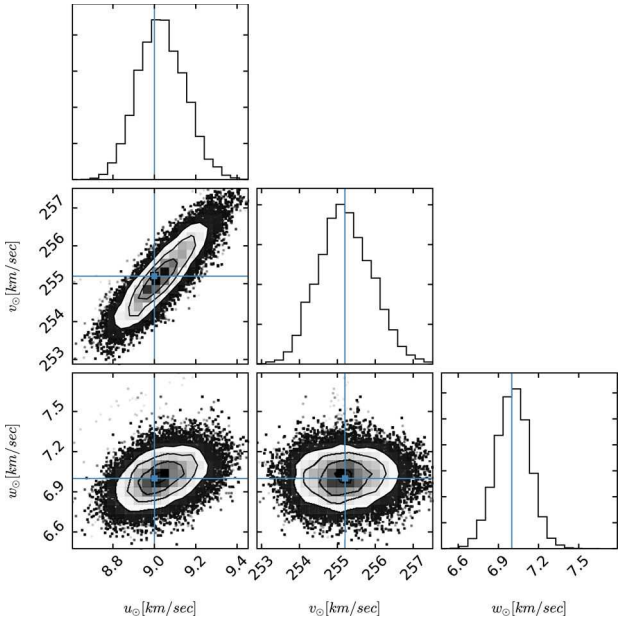

Figure 3. Correlation function plot for the perfect orbit test. The panels represent the probability distribution function and parameter–parameter correlations of the Sun's velocity components obtained through the application of the MCMC algorithm. The blue lines represent the true input values of the Sun's velocity.

clearly establish the proof of concept. We next test if the method works on more physical stellar stream systems and if these could actually be used to constrain the solar motion in the Galaxy.

3.2 Employing *N*-body simulated stream models

In reality, star streams form from the tidal disruption and dissolution of satellites. The escaping stars need to be lifted out of the potential well of their progenitor, and in so doing, they end up with different energies (and hence on different orbits) than their progenitor. Thus to obtain a more realistic description of streams, we decided to produce a set of *N*-body models in the Dehnen & Binney (1998a) Galactic potential model 1. For this, we used the GyrafalcON *N*-body integrator (Dehnen 2000) from the NEMO software package (Teuben 1995).

The initial phase-space distribution of the progenitors of the streams was selected as follows. The initial position of each satellite was drawn at a random direction as seen from the Galactic Center, and with a uniform probability of lying in the Galactocentric distance range of 10–30 kpc. The mean velocity of each satellite was selected randomly from an isotropic Gaussian distribution with (1D) dispersion of 100 km s^{-1} (Harris 1976; van den Bosch et al. 1999).

At these phase-space positions, each progenitor was constructed using a King model (King 1966). The mass, tidal radius and ratio between central potential and velocity dispersion were sampled uniformly between the ranges $M_{\rm sat} = 2$–5×10^4 M$_\odot$, $r_t = 20$–80 pc and $W_{\rm sat} = 2$–4.

Somewhat arbitrarily, we chose to model a set of 22 streams. At present, ∼9 low-mass streams of probable globular cluster progenitors are known within approximately one-fourth of the sky in the North Galactic SDSS footprint: Acheron, Lethe, Cocytos, Styx, Hermus, Hyllus, Palomar 5, NGC 5466 and GD-1 (see e.g. Grillmair 2016). An additional six narrow streams (Ophiuchus, PS1-A,PS1-B, PS1-C, PS1-D and PS1-E) were discovered in the approximately three-fourth of the sky covered by the Pan-STARRS survey (Bernard et al. 2014; Bernard et al. 2016). We expect several more to come to light thanks to the *Gaia* survey, which will cover the full sky and allow for de-contamination of foreground populations by proper motion. Hence, a choice of ∼20 systems for our sample of streams is a conservative estimate of what should be well measured by *Gaia* within a few years.

Once the progenitors were initialized in phase space, they were then evolved independently over a time period between 2–8 Gyr in the same Galactic mass model mentioned above. During this period of time, most of the progenitors were tidally disrupted, giving rise to streams. Those that did not disrupt were re-sampled and evolved. The simulated streams were then transformed from the Galactocentric to the Heliocentric frame (using the *true* parameter set for the Sun) and again only the 5D phase-space information was preserved. Fig. 4(a) represents the Galactic sky structure of these tidal stream models. While we of course do not as yet know the stream discoveries that will be made with the Gaia DR2 catalogue, the distribution shown in Fig. 4 does not appear to be implausible.

To make a fair comparison, the stream models were degraded with realistic uncertainties.

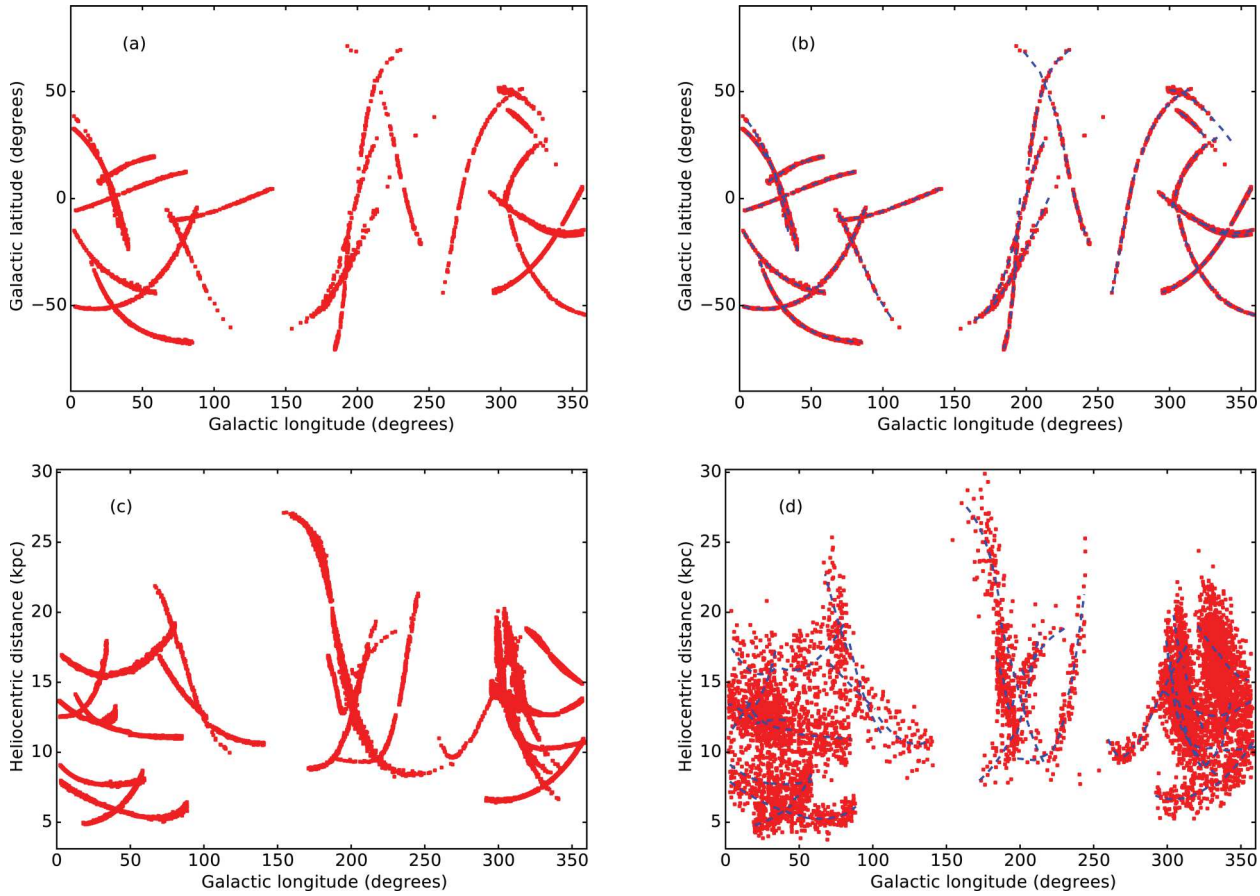

Figure 4. Sky view of the *N*-body tidal stellar streams. The left-hand panels show the positions in Galactic sky (a) and Heliocentric distance (c) that the simulated streams span. The right panels display the same information once the errors in proper motion and distance are applied (consistent with *Gaia* and CFIS survey uncertainties). The red points are the mock stellar points and the blue curves are the fitted curves to these data points. On average, we keep 230 stellar data points per stream.

(i) *Uncertainty in observed proper motions*: We introduced end-of-mission *Gaia* uncertainties for the proper motions into the simulated data. The *Gaia* errors depend upon the colour and magnitude of the stars. For this, we needed to assign magnitudes to the mock data points. This was implemented using the Padova stellar population models (Marigo et al. 2008). A star in the mock stream was selected and its absolute magnitude (M_g) was drawn in the g band from the isochrone metallicity [Fe/H] $= -1.5$ and age 10 Gyr, appropriate for a halo globular cluster. Using perfect distance information of this stellar point and the absolute magnitude, an apparent magnitude was assigned to every star. Using the colour transformations detailed in Jordi et al. (2010), we converted the magnitude to the *Gaia* G band, and limited these to $G = 20.5$. Once the magnitude value was assigned, the uncertainty in proper motion (μ_ℓ, μ_b) was generated using the 'End-of-Mission Sky Average Astrometric Performance Chart'.[1] We also assumed a minimum stream velocity dispersion of 5 km s^{-1}, which is converted into proper motion and added in quadrature to the observational uncertainties.

(ii) *Uncertainty in distance measurements*: We also introduce a 10 per cent uncertainty error in the heliocentric distance ($d_\odot$) measurements to the model stream stars. The motivation for this is that although *Gaia* parallaxes will be excellent for bright nearby stars, the majority of Galactic halo tracers will lie near *Gaia's* faint detection limit, with no geometric parallax information. However, photometric parallaxes will be measurable for such stars, using, for instance, the metallicity-magnitude-distance calibration of Ivezić et al. (2008), which is applicable to main-sequence stars. Ivezić et al. (2008) show that 5 per cent distance uncertainties are achievable with this method with good photometry; our 10 per cent uncertainty value is chosen to be a plausible average value. The necessary photometry (in particular, the u band) is currently being obtained in the Northern hemisphere as part of the Canada–France Imaging Survey,[2] and starting in ∼2021, it will also be available in the Southern hemisphere, thanks to the Large Synoptic Survey Telescope.

After this procedure, the simulated stream particles get smeared out in phase space, as shown in Fig. 4. However, we need the streams to be approximated by a curve along which the vector $\boldsymbol{v}_\mathrm{d}$ can be calculated over the full length of the stream. It is thus necessary to curve-fit the stream data. We implemented this using a simple quadratic polynomial function. The fitting procedure was conducted only in the (2D) sky frame in a coordinate system similar to the Galactic system, but rotated to ensure that both arms of the stream run, as closely as possible, to the equator of the new rotated coordinate frame (this is only approximate, since, in general,

[1] Available on *Gaia's* official website https://www.cosmos.esa.int/web/gaia/sp-table1

[2] http://www.cfht.hawaii.edu/Science/CFIS/

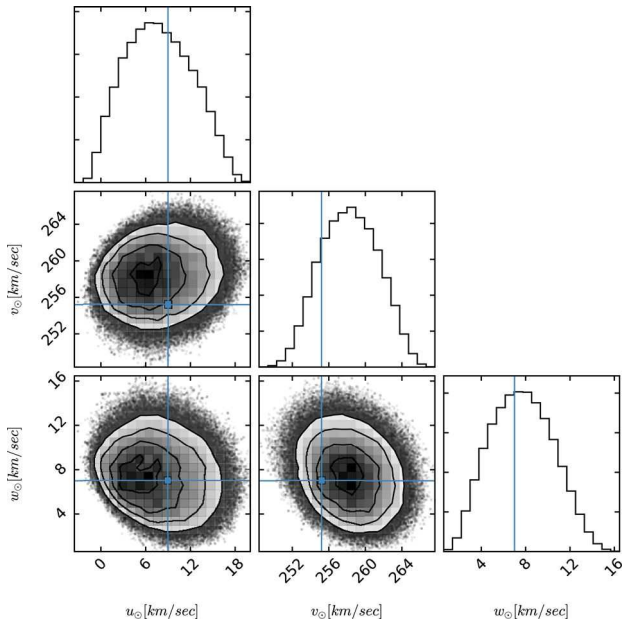

Figure 5. Correlation function plot for the *N*-body stream tests. The model distributions of the $u_\odot$, $v_\odot$ and $w_\odot$ components of the Sun's velocity, are shown, as predicted by our method in 2.0×10^5 MCMC iterations. The input values that were used for the Sun's velocity are displayed with the blue lines and are $(u_\odot, v_\odot \text{ and } w_\odot) = (9.0, 255.2, 7.0)$ km s^{-1}. The MCMC method is clearly able to recover these values to useful accuracy from the stream kinematics.

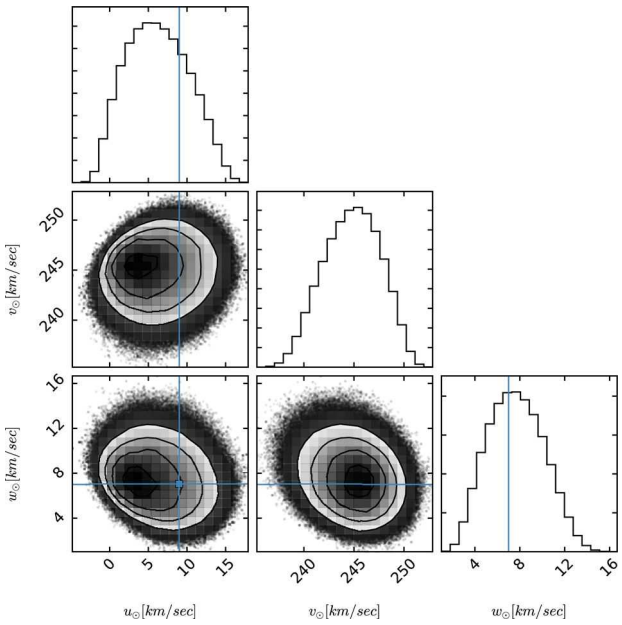

Figure 6. As Fig. 5, but for an underestimated 5 per cent systematic bias introduced into the simulated Heliocentric distance information. In this case, we find a significant bias of $\sim$10 km s^{-1} in the v component of the Sun's motion. The MCMC algorithm was made to run for 2.0×10^5 iterations in this case.

streams do not follow precisely great circle paths). We define the coordinates of the new rotated frame to be $\ell_{\rm new}$ and $b_{\rm new}$. We fitted for $b_{\rm new}$ and $d_\odot$ in the transformed coordinate system ($l_{\rm new}$, $b_{\rm new}$) using a Singular Value Decomposition algorithm with a polynomial functional form

$$b_{\rm new} = a_1 + b_1 \ell_{\rm new} + c_1 \ell_{\rm new}^2 \tag{7}$$

and

$$d_\odot = a_2 + b_2 \ell_{\rm new} + c_2 \ell_{\rm new}^2 \,, \tag{8}$$

where a_i, b_i and c_i are the fitting parameters. The two arms in all of these 22 streams were fitted independently. Once the fitting procedure was complete, the fitted curves were then transformed back to Galactic coordinates. Fig. 4 (right-hand panels) represents the streams with uncertainties introduced along with the curves fitted to them. Once fitting is done, equations (7) and (8) are then used to calculate the vector $\boldsymbol{v}_{\rm d}$ and the heliocentric distances at every stellar point. θ is still the angle between $\boldsymbol{v}_{\rm d}$ and $\boldsymbol{v}_{{\rm o}\mu}$, where $\boldsymbol{v}_{{\rm o}\mu}$ is the observed proper motion vector.

In this case, Sun's Galactic velocity solution (shown in Fig. 5) was recovered as : $(u_\odot, v_\odot, w_\odot) = (7.80, 258.25, 7.69)$ km s^{-1}. This means that the bias estimated between the observed and true value of the Sun's velocity is $(u_\odot - u_{\odot,\rm T}, v_\odot - v_{\odot,\rm T}, w_\odot - w_{\odot,\rm T}) = (-1.20, 3.05, 0.69)$ km s^{-1}, with uncertainties $(\sigma_u, \sigma_v, \sigma_w) = (4.16, 3.04, 2.74)$ km s^{-1}.

3.3 Systematic bias in distance

For completeness, we consider next what the effect of a $\pm$5 per cent distance bias would have on the derivation of the solar velocity; such a bias could arise, in principle, from an incorrect calibration in the photometric distances. To this end, we reran the algorithm on the simulated data and simply forced all of the stellar particles to be 5 per cent less distant. The resulting most likely solution has: $(u_\odot - u_{\odot,\rm T}, v_\odot - v_{\odot,\rm T}, w_\odot - w_{\odot,\rm T}) = (-2.75, -9.69, 0.66)$ km s^{-1}, and uncertainty $(\sigma_u, \sigma_v, \sigma_w) = (3.73, 2.79, 2.45)$ km s^{-1}. The correlation function plot for this case is shown in Fig. 6. Re-running this test using distances that are systematically 5 per cent overestimated gives qualitatively similar results, but with a velocity bias of $(u_\odot - u_{\odot,\rm T}, v_\odot - v_{\odot,\rm T}, w_\odot - w_{\odot,\rm T}) = (-0.99, 13.58, 1.56)$ km s^{-1}.

The bias in the distance measurements clearly affects the vector $\boldsymbol{v}_{\rm r\perp}$ (calculated at the stellar points) and hence affects the solar velocity $\mathbf{V}_\odot$ estimation. In our study (and as can be seen in Fig. 6, $v_\odot$ panel), a large shift was observed in the $v_\odot$ component of the velocity of the Sun from the true $v_\odot$ value, but the other components were less affected. This is not specific to the technique but rather to the overall phase-space distribution of stellar streams with respect to the Sun's motion. The phase-space distribution and orientation of the streams in the example happened to be such that the $v_\odot$ component faced a higher offset from the *true* value than the other two components.

4 DISCUSSION AND CONCLUSIONS

The Galactic Astronomy and Galactic Dynamics communities are greatly looking forward to the second data release of the *Gaia* astrometric satellite. The data from this mission are expected to unveil the phase-space structure of our Galaxy, curing a sort of kinematic 'blindness' we have had until now. *Gaia* will reveal the transverse motion dimensions of the phase space of known stellar streams, and is expected to reveal more stream structures of low contrast that remain hidden in present-day star-count surveys.

In this paper, we presented a geometrical procedure that successfully gauges the Sun's velocity $\mathbf{V}_\odot$ by allowing one to exploit a very basic behaviour of low-mass streams: that the proper motion of the stars should be closely directed along the structure in a frame that is

at rest with respect to the Galaxy. Any perpendicular motion of the stream stars arises (primarily) due to the reflex motion of the observer. This effect is not correlated with the Sun's Galactic distance $R_\odot$ value. The method was demonstrated using *N*-body simulated streams (degraded with *Gaia*-like uncertainties in proper motions and CFHT CFIS-like uncertainties in distance measurements). The reason for using low-mass streams for constraining the solar motion using this method is simple. The high-mass (thick) streams like the Sgr stream formed from the disruption of dwarf galaxies, are highly dispersed in phase space (Ibata et al. 2002; Johnston, Spergel & Haydn 2002). Although their broad trajectory could be curve fitted (or modelled using an orbit) for our purposes, the dispersion in the stream track would result in higher uncertainties in the measured solar motion values.

Our method does not assume any Galactic mass model, which we view as a strength of the technique. If the Galactic potential were well known, it could clearly be used to refine the streams and hence obtain better constraints on $\mathbf{V}_\odot$, but that would also require much more sophisticated modelling of individual tidal streams.

It should also be noted that our analysis determines the Sun's velocity with respect to a sample of streams in the Galactic halo, and this velocity might turn out to be different from the velocity measured with respect to the Galactic Centre or with respect to the LSR for a variety of interesting astrophysical reasons. This could happen, if, for instance, if Sgr A^* is not at rest with respect to the Galaxy, or if the disc possesses significant non-circular motions, or if there is a bulk motion of the streams with respect to the disc (as might happen if there is a substantial ongoing accretion: e.g. the LMC or the Sgr dwarf). Using two independent measurement techniques might give us some insight about the relative motion between the dynamical centres of the inner Milky Way and the outer Milky Way (around which the streams actually orbit).

ACKNOWLEDGEMENTS

The authors would like to thank the anonymous referee for very useful comments that contributed to the clarity and overall improvement of the paper.

REFERENCES

Bernard E. J. et al., 2014, MNRAS, 443, L84
Bernard E. J. et al., 2016, MNRAS, 463, 1759
Bobylev V. V., 2013, Astron. Lett., 39, 95
Bovy J., Hogg D. W., Rix H.-W., 2009, ApJ, 704, 1704
Bovy J., Bahmanyar A., Fritz T. K., Kallivayalil N., 2016, ApJ, 833, 31
Dehnen W., 2000, ApJ, 536, L39
Dehnen W., Binney J., 1998a, MNRAS, 294, 429
Dehnen W., Binney J. J., 1998b, MNRAS, 298, 387
Dehnen W., Odenkirchen M., Grebel E. K., Rix H.-W., 2004, AJ, 127, 2753
Gaia Collaboration et al., 2016, A&A, 595, A2
Grillmair C. J., 2016, Tidal Streams in the Local Group and Beyond. Springer International Publishing, Cham
Grillmair C. J., Dionatos O., 2006, ApJ, 643, L17
Harris W. E., 1976, AJ, 81, 1095
Ibata R., Lewis G. F., Irwin M., Totten E., Quinn T., 2001, ApJ, 551, 294
Ibata R. A., Lewis G. F., Irwin M. J., Quinn T., 2002, MNRAS, 332, 915
Ivezić Z. et al., 2008, ApJ, 684, 287
Johnston K. V., Spergel D. N., Haydn C., 2002, ApJ, 570, 656
Jordi C. et al., 2010, A&A, 523, A48
King I. R., 1966, AJ, 71, 64
Koposov S. E., Rix H.-W., Hogg D. W., 2010, ApJ, 712, 260
Koposov S. E., Irwin M., Belokurov V., Gonzalez-Solares E., Yoldas A. K., Lewis J., Metcalfe N., Shanks T., 2014, MNRAS, 442, L85
Küpper A. H. W., Balbinot E., Bonaca A., Johnston K. V., Hogg D. W., Kroupa P., Santiago B. X., 2015, ApJ, 803, 80
Majewski S. R., Skrutskie M. F., Weinberg M. D., Ostheimer J. C., 2003, ApJ, 599, 1082
Majewski S. R., Law D. R., Polak A. A., Patterson R. J., 2006, ApJ, 637, L25
Marigo P., Girardi L., Bressan A., Groenewegen M. A. T., Silva L., Granato G. L., 2008, A&A, 482, 883
Myeong G. C., Jerjen H., Mackey D., Da Costa G. S., 2017, ApJ, 840, L25
Odenkirchen M. et al., 2001, ApJ, 548, L165
Reid M. J., Brunthaler A., 2004, ApJ, 616, 872
Reid M. J. et al., 2009, ApJ, 700, 137
Rygl K. L. J., Brunthaler A., Reid M. J., Menten K. M., van Langevelde H. J., Xu Y., 2010, A&A, 511, A2
Salomon J. B., Ibata R. A., Famaey B., Martin N. F., Lewis G. F., 2016, MNRAS, 456, 4432
Schönrich R., Binney J., 2009, MNRAS, 396, 203
Schönrich R., Binney J., Dehnen W., 2010, MNRAS, 403, 1829
Sofue Y., Nagayama T., Matsui M., Nakagawa A., 2011, PASJ, 63, 867
Steiman-Cameron T. Y., Durisen R. H., 1990, ApJ, 357, 62
Strömberg G., 1946, ApJ, 104, 12
Teuben P., 1995, in Shaw R. A., Payne H. E., Hayes J. J. E., eds, ASP Conf. Ser. Vol. 77, Astronomical Data Analysis Software and Systems IV. Astron. Soc. Pac., San Francisco, p. 398
Unwin S. C. et al., 2008, PASP, 120, 38
van den Bosch F. C., Lewis G. F., Lake G., Stadel J., 1999, ApJ, 515, 50

This paper has been typeset from a TEX/LATEX file prepared by the author.

CHAPTER 8

SUMMARY AND OUTLOOK

Progress is not simply achieving a milestone. Progress is reaching the milestone but then realising that destination lies further ahead- **me :)**

8.1 Summary

This thesis work was devoted to the detection and the dynamical analysis of stellar streams of the Milky Way galaxy. The first part of the thesis introduced and detailed the workings of a newly developed powerful stream detection algorithm - the `STREAMFINDER` (Chapter 3 and 4), thereby also presenting its application on the ESA/Gaia DR2 catalogue that rendered the first ever all-sky structural and kinematical maps of the stellar streams of the Milky Way halo (Chapter 5). The second part of the thesis established the relevance of the dynamical analysis of stellar streams in constraining the gravitational potential (Chapter 6) and the fundamental parameters (Chapter 7) of the Milky Way galaxy. Each chapter in this thesis was based on a scientific paper that was attached at the end of every chapter.

1. Chapter 1 and 2 set the soil, detailing the major challenges that are being faced by the field of Galactic archaeology, and that how stellar streams recently emerged as important investigatory tools playing useful roles in addressing these fundamental problems.

2. The thesis work discussion begins with Chapter 3 that introduced the `STREAMFINDER` algorithm. This algorithm is a state-of-the art tool that is designed to analyse Gaia data to detect thin and dynamically cold stellar streams in the Milky Way galaxy. `STREAMFINDER` is a generic stream dectection recipe that makes use of as much as possible of our prior knowledge about stellar streams. It can handle heterogeneous datasets that are a combination of

positions and kinematics and its prowess lies in its performance, ability to scan the entire data set for stream structures in an automated way and its capability of detecting even those streams that lie along complex orbital trajectories.

At its heart, the algorithm shoots trial orbits using the present epoch observed phase-space values of the stars in some realistic Milky Way potential model, and it then performs a multidimensional calculation based on both the stellar population and the phase-space distribution of the data stars to detect groups of stars that correspond to a stream. Some initial tests were undertaken using the artificial N-body streams superimposed on the GUMS - mock Gaia catalogue [155] with kinematics degraded to Gaia - like quality. These results manifested that the algorithm, in principle, is capable of discovering even ultra faint stream structures ($\Sigma_G \sim 33\,\mathrm{mag\,arcsec^{-2}}$, number of stars per stream ~ 15) in the end-of-mission ESA/Gaia catalogue. The Chapter described the algorithm's concept, its modus operandi and the results obtained based on trial runs.

The design of the algorithm is such that along with the stream detection, it delivers orbital trajectory along which the stream lies. This is the primary by-product that the algorithm naturally returns and is useful in giving insights about the detected candidate structures. For example, 1) good quality distance measurements and radial velocities for a great majority of halo stars are missing in Gaia DR2 (and later catalogues), and therefore knowing the orbital solutions of the stream structures provides a means to complete the 6D phase-space solutions that are possible for a given stream star, 2) DF(x, v) of streams can be constructed once the complete 6D phase-space distribution of possible orbital solutions are known, that is also extremely useful for re-creating the pre-merging history of the Milky Way, or to perform Schwarzschild modelling to constrain the dark matter distribution in the Galaxy, and 3) since the algorithm offers orbital solutions for every stream, one can easily calculate simple orbital properties of the stream structure such as the eccentricity or energy of the streams.

3. Chapter 4 demonstrated the application of the `STREAMFINDER` algorithm on the Pan-STARRSS1 proper motion dataset in order to detect the GD-1 stream. This analysis, that was done prior to ESA/Gaia DR2, was essential in order to test the sanity and feasibility of the algorithm when applied to a realistic astrophysical dataset. The study was undertaken as a comparison between the Match Filtering technique (the technique using which GD-1 was originally discovered) and the `STREAMFINDER` algorithm by applying them both onto a magnitude limited subset of the Pan-STARRSS1 data. While this trimmed sample led to what was effectively a non-detection with a matched filter search, the application of `STREAMFINDER` onto the very same data readily showed up the GD-1 stream at a significance level of $> 4.4\sigma$. This both validated our algorithm as well as the proper motion measurements in the PS1 catalogue. The positive detection of GD-1 in this PS1 proper motion sample with the `STREAMFINDER` suggested that it would be possible to find other

similar structures in Gaia DR2 (that was yet to be published on 25^{th} April 2018), where the proper motion uncertainties of stars were to be a factor of ~ 25 better.

In addition to GD-1, STREAMFINDER was also able to reproduce the PS1-E stream structure, that appeared to have similar distance and kinematical properties as GD-1 stream. However, this yet requires confirmation.

4. Chapter 5 discussed the first result of the application of the STREAMFINDER algorithm onto the Gaia DR2 catalogue. For the first time, an all-sky structural and kinematical map of the stellar streams of the Milky Way halo was created. A rich network of criss-crossing streams was found in the halo, often with striking kinematic coherence. Along with reproducing the previously known stream structures such as the Sagittarius, GD-1, Orphan, Indus and Jhelum, STREAMFINDER was also able to detect many new stream structures out of which five high confidence stream candidates were claimed as discoveries and were named Gaia -1, 2, 3, 4 and 5.

   The Chapter detailed the method of application of the STREAMFINDER onto Gaia DR2, presented the paranomic view of the Milky Way halo sky, and showcased the phase-space distribution of all the stellar streams that were detected.

5. Chapter 6 demonstrated the power that a mere single stream holds in probing the underlying gravitational potential of the Milky Way by fitting the orbital path of a stream. For this analysis, ESA/Gaia astrometry together with SEGUE's radial velocity measurements of the GD-1 stream [72] were used.

   Assuming a realistic universal model for the halo together with reasonable models for the bulge and the disk, this analysis estimated circular velocity at the Solar radius to be $V_{\rm circ}(R_\odot) = 244^{+6}_{-2}\,{\rm km\,s^{-1}}$, and the density flattening of the halo as $q_\rho = 0.86^{+0.04}_{-0.07}$. This value of $V_{\rm circ}(R_\odot)$ value was found to be in excellent agreement with those obtained by other authors based on different [127, 152] and similar [107] approaches. As for q_ρ, the result was found to be consistent with some previous studies [17]; while being in tensions with a similar GD-1 analysis [106] and also with another study that favoured a prolate halo solution obtained based on analysis of the globular clusters [148].

   With the obtained model of the potential, the mass of the Milky Way in the inner 14.5 kpc, the mean Galactocentric distance of GD-1, was estimated as $M_{MW}(< 14.5\,{\rm kpc}) = 1.75^{+0.06}_{-0.05} \times 10^{11}\,{\rm M}_\odot$. Extrapolating out slightly to $R = 20\,{\rm kpc}$, it was found that $M_{MW}(< 20\,{\rm kpc}) = 2.14 \pm 0.07 \times 10^{11}\,{\rm M}_\odot$. This value too was found to be consistent with various other recent findings of the Milky Way's mass [107, 148, 191].

   Moreover, Gaia's excellent proper motions also allowed the measurement of the velocity dispersion of the GD-1 stream in the direction tangential to the line of sight, that was mea-

sured to be $< 1.25\,\mathrm{km\,s^{-1}}$ (90% confidence limit), confirming the extremely cold dynamical nature of the GD-1 system.

6. Finally, Chapter 7 presented a novel geometrical procedure that successfully gauges the Sun's velocity $\mathbf{V}_\odot$ by exploiting a very basic behaviour of low-mass streams: that the proper motion of the stream stars should be closely directed along the structure in a frame that is at rest with respect to the Galaxy, and any perpendicular motion of the stream stars arises (primarily) due to the reflex motion of the observer. This effect is not correlated with Sun's Galactic distance $R_\odot$ value. The implementation of the method was demonstrated using N-body simulated streams (degraded with Gaia-like uncertainties in proper motions and 10% uncertainty errors in distance measurements as expected from photometric parallaxes derivation), and it was shown that the Sun's motion can be recovered to a useful accuracy through such a procedure.

   Such a method does not assume any Galactic mass model, which must be viewed as a strength of the technique. Also, this prescription determines the Sun's velocity with respect to a sample of streams in the Galactic halo, and this velocity might turn out to be different from the velocity measured with respect to the Galactic centre or with respect to the LSR for a variety of interesting astrophysical reasons. This could happen, if for instance, if Sgr A^* is not at rest with respect to the Galaxy, or if the disk possesses significant non-circular motions, or if there is a bulk motion of the streams with respect to the disk (as might happen if there is a substantial ongoing accretion: e.g., the LMC or the Sgr dwarf). Using two independent measurement techniques might give us some insight about the relative motion between the dynamical centres of the inner Milky Way and the outer Milky Way (around which the streams actually orbit).

   Once we armed with Gaia's proper motion measurements for plenty of stellar streams in the Milky Way, this procedure can be implemented and its feasibility can be verified.

8.2 Future prospects

Presently, the stellar halo formation and evolution scenario is unclear. We do not have a definite answer to what fraction of the Galaxy's stellar halo has been built via accretion and that how does the importance of this process changes with the distance from the Galactic center? There is significant evidence of substructure in the form of streams in the outer halo, but this is still at a rather qualitative level (although see e.g., [6]). Another related and useful question is - can we find any characteristic properties of the accreted objects (in terms of their masses, their star formation, their phase-space distribution and chemical histories) which can be used as filters to discriminate them from rest of the population of stars. Also, we are yet not sure whether there is any evolutionary link between the disk and the halo, or the bulge and the halo? [81] We are

also unware of the dynamical history of our Galaxy, and are unsure about how its mass and gravitational potential evolves with time?

Knowledge of the stellar kinematics complemented with their chemical abundances and ages should allow us to address questions. Therefore, the answers to these and many other questions seem to be within reach in this era of Gaia, where Gaia is being complimented by many other large surveys (RAVE, APOGEE, GALAH, Gaia-ESO) that all-in-all aim at providing a full phase-space-chemical distribution of the Milky Way galaxy.

Motivated by these questions and their relevance in the field of Galactic archaeology, I wish to work towards the following projects in the coming years.

1. **Detection of the Milky Way streams by applying** `STREAMFINDER` **onto Gaia DR2**.

   First results of the `STREAMFINDER` output based on Gaia DR2 gave a rich map of criss-crossing stellar streams in the Milky Way halo. This output employed a single Milky Way potential model (in which the trial orbits are integrated) and only a handful of Stellar population models of Age=10 Gyr that were sampled over [Fe/H] between -2.2 and -1.0. Where I still need to analyze and study the obtained stellar stream maps, I also desire to re-run the algorithm by trying different Galactic potential models and several Stellar Population models (by finely gridding in Age and [Fe/H] space) in order to discover more halo streams. This would be useful in creating a stellar stream census of the Milky Way. Based on such a quantification of streams it should be possible, to some degree, to estimate what fraction of the halo is a consequence of the accretion of smaller mass systems.

   Iterating over different potential models could be also useful in gauging the underlying Galactic potential of the Milky Way.

2. `STREAMFINDER`**–>** `BLOBFINDER` **: detection of blobs of stars**.

   `STREAMFINDER` can be easily converted into a `BLOBFINDER`, an algorithm that is useful to find *blobs* of stars. The idea remains similar to that of `STREAMFINDER`, however instead of integrating orbits `BLOBFINDER` only looks for overdense clumps of stars in multidimensional phase-space-color-magnitude space. Such an algorithm is useful in not only finding low mass stellar systems such as star clusters or ultra-faint dwarf galaxies, but also in detecting similar systems that are presently undergoing disruption.

3. **Development of a coherent and detailed picture of the assembly and evolutionary history of the Milky Way**

   I am strongly inclined working towards the development of a coherent and detailed picture of the assembly and the evolutionary history of the Milky Way and to attempt to reconstruct its distribution function DF (x,v) of the halo accretions. The DF (x,v) of streams could tell us a lot about the pre-merging history of our galaxy and the dark matter distribution. This now appears within reach, thanks to Gaia.

In the hierarchical picture of galaxy formation, galaxies like the Milky Way grow by repeated merging and accretion of their satellites. Some of the disrupted satellites will have contained star clusters [87], which themselves will eventually tidally disrupt to form long streams in the Galactic halo. The famous "Field-of-Streams" map [10], the Pan-STARRS1 synoptic map of halo substructures [12] and the stellar stream map that has been presented in this thesis work, altogether strongly suggest that a significant fraction of the stellar halo population is a result of hierarchical merging. This is something that can be verified for the stars over the entire sky with Gaia's excellent global astrometric solutions. Orbital solutions that `STREAMFINDER` gives for every stream could also prove to be very useful in this endeavour.

4. **Constraining the underlying dark mater distribution of the Milky Way**

   Chapter 6 presented dynamical analysis of the GD-1 stellar stream to probe the underlying shape of the dark matter halo, that in effect rendered quite strong and useful constraints on the circular velocity at the solar radius ($V_{circ}(R_o)$) and the flattening of the dark matter halo density (q_ρ). However, more robust, stringent and global constraints would be placed if a similar exercise is repeated but with an ensemble of streams probing different regions and depths of the Milky Way sky.

   Radial velcoities (v_{los}) for most of the stream stars are missing in the Gaia data. For this, we obtained CFHT/ESPaDOnS time to measure the v_{los} of the detected stream stars that were presented in Chapter 5. Consolidating the stream detection findings and the full 6D dimension measurement of stream stars, I shall then attempt to probe the underlying dark mater distribution via stream dynamical analysis.

5. **Lumpiness in dark matter distribution and its nature**

   CDM simulations predict that there should be hundreds of dark matter lumps in the form of dwarf satellites with M $\geq 10^7 M_\odot$ in the Milky Way halo. However, we know only a few of satellites close to this mass. This challenges the ΛCDM framework. An observational determination of the sub-halo mass spectrum to well below $10^9 M_\odot$ would provide one of the most important astrophysical constraints on the nature of the dark matter.

   In the Milky Way galaxy, one of the most promising methods for detecting low-mass dark matter sub-halos is through their effects on the stellar streams. Sub-halos induce visible gaps when they cross a stream [24, 50]. The dynamical coldness of streams makes them sensitive to the influence of sub-halos with M $\leq 10^8 M_\odot$. Dynamical modeling of the smooth stream itself and of the impact of sub-halos has been shown to be able to detect and characterize subhalos (in terms of their sizes, density and velocities) with masses down to $10^5 M_\odot$ [50]. The dark matter sub-halo phase-space density obtained from "stream-gap" analysis, together with the smooth spatial density of the dark matter halo, would be useful in constructing a complete phase-space distribution of the Milky Way's dark matter halo.

This is another aspect of stream based analysis that I am interested in working towards.

UNIVERSITÉ DE STRASBOURG

Khyati MALHAN

Stellar Streams en tant que sondes de la matière noire: Recherche et analyse dynamique

Résumé

Les flux stellaires comme sondes de la matière noire: recherche et analyse dynamique

Les courants stellaires de marée sont des structures en étoile immaculées qui jouent un rôle central dans la résolution des mystères de longue date de l'archéologie galactique. Étant donné que les flux sont de nature orbitale, ils possèdent intrinsèquement les caractéristiques de résolution de la distribution de masse sous-jacente de la galaxie et peuvent être utilisés pour sonder la forme du halo de matière noire. En plus de tester le scénario de «fusion hiérarchique» de la formation de galaxies, les brèches de ruisseau peuvent également fournir une preuve indirecte de l'existence de sous-halos de matière noire (ce qui, en principe, limite la nature de la particule de matière noire elle-même). Pour toutes ces raisons, l'analyse dynamique des flux stellaires de la Voie Lactée devient naturellement l'un des problèmes les plus intéressants. Cependant, le principal défi consiste à détecter ces structures.

Au cours de la thèse, l'algorithme STREAMFINDER (un algorithme à la pointe de la technologie) a été conçu pour traiter systématiquement le jeu de données Gaia (le nouveau catalogue astrophysique de l'ESA contenant des solutions astrométriques sans précédent de plus de 1,6 milliard d'étoiles) pour la détection des flux stellaires de la Voie lactée. Cette lourde entreprise a permis de détecter 10 structures de flux de confiance, dont 5 étaient considérées comme de nouvelles découvertes. Cette récolte de structures a également facilité, pour la première fois, la création d'une carte structurale et cinématique panoramique des flux stellaires de la rivière Milky. Halo, poussant notre communauté encore plus loin dans l'histoire complexe de la formation de notre galaxie. Ce projet a été immédiatement suivi de l'analyse orbitale de l'un des flux détectés (à savoir GD-1) pour explorer les améliorations des modèles de potentiel gravitationnel de notre galaxie. Les contraintes imposées à la masse de la Voie lactée et à la forme de son halo de matière noire, obtenues simplement en utilisant ce seul flux, ont révélé la puissance potentielle que l'analyse d'un ensemble de flux permettrait de sonder la distribution globale de la masse galactique de notre galaxie.

Ainsi, la thèse a ouvert la voie à de nouvelles découvertes des sous-structures stellaires, soulignant également les perspectives d'avenir dans ce domaine.

Mots clés Structure de la galaxie; étoiles ; ruisseaux stellaires; matière noire.

Résumé en anglais

Title : Stellar Streams as probes of dark matter: Search and dynamical analysis

Tidal stellar streams are pristine star structures that play central role in addressing long standing mysteries of the Galactic archaeology. Since streams are orbital in nature, they inherently possess the characteristics of unravelling the underlying mass distribution of the galaxy, and can be used to probe the shape of the dark matter halo. Besides testing the 'hierarchical merging' scenario of galaxy formation, stream gaps can also provide indirect evidence for the existence of dark matter sub-halos (thereby, in principle, constraining the nature of the dark matter particle itself). Due to all these reasons, the dynamical analysis of stellar streams of the Milky Way Galaxy naturally becomes one of the interesting problems. However, the foremost challenge is to detect these structures.

During the thesis, STREAMFINDER algorithm (a state of the art algorithm) was designed to systematically process the Gaia dataset (ESA's novel astrophysical catalogue containing unprecedented astrometric solutions of over 1.6 billion stars) for the detection of the stellar streams of the Milky Way. This hefty endeavour led to the detection of 10 high confidence stream structures, of which 5 were reported as new discoveries.This harvest of structures also facilitated, for the first time, creation of a panoramic structural and kinematic map of the stellar streams of the Milky Way halo, taking our community a step further in unravelling the complex formation history of our Galaxy. This project was instantly followed by the orbital analysis of one of the detected streams (namely GD-1) to explore the improvements in the gravitational potential models of our Galaxy. The constraints on the Milky Way's mass and that on the shape of its dark matter halo, that were obtained by simply employing this single stream, revealed the potential power the analysis of an ensemble of streams would hold in in probing the overall galactic mass distribtuion of our Galaxy.
Thereby, the thesis paved way for new discoveries of the stellar substructures, also highlighting the future prospects in this field.

Keywords : Galaxy structure ; stars ; stellar streams ; dark matter.

BIBLIOGRAPHY

[1] C. ALLENDE PRIETO, S. R. MAJEWSKI, R. SCHIAVON, K. CUNHA, P. FRINCHABOY, J. HOLTZMAN, K. JOHNSTON, M. SHETRONE, M. SKRUTSKIE, V. SMITH, AND J. WILSON, *APOGEE: The Apache Point Observatory Galactic Evolution Experiment*, Astronomische Nachrichten, 329 (2008), p. 1018.

[2] M. I. ARIFYANTO AND B. FUCHS, *Fine structure in the phase space distribution of nearby subdwarfs*, aap, 449 (2006), pp. 533–538.

[3] J. N. BAHCALL, *The distribution of stars perpendicular to galactic disk*, apj, 276 (1984), pp. 156–168.

[4] J. N. BAHCALL AND R. M. SONEIRA, *The universe at faint magnitudes. I - Models for the galaxy and the predicted star counts*, apjs, 44 (1980), pp. 73–110.

[5] E. BALBINOT, B. X. SANTIAGO, L. N. DA COSTA, M. MAKLER, AND M. A. G. MAIA, *The tidal tails of NGC 2298*, mnras, 416 (2011), pp. 393–402.

[6] E. F. BELL, D. B. ZUCKER, V. BELOKUROV, S. SHARMA, K. V. JOHNSTON, J. S. BULLOCK, D. W. HOGG, K. JAHNKE, J. T. A. DE JONG, T. C. BEERS, N. W. EVANS, E. K. GREBEL, Z. IVEZIĆ, S. E. KOPOSOV, H.-W. RIX, D. P. SCHNEIDER, M. STEINMETZ, AND A. ZOLOTOV, *The Accretion Origin of the Milky Way's Stellar Halo*, apj, 680 (2008), pp. 295–311.

[7] M. BELLAZZINI, R. IBATA, F. R. FERRARO, AND V. TESTA, *Tracing the Sgr Stream with 2MASS. Detection of Stream stars around Outer Halo globular clusters*, aap, 405 (2003), pp. 577–583.

[8] M. BELLAZZINI, H. J. NEWBERG, M. CORRENTI, F. R. FERRARO, AND L. MONACO, *Detection of a population gradient in the Sagittarius stream*, aap, 457 (2006), pp. L21–L24.

[9] V. BELOKUROV, N. W. EVANS, M. J. IRWIN, D. LYNDEN-BELL, B. YANNY, S. VIDRIH, G. GILMORE, G. SEABROKE, D. B. ZUCKER, M. I. WILKINSON, P. C. HEWETT, D. M. BRAMICH, M. FELLHAUER, H. J. NEWBERG, R. F. G. WYSE, T. C. BEERS, E. F. BELL,

J. C. Barentine, J. Brinkmann, N. Cole, K. Pan, and D. G. York, *An Orphan in the "Field of Streams"*, apj, 658 (2007), pp. 337–344.

[10] V. Belokurov, D. B. Zucker, N. W. Evans, G. Gilmore, S. Vidrih, D. M. Bramich, H. J. Newberg, R. F. G. Wyse, M. J. Irwin, M. Fellhauer, P. C. Hewett, N. A. Walton, M. I. Wilkinson, N. Cole, B. Yanny, C. M. Rockosi, T. C. Beers, E. F. Bell, J. Brinkmann, Z. Ivezic, and R. Lupton, *The Field of Streams: Sagittarius and Its Siblings*, apjl, 642 (2006), pp. L137–L140.

[11] E. J. Bernard, A. M. N. Ferguson, E. F. Schlafly, M. Abbas, E. F. Bell, N. R. Deacon, N. F. Martin, H.-W. Rix, B. Sesar, C. T. Slater, J. Peñarrubia, R. F. G. Wyse, W. S. Burgett, K. C. Chambers, P. W. Draper, K. W. Hodapp, N. Kaiser, R.-P. Kudritzki, E. A. Magnier, N. Metcalfe, J. S. Morgan, P. A. Price, J. L. Tonry, R. J. Wainscoat, and C. Waters, *Serendipitous discovery of a thin stellar stream near the Galactic bulge in the Pan-STARRS1 3π Survey*, mnras, 443 (2014), pp. L84–L88.

[12] E. J. Bernard, A. M. N. Ferguson, E. F. Schlafly, N. F. Martin, H.-W. Rix, E. F. Bell, D. P. Finkbeiner, B. Goldman, D. Martínez-Delgado, B. Sesar, R. F. G. Wyse, W. S. Burgett, K. C. Chambers, P. W. Draper, K. W. Hodapp, N. Kaiser, R.-P. Kudritzki, E. A. Magnier, N. Metcalfe, R. J. Wainscoat, and C. Waters, *A Synoptic Map of Halo Substructures from the Pan-STARRS1 3π Survey*, mnras, 463 (2016), pp. 1759–1768.

[13] J. Binney and S. Tremaine, *Galactic Dynamics: Second Edition*, Princeton University Press, 2008.

[14] J. Bland-Hawthorn and O. Gerhard, *The Galaxy in Context: Structural, Kinematic, and Integrated Properties*, araa, 54 (2016), pp. 529–596.

[15] A. Bosma, *The distribution and kinematics of neutral hydrogen in spiral galaxies of various morphological types*, PhD thesis, PhD Thesis, Groningen Univ., (1978), 1978.

[16] J. Bovy, *galpy: A python Library for Galactic Dynamics*, apjs, 216 (2015), p. 29.

[17] J. Bovy, A. Bahmanyar, T. K. Fritz, and N. Kallivayalil, *The Shape of the Inner Milky Way Halo from Observations of the Pal 5 and GD–1 Stellar Streams*, apj, 833 (2016), p. 31.

[18] A. Bowden, *Using stellar streams to probe the galactic potential*, 111 (1111).

[19] A. Bowden, N. W. Evans, and A. A. Williams, *Is the dark halo of the Milky Way prolate?*, mnras, 460 (2016), pp. 329–337.

[20] M. Boylan-Kolchin, V. Springel, S. D. M. White, and A. Jenkins, *There's no place like home? Statistics of Milky Way-mass dark matter haloes*, mnras, 406 (2010), pp. 896–912.

[21] J. S. Bullock and K. V. Johnston, *Tracing Galaxy Formation with Stellar Halos. I. Methods*, apj, 635 (2005), pp. 931–949.

[22] J. S. Bullock, A. V. Kravtsov, and D. H. Weinberg, *Hierarchical Galaxy Formation and Substructure in the Galaxy's Stellar Halo*, apj, 548 (2001), pp. 33–46.

[23] A. Burkert, *The Structure of Dark Matter Halos in Dwarf Galaxies*, in New Light on Galaxy Evolution, R. Bender and R. L. Davies, eds., vol. 171 of IAU Symposium, 1996, p. 175.

[24] R. G. Carlberg, *Dark Matter Sub-halo Counts via Star Stream Crossings*, apj, 748 (2012), p. 20.

[25] B. W. Carney, J. B. Laird, D. W. Latham, and L. A. Aguilar, *A Survey of Proper Motion Stars. XIII. The Halo Population*, aj, 112 (1996), p. 668.

[26] D. Carollo, T. C. Beers, Y. S. Lee, M. Chiba, J. E. Norris, R. Wilhelm, T. Sivarani, B. Marsteller, J. A. Munn, C. A. L. Bailer-Jones, P. R. Fiorentin, and D. G. York, *Two stellar components in the halo of the Milky Way*, nat, 450 (2007), pp. 1020–1025.

[27] K. C. Chambers, E. A. Magnier, N. Metcalfe, H. A. Flewelling, M. E. Huber, C. Z. Waters, L. Denneau, P. W. Draper, D. Farrow, D. P. Finkbeiner, C. Holmberg, J. Koppenhoefer, P. A. Price, R. P. Saglia, E. F. Schlafly, S. J. Smartt, W. Sweeney, R. J. Wainscoat, W. S. Burgett, T. Grav, J. N. Heasley, K. W. Hodapp, R. Jedicke, N. Kaiser, R.-P. Kudritzki, G. A. Luppino, R. H. Lupton, D. G. Monet, J. S. Morgan, P. M. Onaka, C. W. Stubbs, J. L. Tonry, E. Banados, E. F. Bell, R. Bender, E. J. Bernard, M. T. Botticella, S. Casertano, S. Chastel, W.-P. Chen, X. Chen, S. Cole, N. Deacon, C. Frenk, A. Fitzsimmons, S. Gezari, C. Goessl, T. Goggia, B. Goldman, E. K. Grebel, N. C. Hambly, G. Hasinger, A. F. Heavens, T. M. Heckman, R. Henderson, T. Henning, M. Holman, U. Hopp, W.-H. Ip, S. Isani, C. D. Keyes, A. Koekemoer, R. Kotak, K. S. Long, J. R. Lucey, M. Liu, N. F. Martin, B. McLean, E. Morganson, D. N. A. Murphy, M. A. Nieto-Santisteban, P. Norberg, J. A. Peacock, E. A. Pier, M. Postman, N. Primak, C. Rae, A. Rest, A. Riess, A. Riffeser, H. W. Rix, S. Roser, E. Schilbach, A. S. B. Schultz, D. Scolnic, A. Szalay, S. Seitz, B. Shiao, E. Small, K. W. Smith, D. Soderblom, A. N. Taylor, A. R. Thakar, J. Thiel, D. Thilker, Y. Urata, J. Valenti, F. Walter, S. P. Watters,

S. WERNER, R. WHITE, W. M. WOOD-VASEY, AND R. WYSE, *The Pan-STARRS1 Surveys*, ArXiv e-prints, (2016).

[28] B. CHEN, C. STOUGHTON, J. A. SMITH, A. UOMOTO, J. R. PIER, B. YANNY, Z. IVEZIĆ, D. G. YORK, J. E. ANDERSON, J. ANNIS, J. BRINKMANN, I. CSABAI, M. FUKUGITA, R. HINDSLEY, R. LUPTON, J. A. MUNN, AND SDSS COLLABORATION, *Stellar Population Studies with the SDSS. I. The Vertical Distribution of Stars in the Milky Way*, apj, 553 (2001), pp. 184–197.

[29] M. CHIBA AND T. C. BEERS, *Kinematics of Metal-poor Stars in the Galaxy. III. Formation of the Stellar Halo and Thick Disk as Revealed from a Large Sample of Nonkinematically Selected Stars*, aj, 119 (2000), pp. 2843–2865.

[30] E. CHURCHWELL, B. L. BABLER, M. R. MEADE, B. A. WHITNEY, R. BENJAMIN, R. INDEBETOUW, C. CYGANOWSKI, T. P. ROBITAILLE, M. POVICH, C. WATSON, AND S. BRACKER, *The Spitzer/GLIMPSE Surveys: A New View of the Milky Way*, pasp, 121 (2009), p. 213.

[31] C. J. CONSELICE, *The Evolution of Galaxy Structure Over Cosmic Time*, araa, 52 (2014), pp. 291–337.

[32] M. DAVIS, G. EFSTATHIOU, C. S. FRENK, AND S. D. M. WHITE, *The evolution of large-scale structure in a universe dominated by cold dark matter*, apj, 292 (1985), pp. 371–394.

[33] T. J. L. DE BOER, V. BELOKUROV, S. E. KOPOSOV, L. FERRARESE, D. ERKAL, P. CÔTÉ, AND J. F. NAVARRO, *A deeper look at the GD1 stream: density variations and wiggles*, mnras, 477 (2018), pp. 1893–1902.

[34] J. H. J. DE BRUIJNE, *Science performance of Gaia, ESA's space-astrometry mission*, apss, 341 (2012), pp. 31–41.

[35] A. J. DEASON, V. BELOKUROV, N. W. EVANS, S. E. KOPOSOV, R. J. COOKE, J. PEÑARRUBIA, C. F. P. LAPORTE, M. FELLHAUER, M. G. WALKER, AND E. W. OLSZEWSKI, *The cold veil of the Milky Way stellar halo*, mnras, 425 (2012), pp. 2840–2853.

[36] V. P. DEBATTISTA, B. MOORE, T. QUINN, S. KAZANTZIDIS, R. MAAS, L. MAYER, J. READ, AND J. STADEL, *The Causes of Halo Shape Changes Induced by Cooling Baryons: Disks versus Substructures*, apj, 681 (2008), pp. 1076–1088.

[37] V. P. DEBATTISTA, R. ROSKAR, M. VALLURI, T. QUINN, B. MOORE, AND J. WADSLEY, *What's up in the Milky Way? The orientation of the disc relative to the triaxial halo*, mnras, 434 (2013), pp. 2971–2981.

[38] W. DEHNEN AND J. BINNEY, *Mass models of the Milky Way*, mnras, 294 (1998), p. 429.

[39] W. Dehnen, M. Odenkirchen, E. K. Grebel, and H.-W. Rix, *Modeling the Disruption of the Globular Cluster Palomar 5 by Galactic Tides*, aj, 127 (2004), pp. 2753–2770.

[40] A. Dekel, I. Arad, J. Devor, and Y. Birnboim, *Dark Halo Cusp: Asymptotic Convergence*, apj, 588 (2003), pp. 680–695.

[41] M.-H. Demoulin, *Observations of Galaxies with Large amounts of Dust. III. Velocity Field in NGC 3077*, apj, 157 (1969), p. 81.

[42] F. I. Diakogiannis, G. F. Lewis, R. A. Ibata, M. Guglielmo, P. R. Kafle, M. I. Wilkinson, and C. Power, *A novel JEAnS analysis of the Fornax dwarf using evolutionary algorithms: mass follows light with signs of an off-centre merger*, mnras, 470 (2017), pp. 2034–2053.

[43] J. Diemand, M. Kuhlen, P. Madau, M. Zemp, B. Moore, D. Potter, and J. Stadel, *Clumps and streams in the local dark matter distribution*, nat, 454 (2008), pp. 735–738.

[44] J. Dubinski, *The effect of dissipation on the shapes of dark halos*, apj, 431 (1994), pp. 617–624.

[45] J. Dubinski and R. G. Carlberg, *The structure of cold dark matter halos*, apj, 378 (1991), pp. 496–503.

[46] S. Duffau, R. Zinn, A. K. Vivas, G. Carraro, R. A. Méndez, R. Winnick, and C. Gallart, *Spectroscopy of QUEST RR Lyrae Variables: The New Virgo Stellar Stream*, apjl, 636 (2006), pp. L97–L100.

[47] O. J. Eggen, D. Lynden-Bell, and A. R. Sandage, *Evidence from the motions of old stars that the Galaxy collapsed.*, apj, 136 (1962), p. 748.

[48] J. Einasto, *On the Construction of a Composite Model for the Galaxy and on the Determination of the System of Galactic Parameters*, Trudy Astrofizicheskogo Instituta Alma-Ata, 5 (1965), pp. 87–100.

[49] D. Erkal, V. Belokurov, J. Bovy, and J. L. Sanders, *The number and size of subhalo-induced gaps in stellar streams*, mnras, 463 (2016), pp. 102–119.

[50] ——, *The number and size of subhalo-induced gaps in stellar streams*, mnras, 463 (2016), pp. 102–119.

[51] A. Eyre and J. Binney, *Locating the orbits delineated by tidal streams*, mnras, 400 (2009), pp. 548–560.

[52] ——, *The mechanics of tidal streams*, mnras, 413 (2011), pp. 1852–1874.

[53] M. A. Fardal, R. P. van der Marel, D. R. Law, S. T. Sohn, B. Sesar, N. Hernitschek, and H.-W. Rix, *Connecting the Milky Way potential profile to the orbital timescales and spatial structure of the Sagittarius Stream*, ArXiv e-prints, (2018).

[54] W. Forman and C. Jones, *X-ray-imaging observations of clusters of galaxies*, araa, 20 (1982), pp. 547–585.

[55] M. Fouesneau, H.-W. Rix, T. von Hippel, D. W. Hogg, and H. Tian, *Precise Ages of Field Stars from White Dwarf Companions*, ArXiv e-prints, (2018).

[56] K. Freeman and J. Bland-Hawthorn, *The New Galaxy: Signatures of Its Formation*, araa, 40 (2002), pp. 487–537.

[57] K. C. Freeman, *The HERMES Project: Reconstructing Galaxy Formation*, in Galactic Archaeology: Near-Field Cosmology and the Formation of the Milky Way, W. Aoki, M. Ishigaki, T. Suda, T. Tsujimoto, and N. Arimoto, eds., vol. 458 of Astronomical Society of the Pacific Conference Series, Aug. 2012, p. 393.

[58] C. S. Frenk, S. D. M. White, M. Davis, and G. Efstathiou, *The formation of dark halos in a universe dominated by cold dark matter*, apj, 327 (1988), pp. 507–525.

[59] T. K. Fritz, G. Battaglia, M. S. Pawlowski, N. Kallivayalil, R. van der Marel, T. S. Sohn, C. Brook, and G. Besla, *Gaia DR2 Proper Motions of Dwarf Galaxies within 420 kpc: Orbits, Milky Way Mass, Tidal Influences, Planar Alignments, and Group Infall*, ArXiv e-prints, (2018).

[60] Gaia Collaboration, C. Babusiaux, F. van Leeuwen, M. A. Barstow, C. Jordi, A. Vallenari, D. Bossini, A. Bressan, T. Cantat-Gaudin, M. van Leeuwen, and et al., *Gaia Data Release 2: Observational Hertzsprung-Russell diagrams*, ArXiv e-prints, (2018).

[61] Gaia Collaboration, A. G. A. Brown, A. Vallenari, T. Prusti, J. H. J. de Bruijne, F. Mignard, R. Drimmel, C. Babusiaux, C. A. L. Bailer-Jones, U. Bastian, and et al., *Gaia Data Release 1. Summary of the astrometric, photometric, and survey properties*, aap, 595 (2016), p. A2.

[62] Gaia Collaboration, Brown, A. G. A., Vallenari, A., Prusti, T., de Bruijne, J. H. J., and et al., *Gaia data release 2. summary of the contents and survey properties*, A&A, (2018).

[63] Gaia Collaboration, A. Helmi, F. van Leeuwen, P. J. McMillan, D. Massari, T. Antoja, A. Robin, L. Lindegren, U. Bastian, and . co-authors, *Gaia Data Release 2: Kinematics of globular clusters and dwarf galaxies around the Milky Way*, ArXiv e-prints, (2018).

[64] A. M. Ghez, S. Salim, N. N. Weinberg, J. R. Lu, T. Do, J. K. Dunn, K. Matthews, M. R. Morris, S. Yelda, E. E. Becklin, T. Kremenek, M. Milosavljevic, and J. Naiman, *Measuring Distance and Properties of the Milky Way's Central Supermassive Black Hole with Stellar Orbits*, apj, 689 (2008), pp. 1044–1062.

[65] S. Ghigna, B. Moore, F. Governato, G. Lake, T. Quinn, and J. Stadel, *Dark matter haloes within clusters*, mnras, 300 (1998), pp. 146–162.

[66] G. Gilmore, S. Randich, M. Asplund, J. Binney, P. Bonifacio, J. Drew, S. Feltzing, A. Ferguson, R. Jeffries, G. Micela, and et al., *The Gaia-ESO Public Spectroscopic Survey*, The Messenger, 147 (2012), pp. 25–31.

[67] O. Y. Gnedin, W. R. Brown, M. J. Geller, and S. J. Kenyon, *The Mass Profile of the Galaxy to 80 kpc*, apjl, 720 (2010), pp. L108–L112.

[68] J. R. Gott, III, E. L. Turner, and S. J. Aarseth, *N-body simulations of galaxy clustering. III - The covariance function*, apj, 234 (1979), pp. 13–26.

[69] C. J. Grillmair, *Substructure in Tidal Streams: Tributaries in the Anticenter Stream*, apjl, 651 (2006), pp. L29–L32.

[70] ——, *Four New Stellar Debris Streams in the Galactic Halo*, apj, 693 (2009), pp. 1118–1127.

[71] C. J. Grillmair, *Tidal Streams in the Local Group and Beyond*, vol. 420 of Astrophysics and Space Science Library, Springer International Publishing, Cham, 2016.

[72] C. J. Grillmair and O. Dionatos, *Detection of a 63° Cold Stellar Stream in the Sloan Digital Sky Survey*, apjl, 643 (2006), pp. L17–L20.

[73] C. J. Grillmair and R. Johnson, *The Detection of a 45° Tidal Stream Associated with the Globular Cluster NGC 5466*, apjl, 639 (2006), pp. L17–L20.

[74] M. Gustafsson, M. Fairbairn, and J. Sommer-Larsen, *Baryonic pinching of galactic dark matter halos*, prd, 74 (2006), p. 123522.

[75] A. H. Guth, *Inflationary universe: A possible solution to the horizon and flatness problems*, prd, 23 (1981), pp. 347–356.

[76] W. E. Harris, *Spatial structure of the globular cluster system and the distance to the galactic center*, aj, 81 (1976), pp. 1095–1116.

[77] ——, *A New Catalog of Globular Clusters in the Milky Way*, ArXiv e-prints, (2010).

[78] K. Hattori, M. Valluri, E. F. Bell, and I. U. Roederer, *Old, Metal-Poor Extreme Velocity Stars in the Solar Neighborhood*, ArXiv e-prints, (2018).

[79] A. HELMI, *Is the dark halo of our Galaxy spherical?*, mnras, 351 (2004), pp. 643–648.

[80] ——, *Velocity Trends in the Debris of Sagittarius and the Shape of the Dark Matter Halo of Our Galaxy*, apjl, 610 (2004), pp. L97–L100.

[81] ——, *The stellar halo of the Galaxy*, aapr, 15 (2008), pp. 145–188.

[82] A. HELMI, S. D. M. WHITE, P. T. DE ZEEUW, AND H. ZHAO, *Debris streams in the solar neighbourhood as relicts from the formation of the Milky Way*, nat, 402 (1999), pp. 53–55.

[83] HELMI, A., VAN LEEUWEN, F., MCMILLAN, P., AND DPAC, *Gaia data release 2. kinematics of globular clusters and dwarf galaxies around the milky way*, A&A, (2018).

[84] N. HERNITSCHEK, B. SESAR, H.-W. RIX, V. BELOKUROV, D. MARTINEZ-DELGADO, N. F. MARTIN, N. KAISER, K. HODAPP, K. C. CHAMBERS, R. WAINSCOAT, E. MAGNIER, R.-P. KUDRITZKI, N. METCALFE, AND P. W. DRAPER, *The Geometry of the Sagittarius Stream from Pan-STARRS1 3π RR Lyrae*, apj, 850 (2017), p. 96.

[85] R. IBATA, G. F. LEWIS, M. IRWIN, E. TOTTEN, AND T. QUINN, *Great Circle Tidal Streams: Evidence for a Nearly Spherical Massive Dark Halo around the Milky Way*, apj, 551 (2001), pp. 294–311.

[86] R. A. IBATA, G. GILMORE, AND M. J. IRWIN, *A dwarf satellite galaxy in Sagittarius*, nat, 370 (1994), pp. 194–196.

[87] R. A. IBATA, M. J. IRWIN, G. F. LEWIS, A. M. N. FERGUSON, AND N. TANVIR, *One ring to encompass them all: a giant stellar structure that surrounds the Galaxy*, mnras, 340 (2003), pp. L21–L27.

[88] R. A. IBATA, G. F. LEWIS, M. J. IRWIN, AND L. CAMBRÉSY, *Substructure of the outer Galactic halo from the 2-Micron All-Sky Survey*, mnras, 332 (2002), pp. 921–927.

[89] R. A. IBATA, G. F. LEWIS, M. J. IRWIN, AND T. QUINN, *Uncovering cold dark matter halo substructure with tidal streams*, Monthly Notices of the Royal Astronomical Society, 332 (2002), pp. 915–920.

[90] R. A. IBATA, G. F. LEWIS, AND N. F. MARTIN, *Feeling the Pull: a Study of Natural Galactic Accelerometers. I. Photometry of the Delicate Stellar Stream of the Palomar 5 Globular Cluster*, apj, 819 (2016), p. 1.

[91] R. A. IBATA, K. MALHAN, N. F. MARTIN, AND E. STARKENBURG, *Phlegethon, a nearby* 60°*-long retrograde stellar stream*, ArXiv e-prints, (2018).

[92] Z. IVEZIĆ, T. C. BEERS, AND M. JURIĆ, *Galactic Stellar Populations in the Era of the Sloan Digital Sky Survey and Other Large Surveys*, araa, 50 (2012), pp. 251–304.

[93] P. Jethwa, G. Torrealba, C. Navarrete, J. A. Carballo Bello, T. de Boer, D. Erkal, S. E. Koposov, S. Duffau, D. Geisler, M. Catelan, and V. Belokurov, *Discovery of a thin stellar stream in the SLAMS survey*, ArXiv e-prints, (2017).

[94] Y. P. Jing and Y. Suto, *Triaxial Modeling of Halo Density Profiles with High-Resolution N-Body Simulations*, apj, 574 (2002), pp. 538–553.

[95] K. V. Johnston, *The Role of Accretion in Forming the Galactic Halo*, in The Third Stromlo Symposium: The Galactic Halo, B. K. Gibson, R. S. Axelrod, and M. E. Putman, eds., vol. 165 of Astronomical Society of the Pacific Conference Series, 1999, p. 64.

[96] K. V. Johnston, L. Hernquist, and M. Bolte, *Fossil Signatures of Ancient Accretion Events in the Halo*, apj, 465 (1996), p. 278.

[97] K. V. Johnston, D. R. Law, and S. R. Majewski, *A Two Micron All Sky Survey View of the Sagittarius Dwarf Galaxy. III. Constraints on the Flattening of the Galactic Halo*, apj, 619 (2005), pp. 800–806.

[98] K. V. Johnston, D. N. Spergel, and C. Haydn, *How Lumpy Is the Milky Way's Dark Matter Halo?*, The Astrophysical Journal, 570 (2002), pp. 656–664.

[99] M. Jurić, Z. Ivezić, A. Brooks, R. H. Lupton, D. Schlegel, D. Finkbeiner, N. Padmanabhan, N. Bond, B. Sesar, C. M. Rockosi, G. R. Knapp, J. E. Gunn, T. Sumi, D. P. Schneider, J. C. Barentine, H. J. Brewington, J. Brinkmann, M. Fukugita, M. Harvanek, S. J. Kleinman, J. Krzesinski, D. Long, E. H. Neilsen, Jr., A. Nitta, S. A. Snedden, and D. G. York, *The Milky Way Tomography with SDSS. I. Stellar Number Density Distribution*, apj, 673 (2008), pp. 864–914.

[100] N. Kaiser, W. Burgett, K. Chambers, L. Denneau, J. Heasley, R. Jedicke, E. Magnier, J. Morgan, P. Onaka, and J. Tonry, *The Pan-STARRS wide-field optical/NIR imaging survey*, in Ground-based and Airborne Telescopes III, vol. 7733 of procspie, July 2010, p. 77330E.

[101] N. Kallivayalil, R. P. van der Marel, G. Besla, J. Anderson, and C. Alcock, *Third-epoch Magellanic Cloud Proper Motions. I. Hubble Space Telescope/WFC3 Data and Orbit Implications*, apj, 764 (2013), p. 161.

[102] M. Kamionkowski and A. R. Liddle, *The Dearth of Halo Dwarf Galaxies: Is There Power on Short Scales?*, Physical Review Letters, 84 (2000), pp. 4525–4528.

[103] S. Kazantzidis, M. G. Abadi, and J. F. Navarro, *The Sphericalization of Dark Matter Halos by Galaxy Disks*, apjl, 720 (2010), pp. L62–L66.

[104] A. Klypin, A. V. Kravtsov, O. Valenzuela, and F. Prada, *Where Are the Missing Galactic Satellites?*, apj, 522 (1999), pp. 82–92.

[105] S. E. Koposov, M. Irwin, V. Belokurov, E. Gonzalez-Solares, A. K. Yoldas, J. Lewis, N. Metcalfe, and T. Shanks, *Discovery of a cold stellar stream in the ATLAS DR1 data*, mnras, 442 (2014), pp. L85–L89.

[106] S. E. Koposov, H.-W. Rix, and D. W. Hogg, *Constraining the Milky Way Potential with a Six-Dimensional Phase-Space Map of the GD-1 Stellar Stream*, apj, 712 (2010), pp. 260–273.

[107] A. H. W. Küpper, E. Balbinot, A. Bonaca, K. V. Johnston, D. W. Hogg, P. Kroupa, and B. X. Santiago, *Globular Cluster Streams as Galactic High-Precision Scalesm-dashthe Poster Child Palomar 5*, apj, 803 (2015), p. 80.

[108] A. H. W. Küpper, R. R. Lane, and D. C. Heggie, *More on the structure of tidal tails*, mnras, 420 (2012), pp. 2700–2714.

[109] A. Lancon, *Integrated Properties of AGB Stars in Resolved and Unresolved Stellar Populations: Simple Stellar Populations and Star Clusters*, in Why Galaxies Care about AGB Stars II: Shining Examples and Common Inhabitants, F. Kerschbaum, T. Lebzelter, and R. F. Wing, eds., vol. 445 of Astronomical Society of the Pacific Conference Series, Sept. 2011, p. 379.

[110] D. R. Law, K. V. Johnston, and S. R. Majewski, *A Two Micron All-Sky Survey View of the Sagittarius Dwarf Galaxy. IV. Modeling the Sagittarius Tidal Tails*, apj, 619 (2005), pp. 807–823.

[111] D. R. Law and S. R. Majewski, *The Sagittarius Dwarf Galaxy: A Model for Evolution in a Triaxial Milky Way Halo*, apj, 714 (2010), pp. 229–254.

[112] A. C. Layden, R. B. Hanson, S. L. Hawley, A. R. Klemola, and C. J. Hanley, *The Absolute Magnitude and Kinematics of RR Lyrae Stars Via Statistical Parallax*, aj, 112 (1996), p. 2110.

[113] M. Lisanti, *Lectures on Dark Matter Physics*, in New Frontiers in Fields and Strings (TASI 2015) - Proceedings of the 2015 Theoretical Advanced Study Institute in Elementary Particle Physics. Edited by POLCHINSKI JOSEPH ET AL. Published by World Scientific Publishing Co. Pte. Ltd., 2017. ISBN #9789813149441, pp. 399-446, J. Polchinski and et al., eds., 2017, pp. 399–446.

[114] S. R. Loebman, Z. Ivezic, T. R. Quinn, J. Bovy, C. R. Christensen, M. Jurić, R. Roskar, A. M. Brooks, and F. Governato, *The Milky Way Tomography with Sloan Digital Sky Survey. V. Mapping the Dark Matter Halo*, apj, 794 (2014), p. 151.

[115] H. Lux, J. I. Read, G. Lake, and K. V. Johnston, *Constraining the Milky Way halo shape using thin streams*, mnras, 436 (2013), pp. 2386–2397.

[116] D. Lynden-Bell and R. M. Lynden-Bell, *Ghostly streams from the formation of the Galaxy's halo*, mnras, 275 (1995), pp. 429–442.

[117] E. A. Magnier, E. F. Schlafly, D. P. Finkbeiner, J. L. Tonry, B. Goldman, S. Röser, E. Schilbach, K. C. Chambers, H. A. Flewelling, M. E. Huber, P. A. Price, W. E. Sweeney, C. Z. Waters, L. Denneau, P. Draper, K. W. Hodapp, R. Jedicke, R.-P. Kudritzki, N. Metcalfe, C. W. Stubbs, and R. J. Wainscoast, *Pan-STARRS Photometric and Astrometric Calibration*, ArXiv e-prints, (2016).

[118] K. Malhan and R. A. Ibata, *Measuring the Sun's motion with stellar streams*, mnras, 471 (2017), pp. 1005–1011.

[119] ——, *Constraining the Milky Way Halo Potential with the GD-1 stellar stream*, ArXiv e-prints, (2018).

[120] ——, *STREAMFINDER - I. A new algorithm for detecting stellar streams*, mnras, 477 (2018), pp. 4063–4076.

[121] K. Malhan, R. A. Ibata, B. Goldman, N. F. Martin, E. Magnier, and K. Chambers, *STREAMFINDER II: A possible fanning structure parallel to the GD-1 stream in Pan-STARRS1*, mnras, (2018).

[122] K. Malhan, R. A. Ibata, and N. F. Martin, *Ghostly Tributaries to the Milky Way: Charting the Halo's Stellar Streams with the Gaia DR2 catalogue*, ArXiv e-prints, (2018).

[123] P. Marigo, L. Girardi, A. Bressan, M. A. T. Groenewegen, L. Silva, and G. L. Granato, *Evolution of asymptotic giant branch stars. II. Optical to far-infrared isochrones with improved TP-AGB models*, aap, 482 (2008), pp. 883–905.

[124] N. F. Martin, R. A. Ibata, R. M. Rich, M. L. M. Collins, M. A. Fardal, M. J. Irwin, G. F. Lewis, A. W. McConnachie, A. Babul, N. F. Bate, S. C. Chapman, A. R. Conn, D. Crnojević, A. M. N. Ferguson, A. D. Mackey, J. F. Navarro, J. Peñarrubia, N. T. Tanvir, and D. Valls-Gabaud, *The PAndAS Field of Streams: Stellar Structures in the Milky Way Halo toward Andromeda and Triangulum*, apj, 787 (2014), p. 19.

[125] C. Mateu, J. I. Read, and D. Kawata, *Fourteen candidate RR Lyrae star streams in the inner Galaxy*, ArXiv e-prints, (2017).

[126] A. W. McConnachie, *The Observed Properties of Dwarf Galaxies in and around the Local Group*, aj, 144 (2012), p. 4.

[127] P. J. McMillan, *Mass models of the Milky Way*, mnras, 414 (2011), pp. 2446–2457.

[128] P. J. McMillan and J. J. Binney, *The uncertainty in Galactic parameters*, mnras, 402 (2010), pp. 934–940.

[129] M. Miyamoto and R. Nagai, *Three-dimensional models for the distribution of mass in galaxies*, pasj, 27 (1975), pp. 533–543.

[130] G. Monari, B. Famaey, I. Carrillo, T. Piffl, M. Steinmetz, R. F. G. Wyse, F. Anders, C. Chiappini, and K. Janssen, *The escape speed curve of the Galaxy obtained from Gaia DR2 implies a heavy Milky Way*, ArXiv e-prints, (2018).

[131] B. Moore, S. Ghigna, F. Governato, G. Lake, T. Quinn, J. Stadel, and P. Tozzi, *Dark Matter Substructure within Galactic Halos*, apjl, 524 (1999), pp. L19–L22.

[132] ——, *Dark Matter Substructure within Galactic Halos*, apjl, 524 (1999), pp. L19–L22.

[133] H. L. Morrison, *The local density of halo giants*, aj, 106 (1993), pp. 578–590.

[134] H. L. Morrison, A. Helmi, J. Sun, P. Liu, R. Gu, J. E. Norris, P. Harding, T. D. Kinman, A. A. Kepley, K. C. Freeman, M. Williams, and J. Van Duyne, *Fashionably Late? Building Up The Milky Way'S Inner Halo*, apj, 694 (2009), pp. 130–143.

[135] G. C. Myeong, H. Jerjen, D. Mackey, and G. S. Da Costa, *Tidal Tails around the Outer Halo Globular Clusters Eridanus and Palomar 15*, apjl, 840 (2017), p. L25.

[136] ——, *Tidal tails around the outer halo globular clusters Eridanus and Palomar 15*, ArXiv e-prints, (2017).

[137] J. F. Navarro, C. S. Frenk, and S. D. M. White, *The Structure of Cold Dark Matter Halos*, apj, 462 (1996), p. 563.

[138] ——, *A Universal Density Profile from Hierarchical Clustering*, apj, 490 (1997), pp. 493–508.

[139] ——, *A Universal Density Profile from Hierarchical Clustering*, apj, 490 (1997), pp. 493–508.

[140] H. J. Newberg, B. A. Willett, B. Yanny, and Y. Xu, *The Orbit of the Orphan Stream*, apj, 711 (2010), pp. 32–49.

[141] H. J. Newberg and B. Yanny, *The Milky Way's stellar halo - lumpy or triaxial?*, in Journal of Physics Conference Series, vol. 47 of Journal of Physics Conference Series, Oct. 2006, pp. 195–204.

[142] H. J. Newberg, B. Yanny, C. Rockosi, E. K. Grebel, H.-W. Rix, J. Brinkmann, I. Csabai, G. Hennessy, R. B. Hindsley, R. Ibata, Z. Ivezić, D. Lamb, E. T. Nash, M. Odenkirchen, H. A. Rave, D. P. Schneider, J. A. Smith, A. Stolte, and D. G. York, *The Ghost of Sagittarius and Lumps in the Halo of the Milky Way*, apj, 569 (2002), pp. 245–274.

[143] M. Odenkirchen, E. K. Grebel, C. M. Rockosi, W. Dehnen, R. Ibata, H.-W. Rix, A. Stolte, C. Wolf, J. E. Anderson, Jr., N. A. Bahcall, J. Brinkmann, I. Csabai, G. Hennessy, R. B. Hindsley, Z. Ivezic, R. H. Lupton, J. A. Munn, J. R. Pier, C. Stoughton, and D. G. York, *Detection of Massive Tidal Tails around the Globular Cluster Palomar 5 with Sloan Digital Sky Survey Commissioning Data*, apjl, 548 (2001), pp. L165–L169.

[144] J. H. Oort, *Note on the determination of K_z and on the mass density near the Sun.*, bain, 15 (1960), p. 45.

[145] S. Pearson, A. H. W. Küpper, K. V. Johnston, and A. M. Price-Whelan, *Tidal Stream Morphology as an Indicator of Dark Matter Halo Geometry: The Case of Palomar 5*, apj, 799 (2015), p. 28.

[146] P. J. E. Peebles, *The large-scale structure of the universe*, 1980.

[147] Planck Collaboration, P. A. R. Ade, N. Aghanim, M. Arnaud, M. Ashdown, J. Aumont, C. Baccigalupi, A. J. Banday, R. B. Barreiro, J. G. Bartlett, and et al., *Planck 2015 results. XIII. Cosmological parameters*, aap, 594 (2016), p. A13.

[148] L. Posti and A. Helmi, *Mass and shape of the Milky Way's dark matter halo with globular clusters from Gaia and Hubble*, ArXiv e-prints, (2018).

[149] A. M. Price-Whelan and A. Bonaca, *Off the beaten path: Gaia reveals GD-1 stars outside of the main stream*, ArXiv e-prints, (2018).

[150] J. I. Read and P. Steger, *How to break the density-anisotropy degeneracy in spherical stellar systems*, mnras, 471 (2017), pp. 4541–4558.

[151] M. J. Reid and A. Brunthaler, *The Proper Motion of Sagittarius A*. II. The Mass of Sagittarius A**, apj, 616 (2004), pp. 872–884.

[152] M. J. Reid, K. M. Menten, A. Brunthaler, X. W. Zheng, T. M. Dame, Y. Xu, Y. Wu, B. Zhang, and et al., *Trigonometric Parallaxes of High Mass Star Forming Regions: The Structure and Kinematics of the Milky Way*, ApJ, 783 (2014), p. 130.

[153] M. J. Reid, K. M. Menten, X. W. Zheng, A. Brunthaler, L. Moscadelli, Y. Xu, B. Zhang, M. Sato, M. Honma, T. Hirota, K. Hachisuka, Y. K. Choi, G. A. Moellenbrock, and A. Bartkiewicz, *Trigonometric Parallaxes of Massive Star-Forming Regions. VI. Galactic Structure, Fundamental Parameters, and Noncircular Motions*, apj, 700 (2009), pp. 137–148.

[154] M. S. Roberts and R. N. Whitehurst, *The rotation curve and geometry of M31 at large galactocentric distances.*, apj, 201 (1975), pp. 327–346.

[155] A. C. Robin, X. Luri, C. Reylé, Y. Isasi, E. Grux, S. Blanco-Cuaresma, F. Arenou, C. Babusiaux, M. Belcheva, R. Drimmel, C. Jordi, A. Krone-Martins, E. Masana, J. C. Mauduit, F. Mignard, N. Mowlavi, B. Rocca-Volmerange, P. Sartoretti, E. Slezak, and A. Sozzetti, *Gaia Universe model snapshot. A statistical analysis of the expected contents of the Gaia catalogue*, aap, 543 (2012), p. A100.

[156] C. M. Rockosi, M. Odenkirchen, E. K. Grebel, W. Dehnen, K. M. Cudworth, J. E. Gunn, D. G. York, J. Brinkmann, G. S. Hennessy, and Z. Ivezic, *A Matched-Filter Analysis of the Tidal Tails of the Globular Cluster Palomar 5*, aj, 124 (2002), pp. 349–363.

[157] H. J. Rood and J. R. Dickel, *Analytical examination of virial properties of groups of galaxies*, apj, 233 (1979), pp. 418–430.

[158] P. Rosati, S. Borgani, and C. Norman, *The Evolution of X-ray Clusters of Galaxies*, araa, 40 (2002), pp. 539–577.

[159] V. C. Rubin and W. K. Ford, Jr., *Rotation of the Andromeda Nebula from a Spectroscopic Survey of Emission Regions*, apj, 159 (1970), p. 379.

[160] ——, *Rotation of the Andromeda Nebula from a Spectroscopic Survey of Emission Regions*, apj, 159 (1970), p. 379.

[161] V. C. Rubin, W. K. Ford, Jr., and N. Thonnard, *Rotational properties of 21 SC galaxies with a large range of luminosities and radii, from NGC 4605 /R = 4kpc/ to UGC 2885 /R = 122 kpc/*, apj, 238 (1980), pp. 471–487.

[162] V. C. Rubin, N. Thonnard, and W. K. Ford, Jr., *Extended rotation curves of high-luminosity spiral galaxies. IV - Systematic dynamical properties, SA through SC*, apjl, 225 (1978), pp. L107–L111.

[163] S. G. Ryan, J. E. Norris, and T. C. Beers, *Extremely Metal-poor Stars. II. Elemental Abundances and the Early Chemical Enrichment of the Galaxy*, apj, 471 (1996), p. 254.

[164] P. D. SACKETT, *The Shape of Dark Matter Halos*, in Galaxy Dynamics - A Rutgers Symposium, D. R. Merritt, M. Valluri, and J. A. Sellwood, eds., vol. 182 of Astronomical Society of the Pacific Conference Series, Aug. 1999.

[165] J. B. SALOMON, R. A. IBATA, B. FAMAEY, N. F. MARTIN, AND G. F. LEWIS, *The transverse velocity of the Andromeda system, derived from the M31 satellite population*, Monthly Notices of the Royal Astronomical Society, 456 (2016), pp. 4432–4440.

[166] C. SANDERSON AND R. CURTIN, *gmmdiag and gmmfull: C++ classes for multi-threaded gaussian mixture models and expectation-maximisation*, Journal of Open Source Software, 2 (2017).

[167] C. L. SARAZIN, *X-ray emission from clusters of galaxies*, 1988.

[168] R. SCHÖNRICH AND J. BINNEY, *Chemical evolution with radial mixing*, mnras, 396 (2009), pp. 203–222.

[169] L. SEARLE AND R. ZINN, *Compositions of halo clusters and the formation of the galactic halo*, apj, 225 (1978), pp. 357–379.

[170] C. K. SEYFERT, *A Dense Group of Galaxies in Serpens*, pasp, 63 (1951), p. 72.

[171] N. SHIPP, A. DRLICA-WAGNER, E. BALBINOT, P. FERGUSON, D. ERKAL, T. S. LI, K. BECHTOL, V. BELOKUROV, B. BUNCHER, D. CAROLLO, M. CARRASCO KIND, K. KUEHN, J. L. MARSHALL, A. B. PACE, E. S. RYKOFF, I. SEVILLA-NOARBE, E. SHELDON, L. STRIGARI, A. K. VIVAS, B. YANNY, A. ZENTENO, T. M. C. ABBOTT, F. B. ABDALLA, S. ALLAM, S. AVILA, E. BERTIN, D. BROOKS, D. L. BURKE, J. CARRETERO, F. J. CASTANDER, R. CAWTHON, M. CROCCE, C. E. CUNHA, C. B. D'ANDREA, L. N. DA COSTA, C. DAVIS, J. DE VICENTE, S. DESAI, H. T. DIEHL, P. DOEL, A. E. EVRARD, B. FLAUGHER, P. FOSALBA, J. FRIEMAN, J. GARCÍA-BELLIDO, E. GAZTANAGA, D. W. GERDES, D. GRUEN, R. A. GRUENDL, J. GSCHWEND, G. GUTIERREZ, B. HOYLE, D. J. JAMES, M. D. JOHNSON, E. KRAUSE, N. KUROPATKIN, O. LAHAV, H. LIN, M. A. G. MAIA, M. MARCH, P. MARTINI, F. MENANTEAU, C. J. MILLER, R. MIQUEL, R. C. NICHOL, A. A. PLAZAS, A. K. ROMER, M. SAKO, E. SANCHEZ, V. SCARPINE, R. SCHINDLER, M. SCHUBNELL, M. SMITH, R. C. SMITH, F. SOBREIRA, E. SUCHYTA, M. E. C. SWANSON, G. TARLE, D. THOMAS, D. L. TUCKER, A. R. WALKER, R. H. WECHSLER, AND THE DES COLLABORATION, *Stellar Streams Discovered in the Dark Energy Survey*, ArXiv e-prints, (2018).

[172] ——, *Stellar Streams Discovered in the Dark Energy Survey*, ArXiv e-prints, (2018).

[173] M. C. SMITH, G. R. RUCHTI, A. HELMI, R. F. G. WYSE, J. P. FULBRIGHT, K. C. FREEMAN, J. F. NAVARRO, G. M. SEABROKE, M. STEINMETZ, M. WILLIAMS, O. BIENAYMÉ,

J. BINNEY, J. BLAND-HAWTHORN, W. DEHNEN, B. K. GIBSON, G. GILMORE, E. K. GREBEL, U. MUNARI, Q. A. PARKER, R.-D. SCHOLZ, A. SIEBERT, F. G. WATSON, AND T. ZWITTER, *The RAVE survey: constraining the local Galactic escape speed*, mnras, 379 (2007), pp. 755–772.

[174] ——, *The RAVE survey: constraining the local Galactic escape speed*, mnras, 379 (2007), pp. 755–772.

[175] Y. SOFUE, *Grand Rotation Curve and Dark Matter Halo in the Milky Way Galaxy*, pasj, 64 (2012), p. 75.

[176] D. N. SPERGEL AND P. J. STEINHARDT, *Observational Evidence for Self-Interacting Cold Dark Matter*, Physical Review Letters, 84 (2000), pp. 3760–3763.

[177] V. SPRINGEL, J. WANG, M. VOGELSBERGER, A. LUDLOW, A. JENKINS, A. HELMI, J. F. NAVARRO, C. S. FRENK, AND S. D. M. WHITE, *The Aquarius Project: the subhaloes of galactic haloes*, mnras, 391 (2008), pp. 1685–1711.

[178] D. SYER AND S. D. M. WHITE, *Dark halo mergers and the formation of a universal profile*, mnras, 293 (1998), p. 337.

[179] P. TAYLOR AND C. KOBAYASHI, *The effects of AGN feedback on present-day galaxy properties in cosmological simulations*, mnras, 448 (2015), pp. 1835–1846.

[180] THE DARK ENERGY SURVEY COLLABORATION, *The Dark Energy Survey*, ArXiv Astrophysics e-prints, (2005).

[181] G. F. THOMAS, R. IBATA, B. FAMAEY, N. F. MARTIN, AND G. F. LEWIS, *Exploring the reality of density substructures in the Palomar 5 stellar stream*, mnras, 460 (2016), pp. 2711–2719.

[182] J. L. TONRY, C. W. STUBBS, K. R. LYKKE, P. DOHERTY, I. S. SHIVVERS, W. S. BURGETT, K. C. CHAMBERS, K. W. HODAPP, N. KAISER, R.-P. KUDRITZKI, E. A. MAGNIER, J. S. MORGAN, P. A. PRICE, AND R. J. WAINSCOAT, *The Pan-STARRS1 Photometric System*, apj, 750 (2012), p. 99.

[183] E. L. TURNER, S. J. AARSETH, N. T. BLANCHARD, R. D. MATHIEU, AND J. R. GOTT, III, *N-body simulations of galaxy clustering. II - Groups of galaxies*, apj, 228 (1979), pp. 684–695.

[184] R. P. VAN DER MAREL, G. BESLA, T. J. COX, S. T. SOHN, AND J. ANDERSON, *The M31 Velocity Vector. III. Future Milky Way M31-M33 Orbital Evolution, Merging, and Fate of the Sun*, apj, 753 (2012), p. 9.

[185] A. Varghese, R. Ibata, and G. F. Lewis, *Stellar streams as probes of dark halo mass and morphology: a Bayesian reconstruction*, mnras, 417 (2011), pp. 198–215.

[186] A. K. Vivas, R. Zinn, C. Abad, P. Andrews, C. Bailyn, C. Baltay, A. Bongiovanni, C. Briceño, G. Bruzual, P. Coppi, F. Della Prugna, N. Ellman, I. Ferrín, M. Gebhard, T. Girard, J. Hernandez, D. Herrera, R. Honeycutt, G. Magris, S. Mufson, J. Musser, O. Naranjo, D. Rabinowitz, A. Rengstorf, P. Rosenzweig, G. Sánchez, G. Sánchez, B. Schaefer, H. Schenner, J. A. Snyder, S. Sofia, J. Stock, W. van Altena, B. Vicente, and K. Vieira, *The QUEST RR Lyrae Survey. I. The First Catalog*, aj, 127 (2004), pp. 1158–1175.

[187] M. G. Walker and J. Peñarrubia, *A Method for Measuring (Slopes of) the Mass Profiles of Dwarf Spheroidal Galaxies*, apj, 742 (2011), p. 20.

[188] M. S. Warren, P. J. Quinn, J. K. Salmon, and W. H. Zurek, *Dark halos formed via dissipationless collapse. I - Shapes and alignment of angular momentum*, apj, 399 (1992), pp. 405–425.

[189] L. L. Watkins, N. W. Evans, and J. H. An, *The masses of the Milky Way and Andromeda galaxies*, mnras, 406 (2010), pp. 264–278.

[190] L. L. Watkins, N. W. Evans, V. Belokurov, M. C. Smith, P. C. Hewett, D. M. Bramich, G. F. Gilmore, M. J. Irwin, S. Vidrih, Ł. Wyrzykowski, and D. B. Zucker, *Substructure revealed by RRLyraes in SDSS Stripe 82*, mnras, 398 (2009), pp. 1757–1770.

[191] L. L. Watkins, R. P. van der Marel, S. T. Sohn, and N. W. Evans, *Evidence for an Intermediate-Mass Milky Way from Gaia DR2 Halo Globular Cluster Motions*, ArXiv e-prints, (2018).

[192] ——, *Evidence for an Intermediate-Mass Milky Way from Gaia DR2 Halo Globular Cluster Motions*, ArXiv e-prints, (2018).

[193] R. H. Wechsler and J. L. Tinker, *The Connection between Galaxies and their Dark Matter Halos*, ArXiv e-prints, (2018).

[194] S. D. M. White, *The dynamics of rich clusters of galaxies*, mnras, 177 (1976), pp. 717–733.

[195] S. D. M. White and M. J. Rees, *Core condensation in heavy halos - A two-stage theory for galaxy formation and clustering*, mnras, 183 (1978), pp. 341–358.

[196] M. E. K. Williams, M. Steinmetz, S. Sharma, J. Bland-Hawthorn, R. S. de Jong, G. M. Seabroke, A. Helmi, K. C. Freeman, J. Binney, I. Minchev, O. Bienaymé, R. Campbell, J. P. Fulbright, B. K. Gibson, G. F. Gilmore, E. K. Grebel,

U. Munari, J. F. Navarro, Q. A. Parker, W. Reid, A. Siebert, A. Siviero, F. G. Watson, R. F. G. Wyse, and T. Zwitter, *The Dawning of the Stream of Aquarius in RAVE*, apj, 728 (2011), p. 102.

[197] ——, *The Dawning of the Stream of Aquarius in RAVE*, apj, 728 (2011), p. 102.

[198] Y. Xu, L. C. Deng, and J. Y. Hu, *The structure of the Galactic halo: SDSS versus SuperCOSMOS*, mnras, 379 (2007), pp. 1373–1389.

[199] B. Yanny, H. J. Newberg, S. Kent, S. A. Laurent-Muehleisen, J. R. Pier, G. T. Richards, C. Stoughton, J. E. Anderson, Jr., J. Annis, J. Brinkmann, B. Chen, I. Csabai, M. Doi, M. Fukugita, G. S. Hennessy, Z. Ivezić, G. R. Knapp, R. Lupton, J. A. Munn, T. Nash, C. M. Rockosi, D. P. Schneider, J. A. Smith, and D. G. York, *Identification of A-colored Stars and Structure in the Halo of the Milky Way from Sloan Digital Sky Survey Commissioning Data*, apj, 540 (2000), pp. 825–841.

[200] B. Yanny, C. Rockosi, H. J. Newberg, G. R. Knapp, J. K. Adelman-McCarthy, B. Alcorn, S. Allam, C. Allende Prieto, D. An, K. S. J. Anderson, S. Anderson, C. A. L. Bailer-Jones, S. Bastian, T. C. Beers, E. Bell, V. Belokurov, D. Bizyaev, N. Blythe, J. J. Bochanski, W. N. Boroski, J. Brinchmann, J. Brinkmann, H. Brewington, L. Carey, K. M. Cudworth, M. Evans, N. W. Evans, E. Gates, B. T. Gänsicke, B. Gillespie, G. Gilmore, A. Nebot Gomez-Moran, E. K. Grebel, J. Greenwell, J. E. Gunn, C. Jordan, W. Jordan, P. Harding, H. Harris, J. S. Hendry, D. Holder, I. I. Ivans, Z. Ivezic, S. Jester, J. A. Johnson, S. M. Kent, S. Kleinman, A. Kniazev, J. Krzesinski, R. Kron, N. Kuropatkin, S. Lebedeva, Y. S. Lee, R. French Leger, S. Lépine, S. Levine, H. Lin, D. C. Long, C. Loomis, R. Lupton, O. Malanushenko, V. Malanushenko, B. Margon, D. Martinez-Delgado, P. McGehee, D. Monet, H. L. Morrison, J. A. Munn, E. H. Neilsen, Jr., A. Nitta, J. E. Norris, D. Oravetz, R. Owen, N. Padmanabhan, K. Pan, R. S. Peterson, J. R. Pier, J. Platson, P. Re Fiorentin, G. T. Richards, H.-W. Rix, D. J. Schlegel, D. P. Schneider, M. R. Schreiber, A. Schwope, V. Sibley, A. Simmons, S. A. Snedden, J. Allyn Smith, L. Stark, F. Stauffer, M. Steinmetz, C. Stoughton, M. SubbaRao, A. Szalay, P. Szkody, A. R. Thakar, T. Sivarani, D. Tucker, A. Uomoto, D. Vanden Berk, S. Vidrih, Y. Wadadekar, S. Watters, R. Wilhelm, R. F. G. Wyse, J. Yarger, and D. Zucker, *SEGUE: A Spectroscopic Survey of 240,000 Stars with g = 14-20*, aj, 137 (2009), pp. 4377–4399.

[201] D. G. York, J. Adelman, J. E. Anderson, Jr., S. F. Anderson, J. Annis, N. A. Bahcall, J. A. Bakken, R. Barkhouser, S. Bastian, E. Berman, W. N. Boroski, S. Bracker, C. Briegel, J. W. Briggs, J. Brinkmann, R. Brunner, S. Burles,

L. Carey, M. A. Carr, F. J. Castander, B. Chen, P. L. Colestock, A. J. Connolly, J. H. Crocker, I. Csabai, P. C. Czarapata, J. E. Davis, M. Doi, T. Dombeck, D. Eisenstein, N. Ellman, B. R. Elms, M. L. Evans, X. Fan, G. R. Federwitz, L. Fiscelli, S. Friedman, J. A. Frieman, M. Fukugita, B. Gillespie, J. E. Gunn, V. K. Gurbani, E. de Haas, M. Haldeman, F. H. Harris, J. Hayes, T. M. Heckman, G. S. Hennessy, R. B. Hindsley, S. Holm, D. J. Holmgren, C.-h. Huang, C. Hull, D. Husby, S.-I. Ichikawa, T. Ichikawa, Z. Ivezic, S. Kent, R. S. J. Kim, E. Kinney, M. Klaene, A. N. Kleinman, S. Kleinman, G. R. Knapp, J. Korienek, R. G. Kron, P. Z. Kunszt, D. Q. Lamb, B. Lee, R. F. Leger, S. Limmongkol, C. Lindenmeyer, D. C. Long, C. Loomis, J. Loveday, R. Lucinio, R. H. Lupton, B. MacKinnon, E. J. Mannery, P. M. Mantsch, B. Margon, P. McGehee, T. A. McKay, A. Meiksin, A. Merelli, D. G. Monet, J. A. Munn, V. K. Narayanan, T. Nash, E. Neilsen, R. Neswold, H. J. Newberg, R. C. Nichol, T. Nicinski, M. Nonino, N. Okada, S. Okamura, J. P. Ostriker, R. Owen, A. G. Pauls, J. Peoples, R. L. Peterson, D. Petravick, J. R. Pier, A. Pope, R. Pordes, A. Prosapio, R. Rechenmacher, T. R. Quinn, G. T. Richards, M. W. Richmond, C. H. Rivetta, C. M. Rockosi, K. Ruthmansdorfer, D. Sandford, D. J. Schlegel, D. P. Schneider, M. Sekiguchi, G. Sergey, K. Shimasaku, W. A. Siegmund, S. Smee, J. A. Smith, S. Snedden, R. Stone, C. Stoughton, M. A. Strauss, C. Stubbs, M. SubbaRao, A. S. Szalay, I. Szapudi, G. P. Szokoly, A. R. Thakar, C. Tremonti, D. L. Tucker, A. Uomoto, D. Vanden Berk, M. S. Vogeley, P. Waddell, S.-i. Wang, M. Watanabe, D. H. Weinberg, B. Yanny, N. Yasuda, and SDSS Collaboration, *The Sloan Digital Sky Survey: Technical Summary*, aj, 120 (2000), pp. 1579–1587.

UNIVERSITÉ DE STRASBOURG

Khyati MALHAN

Observatoire astronomique de Strasbourg

Stellar Streams en tant que sondes de la matière noire: Recherche et analyse dynamique

Résumé

Les flux stellaires comme sondes de la matière noire: recherche et analyse dynamique

Les courants stellaires de marée sont des structures en étoile immaculées qui jouent un rôle central dans la résolution des mystères de longue date de l'archéologie galactique. Étant donné que les flux sont de nature orbitale, ils possèdent intrinsèquement les caractéristiques de résolution de la distribution de masse sous-jacente de la galaxie et peuvent être utilisés pour sonder la forme du halo de matière noire. En plus de tester le scénario de «fusion hiérarchique» de la formation de galaxies, les brèches de ruisseau peuvent également fournir une preuve indirecte de l'existence de sous-halos de matière noire (ce qui, en principe, limite la nature de la particule de matière noire elle-même). Pour toutes ces raisons, l'analyse dynamique des flux stellaires de la Voie Lactée devient naturellement l'un des problèmes les plus intéressants. Cependant, le principal défi consiste à détecter ces structures.

Au cours de la thèse, l'algorithme STREAMFINDER (un algorithme à la pointe de la technologie) a été conçu pour traiter systématiquement le jeu de données Gaia (le nouveau catalogue astrophysique de l'ESA contenant des solutions astrométriques sans précédent de plus de 1,6 milliard d'étoiles) pour la détection des flux stellaires de la Voie lactée. Cette lourde entreprise a permis de détecter 10 structures de flux de confiance, dont 5 étaient considérées comme de nouvelles découvertes. Cette récolte de structures a également facilité, pour la première fois, la création d'une carte structurale et cinématique panoramique des flux stellaires de la rivière Milky. Halo, poussant notre communauté encore plus loin dans l'histoire complexe de la formation de notre galaxie. Ce projet a été immédiatement suivi de l'analyse orbitale de l'un des flux détectés (à savoir GD-1) pour explorer les améliorations des modèles de potentiel gravitationnel de notre galaxie. Les contraintes imposées à la masse de la Voie lactée et à la forme de son halo de matière noire, obtenues simplement en utilisant ce seul flux, ont révélé la puissance potentielle que l'analyse d'un ensemble de flux permettrait de sonder la distribution globale de la masse galactique de notre galaxie.

Ainsi, la thèse a ouvert la voie à de nouvelles découvertes des sous-structures stellaires, soulignant également les perspectives d'avenir dans ce domaine.

Mots clés Structure de la galaxie; étoiles ; ruisseaux stellaires; matière noire.

Résumé en anglais

Title : Stellar Streams as probes of dark matter: Search and dynamical analysis

Tidal stellar streams are pristine star structures that play central role in addressing long standing mysteries of the Galactic archaeology. Since streams are orbital in nature, they inherently possess the characteristics of unravelling the underlying mass distribution of the galaxy, and can be used to probe the shape of the dark matter halo. Besides testing the 'hierarchical merging' scenario of galaxy formation, stream gaps can also provide indirect evidence for the existence of dark matter sub-halos (thereby, in principle, constraining the nature of the dark matter particle itself). Due to all these reasons, the dynamical analysis of stellar streams of the Milky Way Galaxy naturally becomes one of the interesting problems. However, the foremost challenge is to detect these structures.

During the thesis, STREAMFINDER algorithm (a state of the art algorithm) was designed to systematically process the Gaia dataset (ESA's novel astrophysical catalogue containing unprecedented astrometric solutions of over 1.6 billion stars) for the detection of the stellar streams of the Milky Way. This hefty endeavour led to the detection of 10 high confidence stream structures, of which 5 were reported as new discoveries.This harvest of structures also facilitated, for the first time, creation of a panoramic structural and kinematic map of the stellar streams of the Milky Way halo, taking our community a step further in unravelling the complex formation history of our Galaxy. This project was instantly followed by the orbital analysis of one of the detected streams (namely GD-1) to explore the improvements in the gravitational potential models of our Galaxy. The constraints on the Milky Way's mass and that on the shape of its dark matter halo, that were obtained by simply employing this single stream, revealed the potential power the analysis of an ensemble of streams would hold in in probing the overall galactic mass distribtuion of our Galaxy.
Thereby, the thesis paved way for new discoveries of the stellar substructures, also highlighting the future prospects in this field.

Keywords : Galaxy structure ; stars ; stellar streams ; dark matter.